

**KATHMANDU UNIVERSITY
SCHOOL OF ENGINEERING
DEPARTMENT OF CIVIL ENGINEERING**

DISSERTATION ON



STUDY OF THE EFFECT OF FAULT IN WEAK ROCK MASS ON THE STABILITY OF
TUNNEL

In Partial Fulfillment of the Requirements for
Masters in Science by Research in Civil Engineering

Bimal Chhushyabaga
[Registration number: 025423-19]

September, 2021

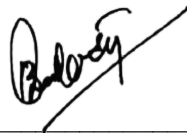
© 2021 Bimal Chhushyabaga

DECLARATION

This master thesis is titled "Study of the effect of Fault in Weak rock mass on the Stability of Tunnel" is submitted to the Department of Civil Engineering for the requirement to partial fulfillment of MS by Research degree in Civil Engineering conducted by Kathmandu University, Nepal. The research work is a genuine, under the supervision of Dr. Shyam Sundar Khadka and has not been submitted to any other universities or institutions.

This study mainly focuses on numerical modeling to study the effect of fault in tunnel and design of its support system in the Himalaya using a case study. A case study has been taken for the study in which tunnel is passing through a fault zone and guideline for the design of required support has been provided by using two-dimensional finite element modelling. A methodology has also been provided for the study of three different tunnel sections such as inverted-D, horseshoe and circular in faulted rock mass, which can be adopted for the design and analysis of tunnel in the Himalayan region. All the data and literature referred from other literary works and cited in this study have been duly acknowledged and provided in the references.

I hereby declare that I am sole author of the thesis. I authorize the Kathmandu University to lend this thesis to other institutions or individuals for the purpose of scholarly research. I further authorize the Kathmandu University to reproduce the thesis by photocopying or by other means, in total or in part, at the request of other institutions or individuals for the purpose of scholarly research.



Bimal Chhushyabaga

[Registration number: 025423-19]

[September, 2021]

DISSERTATION EVALUATION

STUDY OF THE EFFECT OF FAULT IN WEAK ROCK MASS ON THE STABILITY OF TUNNEL

by

Bimal Chhushyabaga

This is to certify that I have examined the above Masters in Science by Research thesis and have found that it is complete and satisfactory in all respects, and that any and all revisions required by the thesis examination committee have been made.



Shyam Sundar Khadka, PhD.
Assistant Professor
Supervisor
Head of Department
Department of Civil Engineering



Er. Shri Ram Neupane
Examiner
Executive Chairman
Megatech Hydro and Infrastructure Pvt.Ltd.



Prof. Manish Pokharel, Ph.D.
Dean
School of Engineering

September, 2021

Acknowledgement

I would like to express my sincere gratitude and warm appreciation to my supervisor Asst. Prof. Dr. Shyam Sundar Khadka for his motivation, encouragement and support for this study of Masters in Science (MS) by Research in Civil Engineering, in Department of Civil Engineering, Kathmandu University. I am fortunate and grateful to my supervisor for the opportunity of Research Assistantship (RA) and MS by Research in Department of Civil Engineering, Kathmandu University. I am indebted to him for his constant guidance and knowledge about tunnel support technology in Himalayan region of Nepal through field visits, laboratory testing and numerical modelling.

Besides my supervisor, I would like to express my gratitude to Energize Nepal Project, Kathmandu University, for the support in field visits to hydropower projects. I would also want to acknowledge my colleague Mr. Sujan Karki and lab assistant Mr. Chetan Sushling Magar for assisting me in laboratory testing in Rock Mechanics and Rock Engineering Laboratory, Department of Civil Engineering. The Laboratory is well equipped and has helped with all the resources required for laboratory testing of collected rock samples from hydropower tunnels. Furthermore, I would also like to thank Dr. Pawan Kumar Shrestha, Hydro Tunnelling and Research Pvt Ltd, for his inputs in numerical modelling of faulted rock mass in Nepal Himalaya.

My sincere thanks also go to Prof. Manish Pokharel, Ph.D., Dean, School of Engineering, Dr. Damber Bahadur Nepali, former Dean of School of Engineering and Assoc. Prof. Dr. Prachand Man Pradhan, former Head of Department of Civil Engineering for their support and guidance in this study. Also, I am grateful to faculties of Department of Civil Engineering, for their suggestions and resources in this study.

Last but not the least, I would like to thank my parents, family members for their spiritual encouragement and support throughout my life, without whom it would not have been possible.

TABLE OF CONTENTS

ACKNOWLEDGEMENT	I
EXECUTIVE SUMMARY	1
LIST OF FIGURES.....	3
LIST OF TABLES.....	7
STUDY TERMINOLOGY	9
1 INTRODUCTION.....	11
1.1 GENERAL.....	11
1.2 NEED OF THE STUDY	12
1.3 OBJECTIVES.....	13
1.4 RESEARCH METHODOLOGY	13
1.5 SCOPE AND LIMITATION	14
1.6 ORGANIZATION CHAPTERS	16
2 CONSTRUCTION PRACTICE OF TUNNEL IN FAULT	17
2.1 GENERAL.....	17
2.2 REVIEW OF HIMALAYAN GEOLOGY.....	18
2.3 FAULT	21
2.4 TUNNEL SUPPORT DESIGN IN FAULT	28
2.4.1 <i>Articulated design approach</i>	29
2.4.2 <i>Anlytical Method</i>	31
2.4.3 <i>Emperical Method</i>	34
2.5 NUMERICAL ANALYSIS.....	40
2.6 CONCLUSION	43
3 DESCRIPTION OF CASE STUDY :MODI KHOLA HYDOELECTRIC PROJECT	44
3.1 GENERAL.....	44
3.2 MODI KHOLA PRESSURE TUNNEL: PROBLEM AND DESIGN IN FAULT ZONE.....	46
3.3 PREVIOUS WORK IN HIMALAYA (INDIAN AND NEPALI TUNNEL DESIGN IN FAULT)	50
3.4 CONCLUSION	56
4 NUMERICAL ANALYSIS.....	58
4.1 GENERAL.....	58
4.2 NUMERICAL MODELLING.....	58
4.2.1 <i>Validation of Numerical Model of Tunnel in Faulted Rock mass in RS2</i>	68
4.2.2 <i>Numerical Modelling in RS2</i>	75

4.3	EFFECTS OF FAULT IN DIFFERENT SHAPE OF TUNNEL	86
4.4	ANALYSIS OF STRUCTURALLY CONTROLLED INSTABILITIES	101
4.5	CONCLUSION	103
5	TUNNEL DESIGN SYSTEM IN FAULT.....	107
6	CONCLUSION AND RECOMMENDATION.....	142
7	REFERENCES.....	144
	ANNEX.....	152
A.	CONVERGENCE CONFINEMENT METHOD.....	152
B.	ROCK MASS CLASSIFICATION	155
C.	PUBLISHED PAPERS	160

Executive Summary

This study deals with stability of the rock mass in tunnel due to the effect of the fault in tunnel in weak rock mass in Nepal Himalaya. Fault is one of the major discontinuities in Nepal which causes excessive deformation and failure of any rock mass and tunnel support. The young mountain system in Himalayan region of Nepal is formed due to the convergent boundary of Indian plate and Eurasian plate. It has resulted the formations of several fault and thrust zones all over the country. Main Frontal Thrust (MFT), Main Boundary Thrust (MBT), Main Central Thrust (MCT), South Tibetan Detachment Systems (STDS) are the major thrusts and faults in Nepal. The hydropower projects in Nepal are located mainly in MBT and MCT. It is evident that the tunnel failures such as wedge failure, block failure, yielding of tunnel support, high deformation are mainly due to weak rock mass and deformation caused by faults and thrusts. Hence, study of the effect of the fault at different location of the tunnel such as crown, right shoulder, left shoulder, left side wall, right side wall, left bottom, right bottom and invert have been done in terms of displacements, stress, plastic zone. As pressure tunnel of Modi Khola hydropower project pass in the vicinity of a fault and thrust zone, it has been selected as a case study. Design of tunnel supports composing of rock bolts, shotcrete and reinforced concrete with sliding gap to account the fault rupture or displacement in a faulted rock has been done using 3D analysis in Unwedge and 2D Finite Element Modelling in RS2.

Roclab, Unwedge and RS2 from Rocscience Inc have been used. Validation of Finite Element Model of tunnel in faulted rock mass is first of all done with field measured deformation data for selected case study and analysis for the effect of fault in the tunnel lining at different key location of tunnel such as crown, invert, shoulder, side wall is done in terms of stress, displacement, shear force, axial force and bending moment. The numerical modeling is done by using the data and parameters of the tunnel and surrounding rock mass based on rock mass classification of Q-systems, GSI system. Strength parameters and mechanical parameters of faulted rock mass are based on Mohr- Coulomb failure criteria, analyzed in RocLab. Unwedge have been used to study the failure due to structurally controlled failure i.e., block or wedge failure in 3-D. Similarly, RS2 have been used to study the effect of fault in tunnel and rock mass in terms of displacements, stress, and design of tunnel support.

3-D Analysis in Unwedge have been done for three sections of headrace tunnel on the basis of chainage: i) 90 m to 400 m ii) 400 to 500 and iii) 500 to 700 m for wedge or block failure. It was found that all the wedges formed around the tunnel in those sections were stable against the sliding failure with factor of safety greater than 2.5.

2-D Numerical analysis RS2 has been be done to study the effect of faulted rock mass in the tunnel and its support design. The study of faults has been done with eight different fault location such as crown, right

shoulder, left shoulder, left side wall, right side wall, left bottom, right bottom and invert with respect to three tunnel of cross sections i) Circular, ii) Inverted D and iii) Horse shoe. The validation of numerical model shows that there is variation of 1.71 % and 5.2 % of modelled deformation with field measured deformations at hill side spring line and hill side bottom respectively. Strength properties of rock mass include tensile strength, compressive strength, frictional angle, cohesive strength. Similarly, data of the fault includes its location, thickness frictional angle, cohesion. The displacement of fault has been assumed as 120 mm on the basis of average rate of displacement given by GPS measurements by Ader et al.,2012 and major seismic energy release 2015 Gorkha Earthquake. Elastic-plastic failure model have been used for modelling of tunnel in weak rock mass (Khadka, 2019).

Articulated system has been used for design of tunnel support in faulted rock mass, which compose of rock bolts, shotcrete and reinforced concrete with sliding gap to account the fault rupture or displacement in a faulted rock. The results obtained show that the tunnel support using articulated system have served well to reduce the bending moment and shear force in tunnel lining of Reinforced Cement Concrete 36 % and 61 % respectively.

List of Figures

Figure 1-1 Research Methodology.....	15
Figure 2-1 Steps to tackle the problem of sheared contact zone of metabasic and quartzite (Goel et al., 1995b).	18
Figure 2-2 a. Seismicity of Nepal and adjacent areas, (Modified after Chamlagain and Niroula, 2020, Di Giacomo et.al., 2014), Figure 2-1 b. Topographical profile (Dahal 2006)	20
Figure 2-3 Types of Fault (a) Normal Fault/Extension, (b) Reverse Fault/Compression (c) Strike-Slip Fault/Transverse (Anderson,1951).....	21
Figure 2-4 Main discontinuities influencing rock mass properties (Palmstrom,1995).....	23
Figure 2-5 Rock Mass Characterization (Martin et al, 1999)	23
Figure 2-6 Definitions of dip and strike for a discontinuity plane (Chapman et.al., 2017).....	24
Figure 2-7 Maximum Horizontal Stress (Zoback,1992) S_v is vertical stress, S_{Hmax} is intermediate stress, S_{Hmin} is horizontal stress.	25
Figure 2-8 Pressuremeter apparatus (Chapman et.al., 2017).	26
Figure 2-9 Primary stress distribution above the groundwater table (Chapman et.al., 2017).....	26
Figure 2-10 Primary stress distribution below the groundwater table (Chapman et.al., 2017)	27
Figure 2-11 Hydraulic fracturing tests (Chapman et.al., 2017).	28
Figure 2-12 Over excavation.....	29
Figure 2-13 Articulated Design.....	29
Figure 2-14 Tunnel behavior across fault boundaries (Russo et. al.,2002).....	30
Figure 2-15 Portion of the longitudinal profile of the Bolu Tunnel with active faults (Russo et. al.,2002).....	31
Figure 2-16 Reinforcement details in lining at side wall and at invert (Russo et al.,2002)	32
Figure 2-17 Ground Reaction Curve and Support Characteristic Curve. (Rocscience, 2005).....	33
Figure 2-18 Longitudinal topographical profile along tunnel alignment (Hoek et. al.,2008).....	34
Figure 2-19 Convergence confinement analysis for sliding joint in Yacambú-Quibor tunnel in the Northern Andes in Venezuela (Hoek et. al.,2008)	34
Figure 2-20 Sliding joint Assembly in Yacambú-Quibor tunnel in the Northern Andes in Venezuela (Hoek et. al.,2008)	35
Figure 2-21 Maximum support capacities for different support system installed in circular tunnel (Hoek, 1998)	36
Figure 2-22 Rock mass types in tectonically disturbed heterogeneous formations such as flysch (Marinos, 2014)	37

Figure 2-23 The new GSI classification chart for heterogeneous rock masses such as flysch (Marinos et. al. 2007)	38
Figure 2-24 General directions for the immediate support measures for every flysch type (Marinos et al., 2011).....	39
Figure 2-25 Shallow Izmir Metro Tunnel of Turkey in RS2 (Kun and Onargan, 2013)	42
Figure 3-1 Plan of Modi Khola Pressure Tunnel (Shrestha & Panthi,2014).....	44
Figure 3-2 Geological profile along the tunnel system of Modi Project (Panthi, 2012).....	45
Figure 3-3 Equal Angle Lower Hemisphere Projection of Pressure Tunnel and Fault of Modi Khola Hydroelectric Project	45
Figure 3-4 Tunnelling through Shear Zone in Modi Khola Hydropower Project, (Paudel et. al.,1998). ...	48
Figure 3-5 Principal tunnel support patterns in Modi Khola Hydroelectric Project (Paudel et. al.,1998). ..	49
Figure 3-6 Flowing mass from the tunnel crown (Himal Hydro, 2001)	50
Figure 3-7 Longitudinal section of Headrace tunnel of Kulekhani III Hydropower (NEA, 1997).....	51
Figure 3-8 Tunnel support in shear zone in Kulekhani III Hydropower Project (NEA, 1997).....	51
Figure 3-9 Longitudinal profile of headrace tunnel of Kaligandaki ‘A’ Hydroelectric Project, (Panthi and Neilson, 2007).....	52
Figure 3-10 Tunnel support in shear zone in Kaligandaki ‘A’ hydroelectric project (Chhushyabaga et. al.2020)	53
Figure 3-11 Longitudinal geological profile of Chameliya headrace tunnel (modified after Khadka,2019)	53
Figure 3-12 Tunnel squeezing Chameliya headrace tunnel. Floor heave (left) and wall closure in hill side (right) (Basnet et. al., 2013).....	54
Figure 3-13 Geological cross-sections along Chhibro-Khodri tunnel (a) original before starting tunneling	54
Figure 3-14 Shear zone treatment in Maneri stage-I project (Lang, 1961).....	55
Figure 3-15 Water inrush in head race tunnel of Maneri stage-I project (Goel et al., 1995a)	55
Figure 4-1 The Mohr- Coulomb strength criterion: (a) shear failure on plane a-b, (b) Strength envelope of shear and normal stresses, and (c) Strength envelope of principal stresses (Zhao, 2000)	60
Figure 4-2 Analysis of Rock Strength of Grouted rock mass using Roclab	64
Figure 4-3 Normal stress distribution in perimeter wedge at chainage of 200 to 400 m of adit tunnel of Modi Khola Hydropower Project.	65
Figure 4-4 Suggested post failure characteristics for different quality of rock mass and tunnel behavior (Hoek, 2007 and Lorig, et al. 2013).....	67
Figure 4-5 Analysis of Rock Strength of Quartzite using Roclab	69

Figure 4-6 Analysis of Rock Strength of faulted rock mass using Roclab	70
Figure 4-7 Analysis of Rock Strength of Phyllitic Schists mass using Roclab.....	71
Figure 4-8 Analysis of Rock Strength of Phyllitic Quartzite using Roclab	72
Figure 4-9 Analysis of Rock Strength of Conglomerate using Roclab.....	73
Figure 4-10 2D Model of Pressure Tunnel of Modi Khola Hydropower Project in RS2	74
Figure 4-11 Deformation obtained in Pressure tunnel of Modi Khola Hydropower project	74
Figure 4-12 b. Definition and Distribution of Fault in Inverted D Tunnel	77
Figure 4-13 b. Definition and Distribution of Fault in Circular Tunnel	79
Figure 4-14 b. Definition and Distribution of Fault in Horseshoe Tunnel.....	81
Figure 4-15 Key points are in inverted D(a), Circular (c) and Horshoe (c) tunnel sections	82
Figure 4-16 Circular Tunnel with Left Side Wall Fault in RS2.....	83
Figure 4-17 Horse Shoe Tunnel with Crown Fault in RS2	84
Figure 4-18 Inverted D Tunnel with Right Shoulder Fault in RS2	85
Figure 4-19 Displacement at tunnel locations at different Fault locations inverted D tunnel.....	87
Figure 4-20 Axial force at tunnel locations at different Fault locations inverted D tunnel.	88
Figure 4-21 Moment at tunnel locations at different Fault locations inverted D tunnel.	89
Figure 4-22 Shear Force at tunnel locations at different Fault locations inverted D tunnel.	90
Figure 4-23 Displacement at tunnel locations at different Fault locations Horseshoe Tunnel	92
Figure 4-24 Axial force at tunnel locations at different Fault locations horseshoe tunnel	93
Figure 4-25 Moment at tunnel locations at different Fault locations horseshoe tunnel.....	95
Figure 4-26 Shear force at tunnel locations at different fault locations horseshoe tunnel	96
Figure 4-27 Displacement at tunnel locations at different Fault locations circular tunnel	97
Figure 4-28 Axial Force at tunnel locations at different Fault locations in circular tunnel	98
Figure 4-29 Moment at tunnel locations at different Fault locations in circular tunnel.....	99
Figure 4-30 Shear Force at tunnel locations at different Fault locations circular tunnel	100
Figure 4-31 Normal stress distribution in perimeter wedge at chainage of 99 to 400 m of Headrace tunnel of Modi Khola Hydropower Project	102
Figure 4-32 Normal stress distribution in perimeter wedge at chainage of 400 to 500 m of Headrace tunnel of Modi Khola Hydropower Project.	102
Figure 4-33 Normal stress distribution in perimeter wedge at chainage of 500 m to 700 m of Headrace tunnel of Modi Khola Hydropower Project	103
Figure 5-1 Tunnel Support Details.....	109
Figure 5-2 Shear force distribution with articulated design Crown Fault.....	110
Figure 5-3 Shear force distribution without articulated design Crown Fault.....	110

Figure 5-4 Moment distribution with articulated design Crown Fault	111
Figure 5-5 Moment distribution without articulated design Crown Fault	111
Figure 5-6 Axial Force distribution with articulated design Crown Fault	112
Figure 5-7 Axial Force distribution without articulated design Crown Fault	112
Figure 5-8 Support capacity plot with articulated design	113
Figure 5-9 Support capacity plot without articulated design	114
Figure 5-10 Axial Force Distribution with articulated design Invert Fault.....	119
Figure 5-11 Moment Distribution with articulated design Invert Fault.....	119
Figure 5-12 Shear Force Distribution with articulated design Invert Fault	120
Figure 5-13 Axial Force distribution without articulated design for Invert Fault.....	120
Figure 5-14 Moment distribution without articulated design for Invert Fault	121
Figure 5-15 Shear Force distribution without articulated design for Invert Fault	121
Figure 5-16 Axial Force Distribution with articulated design for Left Bottom Fault.....	122
Figure 5-17 Moment Distribution with articulated design for Left Bottom Fault	122
Figure 5-18 Shear Force Distribution with articulated design for Left Bottom Fault.....	123
Figure 5-19 Axial Force Distribution without articulated design for Left Bottom Fault.....	123
Figure 5-20 Moment Distribution without articulated design for Left Bottom Fault	124
Figure 5-21 Shear Distribution without articulated design for Left Bottom Fault.....	124
Figure 5-22 Axial Distribution with articulated design for Left Shoulder Fault	125
Figure 5-23 Moment Distribution with articulated design for Left Shoulder Fault.....	125
Figure 5-24 Shear Distribution with articulated design for Left Shoulder Fault	126
Figure 5-25 Axial Distribution without articulated design for Left Shoulder Fault	126
Figure 5-26 Moment Distribution without articulated design for Left Shoulder Fault.....	127
Figure 5-27 Shear Distribution without articulated design for Left Shoulder Fault	127
Figure 5-28 Axial Distribution with articulated design for Left Side Wall Fault	128
Figure 5-29 Moment Distribution with articulated design for Left Side Wall Fault	128
Figure 5-30 Shear Distribution with articulated design for Left Side Wall Fault.....	129
Figure 5-31 Axial Distribution without articulated design for Left Side Wall Fault.....	129
Figure 5-32 Moment Distribution without articulated design for Left Side Wall Fault	130
Figure 5-33 Shear Distribution without articulated design for Left Side Wall Fault.....	130
Figure 5-34 Axial Distribution with articulated design for Right Bottom Fault.....	131
Figure 5-35 Moment Distribution with articulated design for Right Bottom Fault.....	131
Figure 5-36 Shear Distribution with articulated design for Right Bottom Fault	132
Figure 5-37 Shear Distribution without articulated design for Right Bottom Fault	132

Figure 5-38 Axial Distribution without articulated design for Right Bottom Fault.....	133
Figure 5-39 Moment Distribution without articulated design for Right Bottom Fault.....	133
Figure 5-40 Axial Distribution with articulated design for Right Shoulder Fault	134
Figure 5-41 Moment Distribution with articulated design for Right Shoulder Fault.....	134
Figure 5-42 Shear Distribution with articulated design for Right Shoulder Fault	135
Figure 5-43 Axial Distribution without articulated design for Right Shoulder Fault	135
Figure 5-44 Moment Distribution without articulated design for Right Shoulder Fault	136
Figure 5-45 Shear Distribution without articulated design for Right Shoulder Fault.....	136
Figure 5-46 Axial Distribution with articulated design for Right Side Wall	137
Figure 5-47 Moment Distribution with articulated design for Right Side Wall	137
Figure 5-48 Shear Distribution with articulated design for Right Side Wall.....	138
Figure 5-49 Axial Distribution without articulated design for Right Side Wall.....	138
Figure 5-50 Moment Distribution without articulated design for Right Side Wall	139
Figure 5-51 Shear force distribution without articulated design for Right Side Wall	139
Figure 5-52 Comparison of Maximum Moment with and without Articulated Design for Different fault location.....	141
Figure 5-53 Comparison of Maximum Shear force with and without articulated Design for different fault location.....	141
Figure 7-1 Assumed support pressure p_i at different positions (Hoek, 1998)	152
Figure 7-2 Longitudinal displacement profile (Unlu and Gercek,2003).....	154
Figure 7-3 Analysis chart by Palmström and Broch (2006)	158
Figure 7-4 Support recommendations based on Q values Barton et al. (1974)	158
Figure 7-5 General chart for GSI (Marinos et al., 2005)	159

List of Tables

Table 3-1 Faulted rock mass properties in Pressure Tunnel for Modi Khola Hydropower Project (Panthi, 2006).....	45
Table 3-2 Orientation and characteristics of discontinuities in the Headrace Tunnel in Modi Khola Hydroelectric Project. Paudel et. al.,1998	47
Table 3-3 Major tunneling projects with problems faced in fault/ thrust zone and remedial measures (Feng,2017).....	55
Table 4-1 Ratio of increase in displacements in tunnel lining positions due to different fault locations inverted D tunnel.....	87

Table 4-2 Ratio of increase in axial force in tunnel lining positions due to different fault location inverted D tunnel.....	88
Table 4-3 Ratio of increase in moment in tunnel lining positions due to different fault locations inverted D tunnel.	90
Table 4-4 Ratio of increase in shear force in tunnel lining positions due to different fault locations inverted D tunnel.....	90
Table 4-5 Ratio of increase in displacements in tunnel lining positions due to different Fault locations Horseshoe Tunnel	92
Table 4-6 Ratio of increase in axial force in tunnel lining positions due to different fault locations horseshoe tunnel	93
Table 4-7 Ratio of increase in moment in tunnel lining positions due to different fault locations horseshoe tunnel	95
Table 4-8 Ratio of increase in shear force in tunnel lining positions due to different fault location horseshoe tunnel	96
Table 4-9 Ratio of increase in displacement in tunnel lining positions due to different fault locations	97
Table 4-10 Ratio of increase in axial force in tunnel lining positions due to different fault locations in circular tunnel	98
Table 4-11 Ratio of increase in moment in tunnel lining positions due to different fault locations in circular tunnel	100
Table 4-12 Ratio of increase in shear force in tunnel lining positions due to different fault locations in circular tunnel	101
Table 4-13 Ratio of increase in displacement, axial force, bending moment and shear force.....	104
Table 4-14 Critical faults at critical points of tunnel lining in terms of shear force, bending moment, axial force and displacements	105
Table 7-1 Guidelines for excavation and support of rock tunnels based on the RMR system (Bieniawski, 1989).....	155

Study Terminology

Dip: The vertical angle of the line of maximum inclination, measured from a horizontal plane.

Dip direction: The orientation of the horizontal projection of the line of maximum inclination, measured clockwise from the North.

Plunge: Orientation of the tunnel axis to the horizontal, when looking from the opening of the excavation. For instance, horizontal excavations have a zero-degree plunge.

Strike of the plane: Direction of the line of intersection of the plane and a horizontal surface.

Wedge: Triangular rock block created in isolation by intersection of structural discontinuity sets such as fault lines and/or joints but are a part of the fractured soft rock blocky mass.

Block size: Average diameter of a typical rock block measured by observing an exposed rock face at the surface or underground, or rock core obtained by drilling, or from a pile of muck after blasting.

Elastic behavior: This occurs when stress induced is directly proportional to the strain in a material.

Plastic zone: Extent of failure zone resulting from high ground stresses surrounding an excavation and comprising loose unstable rock blocks or wedges.

Crown: Top of the tunnel, also known as the tunnel roof.

Arch: Continuous basic geometry of the tunnel crown.

Invert: Bottom of the tunnel, also known as the tunnel floor.

Wall: Vertical side of a tunnel, which is also called a side wall.

Heading: It is the crown portion of an underground tunnel excavation.

Sequential excavation: Tunnel construction method involving removal of earth in stages including the top heading, bench and invert.

Over break: Unwanted rock removal which is beyond the specified maximum excavation perimeter therefore it is a line outside the pay line. It is also called the B-line.

Under break: Unwanted rock removal that is less than the specified minimum excavation perimeter. It is also called the A-line.

Rock burst: Failure of a significant volume of rock mass which involves sudden collapse of wedges from the tunnel side walls, crown or floor. It is also known as popping.

Spalling: Term for rock bursts from the tunnel side walls.

Stand-up time: Duration for which an excavated surface may be left unsupported before it breaks down. It is also called the bridge-action period.

1 Introduction

1.1 General

Tunnels are underground horizontal civil structures whose lengths are either longer than twice the diameter of the structure or the sum of both the diameter and height of the structure. They are usually constructed by excavating through the ground in places where surface construction is unfavorable due to various factors. Unfavorable factors can be natural barriers, legal requirements, populated cities, existing infrastructure or other existing land uses. Tunnels are built for different utilities purposes such as transportation, storage, irrigation or water conveyance.

A great progress has been made in the tunnel construction in Nepal Himalaya with hundreds of kilometers of already constructed hydropower tunnels and hundreds of kilometers of under construction hydropower tunnels. However, the research about tunnel crossing the active fault is a new subject of interest. Major tunneling problems in the Lesser Himalaya is due to its geology where rock masses are weak and undergoing intense tectonic activities resulting into major faults, folds and other discontinuities. Hence, the need for the geological information becomes very vital in a tunnel where overburden is very high with inaccessible terrain, and tectonically disturbed rock mass. Under such conditions, tunneling unforeseen problems occurs which leads to time and cost over-runs.

The Himalayan range of Nepal, measuring 2400 km from the bend of Indus River from north – northwest to Brahmaputra River is one of the most active and fragile mountain ranges on earth (Dahal, 2006). The complex geological settings, rugged topography, tectonic movements are factors which deduce the rock mass strength, making it very hazardous for the tunnels and underground structures. Fault is a critical geological discontinuity which aids in reducing the strength of rock masses by overstressing the rock mass and creating the displacements and plastic zones. The presence of the faults and the resulted displacements and the plastic zones cause in the formation of structurally controlled instabilities such as wedge/ block failures. Also, rock bursting of brittle and massive rocks, ground squeezing, swellings, ground water inflow are the problems in the tunnel which are directly linked to the mechanism of tectonic movements of faults in the Himalaya.

Stability of tunnel depends on the rock conditions, material properties, residual strength, overburden of tunnel, disturbance factor and tunnel diameter. Poisson's ratio, Young's modulus, shear modulus and stiffness are the properties which influence the magnitude of stresses and deformations in the faulted rock mass (Hochella et al., 1989). It is therefore important to understand rock mineralogy, structure and fabric, discontinuities set, hydrogeology, squeezing and swelling problematic material behavior (Panthi, 2006). The design of tunnels in poor rock masses such as faulted or sheared rock mass presents a major challenge to

geologists and engineers. The complex structure of these materials implies that they cannot effectively be classified in terms of the broadly used rock mass characterisation systems. This chapter includes objectives, research methodology and scope of this research.

1.2 Need of the Study

The majority of hydropower projects in Nepal are located in Himalayan region in deep dissected valleys favorable for large storage and high water. The Himalayan region is tectonically active due to the convergent boundary of Indian plate and Eurasian plate created faults, thrusts such as MFT, MBT, MCT, STDS (Dahal, 2006). There is widespread distribution of fault and shear zone. Hence, most of the hydropower project pass through these zones. It is very difficult to avoid faulted rock mass and problems such as tunnel collapse, overbreak, squeezing ground water ingress. The tunnel support fails due to fault and its associated stress environment which is the combination of gravitational stress, topographic stress, tectonic stress, due to fault zones or shear zones.

There are a number shear zones and faults present in the Nepal Himalaya. These shear zones and faults are located to regional main boundary fault and main central thrust. The contact of two rock types is found to be generally sheared in lesser Himalaya (Goel et al.,1995). The rock mass affected by a shear zone is much larger than the shear zone itself.

Widely used empirical approaches such as Rock Mass Rating (Bieniawski, 1989), Q –system (Barton et al.,1974) have been in the practice for tunnel support estimation. But they have their own applicability i.e they suit best on the parameters and environment on which it has been developed (Norway and Sweden) which is different to the geology of Nepal Himalaya. RMR classification is a conservative approach which can lead to an overestimation of the support measures (Maidl et al., 2008). These classification systems cannot be used to study the faulted rock mass. Paudel et al.,1998 accounts important limitation of the Q-system which does not consider the tunneling direction relative to the direction of the main discontinuities such as faults. The tunnel stability will generally be reduced due to overbreak in such conditions.

The tunnelling conditions in faulted geology, and its numerical modelling for tunnel support design have been a challenging task. Especially at greater excavation and overburden tunnel, tunneling activity induces significant stresses around the tunnel creating difficulty to develop a rational tunnel support design method. It is not surprising to the fact that tunneling have relied on the experience and empirical approaches which has proved to be inadequate. By definition, empirical procedures do not work in the conditions different to those in which it has been developed. Hence, a numerical guideline for the modelling of tunnel support and its design has to be followed. Hence, these empirical methods for tunnel support estimation have been used in hydropower projects in Nepal with modified support systems on the basis of

respective site conditions. This emphasizes the need of alternative way of analysis and design of required support in tunneling and underground structure. Numerical modelling is a best alternative as it can provide solutions in realistic way with better accuracy and precision. Detailed research is a must to develop a standard guideline for the tunnel support design. numerical modeling method using approaches such as FEM, DEM, FDM can serve as a better solution to our problem. Numerical modeling and analysis are comparatively easier for 2-D and 3-D of the rock mass, surrounding the tunnels and tunnel support required to sustain the stress from these rock mass.

1.3 Objectives

Primary Objective:

- To study the effects of the faults on the rock mass around the tunnels and tunnel support design using the numerical modeling.

Secondary Objectives:

- To collect the information in the tunneling approaches in Himalayan region.
- To study the stress distribution around the tunnels due to presence of fault.
- To study the adequacy of tunnel supports in existing hydropower tunnel.
- To provide the reference for the design of the tunnel supports in Himalayan region.

1.4 Research Methodology

Literature Review

Available literatures on the location, orientation, thickness, orientation of faults and their effects on the in-situ stress condition, shear strength, displacement, plastic zones of the different rock mass and the support conditions has been reviewed. Also, the tunnel support approaches used to resist the geological problems from the faults has been studied. Figure 1-1 show the research methodology used in this study.

Selection of case study

Modi Khola Hydroelectric Project has been selected as a case study. The pressure tunnel of Modi Khola Hydropower passes through the faulted zone.

Data Collection

Different hydropower projects have been visited as the primary sources for the data about the rock mass displacement, deformations, plastic zones, and shear strength, in situ stress of around the tunnels and

efficiency of the existing tunnel support. Secondary sources of the data such as research papers, journals, newspapers, feasibility reports have also been reviewed for the additional data.

Calculation of Parameters

Parameters required for the numerical modeling are calculated using the collected data from both the primary and secondary sources and available empirical and analytical relationships based on Q value, GSI value, etc. Mohr Column Failure Criterion have been used as failure criteria and Elastic Plastic model have been used for modelling of rock mass.

Stability Analysis

Based on the data collected and parameters calculated, the stability analysis of the rock mass around the tunnel and tunnel support has been done using various numerical modelling in RS2.

Numerical modeling has been done using finite element modeling in Unwedge, RS2 software provided by Rocscience on the basis of the data collected and the calculated parameters. Validation of modelling has been first done. The analysis on the suitability of the existing supports and the other tunnel supports has been done.

Interpretation

From the results obtained from the numerical modeling conclusion has been drawn about the adequacy of the tunnel supports used for the existing stress conditions from the mechanisms of the fault and tunnel support design.

1.5 Scope and Limitation

The main scope of this project is the detailed study of the fault effected rock mass surrounding the underground tunnel and design of the tunnel support using the numerical modelling for Nepal Himalaya. The scope of the project can be summarized as follows:

- There is widespread distribution of faulted geology in Nepal Himalaya
- Various fault or thrust zone are encountered in Hydropower tunnel projects such as Kulekhani III, Kaligandaki 'A', Modi Khola, etc
- Familiarizations on the effect of the fault and weak planes in stability problems in tunnelling.
- Design of tunnel support in faulted rock mass in Himalayan region of Nepal

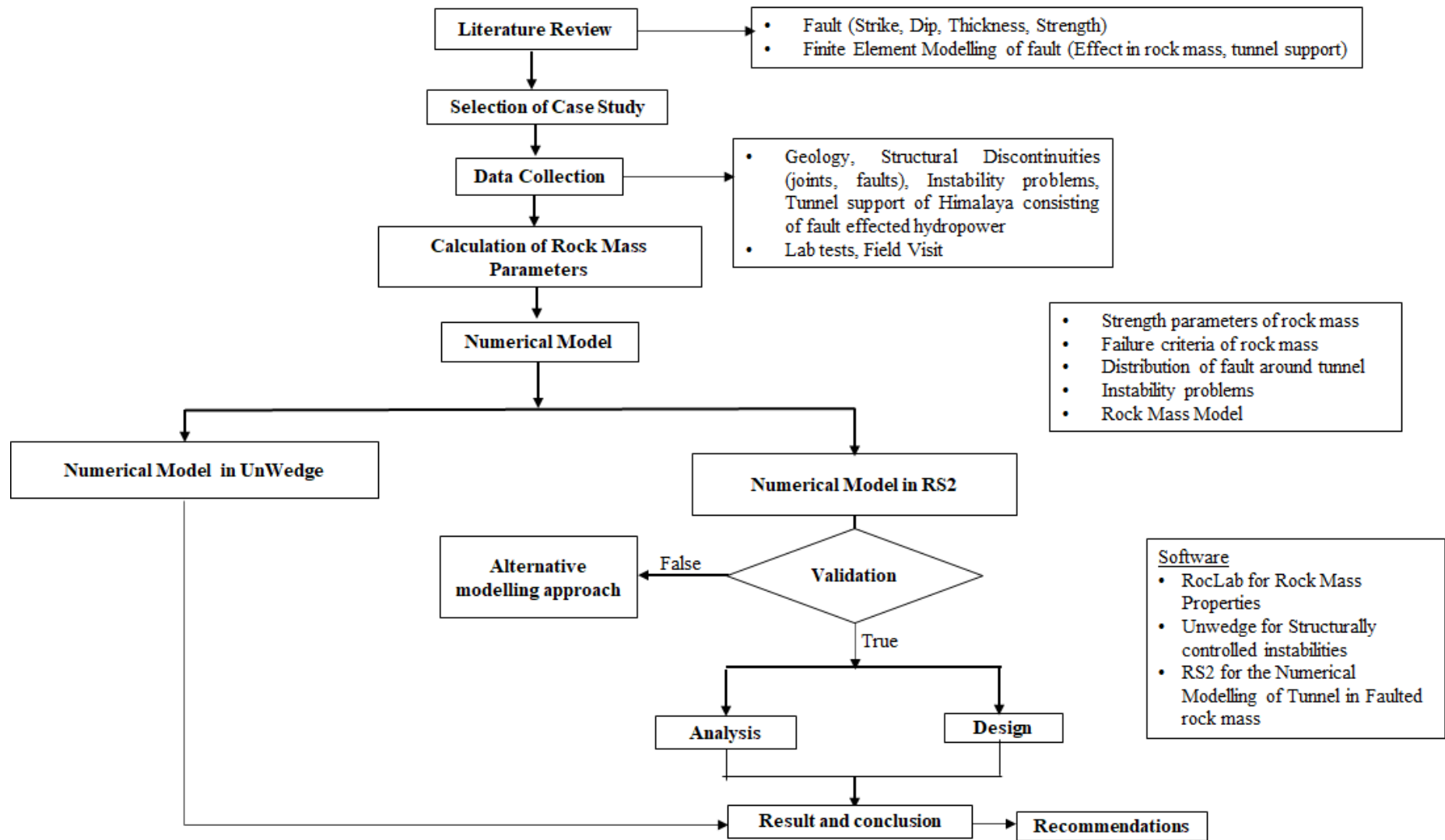


Figure 1-1 Research Methodology

1.6 Organization chapters

The study here comprises of following six chapters.

- **Chapter 1** introduces the study, justifies the relevance of the study, highlights the study. Literature relevant to this study is reviewed in Chapter 2 and 3 to establish a basis for accomplishing the objectives of this study.
- **Chapter 2** covers Geology of Nepal, tunnels in faulted rock mass, their history, types, construction and previous experiences from other tunnels.
- **Chapter 3** discusses the selected case study and previous works in tunnel in faulted rock mass in Lesser Himalaya.
- **Chapter 4** explains the numerical modelling methodology used in this study with a case study
- **Chapter 5** explains the design of tunnel support in fault zone using a case study
- **Chapter 6** concludes this study on the basis of the work done in this study

2 Construction Practice of Tunnel in Fault

2.1 General

In tunnel construction process, layout is first prepared after collecting adequate geological information of project site. Tunneling operations depends upon the reliability of geological data or its predictions. It is easier to collect geological details when the tunneling is done in shallow terrain with flat undisturbed rockmass. In such regions the ideal approach is to make geophysical exploration to identify overburden, geological structures or discontinuities such as faults, shear zones, water bodies etc. Then a conventional geological exploration should be planned for detailing. This approach would optimize the time and cost of for useful geological information with good accuracy. Despite the efforts of the geologists with detailed geological exploration work, most of the project have inadequacies in the prediction of nature of the rock masses. These inadequacies led to different tunneling problems like water-in-rush, roof falls, cavity formation, face collapse, swelling, support failure, etc. In addition, squeezing ground conditions in the weak rock masses tunnelling projects in the Himalaya have also suffered considerable construction problems.

Modi Khola Hydroelectric Project, Kulekhani III Hydropower Project, Kaligandaki 'A' hydroelectric project and Chameliya Hydroelectric Project are some of the hydropower projects located in Nepal constructed in faulted geology. The head race tunnels of these hydropower projects have been constructed in faulted rock mass. The problems of the tunnel in faulted rock mass mainly include squeezing, high pressure and deformation, flowing ground condition, water in rush, cavity formation and high pressure leading to support failure of the tunnel. The tunnel support has been used to solve those problems mentioned above with measures of the support based on the site conditions. It includes stabilization of the fractured rock mass with lattice girders, forepoles, grouting, rock bolts, drainage of ground water and use of flexible support of steel ribs, precast concrete as final support for the movement of ground due to fault. These projects are elaborated in details in section 3.3.

Goel et al., 1995(b) give steps to tackle the problem of sheared contact zone of metabasic and quartzite. Figure 2-1 shows a typical treatment method for shear zones in the roof of tunnel. First the shear zone is excavated with caution up to some depth. After excavation, immediately one thin layer of shotcrete with wire mesh or steel fiber reinforced shotcrete (SFRS) shall be sprayed. The weak zone is then reinforced with inclined rock bolts and finally shotcrete with wiremesh or SFRS (preferably SFRS) should be sprayed ensuring its proper thickness in weak zones. This methodology is effective in the tunnels of the Himalayan region as shear zone and faults zones are frequently found along tunnels and caverns in the Himalaya (Feng, 2017). In case of a thick shear zone ($b \gg 2m$) with sandy gouge, umbrella grouting or rock bolting is used to enhance the strength of roof and walls in advance of tunneling. The excavation is made manually.

Steel ribs are placed closely and shotcreted until the shear zone is crossed. Each (blasting) round of advance should be limited to 0.5m or even smaller depending upon the stand-up time of the material and fully supported before starting another round of excavation (Feng, 2017).

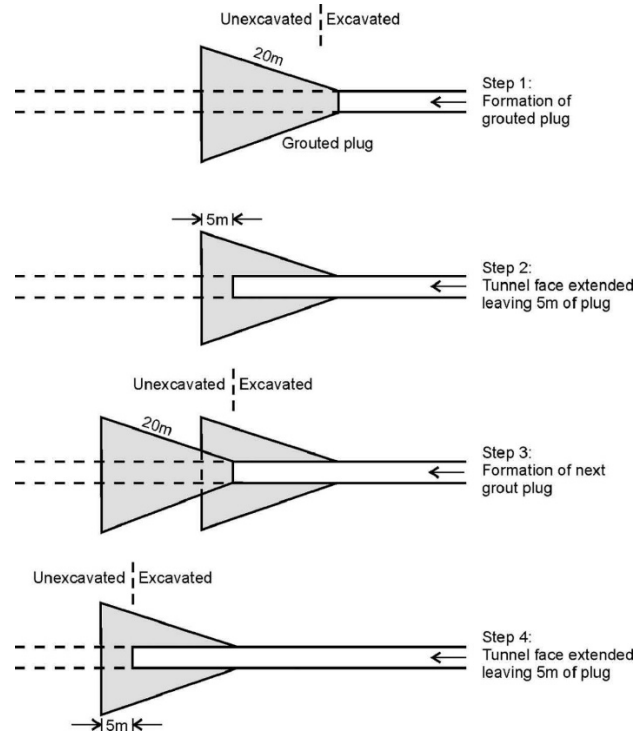


Figure 2-1 Steps to tackle the problem of sheared contact zone of metabasic and quartzite (Goel et al., 1995b).

2.2 Review of Himalayan Geology

Himalaya is a mountain chain is located in Indian subcontinent in the north formed by the collision of the Indian Plate with the Eurasian Plate. The Himalayan range with trends in NW-SE. The uninterrupted convergence of Indian and Eurasian plate since their collision between 40 and 55 million years ago at 50 mm/year has led to the accumulation of widespread strain in the Himalayan frontal arc (Chen and Molnar, 1977). There is variation of thickness of fault zone and shear zone in Nepal from few millimeters to several meters. GPS measurements have shown decrease in rate of collision, i.e., 20 mm/year in the western Nepal Himalaya and 18 mm/year in the eastern Nepal Himalaya (Ader et al., 2012) 25th April, 2015 Gorkha earthquake event increased the Coulomb stress changes by 0.06 MPa at 16 km depth below the site of the 12 May event. (Mandal, 2018). There is an average movement of Fault at the rate of 20 mm / year.

The Shiwaliks are the southern foothills of the Himalaya. With an average height of about 1000 m from mean sea level (MSL), these are generally covered with thick forests and comprise the youngest rocks in

the Himalayan range. The soft, loose, and easily erodible rocks are represented by sand rocks, sandstones, siltstones, clays- tones, mudstones and conglomerates. Water penetrates into these rock masses along the fractures and joints and sometimes creates flowing ground conditions.

The Main Boundary Thrust (MBT)

An analysis of 281 seismic events of earthquake records from 1913 AD to 1987 AD shows that the distribution of earthquake epicenter is due to MBT. All the earthquake epicenters near MBT were less than 5 in magnitude. The only location of earthquake with epicenter at distance 250 km west MBT have magnitude of 6.2. The estimated maximum peak horizontal acceleration related to MBT is 0.46g (NEA, 1997).

Separating the Shiwaliks Formations of the Sub-Himalaya from the older rocks of Lesser Himalaya lying to their north, the Main Boundary Fault is a major structural plane throughout the length of the Himalaya. The irregularity and sinuosity of the fault trace is evidence of a highly inclined plane. The older rocks of the lesser Himalaya are thrust over the Shiwaliks along a series of more or less parallel thrust planes. The Main Boundary Fault is a thrust fault with large-scale movements and is still very active.

The Lower Himalaya are separated from the Shiwaliks by the main boundary fault (MBT). The lower Himalaya are rugged mountain region having an average height of about 4000 m from mean sea level. The lesser Himalaya is made of sedimentary and metamorphic rocks. The sedimentary formations vary from weak slates to massive and thickly bedded dolomites. Limestones, quartzites, shales and claystones are also present. These are intensely folded and faulted. The low grade meta- morphic rocks in the lesser Himalaya are phyllites, quartzites, schists and gneisses.

The Main Central Thrust (MCT)

The main central thrust (MCT), marking the boundary between the lesser and higher Himalaya, is a zone of more or less parallel thrust planes along which the rocks of the central crystallines have moved southwards against, and over the younger sedimentary and metasedimentary rocks.

The higher Himalaya are separated from the lesser Himalaya by the Main Central Thrust (MCT). The topography is rugged and the average height above mean sea level is about 8000 m. The rocks of higher Himalaya are also intensely folded and faulted. Tunnels in Himalaya have high overburden because of its great heights from MSL. Because of these features, various tunneling problems were encountered while excavating tunnels through the Himalaya (Feng, 2017).

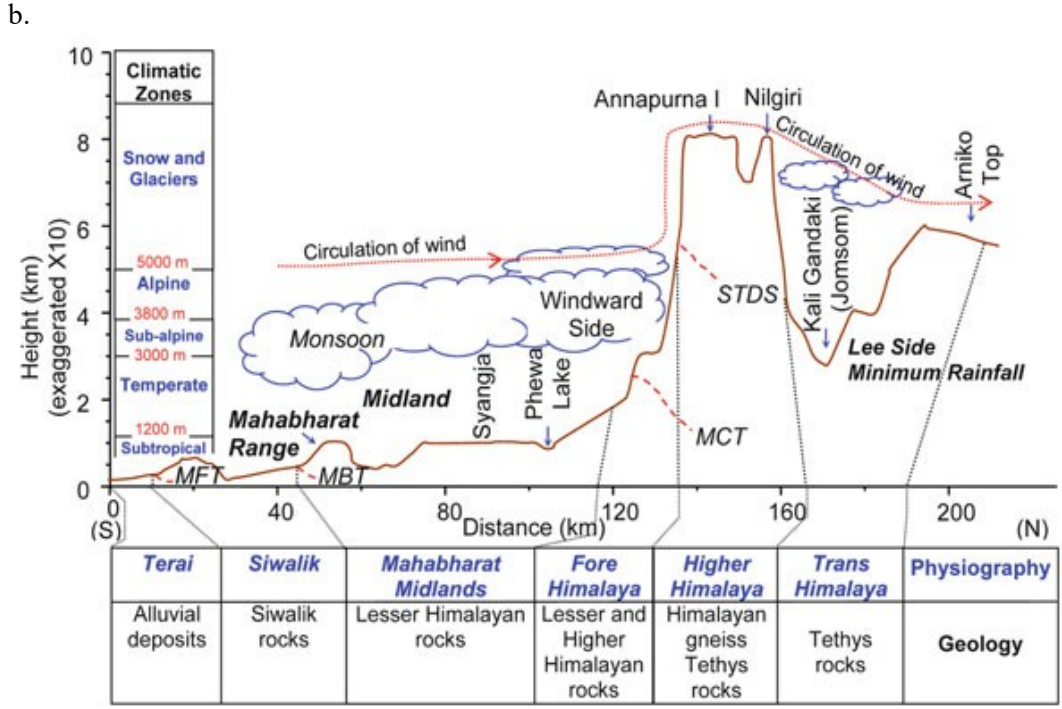
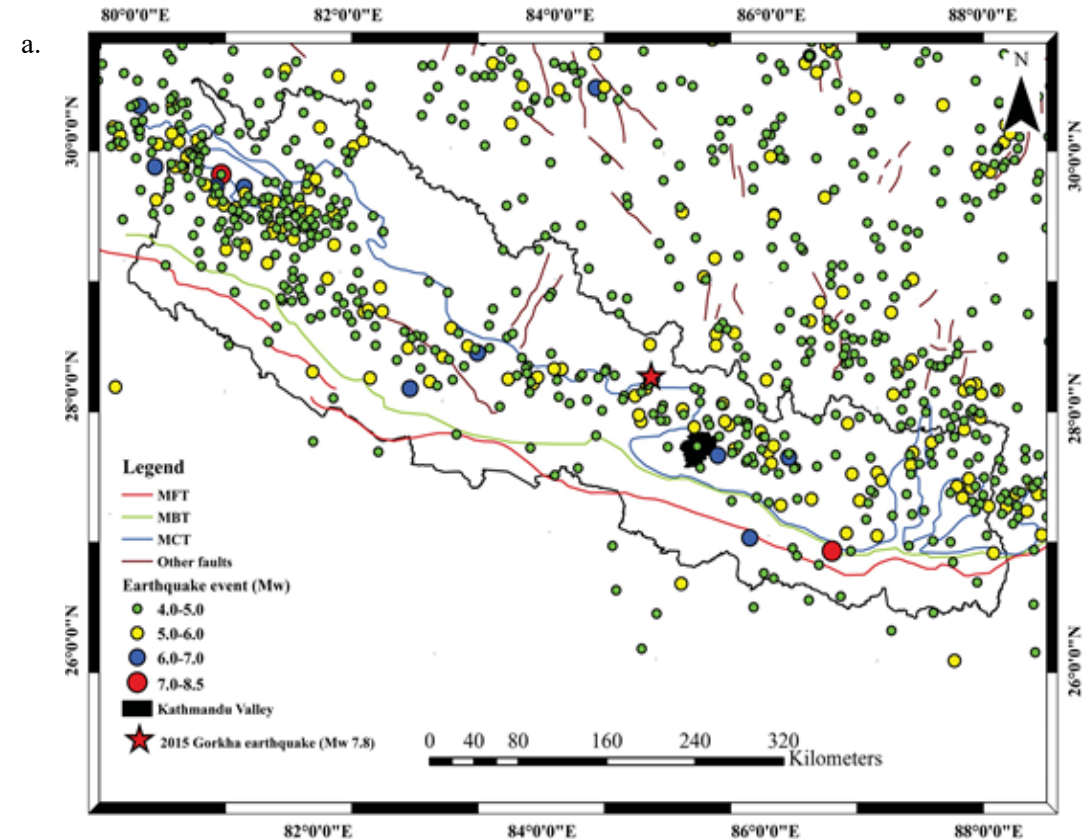


Figure 2-2 a. Seismicity of Nepal and adjacent areas, (Modified after Chamlagain and Niroula, 2020, Di Giacomo et al., 2014), Figure 2-1 b. Topographical profile (Dahal 2006)

2.3 Fault

A fault is a fracture or zone of fractures between two blocks of rock. Faults allow the blocks to move relative to each other. This movement may occur rapidly in the form of an earthquake or may occur slowly, in the form of creep. Faults may range in length from a few millimeters to thousands of kilometers. Most faults produce repeated displacements over geologic time. During an earthquake, the rock on one side of the fault suddenly slips with respect to the other. The fault surface can be horizontal or vertical or some arbitrary angle in between. Dip angle of the fault with respect to the surface and the direction of slip along the fault are used to classify the types of faults. Faults which move along the direction of the dip plane are dip-slip faults and described as either normal or reverse thrust, depending on their motion. Faults which move horizontally are known as strike-slip faults and are classified as either right-lateral or left-lateral. Faults which show both dip-slip and strike-slip motion are known as oblique-slip faults.

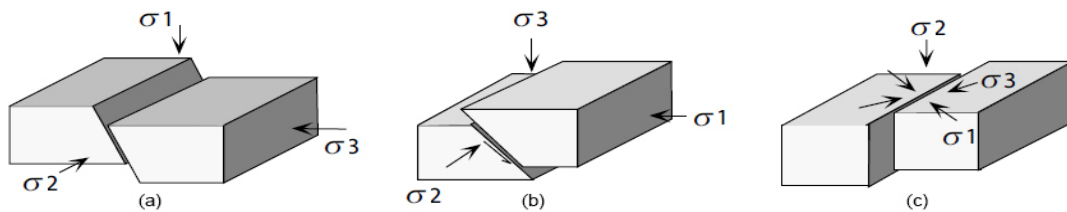


Figure 2-3 Types of Fault (a) Normal Fault/Extension, (b) Reverse Fault/Compression (c) Strike-Slip Fault/Transverse (Anderson,1951)

Rock is naturally stable but changes its mechanical properties, material properties, strength, deformability, permeability and stability of rock masses under extreme conditions, (Palmstrom,1995). Material properties of a rock determines whether it is suitable for construction or not and the precautions required when using it. Anderson in 1951, reformulated the Mohr-Coulomb law in terms of differential stress ($\sigma_d = \sigma_1 - \sigma_3$) and lithostatic stress ($\sigma_L = \rho g z$) instead of shear stress and normal stress. He took three cases to represent reverse faults, normal faults and strike slip faults and assumed that $\sigma_L = \sigma_3$, $\sigma_L = \sigma_1$ and $\sigma_L = \sigma_2 = 0.5(\sigma_1 + \sigma_3)$ for each of these cases, respectively (Eq.(2.1), Eq.(2.2), Eq.(2.3)). Then, the differential stress as a function of depth (or σ_L) may be written as equation ,and P_w is the pore fluid pressure.

The damage to the tunnel is dependent on the nature of the fault. On the basis of the failure mechanism of the tunnel, faults can be classified as **Active fault and Inactive fault**

Active fault

The active fault is generally defined as a fault that is expected to cause sub-surface deformation in the future. Earthquake excitation and fault displacement are the prime reasons for serious damage to fault-

crossing tunnels. Considering the different damage patterns observed in fault-crossing tunnels, and in order to clarify the mechanism causing seismic damage, the active faults that tunnel cross through are further divided into two types: Causative fault and displaced secondary fault.

$$\text{For normal fault, } \sigma_d = \sigma_1 - \sigma_3 = \frac{2(c - \mu(\sigma_L - P_w))}{\sqrt{\mu^2 + 1} + 1} \quad \text{Eq.(2.1)}$$

$$\text{For reverse fault, } \sigma_d = \sigma_1 - \sigma_3 = \frac{2(c + \mu(\sigma_L - P_w))}{\sqrt{\mu^2 + 1} - 1} \quad \text{Eq.(2.2)}$$

$$\text{For strike slip fault, } \sigma_d = \sigma_1 - \sigma_3 = \frac{2(c + \mu(\sigma_L - P_w))}{\sqrt{\mu^2 + 1}} \quad \text{Eq.(2.3)}$$

For causative fault, the displacement of fault is proportional to the magnitude of the earthquake. For displaced secondary fault, there is no direct relationship between the displacement of fault and the magnitude, so the damage patterns of the tunnel crosses displaced secondary fault might not be the same as that of the tunnel crossing causative fault

Inactive fault

Inactive fault does not cause dislocation in an earthquake, so the influence of fault on the tunnel is similar to fracture zone in an earthquake. Due to the existence of such a fault, tunnel structure on both sides of fault may suffer from shear action of fault as a result of the inconsistent movement of surrounding rock on both sides of the fault. Failure mechanism of the tunnel in inactive fault zone is the discrepant seismic response caused by different rock properties between fault and the surrounding better rock quality, while the seismic response is mainly related with specific rock parameters. (Zhang et. al., 2020)

The engineering behavior of the ground is dependent on strength and stiffness of the rock or soil, joints, faults. The main features which define rock wedges include faults, fractures, shear zones, bedding planes, joints, joint infilling, foliation (Byrne et al, 1995). shows seven main types of discontinuities which directly influence deformation of the rock mass. They are faults, joints, partings, cracks, fissures, bedding planes, shears and weak zones (Palmström,1995). These geological descriptions can influence engineering characteristics by controlling stress redistributions around the tunnel, influence the support requirements, overall rock mass strength, behavior, stability, loads. (Eberhardt, 2012).

It causes structural breaks and interruptions in the intact homogeneous rock mass which convert it into a combination of discrete wedges whose shape and size are defined by their boundary margins (Hack, 2006). The orientation of the discontinuities is represented using graphical projection or stereographic projections as shown in Strike is the direction in which a horizontal line can be drawn on a plane in relation to

geographic north. Dip is the angle of maximum slope of the beds of rock measured from the horizontal at any point

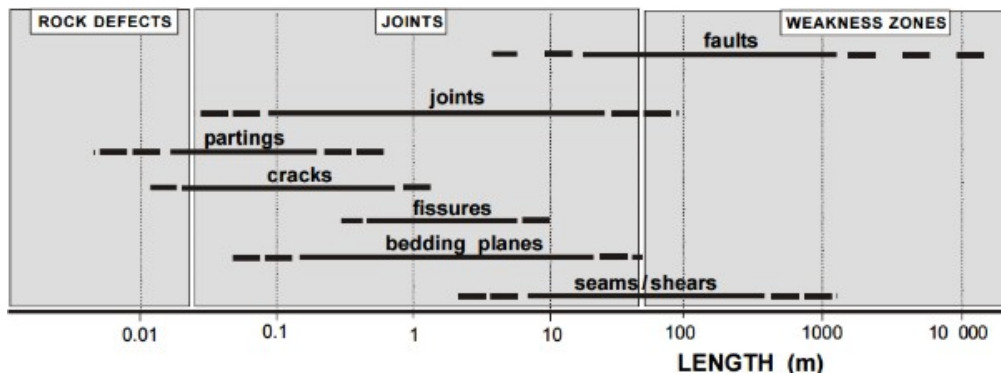


Figure 2-4 Main discontinuities influencing rock mass properties (Palmstrom, 1995)

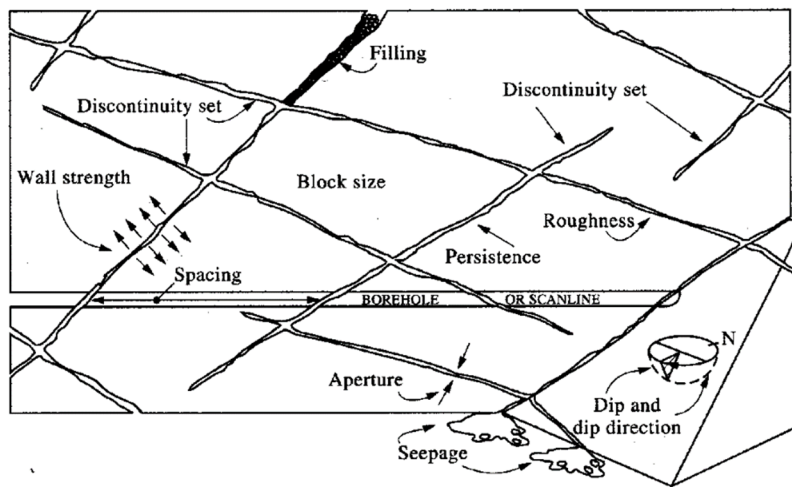


Figure 2-5 Rock Mass Characterization (Martin et al, 1999)

Earthquakes and Stress orientation in the Himalaya

The Himalaya is tectonically active region with number of earthquakes in the past century. Himalayan region is seismically active zone due to continuous movement of fault described in section 2.2 above. Many earthquakes of magnitude greater than 8 have occurred during the past century. 1897 AD earthquake of Magnitude 8.7 due to the rupture of fault in south of Himalaya beneath the Shillong plateau, 1905 AD Kangra earthquake of Magnitude 8.6, 1934 AD Bihar–Nepal earthquake of Magnitude 8.4, 1950 AD Assam earthquake of Magnitude 8.7 are the major earthquakes of magnitude greater than 8 (Feng, 2017). Similarly, an earthquake of magnitude 7.8 occurred in Gorkha on 25th April 2015 AD in the Himalayan Front. The location of various faults and its associated earthquake in Nepal in past century. Weak and fragile rocks, with regional and smaller structural features, resulting stress due to earthquake and fault movement have made the tunnelling difficult in the Himalaya. It has made the tunneling in the Himalaya a challenging task.

The tectonic stress distribution is shown in Figure 2-7. It shows that there is stress distribution due to normal faulting, strike-slip faulting, and thrust faulting. It has been observed that most of stress have been oriented form focal mechanism.

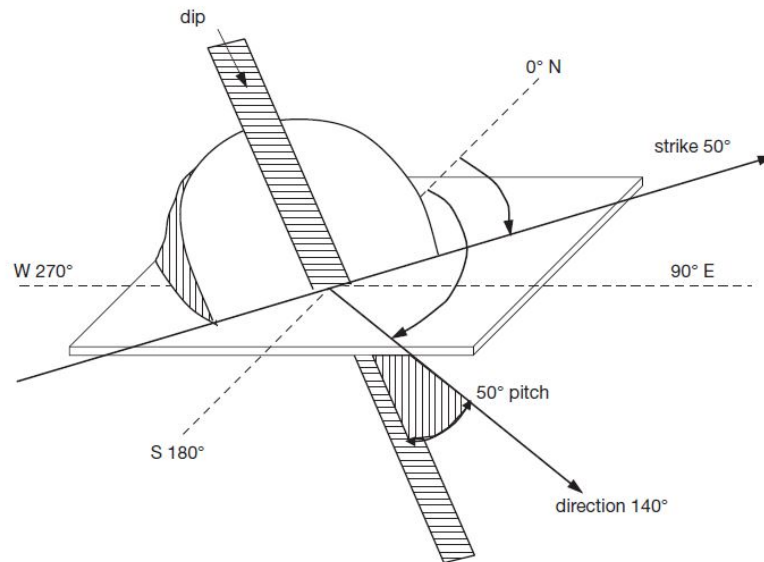


Figure 2-6 Definitions of dip and strike for a discontinuity plane (Chapman et.al., 2017)

The red data show the stress orientation due to normal faulting in which vertical stress (S_v) is greater than horizontal stress (S_{hmin}) and intermediate stress (S_{Hmax}) in the order of $S_v > S_{Hmax} > S_{hmin}$. Green data show strike-slip faulting in which intermediate stress (S_{Hmax}) is greater than vertical stress (S_v) and horizontal stress (S_{hmin}) in the order of $S_{Hmax} > S_v > S_{hmin}$. Purple data show thrust faulting regime in which intermediate (S_{Hmax}) stress is greater than horizontal stress (S_{hmin}) and vertical stress (S_v) in the order of $S_{Hmax} > S_{hmin} > S_v$. Hence, the orientation of maximum stress during tunnelling is site specific. The maximum stress can be either in vertical direction or in horizontal direction or in out of the plane of face of tunnel. It signifies the importance of measurement of field stress for the correct simulation of tunnel excavation and support installation.

Therefore, there should be accurate measurement of the principal stress. Methods such as pressuremeter and hydraulic jacking can be used for this purpose.

Pressuremeter

It is used as a loading test in boreholes with a defined diameter(d) to determine the deformation modulus and horizontal stress. The pressuremeter consists of a cylindrical pressure cell containing strain arms within

a cylindrical rubber membrane, which is pressed hydraulically against the borehole wall. The borehole walls are loaded and then unloaded cyclically causing the borehole walls to deform. The obtained deformation is measured by the strain arms, and estimation of the deformation modulus of the material is done (Chapman et.al., 2017). Figure 2-8 show apparatus of pressuremeter.

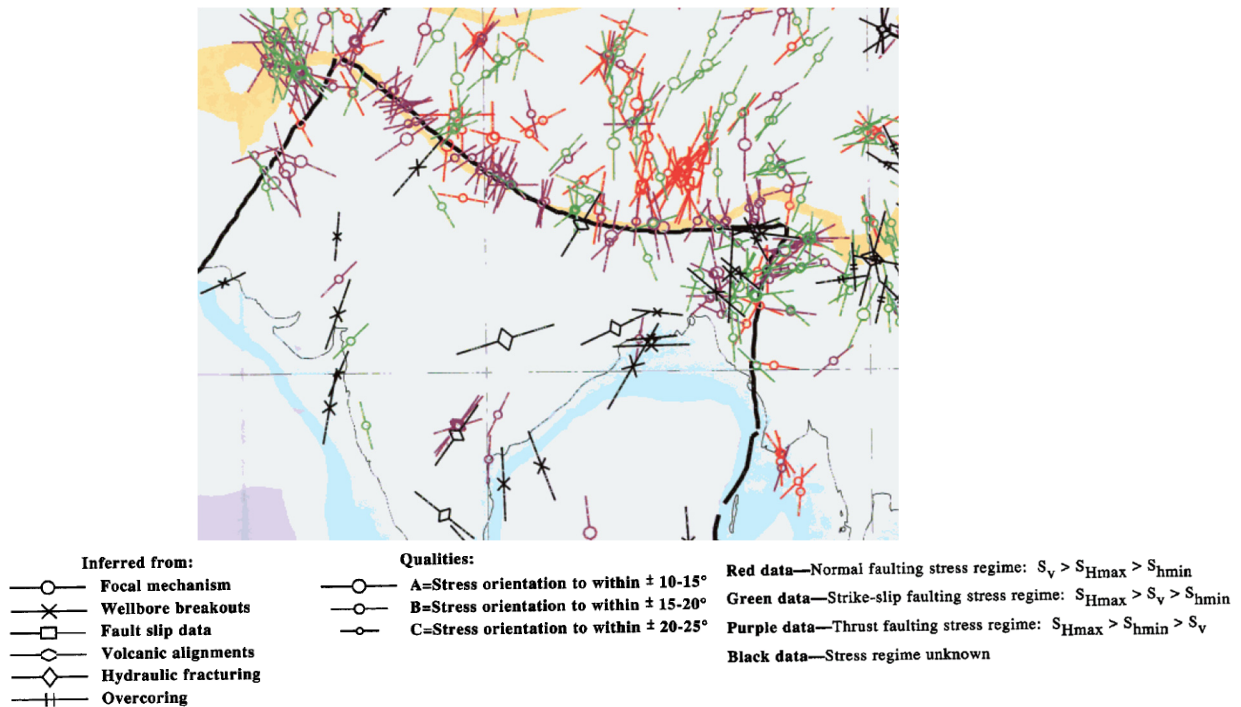


Figure 2-7 Maximum Horizontal Stress (Zoback,1992) S_v is vertical stress, S_{Hmax} is intermediate stress, S_{hmin} is horizontal stress.

In soft ground with faulted rock and weak rock, 1 m long and 74 mm diameter pressuremeter are lowered into a slightly oversized pre-bored hole, replacing the soil. It can operate up to pressures of approximately 4.5 MN/m^2 for measuring horizontal stress. For any tunnel construction it is important to determine the primary stresses, i.e. the stresses in the ground prior to construction of the tunnel. This will help the tunnel designer to estimate the likely stress redistribution and loading on the tunnel lining. Principal stresses are major stress which are concerned in tunnelling they are the largest and smallest possible stress where the shear stress is equal to zero. Primary stress distribution above and below the ground water table are show in Figure 2-9 and Figure 2-10.

The vertical principal stress can easily be determined by Eq.(2.4), i.e. $\sigma_v = \gamma H$. γ the unit weight of the rock mass, H is overburden depth. The horizontal principal stress is given by Eq.(2.5) , $\sigma_h = K_0 \gamma H$. The value of K_0 , the coefficient of lateral earth pressure at rest which vary in magnitude in different directions

K_0 can be calculated from Poisson's ratio by Eq.(2.8) and shown in Figure 2-9 . It is assumed that the principal stresses are initially acting vertically and horizontally (Chapman et.al., 2017).

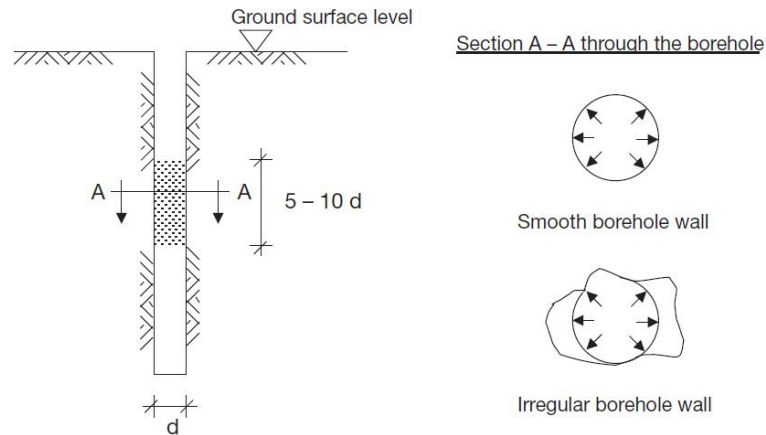


Figure 2-8 Pressuremeter apparatus (Chapman et.al., 2017).

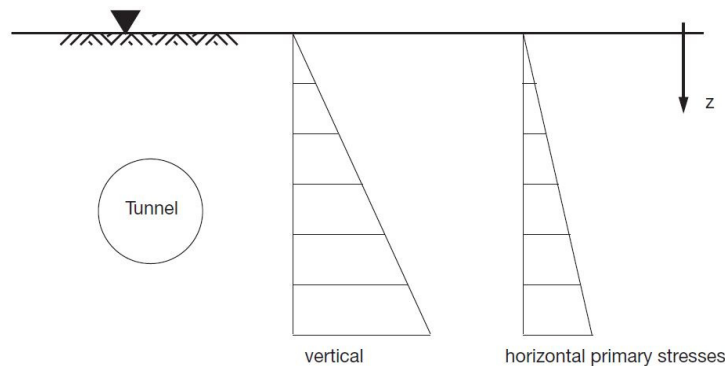


Figure 2-9 Primary stress distribution above the groundwater table (Chapman et.al., 2017)

The value of K_0 is determined empirically. ' μ ' is generally in the range 0 to 0.5, using Eq.(2.8) would lead to K_0 values in the range of 0 to 1.0. The realistic range of μ for the ground is between 0.2 to 0.35, which leads to K_0 values of between 0.25 and 0.54. This example calculation shows that K_0 values of greater than 1.0 are not possible with this equation and values of K_0 of greater than 0.54 are only fully covered if one uses a μ value, which is not necessarily realistic for the ground. This equation represents a simplified case and is based on the assumption of elasticity in the ground and is only valid in rare circumstances in underground construction. Also, the angle of internal friction, ϕ and K_0 are related as $K_0 = 1 - \sin\phi$. (Kim and Yoo, 2002).

To determine its value one needs to take into account the historical development of the earth, and hence the rock. Shrestha and Panthi (2014) proposed Eq.(2.6) in case of Nepal himalaya, σ_{tectonic} is horizontal

tectonic stress. Shrestha and Panthi (2014) give fairly good grounds to assume that the magnitude of tectonic horizontal stress in the faulted rock mass is in the range of 4 ± 0.5 MPa .However, it is very difficult to measure the magniude and direction of tectonic stress as it constantly increases with the tectonic movement due to faults.

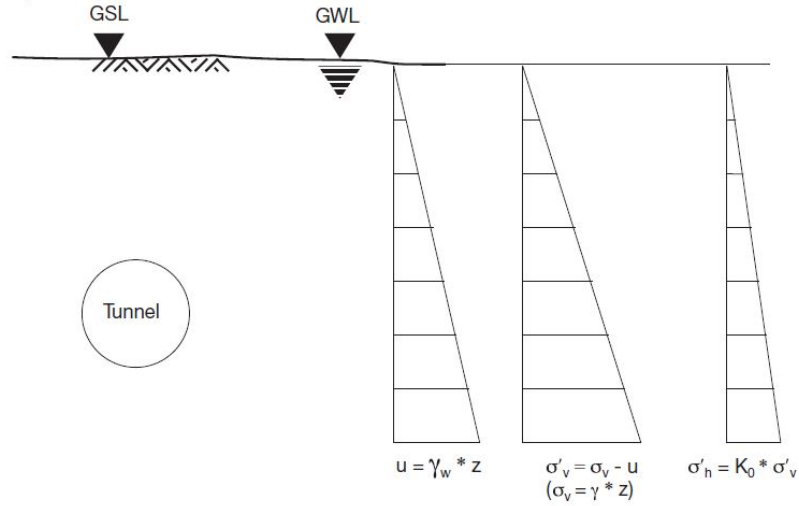


Figure 2-10 Primary stress distribution below the groundwater table (Chapman et al., 2017)

Similarly, Chhushyabaga et al., 2020 suggested Eq.(2.7) by Jaeger and Cook, 1971 to obtain the tectonic stress in faulted rock mass. Eq.(2.7) is obtained from 2D Faulting theory which assumes that the failure is only a function of the difference between the principal stresses σ_1 and σ_3 (Zoback,1992). The principal stresses in Nepal Himalaya.25th April, 2015 AD Gorkha earthquake event increased the Coulomb stress changes by 0.06 MPa at 16 km depth below the site of the 12 May event. (Mandal, 2018). Hence all the parameters mention abouve should be considered to determine the principal stress in the faulted rock mass in Nepal Himalaya.

$$\sigma_v = \gamma H \quad \text{Eq.(2.4)}$$

$$\sigma_h = k_0 \sigma_v \quad \text{Eq.(2.5)}$$

$$\sigma_h = k_0 \sigma_v + \sigma_{\text{tectonic}} \quad \text{Eq.(2.6)}$$

$$\frac{\sigma_1}{\sigma_3} = ((\mu^2 + 1)^{\frac{1}{2}} + \mu)^2 \quad \text{Eq.(2.7)}$$

$$k_0 = \frac{\mu}{1 - \mu} \quad \text{Eq.(2.8)}$$

Hydraulic fracturing

In order to determine the principal stress a practical method Hydraulic fracturing tests can be used. The following procedure is used to determine the smallest lateral pressure and its direction in a borehole.

Reasonable length of borehole above and below the location of the measurement without crack is maintained. This section is then sealed with packers and pressurized with air or water until there is a sudden drop in measured pressure. The maximum pressure is noted and the system is closed. The pressure drop develops when the ground fractures and the liquid flows into the ground so the noted pressure is adjusted according to it. Two main fractures occur in the direction of the largest principal stress, σ_1 .

Figure 2-11 shows example of the hydraulic fracturing test (Chapman et.al., 2017) . In this figure, x and y are the principal stress directions and σ_1 and σ_2 are the principal stresses. In this example, the direction of the largest deformation gives the smallest principal stress direction and thus the smallest value of K_0 . The largest value of K_0 in this example is found in the y-direction, but cannot be determined in this experiment. The value of K_0 determined from this experiment is still only an estimation and it is therefore advisable to do design calculations for a range of K_0 values.

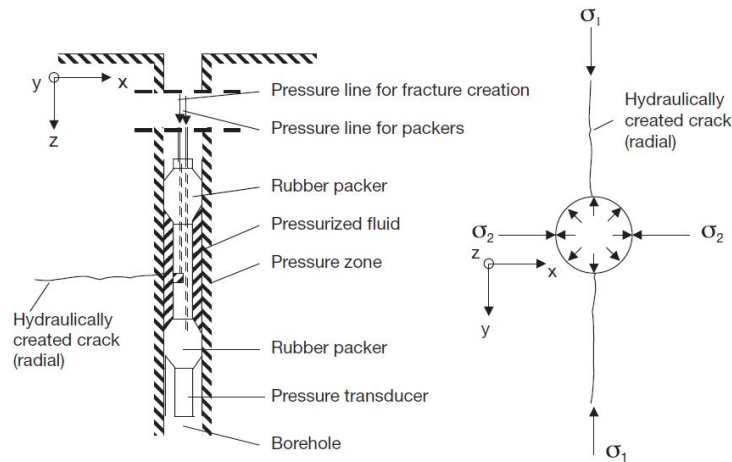


Figure 2-11 Hydraulic fracturing tests (Chapman et.al., 2017).

2.4 Tunnel Support Design in Fault

The tunnel support design in the faulted rock mass is done to cover predicted the rupture or displacement of rock mass due to fault. It is a three-dimensional problem with interactions of the rock mass and the tunnel support. This interaction is dependent on the location, i.e., relative to the tunnel face and dependent on time, i.e., application of tunnel support in the rock mass.

Generally, tunnel is driven through the fault with enlarged cross section (Figure 2-12). A double lining is installed which is filled by a porous material or foam concrete in between the lining. The gap between the outer and inner linings provides a clearance profile when there is fault rupture . This solution is effective when a fault rupture concentrated to short length of tunnel i.e., in a few meters is expected as excavation

cost increases with increase in the length of tunnel (Russo et. al, 2002). Some of the methods which have been used in tunnel support design are as follows.

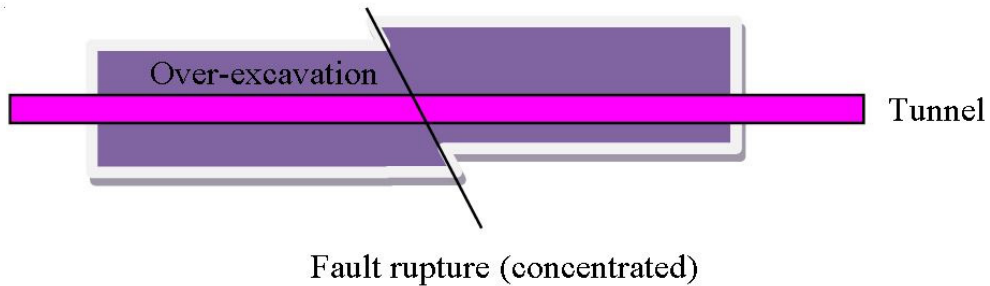


Figure 2-12 Over excavation

2.4.1 Articulated design approach

Articulated design approach consists of using lining segments in reinforced concrete lining as independent sections across the fault over a certain length beside the fault (Figure 2-13). It helps to concentrate the movement of the fault rupture at the joints linking the segments to accommodate the movement on a certain distance. This solution has advantage of concentrating potential damages at elements only at lining located at the fault without uncontrolled propagation to other locations. The maximum length of element depends on width of the cross section, expected movement of the fault, compressibility of the surrounding soil (Russo et. al, 2002). Articulated design has been used in twin Bolu tunnel, Turkey (Russo et. al, 2002).

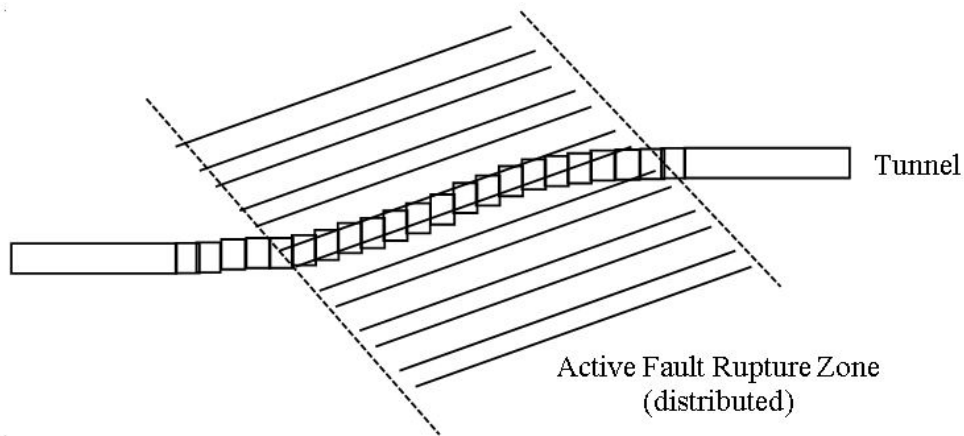


Figure 2-13 Articulated Design

Bolu Tunnel

Bolu tunnel is a twin motorway tunnel of about 3 km length in Turkey. The Bakacak Fault encountered in this tunnel has been recognized as active (Figure 2-15). The tunnel was heavily damaged by the 1999

Düzce earthquake, whose epicenter was in proximity to the construction site. About 350 m collapsed in both tubes with major damages to linings and invert. When the Bakacak fault was recognized as active the shape and type of the cross section adopted was already defined. Consequently, the articulated design solution has been adopted to maintain the shape of the static design of the tunnel (Russo et. al.,2002).

The assumptions made in this method are as follows in this method are as follows:

- Following to a fault rupture, the tunnel will act longitudinally as an embedded beam whose extremities are displaced by the lateral offset of the fault. The fault will rupture with higher probability by a uniformly distributed rupture across the fault boundaries.
- Shear strain (γ) in the fault rock mass is assumed as the ratio between expected offset and width of the fault at tunnel level. Due to rupture, tunnel will be sheared and bent as an embedded beam (Figure 2-14). Once the shear resistance of joints is attained, each segment will be free to move independently according to external loads.
- A displacement is gradually applied to extremities of the tunnel linings.

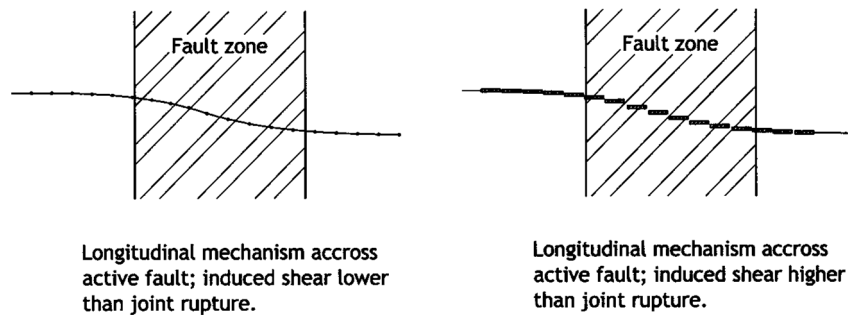


Figure 2-14 Tunnel behavior across fault boundaries (Russo et. al.,2002)

The segments geometry was defined by considering a ratio between length and width of the tunnel segment equal to 1/3 resulting in an element length of about 5 m. This geometry allowed to keep the lateral increment of load on the single crown segment below an acceptable threshold value. For practical reasons the length of the segments was reduced to 4.4 m and the joint gap width was 50 cm at invert. This allowed to maintain modular reinforcement cage Figure 2-16.

Across the fault zone support measures for the rock support was adopted: which consisted of an 80 cm intermediate concrete (40 N/mm^2) with the primary lining and the inner lining based on articulated design (Figure 2-13). The reinforcement bars have been placed only in the inner (final) lining and at invert, while the shotcrete and intermediate linings have been fiber reinforced (Figure 2-16). The reinforcement design primary aim was to provide a high ductility to the lining. This was gained firstly by introducing stirrups at shear keeping the spacing below 30 cm, and also by introducing a light dosage of steel fibers in the concrete

mix, or applying an equivalent double mesh layer. These measures were applied within the fault and up to a distance of 30 to 40 m from the fault borders (Russo et. al.,2002).

The joints at 4.20 m spacing had been detailed to prevent soil squeezing between the segments and to bridge the static soil pressure to the surrounding elements. 0.40 m thick fiber reinforced shotcrete beam has been applied to bridge the gap and to provide ring closure of the joint at the invert. At crown the regular shotcrete preliminary lining (40 cm thick) has been assessed sufficient. Ytong blocks closing the invert segment have been used. The advantages of the Ytong blocks are the economy, their compressibility and the fact that they can be easily assembled to create slabs. The 50 cm wide joint is filled by two layers Ytong blocks A waterproofing membrane is installed below the Ytong blocks slabs and the invert (Russo et. al.,2002).

At crown three levels linings are installed: a shotcrete lining, an intermediary lining of poured concrete and a reinforced final lining. The waterproofing membrane bridges the seismic joint gap between intermediary and final lining. The joint opening in the final lining has been enlarged to 70 cm, the gap will be covered for ventilation purposes and fire resistance by a steel plate.

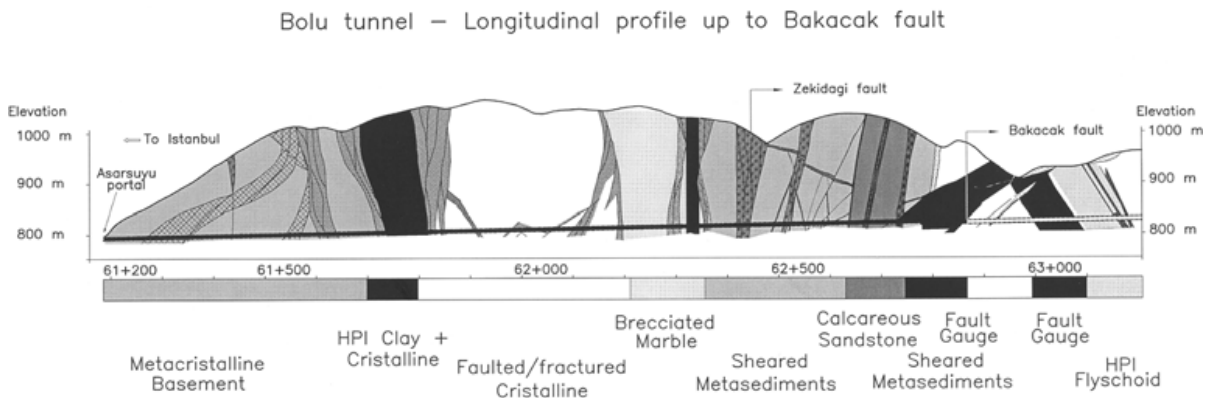


Figure 2-15 Portion of the longitudinal profile of the Bolu Tunnel with active faults (Russo et. al.,2002)

2.4.2 Analytical Method

Convergence Confinement Method (Carranza-Torres and Fairhurst, 2000) is tunnel design approach which is basically a two-dimensional plane strain model of a hole in an infinite pre-stressed slab. The effect of the third dimension i.e., distance to tunnel face is introduced by successive release of an internal pressure, which corresponds to the primary stress at the starting point. Convergence confinement method can be applied to study tunnel behavior along the different stages of excavation. The study of tunnel behavior allows the definition of different solutions to the support and excavation types needed to a safe tunnelling construction. The details of CCM are included in Annex A.



Figure 2-16 Reinforcement details in lining at side wall and at invert (Russo et al.,2002)

There are closed mathematical solutions for elastic and elasto-plastic material and isotropic stress conditions. The displacement response of the tunnel perimeter versus the internal stress is called Ground Reaction Curve (GRC). In the case of a supported tunnel the load release on the rock mass is partially absorbed by yielding of the rock and partially transferred to the support. The load transfer from the rock mass into the support is represented by the Support Characteristic Curve (SCC). The tunnel deformation behavior ahead and behind of the face is represented by the longitudinal displacement profile (LDP).

This method has been used in design of tunnel support in faulted rock mass in Yacambú-Quibor tunnel in Venezuela (Guevara ,2004). This analysis involves new construction within the central portion of a 25 km tunnel, 5.2 m in diameter, in highly variable metamorphic rock at depths of up to 1200 m below surface (Figure 2-18). The design problem is highly deformed graphitic phyllite. The deformation in the rock mass is the result of the tectonic processes inherent in the Andes Mountains and a large regional fault .The fault passes through the tunnel as seen in Figure 2-18. (Guevara ,2004)

This analysis with CCM is done in section of 1150 m overburden. The in-situ stresses at depth are assumed to be approximately equal (30 MPa) in all directions as a result of the low shear resistance due to the fact that the tectonic history of the rock mass has reduced its properties to their residual values.

The mechanism of CCM method is explained as follows. The example shows an installation of the support 1.5 m behind the tunnel face. Figure 2-17 shows a typical construction and interaction between the ground reaction curve and the support characteristic curve. The internal pressure corresponding to the GRC construction is decreasing with inward displacement of the tunnel beginning before excavation takes place. At the tunnel face i.e., dashed line the displacement is u_0 . After setting the support into place it gradually starts to receive load from the continuously deforming wall of the tunnel. This will be happening up to the point where, either equilibrium is reached and the tunnel ceases its short-term radial displacement, or the

support maximum pressure is reached. If this last condition is met, lining materials yield. To avoid excessive yield of the support, either maximum support pressure can be increased, or more displacement allowed to take place. This mechanism has been used to yield the excess displacement in circular steel sets, shotcrete and reinforced shotcrete with two sliding joints in the faulted rock mass Yacambú-Quibor tunnel in Venezuela.

Hoek, 1998 developed the chart to provide the combination of tunnel support based on the support pressure obtained. Figure 2-21 shows maximum support capacities for different support system installed in a circular tunnel. The circular steel sets of Circular steel arches (W 6 X 20), 20 cm of shotcrete, final 60 cm of reinforced shotcrete section have been used based on Figure 2-21 for obtained support pressure of 30 MPa. In order to yield the displacement due to faulted rock mass, two sliding joints have been used. Figure 2-20 shows the use of Yielding support in squeezing ground condition in the faulted rock mass in Yacambú-Quibor tunnel in Venezuela (Hoek, 1998).

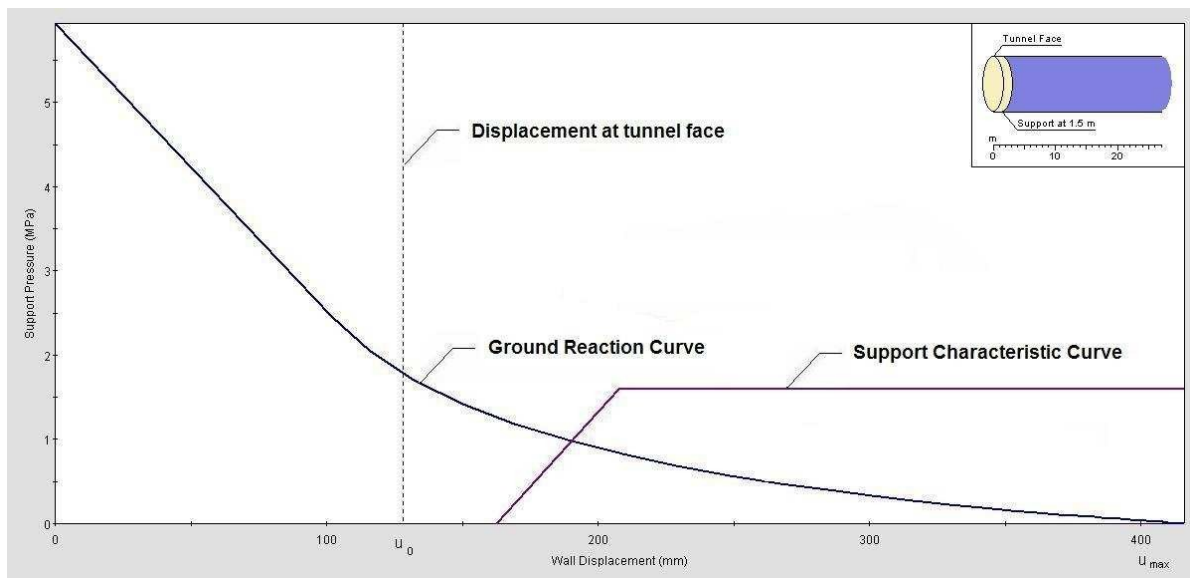


Figure 2-17 Ground Reaction Curve and Support Characteristic Curve. (Rocscience, 2005).

Dashed support load curve in Figure 2-19 represents delayed loading due to sliding joint which has helped in reducing the deformation in the tunnel due to faulted rock mass and has made the design safe. The details of Rock Mass Classification are included in Annex B in this report.

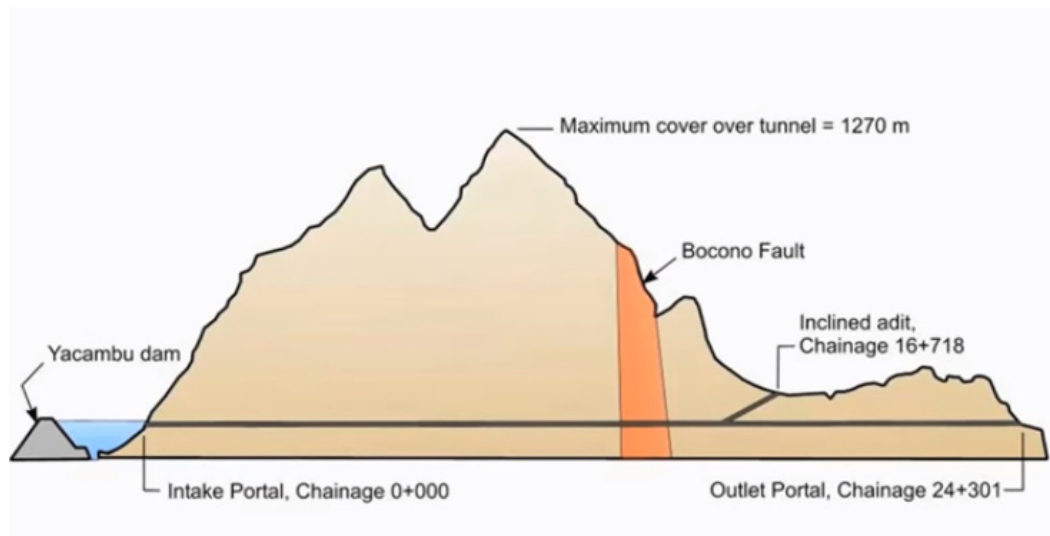


Figure 2-18 Longitudinal topographical profile along tunnel alignment (Hoek et. al.,2008)

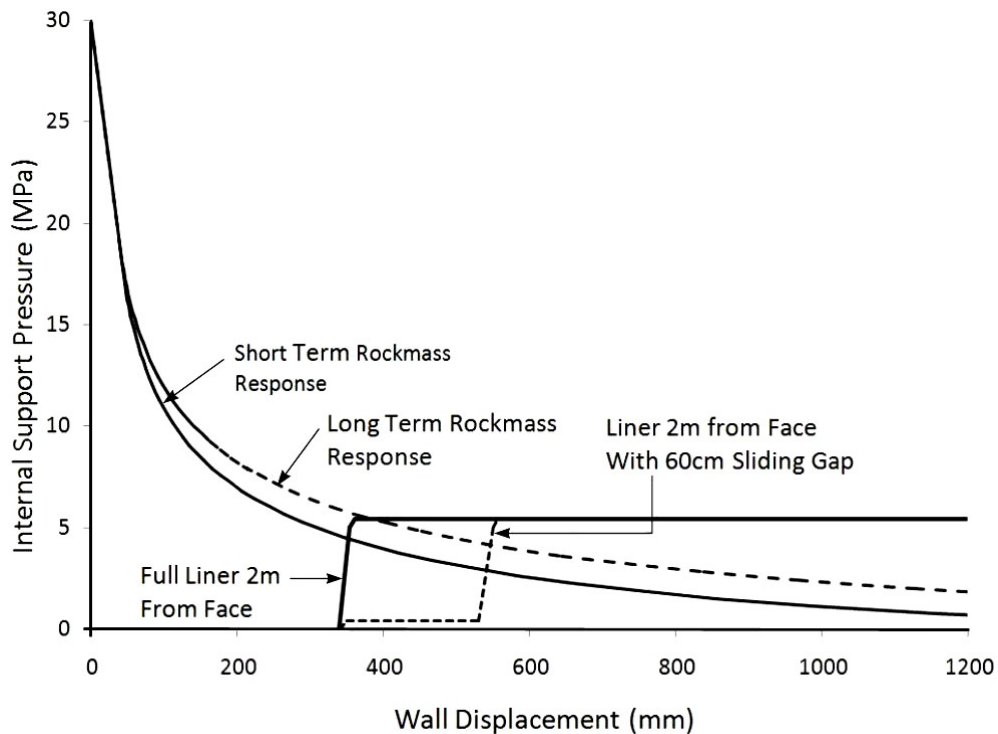


Figure 2-19 Convergence confinement analysis for sliding joint in Yacambú-Quibor tunnel in the Northern Andes in Venezuela (Hoek et. al.,2008)

2.4.3 Empirical Method

Marinos et. al. 2007; Marinos et al., 2011; Marinos, 2014; Marinos, 2019; developed a new GSI classification chart for heterogeneous rock masses such as flysch which is basically sheared or fractured rock mass to characterize and provide the temporary support or immediate support during the construction

of tunnel and underground structure. Faulted and sheared rock mass causes problems or challenges in design and construction of tunnel and underground structure. The overall rock mass is heterogeneous, anisotropic and influenced by extensional faulting. The structural deformation due to tectonism decreases the quality of the rock mass. Such tectonically effected rock mass are classified into 11 rock mass types (I to XI) on the basis of the quality of the rock mass due to tectonism (Figure 2-22). The classification has been done by developing a new Geological Strength Index (GSI) chart. Figure 2-23 shows the new GSI classification chart for heterogenous rock masses (Marinos et al., 2007). On the basis of the classified rock masses, immediate support type and excavation step has been defined, which is given in a chart shown in Figure 2-24. Figure 2-24 shows the general directions for the immediate support measures for tectonically effected rock masses.

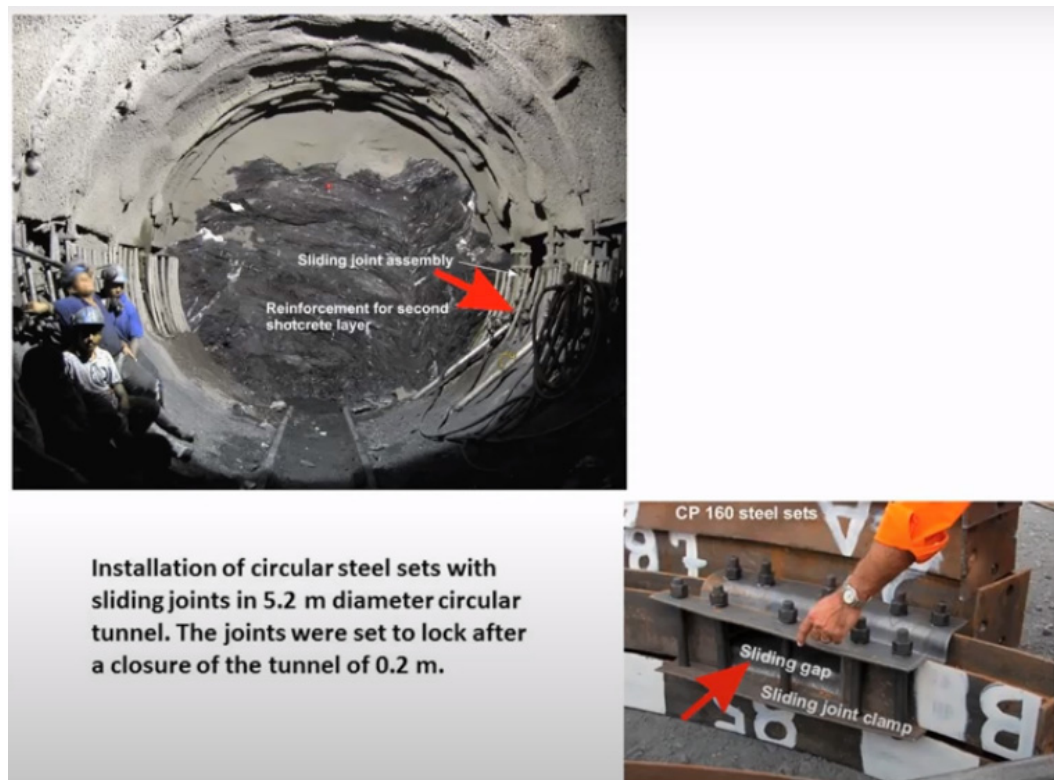
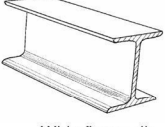
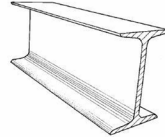
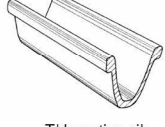
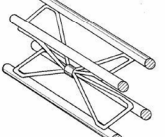
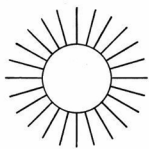
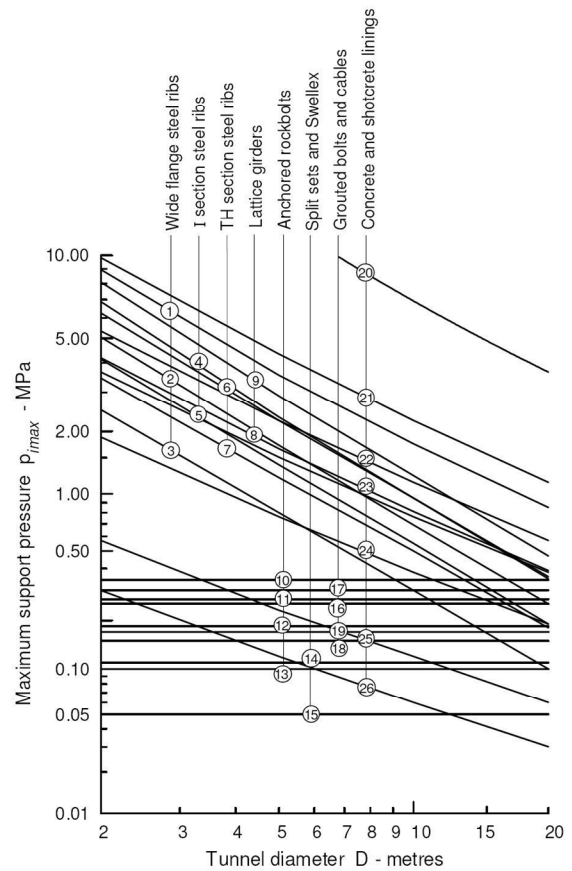


Figure 2-20 Sliding joint Assembly in Yacambú-Quibor tunnel in the Northern Andes in Venezuela (Hoek et. al.,2008)

Support type	Flange width - mm	Section depth - mm	Weight - kg/m	Curve number	Maximum support pressure $p_{i\max}$ (MPa) for a tunnel of diameter D (metres) and a set spacing of s (metres)
 Wide flange rib	305	305	97	1	$p_{i\max} = 19.9D^{-1.23}/s$
	203	203	67	2	$p_{i\max} = 13.2D^{-1.3}/s$
	150	150	32	3	$p_{i\max} = 7.0D^{-1.4}/s$
 I section rib	203	254	82	4	$p_{i\max} = 17.6D^{-1.29}/s$
	152	203	52	5	$p_{i\max} = 11.1D^{-1.33}/s$
 TH section rib	171	138	38	6	$p_{i\max} = 15.5D^{-1.24}/s$
	124	108	21	7	$p_{i\max} = 8.8D^{-1.27}/s$
 3 bar lattice girder	220	190	19	8	$p_{i\max} = 8.6D^{-1.03}/s$
	140	130	18		
 4 bar lattice girder	220	280	29	9	$p_{i\max} = 18.3D^{-1.02}/s$
	140	200	26		
 Rockbolts or cables spaced on a grid of $s \times s$ metres	34 mm rockbolt			10	$p_{i\max} = 0.354/s^2$
	25 mm rockbolt			11	$p_{i\max} = 0.267/s^2$
	19 mm rockbolt			12	$p_{i\max} = 0.184/s^2$
	17 mm rockbolt			13	$p_{i\max} = 0.10/s^2$
	SS39 Split set			14	$p_{i\max} = 0.05/s^2$
	EXX Swellex			15	$p_{i\max} = 0.11/s^2$
	20mm rebar			16	$p_{i\max} = 0.17/s^2$
	22mm fibreglass			17	$p_{i\max} = 0.26/s^2$
	Plain cable			18	$p_{i\max} = 0.15/s^2$
	Birdcage cable			19	$p_{i\max} = 0.30/s^2$

Support type	Thickness - mm	Age - days	UCS - MPa	Curve number	Maximum support pressure $p_{i\max}$ (MPa) for a tunnel of diameter D (metres)
 Concrete or shotcrete lining	1m	28	35	20	$p_{i\max} = 57.8D^{-0.92}$
	300	28	35	21	$p_{i\max} = 19.1D^{-0.92}$
	150	28	35	22	$p_{i\max} = 10.6D^{-0.97}$
	100	28	35	23	$p_{i\max} = 7.3D^{-0.98}$
	50	28	35	24	$p_{i\max} = 3.8D^{-0.99}$
	50	3	11	25	$p_{i\max} = 1.1D^{-0.97}$
	50	0.5	6	26	$p_{i\max} = 0.6D^{-1.0}$



Source : Hoek (1999)

Figure 2-21 Maximum support capacities for different support system installed in circular tunnel (Hoek, 1998)

ROCKMASS TYPE	STRUCTURE	ROCKMASS TYPE	STRUCTURE	ROCKMASS TYPE	STRUCTURE
TYPE I. Undisturbed, with thick to medium thickness sandstone beds with sporadic thin films of siltstone.		TYPE II. Undisturbed massive siltstone with sporadic thin interlayers of sandstones		TYPE III. Moderately disturbed sandstones with thin films of interlayers siltstone	
TYPE IV. Moderately disturbed rockmass with sandstone and siltstone similar amount		TYPE V. Moderately disturbed siltstones with sandstone interlayers		TYPE VI. Moderately disturbed siltstones with sparse sandstone interlayers	
TYPE VII. Strongly disturbed, folded rockmass that retains its structure, with sandstone and siltstone in similar extend		TYPE VIII. Strongly disturbed, folded rockmass, with siltstones and sandstone interlayers. The structure is retained and deformation - shearing is not strong		TYPE IX. Disintegrated rockmass	
TYPE X. Tectonically deformed intensively folded/ faulted siltstone or clay shale with broken and deformed sandstone layers forming an almost chaotic structure		TYPE XI. Tectonically strongly sheared siltstone or clayey shale forming a chaotic structure with pockets of clay.			

Figure 2-22 Rock mass types in tectonically disturbed heterogeneous formations such as flysch (Marinos, 2014)

ROCKMASS TYPE	STRUCTURE	TEMPORARY SUPPORT RECOMMENDATIONS
Type I. Undisturbed, with thick to medium thickness sandstone beds with sporadic thin films of siltstone.		<ul style="list-style-type: none"> Excavation step: $\geq 3.0\text{m}$ Installation of split-set bolts (e.g. Swellex) to support the unstable wedges (Sparse installation is not recommended due to the large dimensions of typical transportation tunnels)
Type II. Undisturbed massive siltstone with sporadic thin interlayers of sandstones.		<ul style="list-style-type: none"> Excavation step: 2-3m Bolts installation to support the unstable wedges and control the deformation in case of high overburden Light steel sets in case of weathered rockmass, depending on excavation depth
Type III. Moderately disturbed sandstones with thin of siltstone interlayers.		<ul style="list-style-type: none"> Excavation step: 1.5-2m Installation of split-set bolts (e.g. Swellex type) for the support of unstable wedges Light steel sets in case of loose structure
Type IV. Moderately disturbed rock mass with sandstone and siltstone similar amounts.		<ul style="list-style-type: none"> Excavation step: 1.5-2m Systematic bolt installation to support the unstable wedges, prevent the rockmass loosening and control the deformation in case of high overburden Spiles and light steel sets in case of loose structure and weathered rockmass to avoid local chimney type failures
Type V. Moderately disturbed siltstones with thin sandstone interlayers.		<ul style="list-style-type: none"> Excavation step: 1.5-2m Systematic bolt installation to support the unstable wedges, prevent rockmass loosening and control the deformation under high overburden Light steel sets to increase the rigidity and strength of the support shell Spiles in case of loose and weathered structures to avoid chimney type failures Face retaining measures: Depending on excavation depth (fibreglass nails)
Type VI. Moderately disturbed siltstones with sparse sandstone interlayers.		<ul style="list-style-type: none"> Excavation step: 1.5-2m Dense bolt pattern to control the deformation and prevent rockmass loosening Steel sets to increase the rigidity and strength of the support shell Spiles to stabilise loose and weathered structures and avoid chimney type failures Face retaining measures: Depending on excavation depth (fibreglass nails) Depending on bedding orientation, anisotropic stress induced deformations may be observed
Type VII. Strongly disturbed, folded rock mass that retains its structure, with sandstone and siltstone in similar extent.		<ul style="list-style-type: none"> Excavation step: 1.5-2m Dense bolt pattern to control of deformation and rockmass loosening prevention Steel sets to increase the rigidity and strength of the support shell Face retaining measures: Depending on excavation depth (fibreglass nails or/and forepolling)
Type VIII. Strongly disturbed, folded rock mass with siltstones and sandstone interlayers. The structure is retained and deformation – shearing is not strong.		<ul style="list-style-type: none"> Excavation step usually small: 1-1.5m Dense bolt pattern to control the deformation Steel sets to increase the rigidity and strength of the support shell Face retaining measures: Depending on excavation depth (fibreglass nails or/and forepolling) Permanent and probably temporary invert to improve the shell rigidity.
Type IX. Disintegrated rockmass that can be found in wide zones of faults or/and of high weathering.		<ul style="list-style-type: none"> Excavation step usually small (~1m) Face buttress Dense pattern of self-drilling anchors. Grouting to locally increase the rockmass cohesion Steel sets to increase the rigidity and strength of the support shell Spiles to presupport tunnel roof and prevent the development of chimney type failure Alternatively in case of completely cohesionless rockmass grouting around tunnel section is proposed (e.g. through perforated forepolls)
Type X. Tectonically deformed intensively folded/faulted siltstone or clay shale with broken and deformed sandstone layers forming an almost chaotic structure.		<ul style="list-style-type: none"> Small excavation step (~1m) Dense bolt pattern to control the deformation Steel sets in order to increase the rigidity and strength of the support shell Face retaining measures: Depending on excavation depth (fibreglass nails or/and forepolling) Permanent and temporary invert to improve the shell rigidity
Type XI. Tectonically strongly sheared siltstone or clayey shale forming a chaotic structure with pockets of clay.		<ul style="list-style-type: none"> Small excavation step (~1m) Dense bolt pattern and steel sets to increase the rigidity and strength of the support shell Face retaining measures: Depending on excavation depth (fibreglass nails or/and forepolling) Permanent and temporary invert to improve the shell rigidity In case of very high overburden (>100-150m) the construction of a flexible support system using yielding elements may be required.
<p>Remarks:</p> <ul style="list-style-type: none"> The excavation is referred to Top heading and Bench method. Full face excavation in weak rockmasses imposes strong face retaining measures and small distance between temporary support and final lining. Shotcrete is not referred in the recommendations due to its wide application. More specifically, when shotcrete is used to avoid rockmass loosening and to ensure the personnel safety, its thickness is generally small and it is determined according to experience and evaluation of the magnitude of possible wedge failure. In stress induced phenomena due to the combination of weak rockmass and high excavation depth or/and swelling phenomena, shotcrete should be analysed as a structural element and the requisite thickness and reinforcement is determined through numerical analyses. The excavation step will be determined according to: (a) the anticipated size of wedges in the case of competent undisturbed rockmasses (b) the size of the wedges and the structure loosening prevention, in the case of disturbed rockmasses with no deformation problems (c) the prevention of structure loosening and decrease of deformation, in the case of weak rock masses where significant deformation is anticipated. However, the installation of spiles allows the increase of the excavation step. Drainage holes are proposed in case of permeable sandstone beds and relief holes in case of trapped, low permeable, groundwater zones under the water table. Special support requirements should be considered in case of swelling rockmasses (e.g. possible in type VI, VIII, X, XI). 		

Figure 2-24 General directions for the immediate support measures for every flysch type (Marinos et al., 2011).

2.5 Numerical Analysis

Numerical analysis is one of the modern analysis approaches to simulate the tunneling process. This approach helps in realistic simulation of excavation and construction of tunnel and underground structures. It helps us to understand mechanical nature, interaction of complicated system between tunnel and surrounding geology. Nature of the failure mode during the tunneling and measures to prevent the failure or design of suitable support can be easily developed.

In the context of the tunnel in the faulted rock mass, the extent of the behavior of the tunnel opening should be fully understood, i.e., the maximum stress and displacement during the tunneling cycle. Generally, tunnels reach their maximum displacement during at the excavation distance of three times the diameter of the tunnel from the face of the tunnel.

In this section the methodology of numerical modelling of tunnel in faulted rock mass has been studied. Beam spring models, finite element methods, and finite difference methods, have been used for numerical modelling in the faulted rock mass. Jeon et al., 2004 used scaled model test and numerical analysis FLAC2D to show that deformation and plastic region increases when the fault distance to the tunnel decreases. They showed deformation in crown of the tunnel is more when fault is located above the crown than that of side of the wall. Hao and Azzam, 2005 used UDEC numerical solution for evaluating the effects of fault dips, fault location, fault shear strength and insitu stress state on the behaviour of rock mass failure and deformation around the large scale underground openings. With increasing value of frictional angle, magnitudes of rock mass plastic zones, displacement, asymmetrical phenomenon can be reduced. There is positive correlation between displacement and shear strain in the tunnel to thickness of fault (Childs et. al., 2009).

Similarly, Shahidi & Vafaeian, 2005 analysed longitudinal displacement profile of Koohrang-III tunnel in the active faulted zone and design the flexible lining and joints. Caulfield et al, 2005 used innovative seismic design measures for the retrofit of the claremont tunnel. The retrofit project involves construction of a new by pass tunnel through the Hayward Fault zone using systematic contact grouting, localized structural repair of the existing concrete liner, oversized tunnel cross section, backfill concrete side drifts, seismic isolation of an internal structural pipe, and shear fuses in the final lining.

Gregor et al, 2007 analysed and designed underground structures in FLAC 3D model crossing an active fault in Coronado, California using Precast Concrete Tunnel Lining System with circumferential joint opening control. Lanzano et al., 2008 collected case studies of earthquake effected Tunnels under seismic loading to highlight and classify the damages in groups, find out the causes of the damage and improve the performance based seismic design of tunnel.

2D circular model of reinforced concrete has been studied by Dalgıç, 2002 to show earthquake, fault geology, structural properties are influential parameters when tunnel is passing through an active fault. Seismic impacts on tunnel are ground shaking and ground failure such as liquefaction, slope instability, fault displacements. During fault rupture large displacement or strains can cause spalling and closure of tunnel structure. A collapse within the clay zone in Bolu tunnels in Turkey was observed by near-fault seismic intensity or local ground instability due to 1999 Duzce Earthquake, Turkey (Dalgıç, 2002). So, design of tunnel structure should be done for small predicted displacements and account for the potential damages.

Special consideration should be given in the designed of tunnel in the vicinity of fault. Desai et al., 1991 used flexible joints between single tunnel elements to accommodate differential movements and to keep leakage at a minimum for the Los Angeles water tunnels crossing active faults. Similarly, system of two row steel wire mesh, lattice girder, umbrella arch, shotcrete, facebolts, system of rock bolts were proposed in Izmir Metro Tunnel, Western Turkey (Kun & Onargan, 2013). The support system was proposed with numerical analysis in commercially available software RS2.

Rock mass properties used in the continuum modelling are determined using Geological Strength Index (GSI) and Hoek Brown Failure Criterion. The parameters of intact rock such as compressive strength, poisons ratio, modulus of elasticity and rock mass parameters such as joint number, spacing, orientation, ground water conditions are used in determination of rock mass properties. Hoek-Brown envelope can be linearized into Mohr-Coulomb over appropriate stress range in insitu stress conditions. It has been emphasized that numerical modelling of tunnel in faulted rock mass can be done in commercially available software i.e., RS2 (Rocscience).

Kun & Onargan, 2013 modelled influence of fault in Izmir Metro Tunnel of Turkey in RS2 in two dimensions (Figure 2-25). Effects of tunneling on the building and other surface structures built in the influence zone of the tunnel and fault were numerically investigated. In this study, rock mass around the tunnel was simulated by finite element, rock mass in immediate and far field of excavation face was simulated by boundry elements with elasto plastic behaviours (Figure 2-25). Mohr-Colomb failure criteria was used as the failure criteria for the rock mass. The boundry conditions have been restrained in both directions in bottom boundry. Top boundry have been free to move . Similarly left and right boundry have been restrained in X-directions and free to move in Y-directions. Youngs modulus, Poissons ratio, frictional angle, cohesion are the engineering properties of the rock formations in and around the fault zone. Pressure applied by the buildings on the tunnel route was incorporated by assuming surcharge load of 6-storey building of 0.01 MN/m^2 .

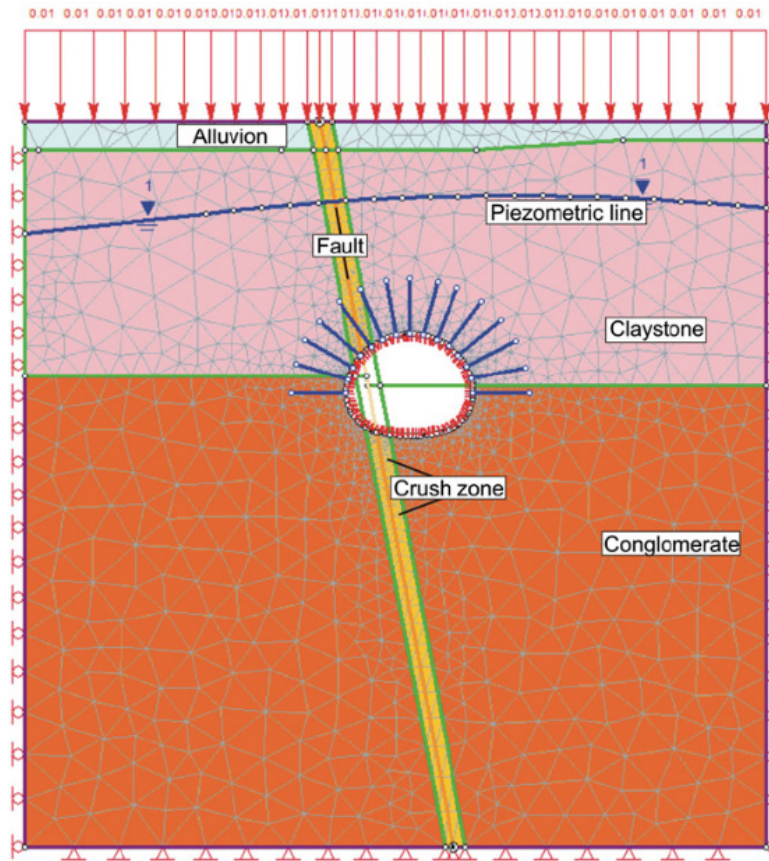


Figure 2-25 Shallow Izmir Metro Tunnel of Turkey in RS2 (Kun and Onargan, 2013)

They have validated their work by comparing the obtained deformations from the modelling with the measured deformations in the site. Subsidence values were obtained as 18 mm and 19 mm from numerical modelling and field measurement respectively. The subsidence deformation of the superstructure from the model was obtained with a variation of 5 percent from measurement for tunnel geometry 1. Similarly, convergence values were obtained as 12 mm and 11 mm from numerical modelling and field measurements respectively. The convergence of the tunnel in the model was obtained with a variation of 9 percent from the field measurement for tunnel geometry 2.

Similarly, Chhushyabaga et al., 2020 (a) emphasize the problems of faulted rock mass in the Nepal Himalaya as tunnel deformation and yielding through numerical modelling in RS2. They have proposed the use of a system of tunnel support for strengthening the faulted rock mass around the tunnel using forpoles in the Kulekhani III headrace tunnel.

2.6 Conclusion

There is wide spread distribution of fault in Nepal so there is high probability that tunnel experience faulted geology, its associated problems. Some of the conclusions are as follows:

- Tunnelling in the faulted rock mass is unpredictable as problems water-in- rush, roof falls, cavity formation, face collapse, swelling, support failure occurs which leads to time and cost over-runs.
- Stabilization of the fractured rock mass with lattice girders, forepoles, grouting, rock bolts, drainage of ground water and use of flexible support of steel ribs, precast concrete as final support for the movement of ground due to fault has been done in tunnels constructed in Nepal Himalaya.
- The maximum stress in the faulted geology can be either in vertical direction or in horizontal direction or in out of the plane of face of tunnel. It signifies the importance of measurement of field stress for the correct simulation of tunnel excavation and support installation. Pressuremeter and hydraulic fracturing should be used for the stress measurement in faulted zoology.
- Numerical Modelling of faulted rock mass can be done in FEM based software RS2 (Rocscience).
- Articulated design approach (Russo et. al, 2002), Analytical Method using CCM approach (Carranza-Torres and Fairhurst, 2000), and Empirical method (Marinos et. al. 2007;, Marinos et al., 2011; Marinos, 2014;, Marinos, 2019) are three methods which can be used in design of tunnel in faulted rock mass.

3 Description of Case Study :Modi Khola Hydroelectric Project

3.1 General

Modi Khola Hydroelectric Project lies about 45 km west of Pokhara in Nepal. A 423 m long inverted-D shaped pressure tunnel with a varying cross sectional area of 22 m² to 27 m² pass through fault zone upstream of junction of Audit 2 (Figure 3-2).The pressure tunnel passes through altered, disintegrated and weathered green quartzite with occasional intercalation of phyllitic schist .The rock mass at this tunnel reach was of very poor to fair quality, with Q-value ranging from 0.18 to 4.1 (Himal Hydro, 2001). This fault has overlaying conglomerate above the tunnel alignment and overburden soil on the valley side slopes. This fault consists mainly of extremely to exceptionally poor rock mass, which is composed of completely decomposed fault gouge and fault breccia.

The fault has thickness of 16.7 m and orientation of 32°/ 308° tunnel has trend of 12° / 192 °. Figure 3-3 shows equal angle lower hemisphere projection of pressure tunnel and fault of Modi Khola Hydroelectric Project at 65 m upstream of Adit-2. The angle between fault and tunnel is 26° (Himal Hydro, 2001). The strength properties of the faulted rock mass are given in (Table 3-1)

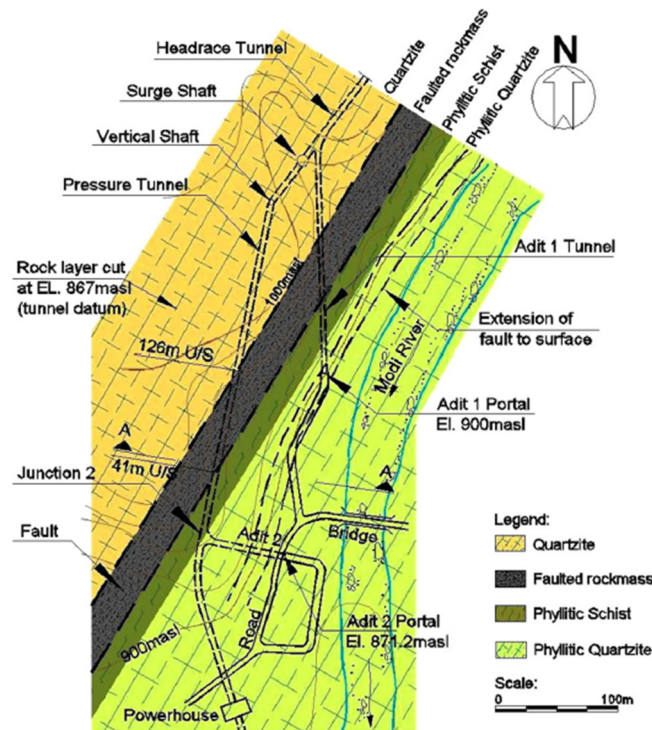


Figure 3-1 Plan of Modi Khola Pressure Tunnel (Shrestha & Panthi,2014)

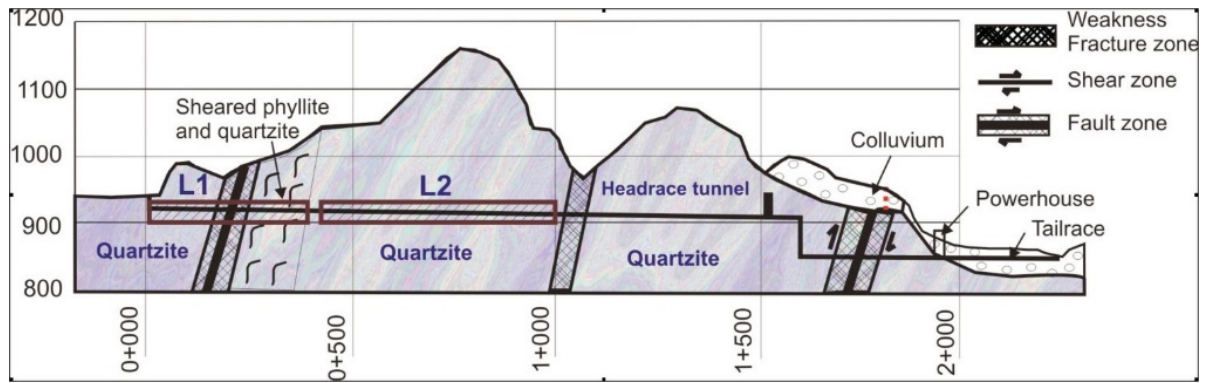


Figure 3-2 Geological profile along the tunnel system of Modi Project (Panthi, 2012).

Table 3-1 Faulted rock mass properties in Pressure Tunnel for Modi Khola Hydropower Project (Panthi, 2006).

Description	Quartzite	Fault Core	Phyllitic Schist	Phyllitic Quartzite	Conglomerate	Grouted rock mass
Intact rock strength (r_{ci}), MPa	225	1	16	100	35	5
Rock Mass Rating (RMR_{89})	27	15	17	24	50	20
$GSI = RMR - 5$	22	10	12	19	45	15
Material constant (m_i)	20	20	9	16	21	20
Disturbance factor (D)	0	0	0	0	0	0
Poisson's ratio (m)	0.2	0.2	0.1	0.17	0.2	0.2
Dry unit weight ^b , gr/cm^3	2.66	2.66	2.73	2.68	2.60	2.66
Overburden, m	80	80	80	80	100	80

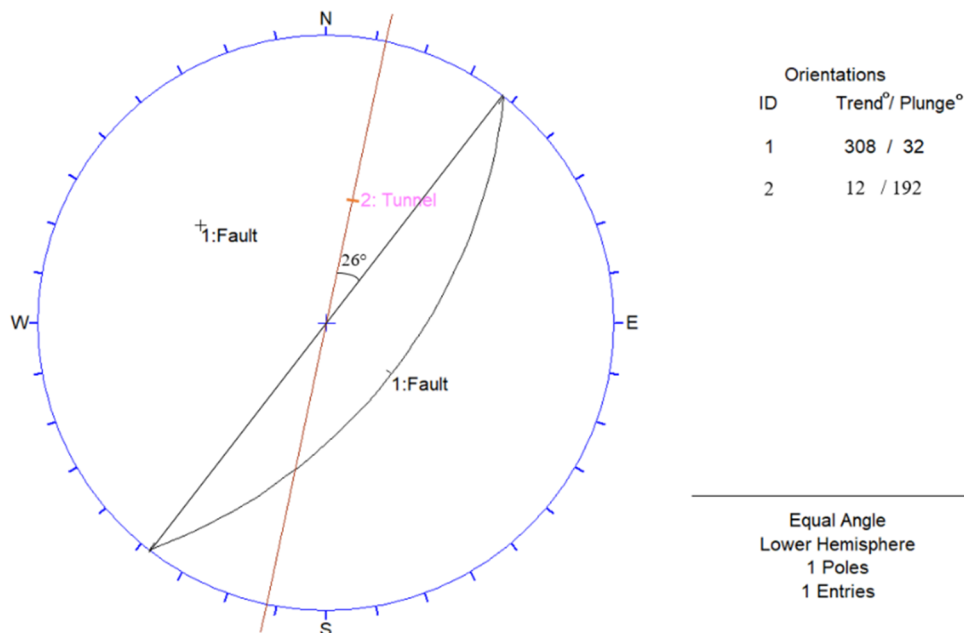


Figure 3-3 Equal Angle Lower Hemisphere Projection of Pressure Tunnel and Fault of Modi Khola Hydroelectric Project

3.2 Modi Khola Pressure Tunnel: Problem and Design in Fault zone

A 76.5 m long Adit No. 2 was designed for the excavation of Pressure Tunnel. The design was done as for a major shearzone to cross along the upstream part from junction Figure 3-2. It was done as per the side conditions and problems encountered during the tunnel excavation process. Initial and final support was given in two stages. In first stage primary or initial support was given which tunnel excavation and final support was given to it. Figure 3-4 show the tunnelling process in the fault zone for initial stage.

The tunneling in the fault zone and its support measures for initial stage are explained as follows. The alignment of the pressure tunnel was changed with a vertical shaft as the penstock was previously exposed to surface of the ground. As a result the weakzone continued for a long distance. On further excavation, a major shear zone composed of fully decomposed soft fault gouge and shattered fault breccia collapsed at upstream face chainage of 26 and 41 m (Paudel et. al.,1998).

Since, the Pressure Tunnel alignment was 7 m to 10 m below the river bed level, high rate of ground water inflow further made the condition worse. The slide material was piled up at the face and consolidation grouting was started to stabilize the collapse. The grouting was done by injecting in ratio of 1:1 (cement:water) through 3 m to 8 m long perforated Galvanised pipes. After consolidation grouting in the perimeter and above the crown, heading and benching method was followed for further excavation (Paudel et. al.,1998). Heading by steel arch installation above SPL at 30 cm to 50 cm spacing and lagging behind with steel bars was done in the first stage. In the second stage full section excavation was done by erecting the post and struts with concrete foundation at 30 cm to 50 cm spacing. After excavating 14 m in the shear zone following the heading and benching method, horizontal probe hole drilling was started to find out the width of the shear zone. Core samples of fractured quartzites were obtained from about 18 m onwards from the drilling face showed shearzone was found to be about 32 m (Paudel et. al.,1998).

After the installation of initial or primary support final support was applied. Grouting in the perimeter and spilling bars at 20 cm spacing was given per meter length of tunnel. Steel ribs support with 75 to 100 mm thick fibre reinforced shotcrete was used throughout the weak zone. Provisions of compressible packing between rock and the support was used to resist all the movements due to fault to allow deformation under controlled condition and final lining with flexible joints of the tunnel. These are the important tunnel support design in the context of tectonically active zones of Modi Khola Hydroelectric Project (Paudel et. al.,1998). Figure 3-5 show principal tunnel support patterns in Modi Khola Hydroelectric Project. It consists of rock bolts, spot bolting, systematic rock bolting, grouted bolting, expansion rock bolt, steel fibre reinforced shotcrete, wire mesh, stone masonry with precast arch of concrete, circular steel rib and reinforced concrete.

Table 3-2 Orientation and characteristics of discontinuities in the Headrace Tunnel in Modi Khola Hydroelectric Project. Paudel et. al.,1998

Tunnel Location	Chainage(m)	Bedding/Joint	Orientation	In filling	Opening (mm)	Spacing (cm)	Roughness
HRT from Inlet	99-120	Bedding	N 25°E/35°N W	Clay	-	200-300	Slickensided
	120-130	Bedding	N 27°E/37°NW	Clay		200-300	Planar
	330-400	Joint	125°/60°NE	Sandy clay	-	30-100	Planar
	400-440	Joint	12°/70° SE	-	2-3	50-100	Smooth
	400-440	Bedding	N 45°E/23°NW	Sandy clay	-	50-150	Undulated
	440-500	Joint	N 45°E/85° SE	-	3-5	100-200	Smooth
	500-600	Joint	200°/44° SE	Clay	-	40-100	Planar
	600-660	Bedding	N 31°E/35°NW	Clay	-	50-100	Undulated
	660-690	Joint	N-S/62°E	Sandy Clay		20-50	Planar
Adit – 1 Upstream	0-200	Bedding	N 30°E/24°NW	Sandy Clay	-	100-200	Slickensided
	0-200	Joint	N 20°E/65° SE	-	3-5	40-100	Smooth
	200-360	Bedding	N 27°E/28° NW	Sandy Clay	-	60-100	Slicken sided
	200-360	Joint	78°E/74°SE	-	2-5	20-60	Rough/Planar
	360-390	Joint	N95°/6°SW	-	-	100-300	Rough/tight
	390-530	Joint	220°/66°SE	-	5-10	50-100	Rough/Planar
	530-550	Joint	42°/72 °SE	Sandy Clay	-	30- 100	Rough/Planar
	550-600	Joint	175°/66° NE		5-10	50-100	Smooth
	600-660	Joint	340°/60°NE	Silt + clay	-	40-100	Smooth
	660-705	Joint	90°/70°S	-	3- 5	50-150	Smooth
	705-795	Bedding	45°/35° NW	Clay	-	200-300	Planar
	705-795	Joint	330°/65° NE	-	2-6	100-150	Smooth/Planar

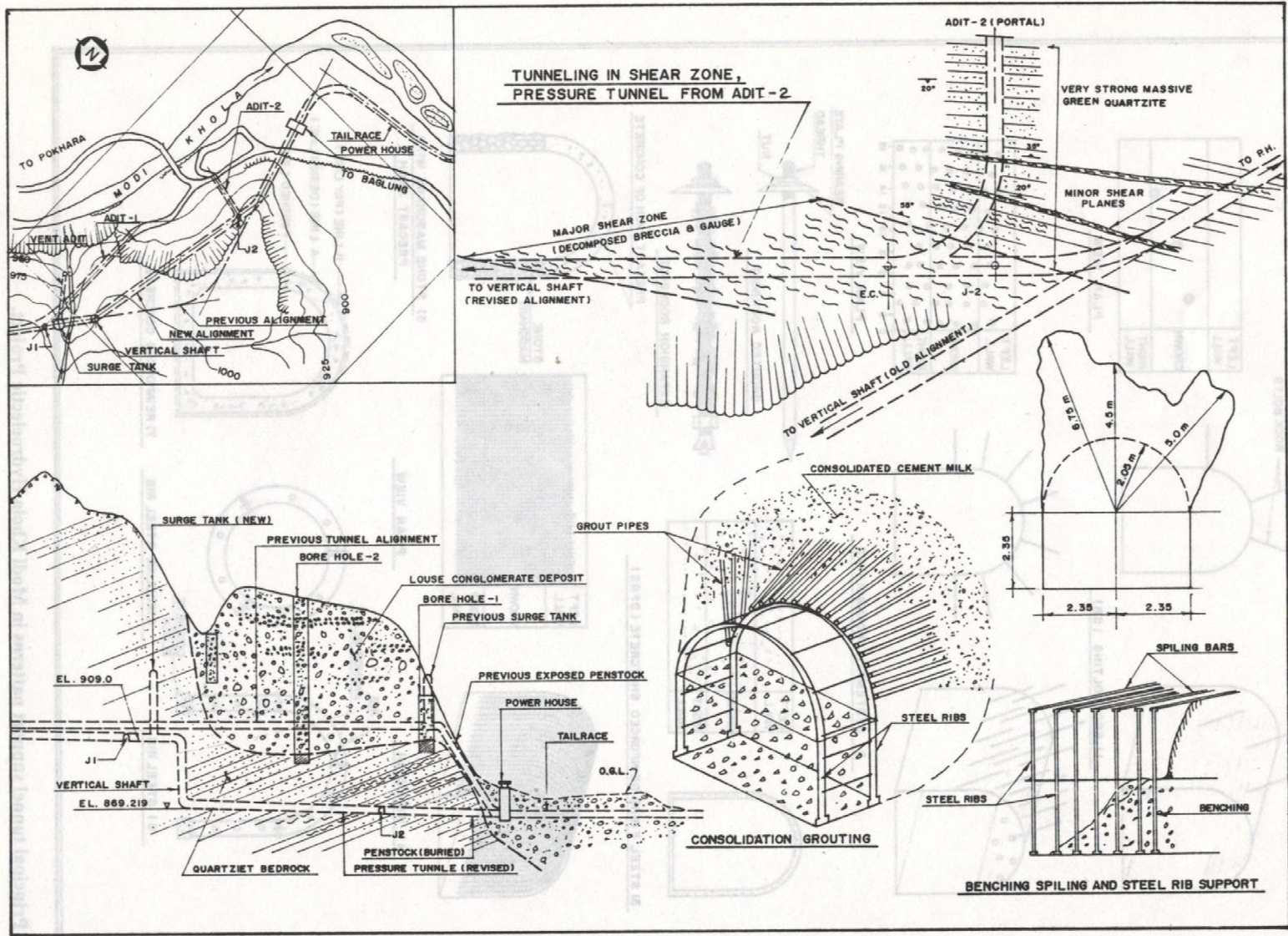


Figure 3-4 Tunnelling through Shear Zone in Modi Khola Hydropower Project, (Paudel et. al.,1998).

3.3 Previous work in Himalaya (Indian and Nepali tunnel design in Fault)

Fault zone and thrust zones are frequently encountered while tunneling in the case of Lesser Himalaya. There are different projects in Nepal and India which have encountered various tunnel support failure problems in fault zone. It has been found that tunneling in fault zone is site specific. Tunnel supports in the weak zone in the fault are applied on the basis of the problems such as squeezing, ground water ingress, overbreak. This section describes the work on the problems and support measures in tunneling in fault zone located various projects located in Lesser Himalaya in Nepal and India. It is elaborated in details as follows.

In Modi Khola Hydroelectric Project, Nepal, there was existence of fault in Adit No. 2 of Pressure Tunnel (Figure 3-2). As the tunnel excavation proceeded across the fault and reached 83 m upstream from the Adit-2 junction, severe squeezing was observed at several locations behind the tunnel face. Flowing rock mass from the crown of the tunnel in Modi Khola Hydroelectric Project was encountered (Figure 3-6). Rock squeezing initiated with failure of joints in steel ribs along the spring line of the tunnel and continued throughout the fault zone. Severity of squeezing reached its maximum mainly to the hill side wall-bottom. However, the extent of squeezing to the river side wall was relatively less (Shrestha and Panthi, 2014). The pressure tunnel lost considerable dimension due to squeezing, and the minimal workable space behind the steel pipe became insufficient. Thus, re-excavation of the squeezed tunnel wall was carried out, and the tunnel invert was lowered. Damaged steel ribs were removed in pieces, walls and crowns were excavated with due care, additional shotcrete was applied, and new steel ribs were installed. Also, horizontal H-beam struts were also provided at the lowered tunnel invert (Himal Hydro, 2001).



Figure 3-6 Flowing mass from the tunnel crown (Himal Hydro, 2001)

Similarly, in Kulekhani III Hydropower Project, Nepal, MBT is located about 600 m south of powerhouse site in the tectonic contact between tertiary sedimentary rock and metasedimentary rock of Paleozoic age. Mahabharat Thrust (MT) separates crystalline rocks in the north from metasedimentary rock in the south (Figure 3-7). MT is as an extension of MCT. The general trend of Thrust is West-North-West to East-South- East and dips at 65° towards north east. The thrust crosses tunnel at chainage 1+450 m chainage. The rate of northward movement is considered to be 5cm/year in recent years (NEA, 1997). The headrace tunnel of diameter 3.5 m, 4.7 km length passes through sheared schist, sheared phyllite. There was heavy squeezing in shear zone in headrace tunnel which required re-excavation with heavy support of steel ribs, concrete lining, bolts and reinforced concrete (Figure 3-8).

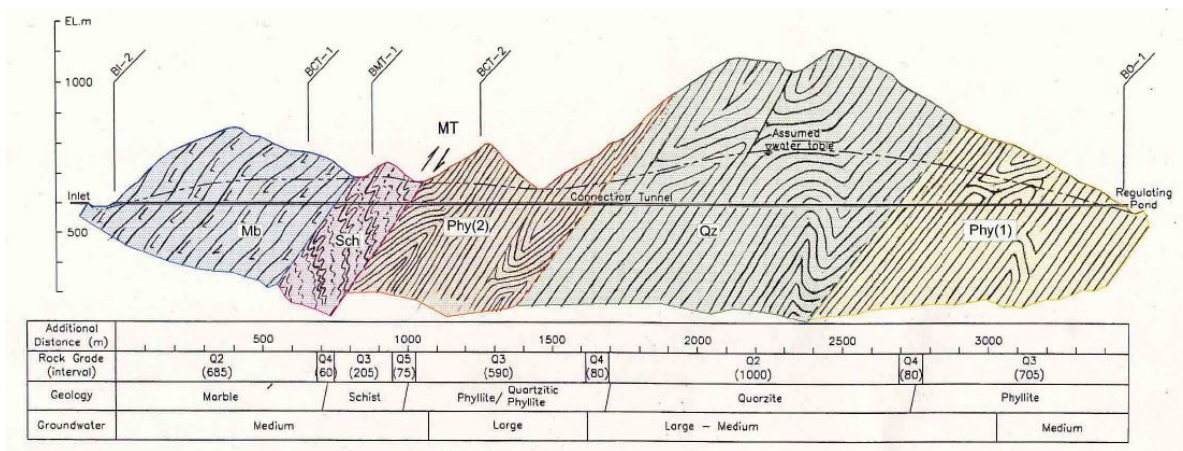


Figure 3-7 Longitudinal section of Headrace tunnel of Kulekhani III Hydropower (NEA, 1997)

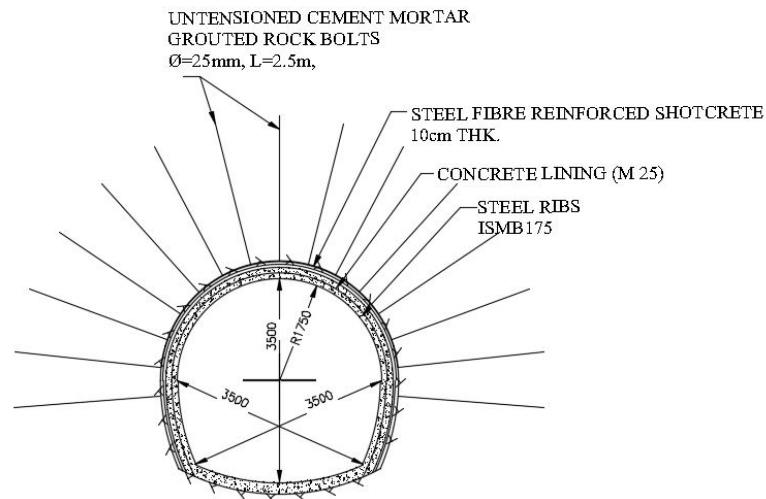


Figure 3-8 Tunnel support in shear zone in Kulekhani III Hydropower Project (NEA, 1997).

Similarly, Kaligandaki 'A' hydroelectric project, Nepal is located in the lesser Himalayan region and is relatively close to Main Boundary Thrust. The length of 5950 m long horseshoe shaped headrace tunnel

with 4.35 m. The headrace tunnel passes through highly deformed siliceous and graphitic phyllite that varies in mineral composition and degree of metamorphism. The rock mass in the area has been subjected to shearing, folding and faulting due to active tectonic movement (Figure 3-9). The phyllite is of poor quality, thinly foliated and highly weathered. The orientations and dips of the joints sets are highly scattered due to extreme folding and shearing, giving no distinct joint system except for foliation joints. In general, the foliation joints are oriented in Southeast to Northwest direction and dip towards Southwest. The maximum rock cover above the tunnel is approximately 600 m, and more than 80% of the tunnel alignment has overburden exceeding 200 m. The tunnel is closed to Main Boundary Thrusts (MBT) and different shear zones.

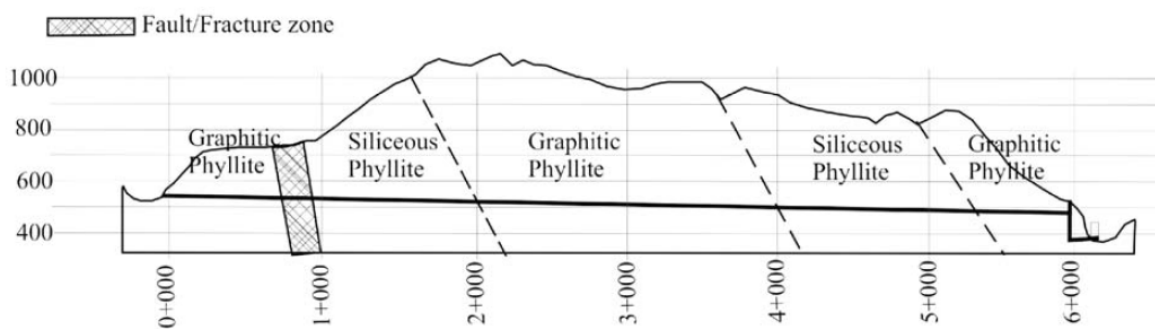


Figure 3-9 Longitudinal profile of headrace tunnel of Kaligandaki 'A' Hydroelectric Project, (Panthi and Neilson, 2007)

The head race tunnel was excavated by drill & blast method with heading and benching method and faced severe squeezing due to shear zone of deformed siliceous and graphitic phyllite. The primary rock support applied during construction mainly consisted of steel ribs of ISMB 125 spaced at an interval ranging from 0.6 to 1.5 m, steel fiber reinforced shotcrete having thickness ranging from 15 to 60 cm and 4-m-long 25-mm diameter fully grouted rock bolts (Panthi and Shrestha , 2018). The tunnel was supported with steel ribs at 1 m spacing centre to centre, 200–250 mm thick reinforced shotcrete and radial bolting. Load cells and closure studs were installed up to 3 m behind the face. Tunnel deformation and support pressure were measured to be 1.4–8.5% and 0.90–1.27 MPa. (Dwivedi et al, 2014). Chhushyabaga et. al.2020, used numerical analysis in RS to design the tunnel support in the fault zone which composed of Grouted rock bolts of 34 mm diameter, 200 mm concrete (M 25) and steel ribs of ISMB 310 (Figure 3-10).

Similarly, Chameliya Hydroelectric Project, Nepal is located in the west-central part of the Lesser Himalayan Zone and is 60 km north of the Main Boundary Thrust (MBT) and close to the Main Central Thrust (MCT). The headrace tunnel is horseshoe shape cross section area of 21 m². During excavation headrace tunnel at chainage of 3+100 m to 3+900 m (Figure 3-11) thrust zone and fault zone were encountered. Due to which heavy tunnel squeezing and tunnel collapse was registered with significant floor heaving and wall convergence (Figure 3-12). Over excavation was used which was unsuccessful with

heavy squeezing (Figure 3-12). Sequential excavation of top heading and benching with fore-poling, lattice girder, steel ribs with flexible joints were used to cross the fault zone at chainage 3+100 m to 3+900 .

In Chhibro-Khodri tunnel of Yamuna hydroelectric project India, recurrence of Krol and Nahan thrusts have resulted in changing geology along the tunnel alignment due to thrust zone (Figure 3-13(a)).

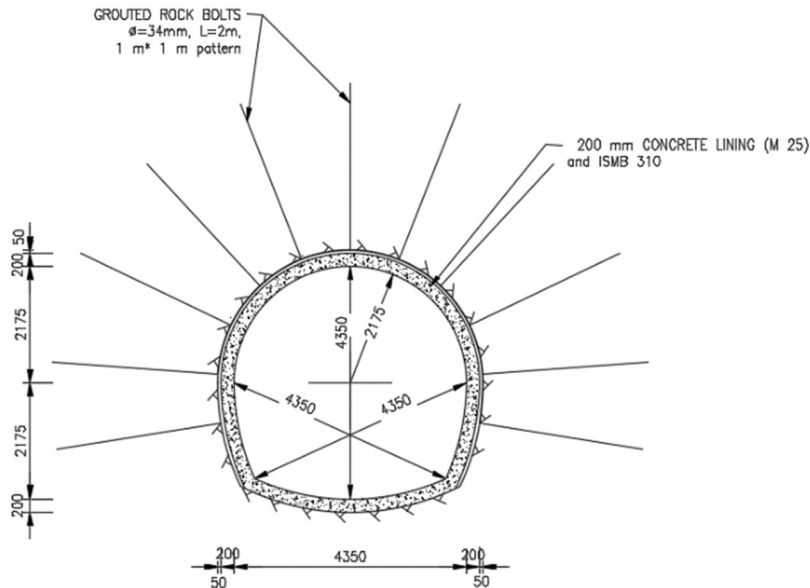


Figure 3-10 Tunnel support in shear zone in Kaligandaki 'A' hydroelectric project (Chhushyabaga et. al.2020)

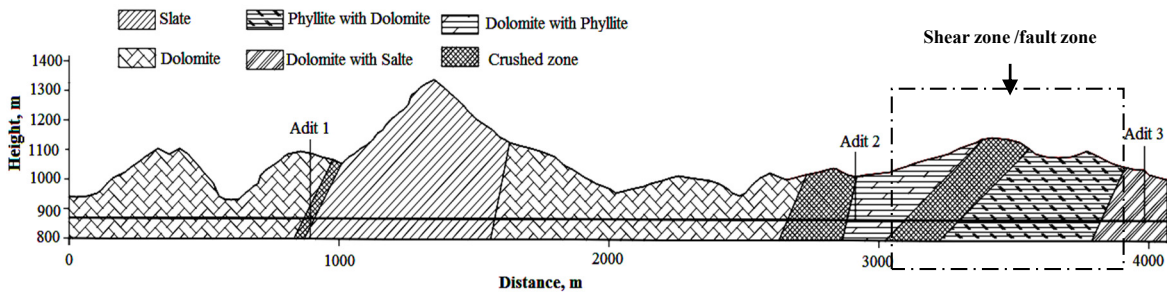


Figure 3-11 Longitudinal geological profile of Chameliya headrace tunnel (modified after Khadka,2019)

. The tunnel is of 7.5 m diameter with length of 6.2 km with tunnel depth greater than 600 m. This resulted in the problems of water-inrush and squeezing ground conditions during tunneling through the intra-thrust zone, which delayed the project. This resulted the change in the tunnel alignment . The difference was mainly in terms of the position of faults and thrusts, which were struck as surprise and resulted in the delay in completion of tunnel. Forepoling steel supports, shotcreting and rock bolting in squeezing grounds in thrust zone was used with changed tunnel alignment to cross thrust zone (Jethwa et al., 1980).



Figure 3-12 Tunnel squeezing Chameliya headrace tunnel. Floor heave (left) and wall closure in hill side (right) (Basnet et. al., 2013).

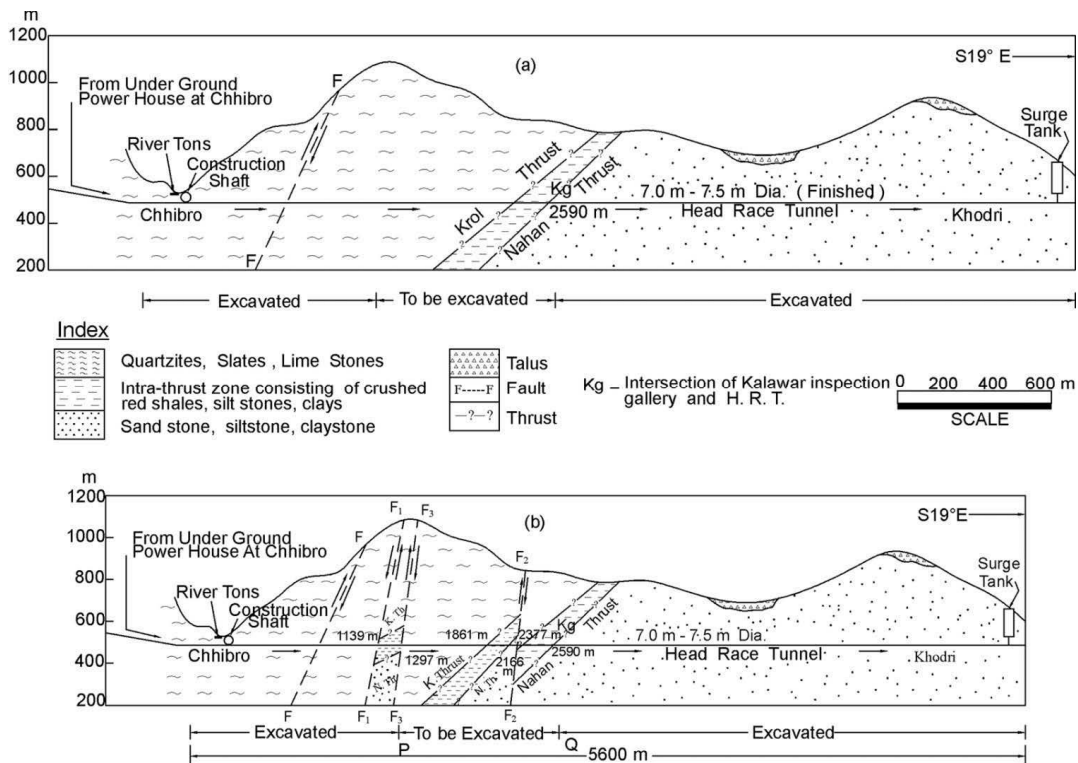


Figure 3-13 Geological cross-sections along Chhibro-Khodri tunnel (a) original before starting tunneling (b) actual encountered during tunneling (Jethwa et al., 1980).

Similarly, in the case of Maneri stage-I project head race tunnel in India, the trapped water in quartzites above impervious shear zone rushed in to the tunnel causing roof collapse and debris flow flooding the tunnel (Figure 3-15). Wire mesh, shotcrete, rock bolt shown in Figure 3-14 were used as the tunnel support for shear zone treatment in Maneri stage-I project. Tunnelling problems and their remedial measures and supports in fault zone and shear zone located in different hydropower projects in India such as Maneri

Stage-II Hydroelectric Project, Maneri Stage-I Hydroelectric Project, Tehri Project, Uttarakhand, Dul Hasti Hydroelectric Project, Ranganadi Hydroelectric Project, Rohtang Highway Tunnel, Chenani - Nashri Highway Tunnel, Parbati Stage-II Hydroelectric Project, Ranjit Sagar Hydroelectric Project are illustrated in Table 3-3.

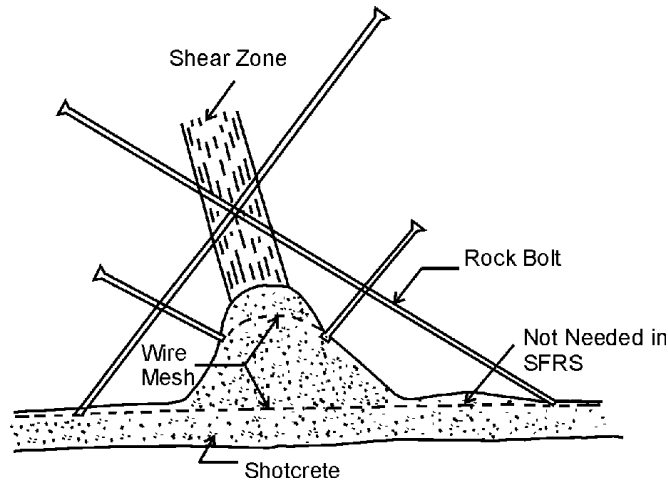


Figure 3-14 Shear zone treatment in Maneri stage-I project (Lang, 1961).

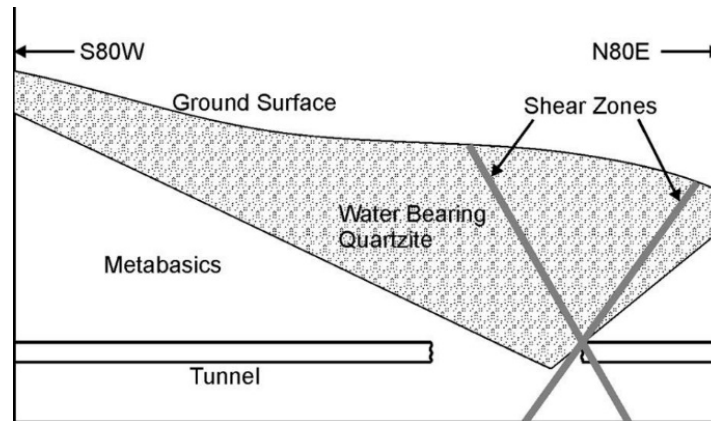


Figure 3-15 Water inrush in head race tunnel of Maneri stage-I project (Goel et al., 1995a)

Table 3-3 Major tunneling projects with problems faced in fault/ thrust zone and remedial measures (Feng,2017)

Name of the Project, Name of Tunnel, Length, Size	Rock Type	Tunneling Problems	Remedial Measures & Supports
Maneri Stage-II Hydroelectric Project, Uttarakhand: HRT-16.0km long, 6.5m wide horse-shoe, tunnel depth > 1000m	Quartzite, gneisses, phyllites, greywackes, slates, limestone, epidiorite; Srinagar thrust and faults	The lithological contacts were sheared, squeezing, high pressure and deformation, flowing ground condition	Forepoling, grouting to tackle the crushed and weak rocks; cavity was grouted using bulkhead and inserting the bolts, steel rib supports with concrete backfill; excavation of bypass drift to release the water pressure
Maneri Stage-I Hydroelectric Project, Uttarakhand: HRT-8.56km long, 5.0m dia.,	Quartzite, metabasic, Chlorite schist, quartzite with minor	Water-in-rush, cavity formation and high pressure because of	Tunneled through alternate alignment to avoid water-charged zone; formation of grouted zone around tunnel to tackle the highly jointed and crushed metabasics

circular, maximum tunnel depth 800m	slate; fault and recurrence of folds	squeezing condition leading to support failure	and quartzites in cavity area; heavy steel rib supports with steel lagging to tackle squeezing condition; secondary support of concrete lining
Tehri Project, Uttarakhand: HRT (4 nos.) – 1km long each, 8.5m dia.	Thinly/thickly bedded phyllites of various grades, sheared phyllites	Minor tunneling problems generally in sheared phyllites	Steel rib supports with final concrete lining in HRTs.
Dul Hasti Hydroelectric Project, J&K: HRT – 10.6km long, 7.5m dia. circular/ horse-shoe	Schist/gneiss on west, quartzite/phyllite on east; Kishtwar fault separating the two lithological units	Water ingress, cavity formation, TBM did not succeed in a smooth manner	Advanced probe holes and use of conventional DBM, use of 20mm wiremesh at crater location to stop the muck flow, filling of cavities with concrete, drainage
Ranganadi Hydroelectric Project, NE Himalaya: HRT – 8.5 km long, 6.8m dia.	Schist, gneiss, shiwalik sandstone besides mica chlorite/mica schist, granitic gneiss, carbonaceous shales and soft sandstone	Intake portal collapse, squeezing ground, intra-thrust zone, methane gas, chimney formation, roof falls and over breaks, crushed rock and flowing water from roof	Forepoling and drainage then tunnel driving, steel supports in squeezing grounds, shotcreting and rock bolting etc., changed tunnel alignment to cross main central thrust (MCT)
Rohtang Highway Tunnel, H.P.: 8.9km long, 10.0m wide horse-shoe, Maximum tunnel depth 1900m	Uniformly dipping alternate sequence of quartzites, quartzitic-schist, and quartz-biotite schist with thin bands of phyllites; Serinala fault passes through the tunnel	Roof collapse; loose rock falls at various places; squeezing; high deformations of roof; Serinala fault flooded tunnel with rock debris	NATM was used. Shotcrete and rock bolt supports was strengthened; longer rock bolts were used; yieldable steel rib supports are planned in poor rock conditions; DRESS technology was used to tackle the fault zone; the concrete lining will be used as final support
Chenani-Nashri Highway Tunnel, J&K: 9.0km long, 6.0m wide horse-shoe escape tunnel and 12m wide horse-shape main tunnel, maximum tunnel depth 1200m	Sandstone, siltstone and claystone; minor shear zones	High deformation for longer period; roof falls at places	Tunneling by NATM; longer rock bolts and additional layer of shotcrete along with lattice girders have been used as primary support with final concrete lining
Parbati Stage-II Hydroelectric Project, H.P.: HRT- 31.5km long, 7.0m dia., circular, maximum tunnel depth 1300m	Granite, gneissic granite and quartzite; folded, faulted and jointed	Mild rock burst, water inundation from probe holes flooding the tunnel and TBM, work stopped from TBM side, likely to resume soon.	High capacity steel rib supports were installed in drill and blast excavated section; secondary concrete lining; rock bolts, wiremesh shotcrete and hexagonal precast concrete segments were installed in TBM excavated section
Ranjit Sagar Hydroelectric Project, Sikkim: HRT- 3km long, 4.5m dia.	Phyllitic zone, intake portal at slope-wash /talus	Number of shear zones with flowing conditions	Cold bend rib supports, precast lagging, forepoling and backfill concrete

Where HRT is Headrace tunnel, TBM is tunnel boring machine

3.4 Conclusion

Tunnelling in the lesser Himalaya is very challenging and difficult due to presence of fault and thrust zones. Quartzite, Gneisses, Phyllite, Slate, limestone, Metabasic, Chlorite schist, sand stones are the common types of the rock mass found in the fault and thrust zone in this zone. These rock masses are unstable when tunnel and underground structures are excavated. They encounter problems such as squeezing, high pressure and deformation, flowing ground condition, water in rush, cavity formation and high pressure leading to support failure of the tunnel.

This requires a design of the tunnel support with consideration of the weak rock mass of the fault and thrust zone. Most of the hydropower projects in located in fault and thrust zone in lesser Himalaya have encountered and solves those problems mentioned above with measures of the support based on the site conditions. It includes stabilization of the fractured rock mass with drainage of ground water and use of final support for the movement of ground due to fault. Some of those measures in the design of tunnel support used in faulted rock mass are as follows:

- Forepoling, grouting to tackle the crushed and weak rocks
- longer rock bolts and additional layer of shotcrete along with lattice girders
- Cavity grouting using bolts
- Steel rib supports with concrete backfill
- Excavation of bypass drift for drainage to release the water pressure
- Heavy steel rib supports with steel flexible joints, lagging to tackle squeezing condition
- Secondary support of concrete lining and steel rib supports with final concrete lining
- Wire mesh at crater location to stop the muck flow, filling of cavities with concrete

Hence, we can conclude that tunnel support in the fault zone have been applied in two stages. In first stage rock mass have been stabilized with lattice girders, forepoles, grouting, rock bolts, drainages of water with bypass drifts. In second stage the final support with flexible support of steel ribs, precast concrete has been used to account the fault rupture and displacements.

4 Numerical Analysis

4.1 General

Numerical analysis is popular approach to investigate the effect of the fault in tunneling with real behavior of faulted rock mass. Remarkable discontinuity and large deformability are two main properties of a fault in the tunnelling. It is considered that if a numerical method can equivalently simulate these two properties, it is preferable to apply in tunnel stability analysis and succeed in realistically simulation the influence of a fault on the tunnel surrounding rockmass and supporting system (Zhang et. al., 2017). In this study finite element modelling was done to study the effect of the fault at different sections i.e., circular, horseshoe and inverted-D following after validation model of tunnel in faulted rock mass for the case study of Modi Khola Hydropower Project in chapter 3.

4.2 Numerical modelling

Three commercial softwares a) RocLab, b) Unwedge c) RS2 from Rocscience Inc have been used in this study. Roc Lab have been used to obtain the mechanical strength parameters of rock mass. Unwedge have been used to study the structurally controlled failure in tunnel. Similarly, RS2 have been used to study the effect of the fault at different sections i.e., circular, horseshoe and inverted-D and have also been used in design of required tunnel supports. The procedure and modelling approaches are elaborated in details are follows.

a) RocLab

Rock mass properties are important parameters used in the numerical modeling of tunnel, underground structures and its excavations. RocLab is a software program which product of Rocscience Inc used for determining soil and rock mass strength parameters through analysis of laboratory or field triaxial or direct shear data. The program can fit the linear Mohr-Coulomb strength criterion and generalized Hoek-Brown. RocLab includes built-in tables for estimating typical strength parameters for various rock and soil types (RocLab, 2002). Various constitutive models are used in numerical analysis programs for tunnel excavation and design of supports. The analysis is limited if reliable estimate of geotechnical input parameters cannot be done. RocLab provides tools for quickly and easily testing out hypotheses on four of the most widely used and accepted strength models for soils and rock. The program can be used to determine strength models that best describe laboratory or field data. RocLab is designed to aid engineers at various stages of design. It provides implementations of the failure criteria such as Generalized Hoek-Brown and Mohr- Coulomb failure criteria. The program enables users to easily visualize the effects of changes in input parameters on rock and soil failure envelopes. In addition, RocLab comes with built-in tables of typical strength parameter

values for various rock and soil types, compiled from very credible sources. This allows users to obtain reliable estimates of the strength properties of a wide variety of rocks and soils. The task of determining rock and soil mass properties is carried out in order to obtain input material properties for use in limit equilibrium or numerical analysis of geotechnical structures. The material properties determined from RocLab are used as input for analysis in RS2 for finite element stress analysis and support design for excavations.

Procedure of using RocLab

The procedure of using RocLab is as follows:

i. Determine Strength Parameters

For Generalized Hoek-Brown Criterion, parameters of a rock mass (m_b , s and a) are determined based on input data such as Unconfined compressive strength of intact rock σ_{ci} , the intact rock parameter m_i , geological strength index GSI, disturbance factor D . These are obtained from Triaxial Strength Test. The Hoek–Brown strength criterion is an empirical failure criterion of rock mass which has been developed specifically for rock materials and rock masses. It has been applied in rock engineering successfully to a wide range of intact and fractured rock types. This method is based on the observed behavior of rock masses to simulate the failure mechanism of jointed rock, and triaxial compression tests of fractured rock (Hoek et al., 2002). The criterion includes procedures developed to estimate rock mass strength from laboratory test values and field observations. Hoek–Brown assumes independence of the intermediate principal stress. It has been used widely in rock engineering practice Priest (2005).

The original non-linear Hoek–Brown strength criterion for intact rock is defined by Eq.(4.1)
Eq.(4.1)Eq.(4.1)

$$\sigma'_1 = \sigma'_3 + \sigma_c \left(m \frac{\sigma'_3}{\sigma_c} + s \right)^{0.5} \quad \text{Eq.(4.1)}$$

Where, σ_c is the unconfined compressive strength of the intact rock; σ'_1 and σ'_3 are the major and minor effective principal stresses, respectively; and m and s are material constants. This criterion was later updated (Hoek & Brown, 1997) to the current generalized form as Eq.(4.2).

$$\sigma'_1 = \sigma'_3 + \sigma_c \left(m_b \frac{\sigma'_3}{\sigma_c} + s \right)^a \quad \text{Eq.(4.2)}$$

where m_b is the reduced value of material constant m_i for the rock mass; and s and a are constants that depend on the characteristics of the rock mass. The parameters m_b , s and a can be estimated from the Geological Strength Index (GSI) as follows (Hoek et al., 2002):

$$m_b = m_i \exp\left(\frac{GSI - 100}{28 - 14D}\right) \quad \text{Eq.(4.3)}$$

$$s = \exp\left(\frac{GSI - 100}{9 - 3D}\right) \quad \text{Eq.(4.4)}$$

$$a = \frac{1}{2} + \frac{1}{6} \left(e^{\frac{-GSI}{15}} - e^{\frac{-20}{3}} \right) \quad \text{Eq.(4.5)}$$

Where, D is a factor of degree of disturbance to which the rock mass has been disturbed by blast damage and stress relaxation. It varies from 0 for undisturbed to 1 for very disturbed rock mass in situ rock masses. The unconfined compression strength (σ_c) and tensile strength (σ_t) is obtained by setting $\sigma'_3=0$ in 20. giving the expression as:

$$\sigma_c = \sigma_{ci} s^a \quad \text{Eq.(4.6)}$$

$$\sigma_t = -\frac{s\sigma_{ci}}{m_b} \quad \text{Eq.(4.7)}$$

For Mohr-Coulomb Strength Criterion parameters, c (cohesive strength), and ϕ (friction angle) of rock mass. These are obtained from Direct Strength Test

Mohr- Coulomb failure criterion

The Mohr-Coulomb failure criterion is a set of linear equations in the form of principal stress describing the failure conditions for an isotropic material. The basic concept of this criterion suggests that the shear strength of a rock material is made up of two parts: a constant cohesion; and a friction varying with normal stress. Mohr's condition assumes that failure envelope which can be linear or non-linear is the locus of σ , τ acting on a failure plane. Coulomb's conditions are based on a linear failure envelope to determine the critical failure on rock plane (Labuz and Zang, 2012).

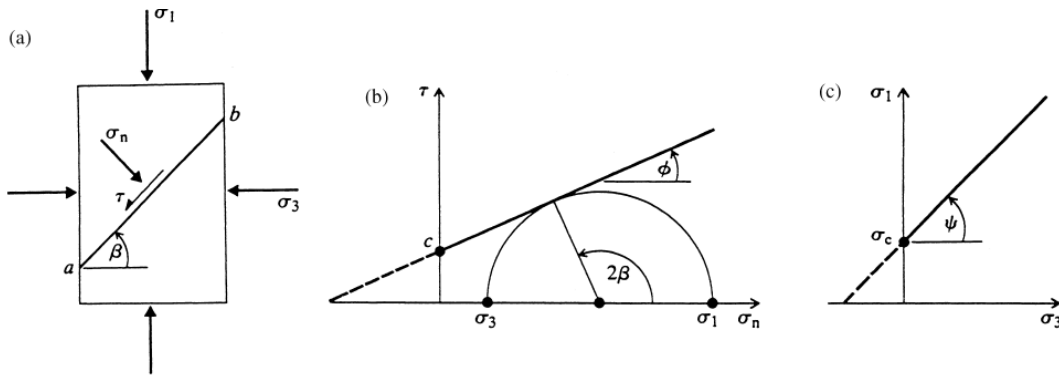


Figure 4-1 The Mohr- Coulomb strength criterion: (a) shear failure on plane a-b, (b) Strength envelope of shear and normal stresses, and (c) Strength envelope of principal stresses (Zhao, 2000)

The shear strength, τ , that can be developed on a plane such as a-b in (a) is given by Eq.(4.8)

$$\tau = c + \sigma_n \tan \phi \quad \text{Eq.(4.8)}$$

where c is cohesion, σ_n is the normal stress acting on plane a-b, and ϕ is the angle of internal friction.

Applying the stress transformation equations gives

$$\sigma_n = \frac{1}{2}(\sigma_1 - \sigma_3) + \frac{1}{2}(\sigma_1 - \sigma_3) \cos 2\beta \quad \text{Eq.(4.9)}$$

$$\tau = \frac{1}{2}(\sigma_1 - \sigma_3) \sin 2\beta \quad \text{Eq.(4.10)}$$

Substituting for σ_n and τ and rearranging gives the limiting stress condition on any plane defined by β as

$$\sigma_1 = \frac{2c + \sigma_3[\sin 2\beta + \tan \phi(1 - \cos 2\beta)]}{\sin 2\beta - \tan \phi(1 + \cos 2\beta)} \quad \text{Eq.(4.11)}$$

There will be a critical plane on which the available shear strength will be first reached as σ_1 is increased. The Mohr circle construction of (b) gives the orientation of this critical plane as

$$\beta = \frac{\pi}{4} + \frac{\phi}{2} \quad \text{Eq.(4.12)}$$

For the critical plane, $\sin 2\beta = \cos \phi$, $\cos 2\beta = -\sin \phi$, reduces to

$$\sigma_1 = \frac{2c \cos \phi + \sigma_3(1 + \sin \phi)}{1 - \sin \phi} \quad \text{Eq.(4.13)}$$

This linear relation between σ_3 and the peak value of σ_1 is shown in (c). Note that the slope of this envelope is related to ϕ by the equation

$$\tan \psi = \frac{1 + \sin \phi}{1 - \sin \phi} \quad \text{Eq.(4.14)}$$

and that the uniaxial compressive strength (σ_c) and uniaxial tensile strength (σ_t) are related to c and ϕ by

$$\sigma_c = \frac{2c \cos \phi}{1 - \sin \phi} \quad \text{Eq.(4.15)}$$

$$\sigma_t = \frac{2c \cos \phi}{1 + \sin \phi} \quad \text{Eq.(4.16)}$$

It can be noted that σ_c , σ_t and c are proportionally related if ϕ is constant.

These data can be imported from Microsoft Excel through the clipboard, from tab-delimited or comma separated value text files, from RocLab or RocData files, or Entered into the program directly using a built-in spreadsheet.

ii. Curve Fitting

RocLab provides three methods for fitting strength models to test data.

- The Levenberg-Marquardt method is the default technique for fitting all strength criteria to data points. This robust algorithm has become the standard for non-linear regression. It is very reliable in practice, and has the ability to converge quickly from a wider range of initial guesses than other typical methods.
- The Simplex method is one of the best curve fitting methods, and has a reputation for being very reliable.
- Linear Regression (linear least-squares) curve fitting is the third technique provided in RocData. It can be used to only fit the Hoek- Brown criterion for intact rock, and the Mohr-Coulomb strength model to lab data.

iii. Plot Failure Envelopes

Plot the failure envelopes of the strength models in principal and or shear-normal stress space. Interactively change the parameters of the various strength models to see how they influence the failure envelopes.

iv. Equivalent Mohr-Coulomb Parameters

For the non-linear strength criteria (Hoek-Brown, calculate equivalent Mohr-Coulomb strength parameters (cohesion and friction angle). The best-fit Mohr-Coulomb strength envelope is determined over a stress range that you can define based on your application (i.e., tunneling or slope stability). Plot the equivalent Mohr-Coulomb failure envelope in principal and / or shear-normal stress space.

Graphically sample any failure envelope to determine specific stress (principal, shear or normal stress) values at any point along the envelope.

RocData calculates then rock mass parameters such as tensile strength, uniaxial compressive strength and deformation modulus for the Generalized Hoek-Brown criterion.

b) Unwedge

UnWedge (Rocscience Inc) is a 3D stability analysis and visualization program for tunnel and underground excavations in rock containing intersecting structural discontinuities. Potentially unstable wedges formed due to intersecting structural discontinuities are modelled support are added to obtain desired factor of safety. It provides 3D visualization of the formed wedge around the underground structures and required support. Support contains various types of pattern bolting, spot bolting and shotcrete.

UnWedge provides enhanced support models for bolts, shotcrete and support pressures. It has the ability to optimize tunnel orientation and an option to look at different combinations of three joint sets based on a list of more than three joint sets. UnWedge uses analysis engine based on Goodman and Shi's block theory, 1985, which includes the ability to incorporate induced stress around the excavation and the effect on stability.

It also uses new strength models such as Barton-Bandis (Barton and Bandis, 2017; Barton and Bandis, 1982) and Power Curve with the ability to improve the scaling and sizing of wedges. Figure 4-3 show normal stress distribution in perimeter wedge at chainage of 200 to 400 m of adit tunnel of Modi Khola Hydropower Project.

The wedges formed cannot slide inside the tunnel as the factor of safety of all the wedges are well above 2.5 limit. Hence, it is safe for structurally controlled failure induced due to gravity and hence no support is required for it. The support is to be provided as per the analysis for the stress induced failure. The strength parameters have been taken as per Mohr-Column failure criteria.

Procedure of modelling in Unwedge

- i. Defining the Cross-Section of an Opening of the tunnel
- ii. Entering Input Data i.e. Dip and dip direction of tunnel axis, joint orientations, joint properties include strength properties as per Mohr-Column failure criteria and field stress. If the seismic data is available, it can also be included in the form of tectonic stress.
- iii. Viewing Formed Wedges (3D wedge view) with factor of Safety i.e. distribution of field stress, normal Stress, shear Stress. If the wedge has factor of safety less than desired value. In most of the case it is taken as 2.5. Support contains various types of pattern bolting, spot bolting and shotcrete are used to obtain the factor of safety greater than 2.5.

c) RS2

RS2 has been done to study the effect of faulted rock mass in the tunnel and its support design. In numerical modeling, the rock mass around the tunnel, in the immediate and far field of excavation face was simulated by finite elements. It helps in evaluation of the rock mass together with the fault planes, displaying non-linear i.e., elastic plastic behavior. 2-D Numerical analysis

RS2 (Formerly RS2 or Phase2) is a powerful 2D finite element program for soil and rock applications, which is used for tunnel and underground structure for excavation design. Multi-staged models of tunnels in weak jointed, faulted or thrust rock mass can be easily created and analyzed with progressive failure, support interaction with various widely known failure criteria such as Mohr-Coulomb and Generalized

Hoek-Brown for finite element results of tunneling. Material models for rock and soil in RS2 include Mohr-Coulomb, Generalized Hoek-Brown. RS2 offers a wide range of support modeling options. Liner elements can be applied in the modeling of shotcrete, concrete, steel set systems, retaining walls, piles, multi-layer composite liners, geotextiles, and more. Liner design tools include support capacity plots, which allow you to determine the safety factor of reinforced liners. Bolt types include end anchored, fully bonded, cable bolts, split sets, and grouted tiebacks. Liners include Simple liners a single layer of shotcrete, Composite Liners of multiple layers of material, Pile walls of a structural beam element with a joint on both sides, Geosynthetic support such as geogrids and geotextiles, Reinforced concrete, Cable Truss and Struts. Liners may consist of beam elements which can resist axial, bending and shear forces, or truss elements which only possess axial properties.

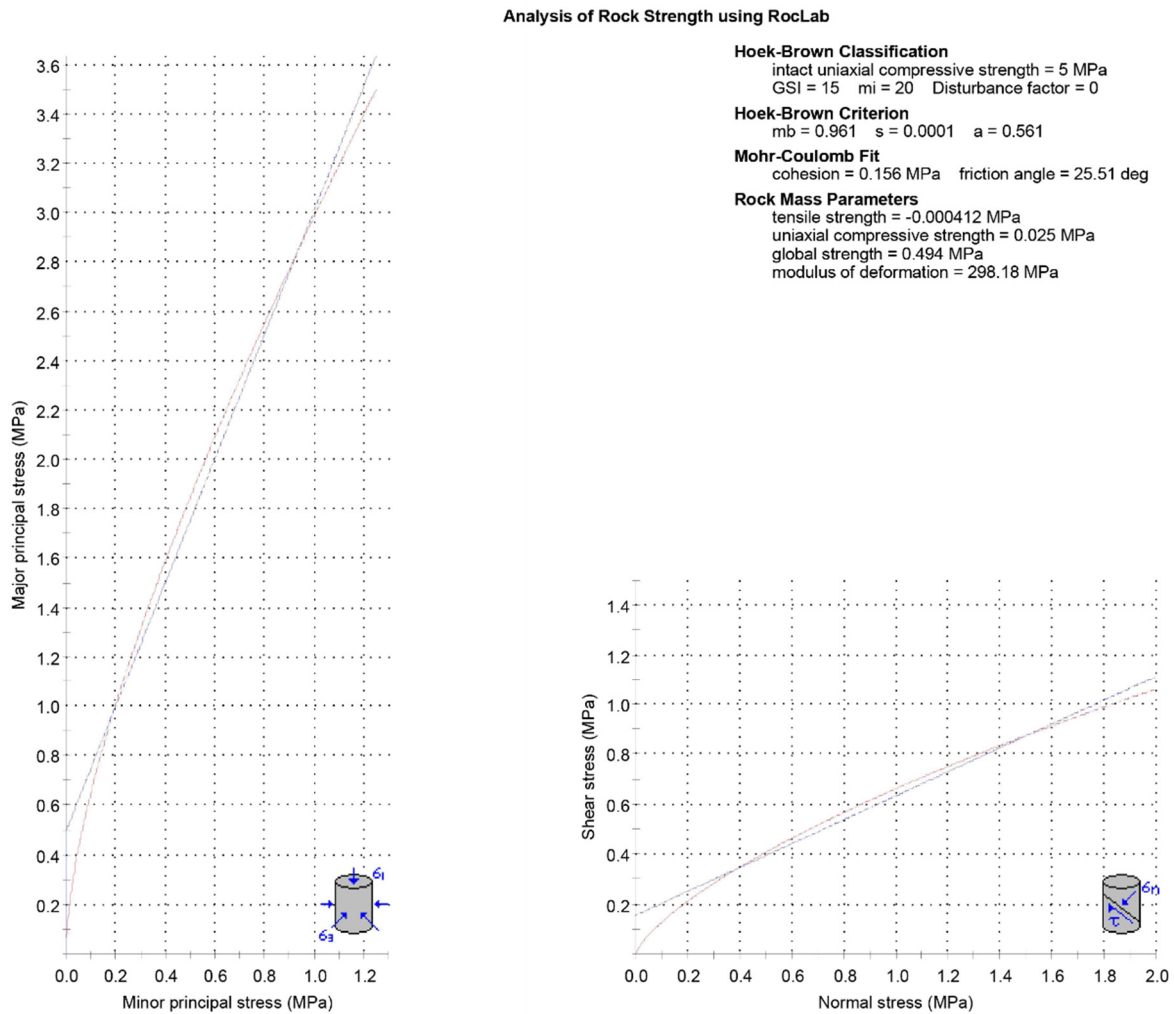


Figure 4-2 Analysis of Rock Strength of Grouted rock mass using Roclab

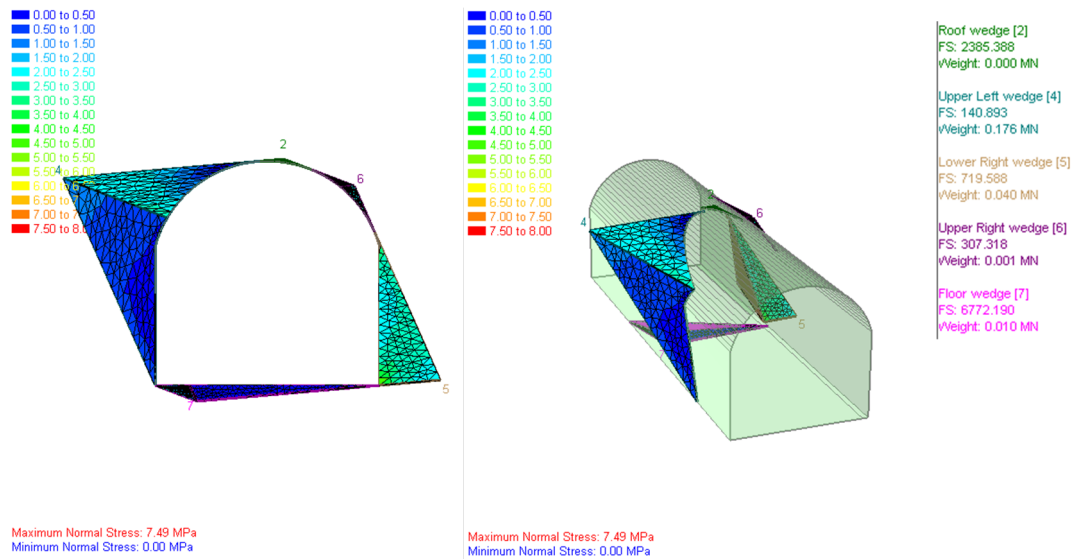


Figure 4-3 Normal stress distribution in perimeter wedge at chainage of 200 to 400 m of adit tunnel of Modi Khola Hydropower Project.

Procedure of modelling in RS2

Following is the procedure which is followed for the design of tunnel support in faulted rock mass of Modi Khola Hydropower Project with 2D modelling in RS2

i. Determination of Parameters:

First of all, geotechnical investigation is done to obtain the geology of selected case study. Then, parameters representing mechanical strength properties of rock mass are obtained by the Generalized Hoek-Brown failure criterion or Mohr-Coulomb. Similarly, the ground water table, in-situ stress on the basis of the topography and seismicity is determined. For the ground water the piezometric lines the pore fluid pressure has been taken as 0.00981 MN/m^3 .

ii. Boundary Conditions

The diameter of tunnel, fault thickness, fault orientation, strength parameters of faulted rock mass on the basis of Mohr-Coulomb are obtained. The size of model is made with expansion of six times tunnel diameter with hinged support at the external of model boundary, i.e. restrained at x and y direction. For the modelling of fault boundary, displacement of 120 mm has been assumed in South to North orientation. Assumption has been made based on the GPS measurements by Ader et al., 2012 and number of years since large stress release event in Nepal Himalaya i.e., 25th April, 2015 Gorkha earthquake. There is average movement of fault at the rate of 20 mm / year in major thrust zone (Ader et al., 2012). So, total displacement of 120 mm has been assumed (i.e., average fault movement times number of years since 2015 Gorkha Earthquake)

iii. Three-dimensional Effect

Internal pressure reduction method has been used with total of 15 number of stages. Internal Pressure have been reduced linearly with respect to field induced stress in 15 stages to represent three dimensional tunneling and support installation procedure.

iv. Meshing

The modelling is done with mesh type of three noded graded triangles with gradation factor of 0.1.

v. Analysis Method

The analysis has been done using plane strain analysis with Gaussian elimination as the solver. For the stress analysis number of maximum iterations taken is 500 with tolerance of 0.001 with convergence type of absolute energy method. It has been taken that the tensile failure reduces the shear strength to zero when there is shear failure. Also, joint tension reduces the joint stiffness by the factor of 0.01.

vi. Rock mass model

For numerical modeling of rock mass in Nepal Himalaya, finite element model suggested by Khadka, 2019 has been used. For extremely poor rock mass, i.e., GSI less than 30, the elastic-perfectly- plastic failure model is more appropriate with the disturbance factor taken as zero. It is found that the disturbance factor has great influence on the modeling of such weak rock mass in the Himalayan region. For the rock mass for which the GSI value is greater than 30, the strain-softening failure model is more appropriate in this region. In this case, the disturbance factor is taken as 0.5. In strain- softening, the residual value is considered by lowering the peak GSI value which represented crushing of the intact rock and wearing joint surface roughness. For very poor to moderately jointed and weathered rock mass ($30 < \text{GSI} < 50$), the residual strength parameters are taken between 60 and 70 % of peak values while for fair to good, jointed rock ($50 < \text{GSI} < 60$), the residual strength parameters are taken between 40 and 50% of peak values.

Cai et al., 2007, emphasized that the peak and residual strength understanding of the rock mass strength behavior will guide in effective design of tunnel support. Hoek, (2007) suggested different post failure characteristics for different quality of rock masses. Very good quality hard rock mass has elastic-brittle behavior, average quality rock mass has strain-softening behavior, and very poor-quality rock mass has elastic-plastic failure behavior. These behaviors are shown in Figure 4-4.

vii. Support in Faulted rock mass

For the support of tunnel in the faulted rock mass, Elastic standard beam liner type with sliding gap with strain locking is used to model a liner which has flexural rigidity, i.e., resistance to bending such as a

simple shotcrete or concrete liner. A Standard Beam liner is made up of "beam elements" which can respond to flexural, axial, compressive, tensile, and shear loads. For a Standard Beam liner there are two ways of defining the liner cross-section: thickness or area and moment of inertia. Thickness method have been used with a constant cross-section, and uniform properties layer. The liner axial and flexural properties is based on a cross-sectional area = Thickness x 1 (unit width).

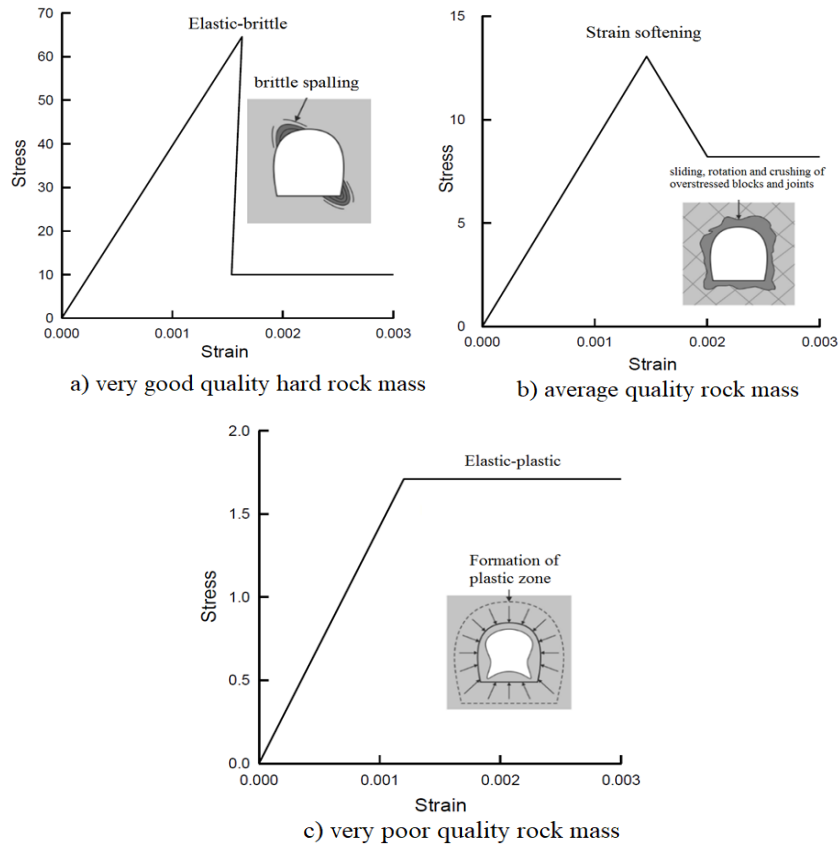


Figure 4-4 Suggested post failure characteristics for different quality of rock mass and tunnel behavior (Hoek, 2007 and Lorig, et al. 2013)

Sliding Gap

The Sliding Gap option has been used a specialized option for modeling excess deformation due to the fault movement or rupture as a type of support system. This type of support system incorporates one freely sliding joint(s), which allow support to freely close in the circumferential direction, until a pre-determined gap has been closed. After the gap closes, the support locks and axial load can be transmitted through the liner.

Mechanism of strain at Locking

In RS2 the length of the sliding gap is specified in terms of an equivalent circumferential strain in the liner.

The value of strain at locking depends on the length of liner you are considering. for a fully lined, circular tunnel of 6 meter diameter, and a total Sliding Gap = 1 meter, the Strain at Locking = $100/(\pi \times 6)$ % = 5.3 %. If more than one sliding gap exists, then add up the total gap length, and divide by the total liner length, to determine the Strain at Locking.

4.2.1 Validation of Numerical Model of Tunnel in Faulted Rock mass in RS2

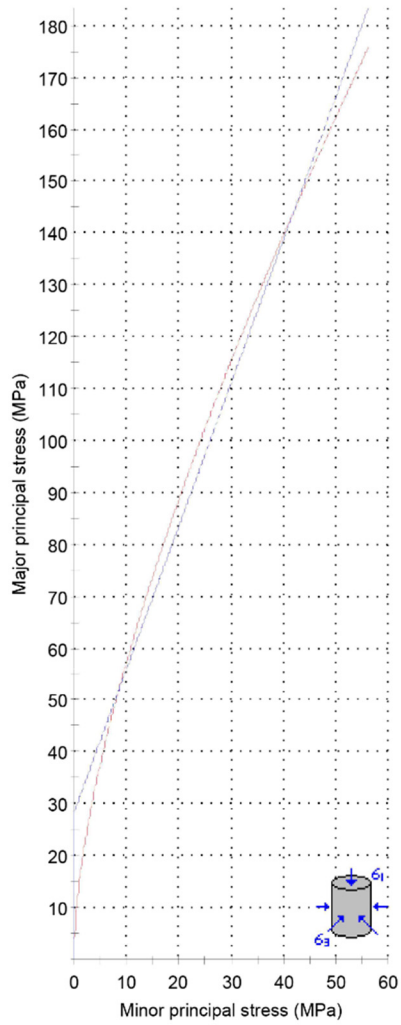
In order to use RS2 as a tool of numerical modelling of tunnel in faulted rock mass its validation have been done by comparing deformation modelled with the field measurement. For this purpose a tunnel section of pressure tunnel at 65 m upstream of Adit-2 of Modi Khola Hydroelectric Project in the vicinity of fault have been modeled (Figure 4-10).

Finite Element model of tunnel have been done using elastic plastic plain strain analysis. The behavior of the rock mass after yielding can only be simulated with the plastic deformations (Cai et al, 2007). Hence, the elastic plastic analysis has been done. Heading and benching have been used for the excavation of tunnel by incorporating the three dimensional effect (i.e, number of stages with field stress vector in decreasing order). The rock mass is composed of Phyllitic Schists, Colluvial deposits, Alluvial deposits, Phyllitic quartzite, Conglomerate, Quartzite. The mechanical parameters are listed in Table 3-1.

Field stress, $\sigma_1 = 2.08$ MPa, $\sigma_3 = 1.33$ MPa, $\sigma_2 = 1.33$ MPa has been taken as given by Chhushyabaga et al., 2020. It has been done based on the back calculation by Shrestha and Panthi, 2014 in faulted Modi Khola Pressure Tunnel. They calculate the principal stresses $\sigma_1=2.08$ MPa and $\sigma_3=1.33$ MPa which is similar to the values $\sigma_1=2.08$ MPa and $\sigma_3=1.39$ MPa given by Eq.(2.7) suggested by Jaeger and Cook in 1971. Eq.(2.7) is obtained from 2D Faulting theory which assumes that the failure is only a function of the difference between the principal stresses σ_1 and σ_3 (Zoback,1992).

For the estimation of the rock mass properties of headrace tunnel of Modi Khola Hydroelectric project, RocLab has been used with Generalized Hoek and Brown failure criteria (2002) and equivalent Mohr Coulomb fit. The procedure of using RocLab has been explained in 4.2 (a). The rock mass parameters of quartzite, fault Core, phyllitic schist, phyllitic quartzite, conglomerate, and grouted rock mass have been obtained with the failure envelope of Mohr Column failure Criteria and Generalized Hoek Brown Failure Criteria. Figure 4-5 shows analysis of rock strength of Quartzite, Figure 4-6 shows analysis of rock strength of faulted rock mass, Figure 4-7 shows analysis of rock strength of Phyllitic Schists, Figure 4-8 shows analysis of rock strength of phyllitic quartzite,

Analysis of Rock Strength using RocLab



Hoek-Brown Classification

intact uniaxial compressive strength = 225 MPa
 GSI = 22 $m_i = 20$ Disturbance factor = 0

Hoek-Brown Criterion

$m_b = 1.234$ $s = 0.0002$ $a = 0.538$

Mohr-Coulomb Fit

cohesion = 8.529 MPa friction angle = 27.87 deg

Rock Mass Parameters

tensile strength = -0.031 MPa
 uniaxial compressive strength = 2.120 MPa
 global strength = 28.320 MPa
 modulus of deformation = 1995.26 MPa

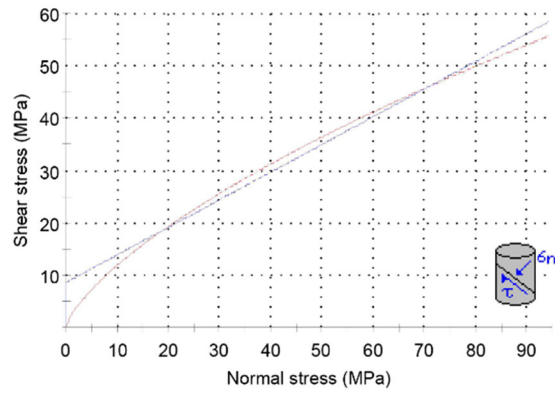
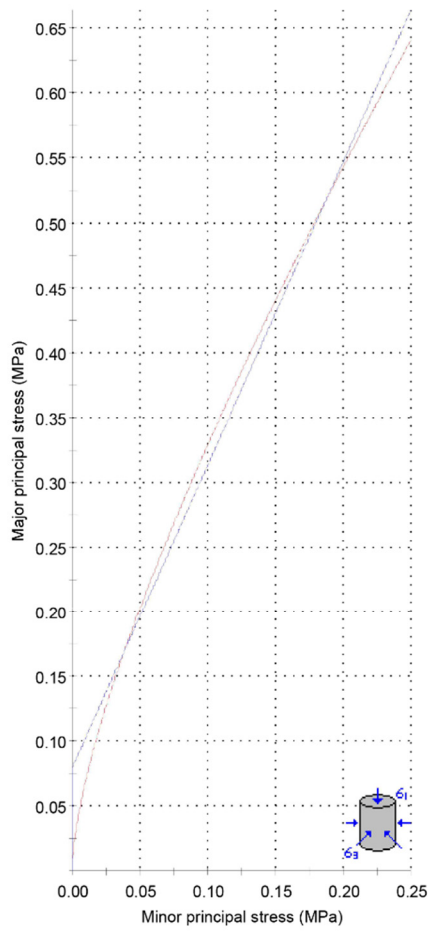


Figure 4-5 Analysis of Rock Strength of Quartzite using Roclab

Analysis of Rock Strength using RocLab



Hoek-Brown Classification

intact uniaxial compressive strength = 1 MPa
 GSI = 10 $m_i = 20$ Disturbance factor = 0

Hoek-Brown Criterion

$m_b = 0.804$ $s = 4.54e-5$ $a = 0.585$

Mohr-Coulomb Fit

cohesion = 0.026 MPa friction angle = 23.65 deg

Rock Mass Parameters

tensile strength = $-5.65e-5$ MPa
 uniaxial compressive strength = 0.003 MPa
 global strength = 0.079 MPa
 modulus of deformation = 100.00 MPa

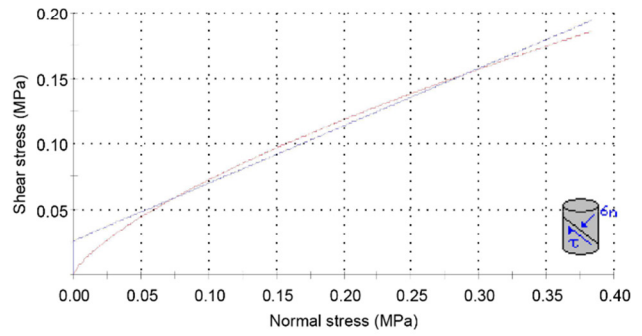
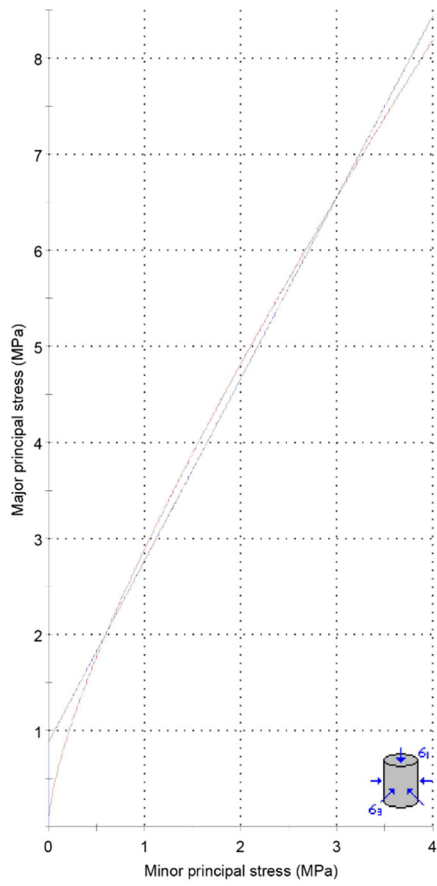


Figure 4-6 Analysis of Rock Strength of faulted rock mass using Roclab

Analysis of Rock Strength using RocLab



Hoek-Brown Classification
 intact uniaxial compressive strength = 16 MPa
 GSI = 12 mi = 9 Disturbance factor = 0

Hoek-Brown Criterion
 mb = 0.388 s = 0.0001 a = 0.575

Mohr-Coulomb Fit
 cohesion = 0.320 MPa friction angle = 17.94 deg

Rock Mass Parameters
 tensile strength = -0.002 MPa
 uniaxial compressive strength = 0.058 MPa
 global strength = 0.881 MPa
 modulus of deformation = 448.81 MPa

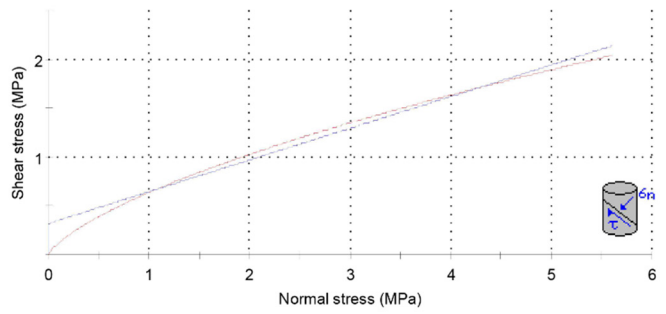
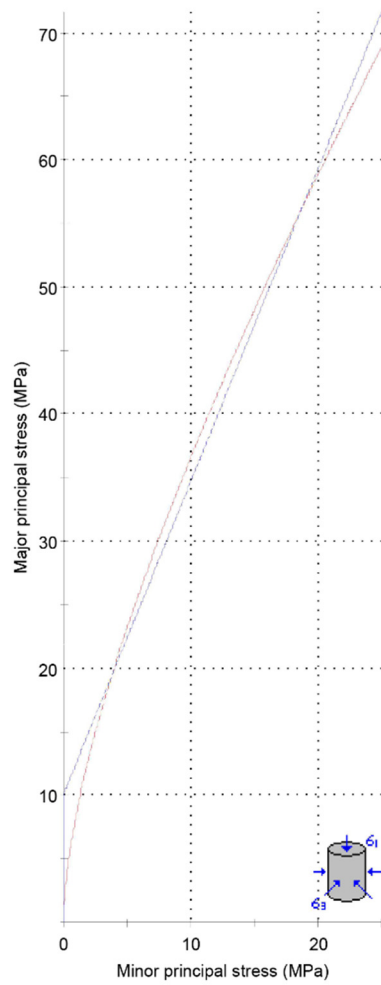


Figure 4-7 Analysis of Rock Strength of Phyllitic Schists mass using Roclab

Analysis of Rock Strength using RocLab



Hoek-Brown Classification

intact uniaxial compressive strength = 100 MPa
 GSI = 19 mi = 16 Disturbance factor = 0

Hoek-Brown Criterion

mb = 0.887 s = 0.0001 a = 0.547

Mohr-Coulomb Fit

cohesion = 3.226 MPa friction angle = 24.97 deg

Rock Mass Parameters

tensile strength = -0.014 MPa
 uniaxial compressive strength = 0.729 MPa
 global strength = 10.121 MPa
 modulus of deformation = 1678.80 MPa

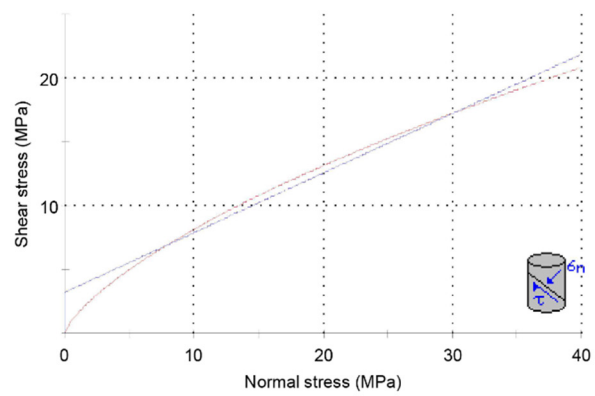
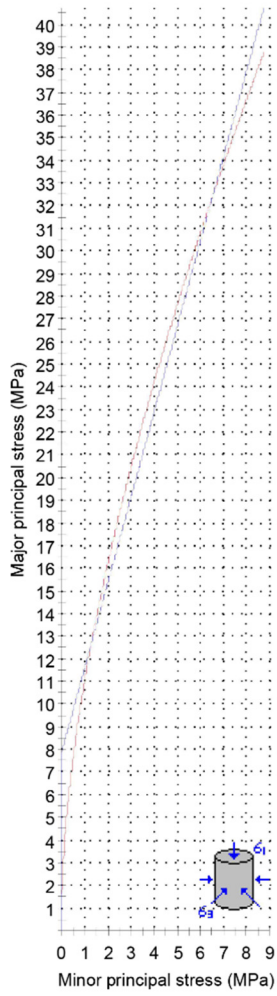


Figure 4-8 Analysis of Rock Strength of Phyllitic Quartzite using Roclab

Analysis of Rock Strength using RocLab



Hoek-Brown Classification
 intact uniaxial compressive strength = 35 MPa
 GSI = 45 $m_i = 21$ Disturbance factor = 0

Hoek-Brown Criterion
 $m_b = 2.945$ $s = 0.0022$ $a = 0.508$

Mohr-Coulomb Fit
 cohesion = 2.032 MPa friction angle = 35.41 deg

Rock Mass Parameters
 tensile strength = -0.026 MPa
 uniaxial compressive strength = 1.569 MPa
 global strength = 7.877 MPa
 modulus of deformation = 4436.43 MPa

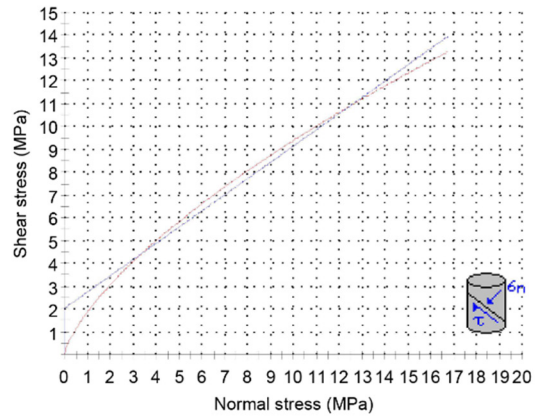


Figure 4-9 Analysis of Rock Strength of Conglomerate using Roclab

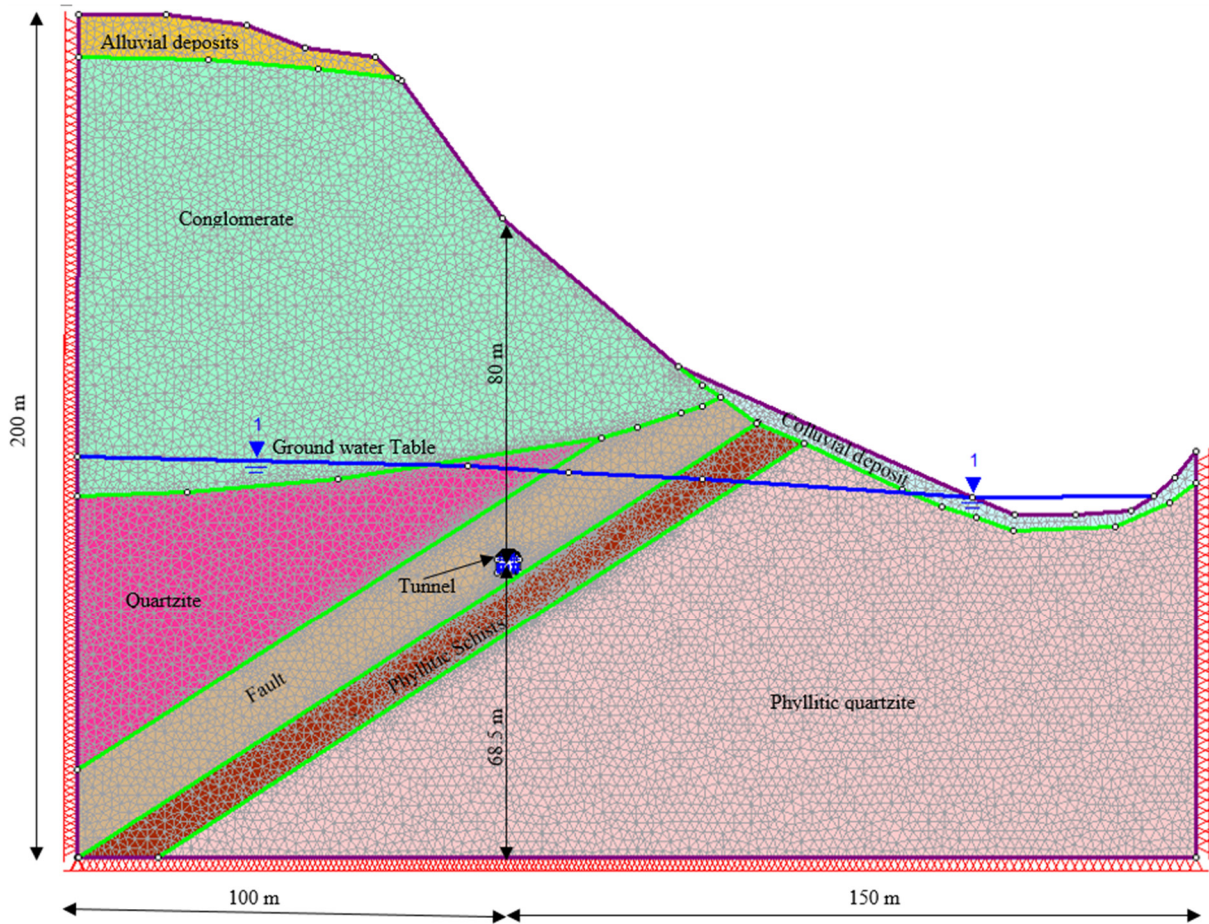


Figure 4-10 2D Model of Pressure Tunnel of Modi Khola Hydropower Project in RS2

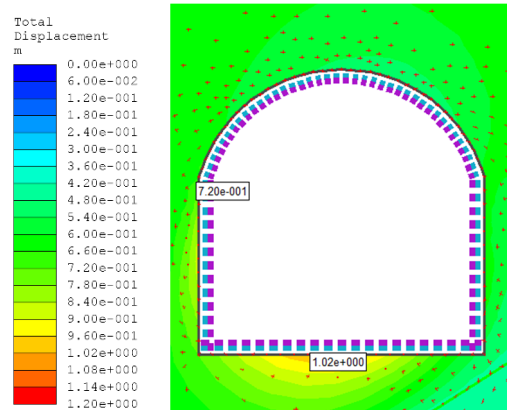


Figure 4-11 Deformation obtained in Pressure tunnel of Modi Khola Hydropower project

Deformation in pressure tunnel of Modi Khola Hydroelectric Project in faulted geology have been measured. The measured deformation at hill side spring line and hill side bottom are 0.7 m and 0.96 m respectively (Himal Hydro, 2001). Hence, comparison of the deformation obtained from numerical

modelling and field measurement have been done for the validation. The modelled deformation at hill side spring line and hill side bottom are 0.688 m and 1.01 m respectively (Figure 4-11). The obtained deformations from the modelling and the measured deformations are similar to each other. There is variation of 1.71 % and 5.2 % of modelled deformation with field measured deformations. Hence, we can conclude that the modelling of tunnel in faulted rock mass in RS2 gives the result at reasonable accuracy. Therefore, the study of the effect of the fault in tunnel can be done.

4.2.2 Numerical Modelling in RS2

The stability of the tunnel and surrounding rock mass are predominately affected by fault around tunnel. A good understanding of fault in surrounding rock mass of tunnel is very vital. In tunnelling, distribution and thickness of fault are important factors in the stability of rock mass (Zhang et. al., 2017). To study the influence of fault in tunneling, Finite Element Models were developed in RS2 in which location of the fault, its orientation, were varied for three different cross sections such as circular, inverted-D and horseshoe.

The tunnel sections are divided into six segments such as Crown, Left Shoulder, Right Shoulder, Invert, Right Side Wall, and Left Side Wall. When the fault of thickness ‘T’ is located in perpendicular distance of ‘D_s’ from a section of the tunnel, a name of fault is assigned with corresponding section.

For example: if a fault is located in crown segment it has been defined as the crown fault (Fig. 4-12 (b)). Similarly, the definition of other faults is done as follows: If a fault is located in Left Shoulder segment it has been defined as the Left Shoulder Fault (Fig. 4-12 (d)). If a fault is located in Right Shoulder segment it has been defined as the Right Shoulder Fault (Fig. 4-12 (c)). If a fault is located in Invert segment it has been defined as the Invert Fault (Fig. 4-12 (f)). If a fault is located in Right Side Wall segment it has been defined as the Right Side Wall fault (Fig. 4-12 (e)). If a fault is located in Left Side Wall segment it has been defined as Left Side Wall fault (Fig. 4-12 (a)). If a fault is located in Left Bottom segment it has been defined as the Left Bottom Fault (Fig. 4-12 (g)). If a fault is located in Right Bottom segment it has been defined as the Right Bottom Fault (Fig. 4-12 (h)).

It has been for all three sections of inverted-D, circular, and horseshoe and it is illustrated in Figure 4-12, Figure 4-13, and Figure 4-14. Figure 4-12 show the definition and distribution of fault in inverted D tunnel. Similarly, Figure 4-13 show the definition and distribution of fault in circular tunnel. Figure 4-14 show the definition and distribution of fault in horseshoe tunnel. Diameter of tunnel ‘D’ is taken as 5.1 m with the distance of fault from tunnel, $D_s = 0.1 D$ equal to 0.51 m. and thickness of the fault ‘T’ of 0.51 m. Key points are defined as the mid point of tunnel sections such as Crown, Left Shoulder, Right Shoulder, Invert, Right Side Wall, Left Side Wall, Left Bottom and Right Bottom. They are named as A, B, C, D, E, F, G, H, I, J, K and L for circular, Inverted-D and horseshoe. These key points have been divided on the basis of

the distance of a locus of a point in the circumference of tunnel in anticlockwise direction. The displacement and stress in key points such as crown, invert, shoulders, walls on the tunnel limit are chosen to be analyzed as the representative of the displacement and stress of the tunnel (Zhang et. al., 2017). The influence has been studied in key points on the terms of displacements field, plastic zone in rock mass and internal forces such as shear force, axial force and bending moment in tunnel. Elastic Concrete beam liner of thickness 0.3 m and grade 25 MPa is taken as the tunnel support.

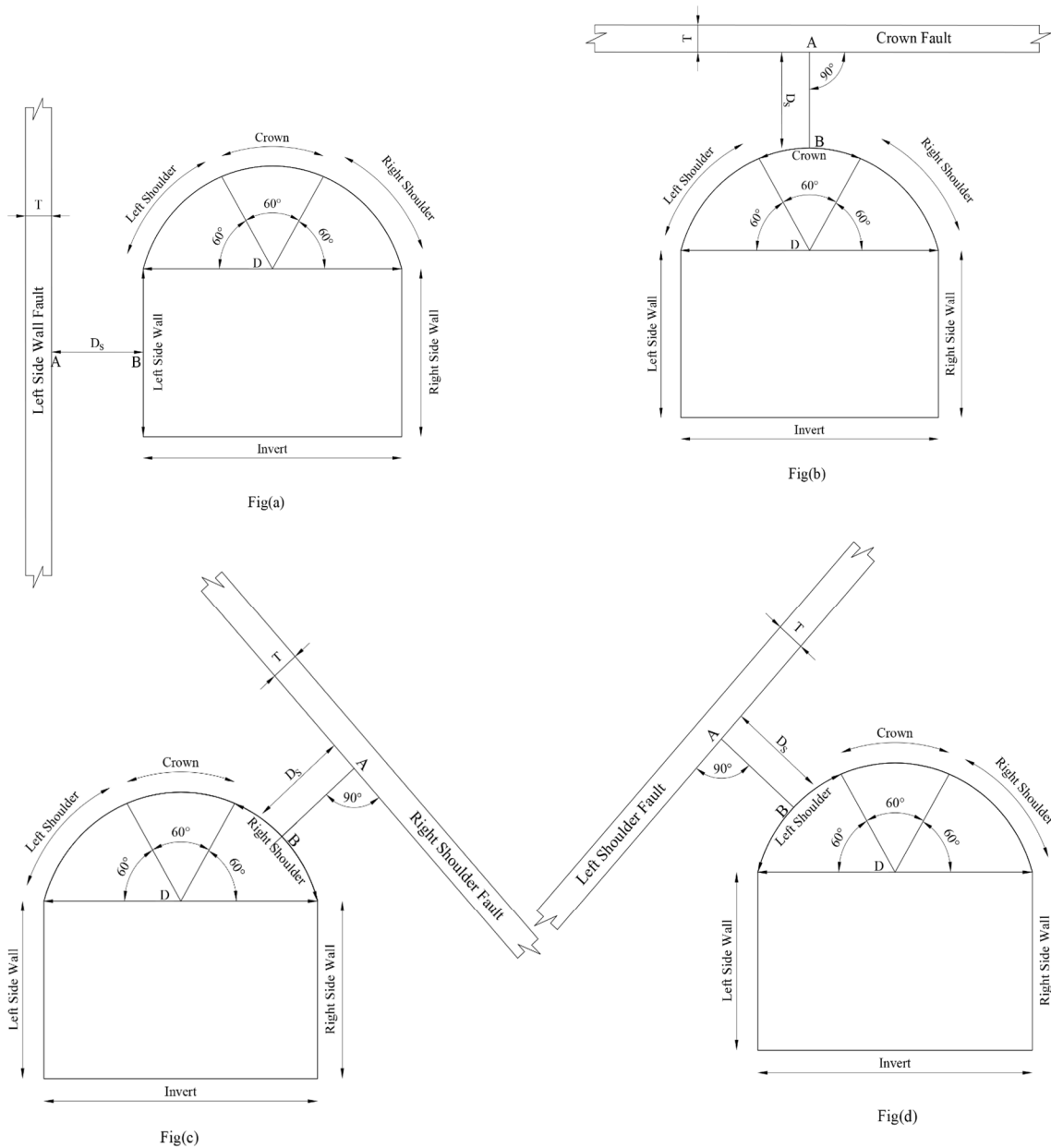
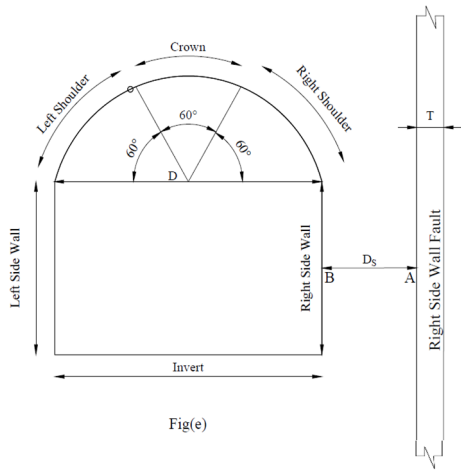
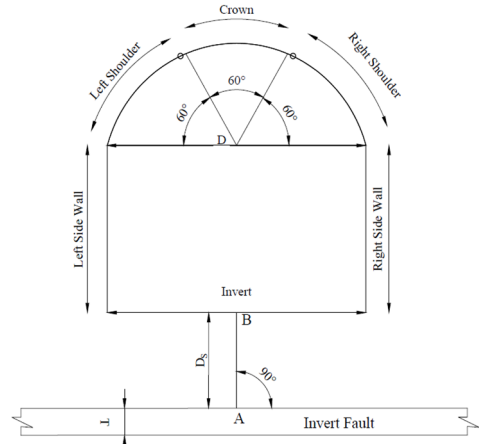


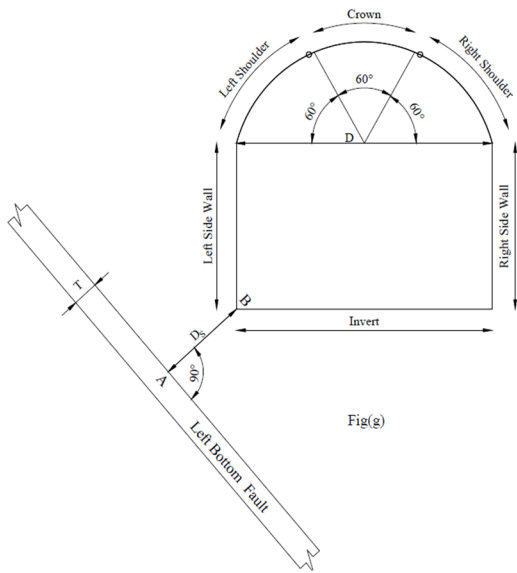
Figure 4-12 a. Definition and Distribution of Fault in Inverted D Tunnel



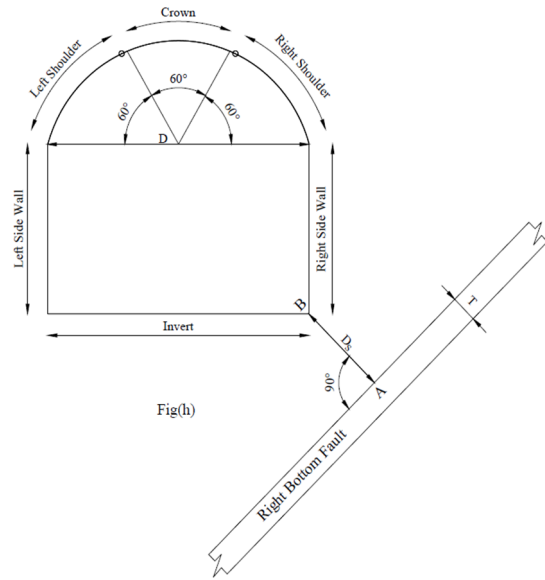
Fig(e)



Fig(f)



Fig(g)



Fig(h)

Figure 4-12 b. Definition and Distribution of Fault in Inverted D Tunnel

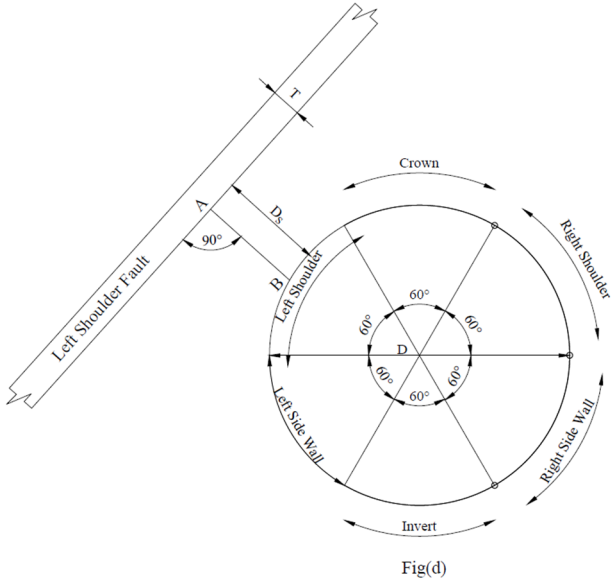
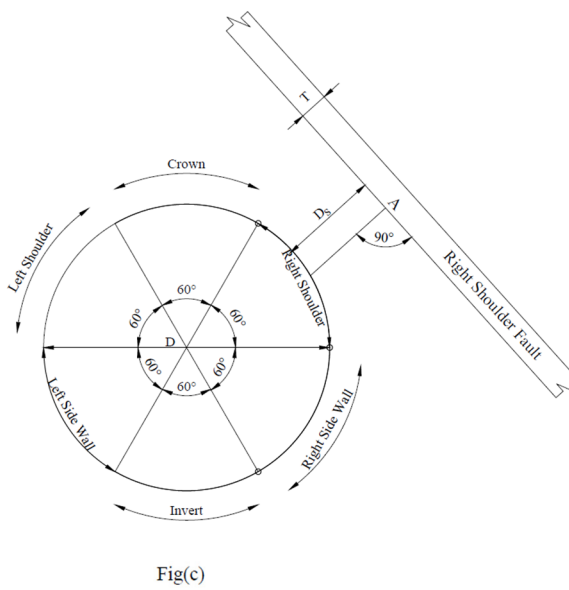
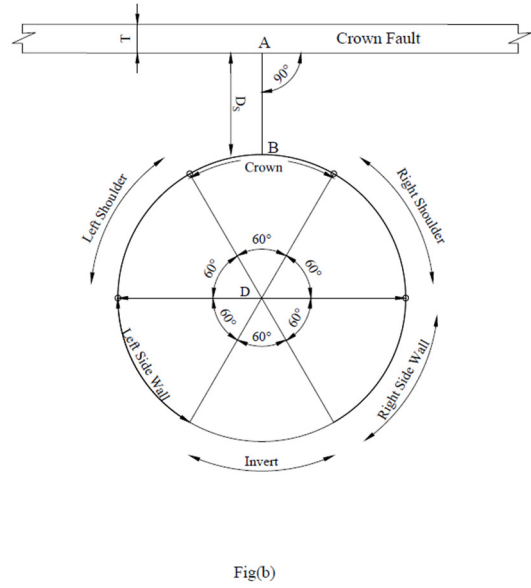
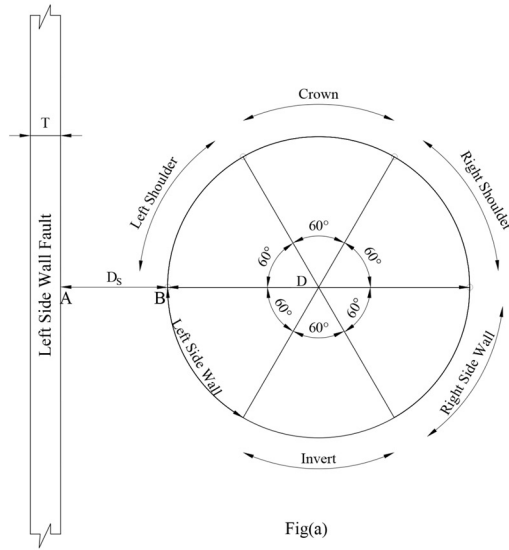


Figure 4-13 a. Definition and Distribution of Fault in Circular Tunnel

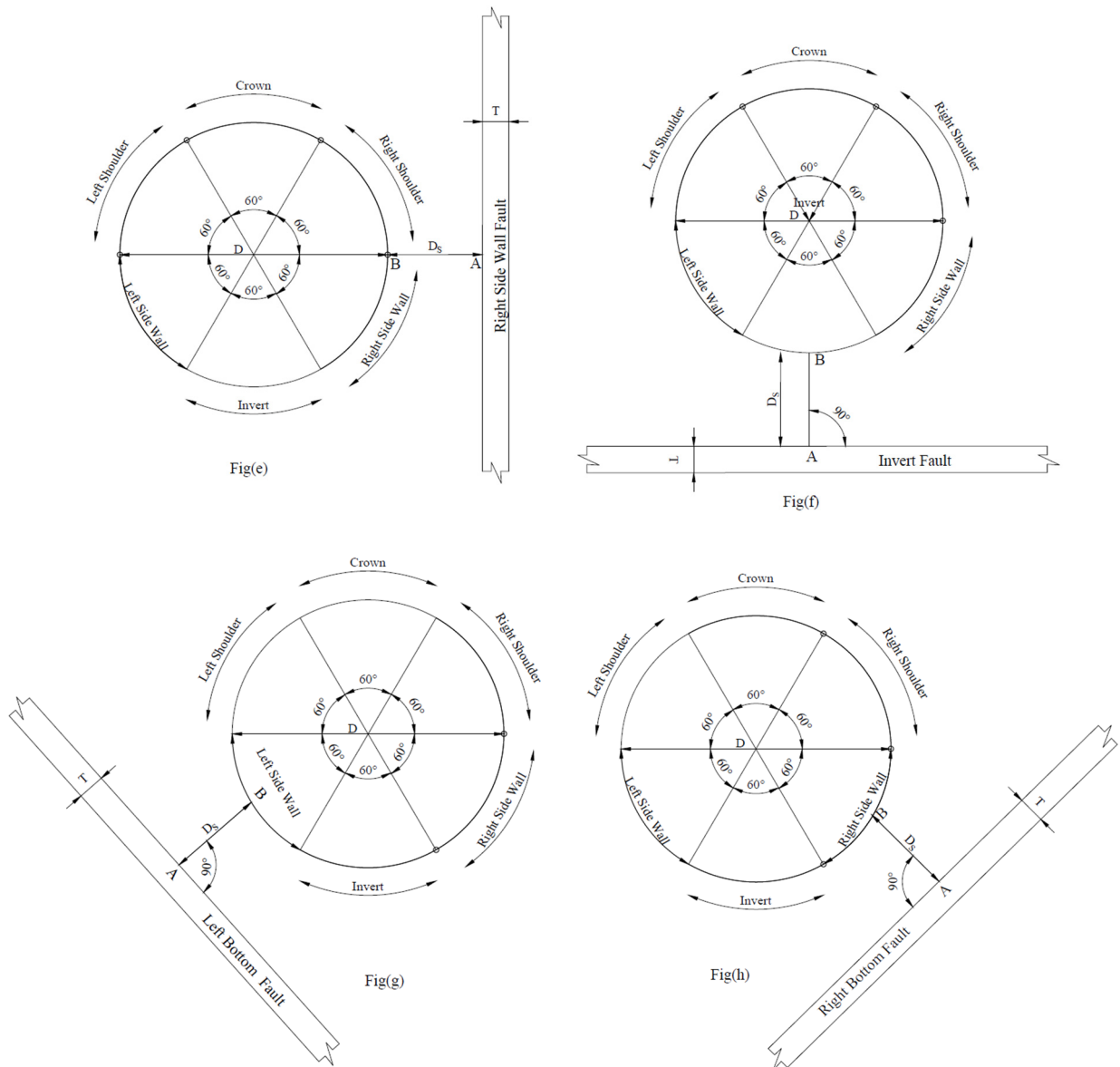


Figure 4-13 b. Definition and Distribution of Fault in Circular Tunnel

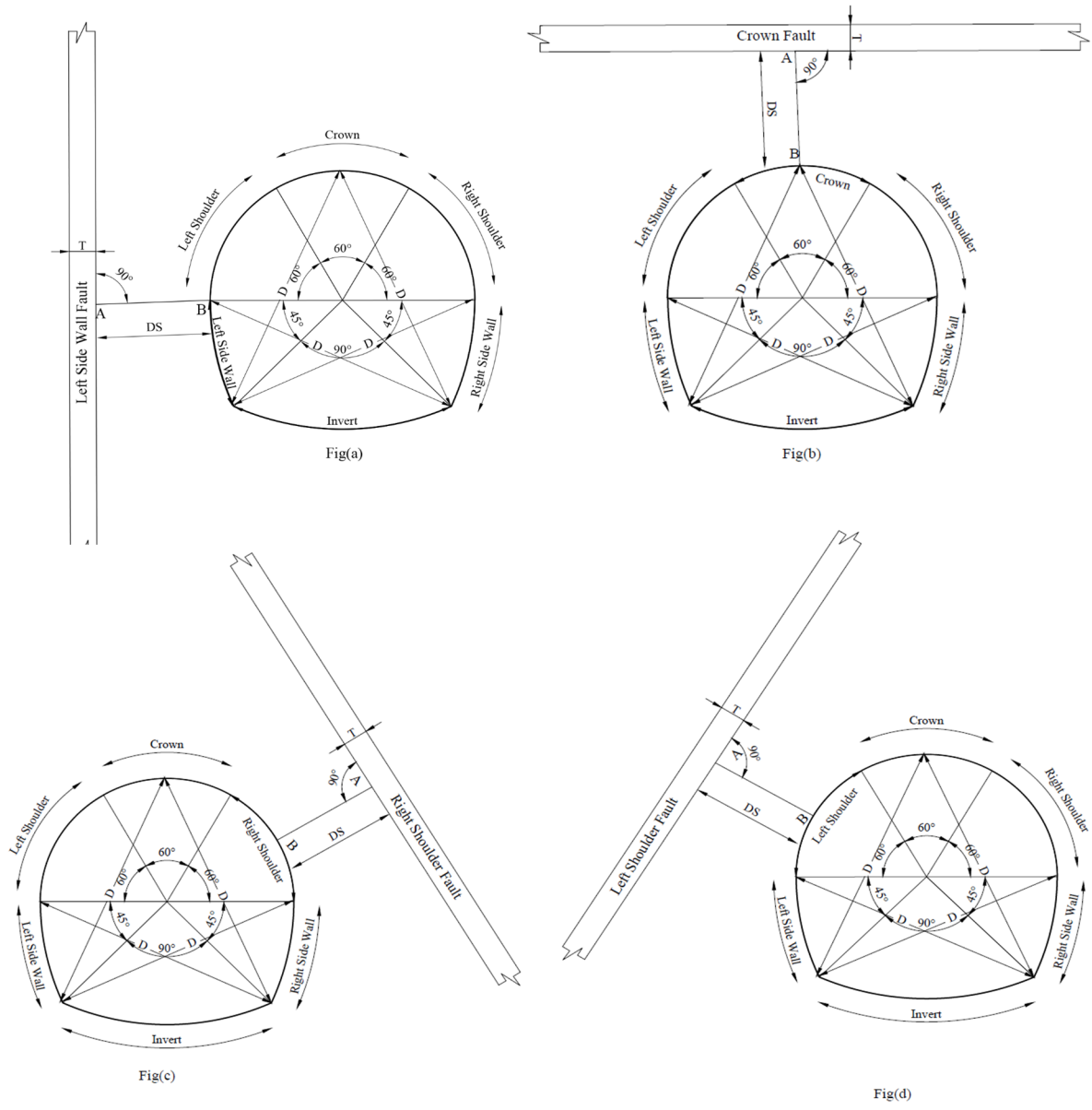


Figure 4 14 a. Definition and Distribution of Fault in Horseshoe Tunnel

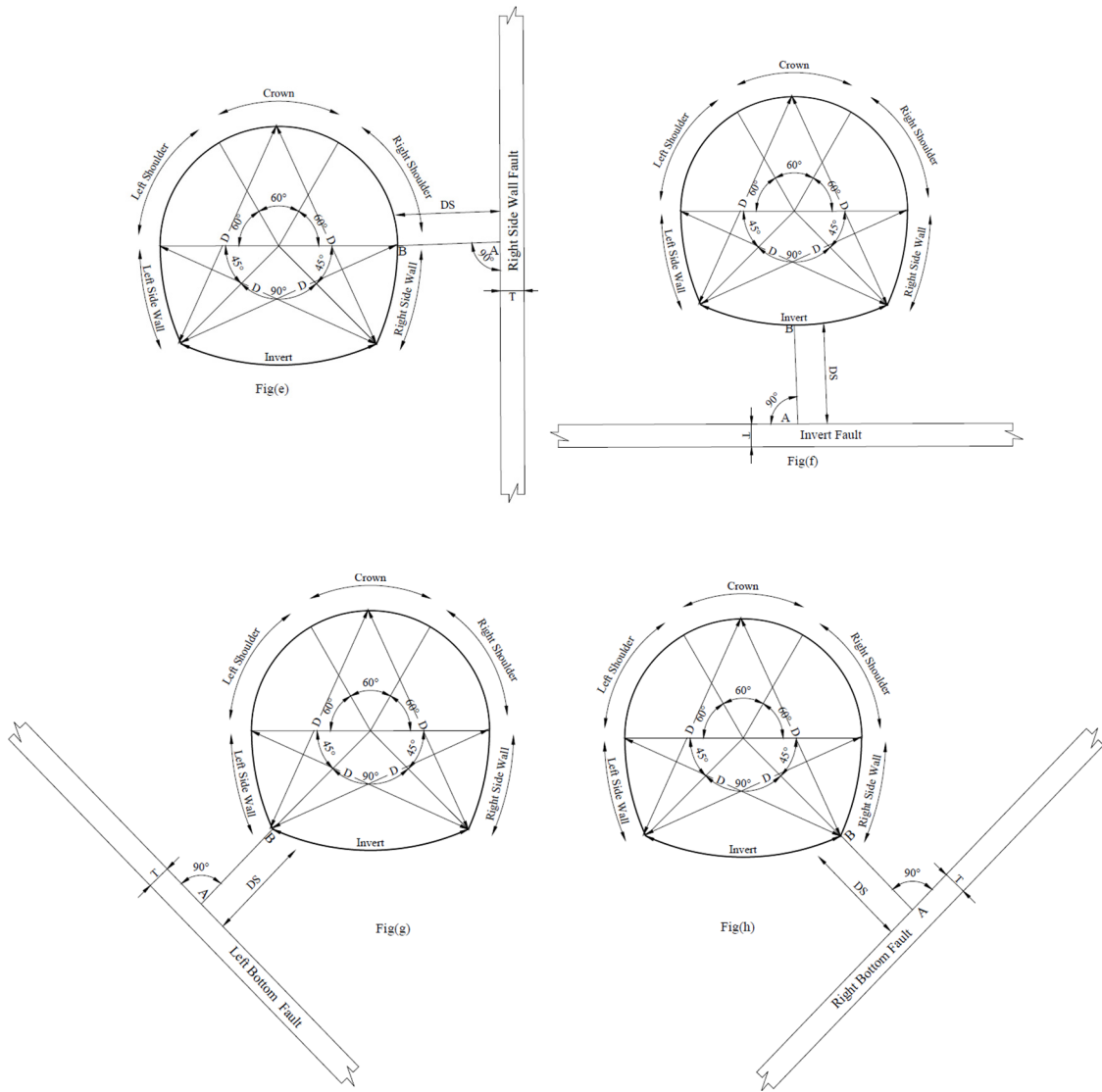


Figure 4-14 b. Definition and Distribution of Fault in Horseshoe Tunnel

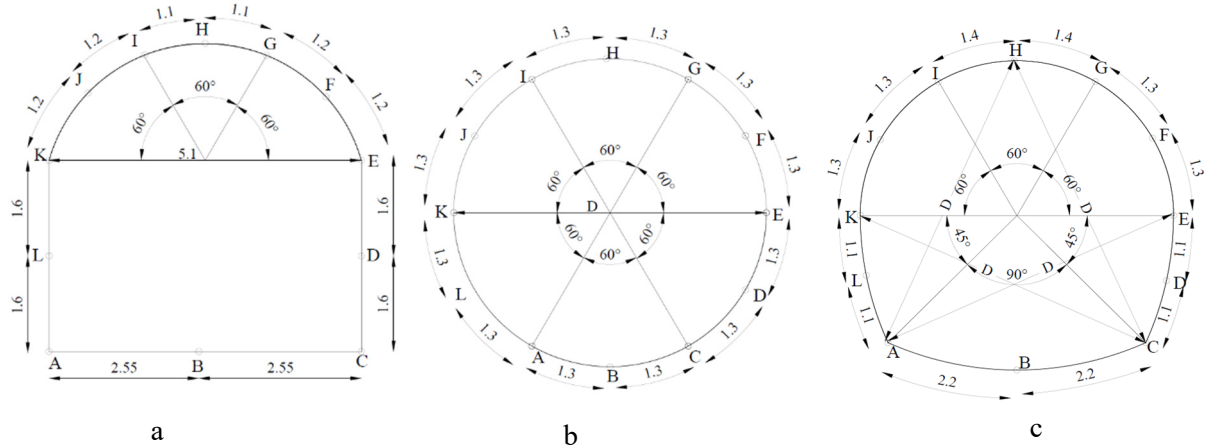


Figure 4-15 Key points are in inverted D(a), Circular (b) and Horseshoe (c) tunnel sections

Similarly, a ratio parameter has been defined for displacement, shear force, axial force and bending moment at key points of tunnel lining to study the influence of the fault. It is defined as:

$$\text{Ratio} = \frac{\text{displacement or shear force or axial force or bending moment at key points of tunnel lining with fault}}{\text{displacement or shear force or axial force or bending moment at key points of tunnel lining without fault}}$$

For displacement, RC_d is displacement ratio due to crown fault, RLS_d is displacement ratio due to left shoulder fault, RRS_d is displacement ratio due to right shoulder fault, RI_d is displacement ratio due to invert fault, $RRSW_d$ is displacement ratio due to right side wall fault, $RLSW_d$ is displacement ratio due to left side wall fault, RLB_d is displacement ratio due to left bottom fault, and RRB_d is displacement ratio due to right bottom fault.

For shear force, RC_s is shear force ratio due to crown fault, RLS_s is shear force ratio due to left shoulder fault, RRS_s is shear force ratio due to right shoulder fault, RI_s is shear force ratio due to invert fault, $RRSW_s$ is shear force ratio due to right side wall fault, $RLSW_s$ is shear force ratio due to left side wall fault, RLB_s is shear force ratio due to left bottom fault, and RRB_s is shear force ratio due to right bottom fault

Similarly, for axial force, RC_a is axial force ratio due to crown fault, RLS_a is axial force ratio due to left shoulder fault, RRS_a is axial force ratio due to right shoulder fault, RI_a is axial force ratio due to invert fault, $RRSW_a$ is axial force ratio due to right side wall fault, $RLSW_a$ is axial force ratio due to left side wall fault, RLB_a is axial force ratio due to left bottom fault, and RRB_a is axial force ratio due to right bottom fault

Similarly, for bending moment, RC_m is bending moment ratio due to crown fault, RLS_m is bending moment ratio due to left shoulder fault, RRS_m is bending moment ratio due to right shoulder fault, RI_m is bending moment ratio due to invert fault, $RRSW_m$ is bending moment ratio due to right side wall fault,

RLSW_m is bending moment ratio due to left side wall fault, RLB_m is bending moment ratio due to left bottom fault, and RRB_m is bending moment ratio due to right bottom fault

The mechanical and strength parameters of faulted and surrounding rock mass (Table 3-1) are estimated from using Mohr Columnb failure criteria in RocLab as the procedure explained in section 4.2. The modelling procedure described in 4.2(c) have been used to model in RS2. Figure 4-16 show circular tunnel with left side wall fault. Similarly, Figure 4-17 show horseshoe tunnel with crown fault. Figure 4-18 show inverted D tunnel with right shoulder fault in RS2.

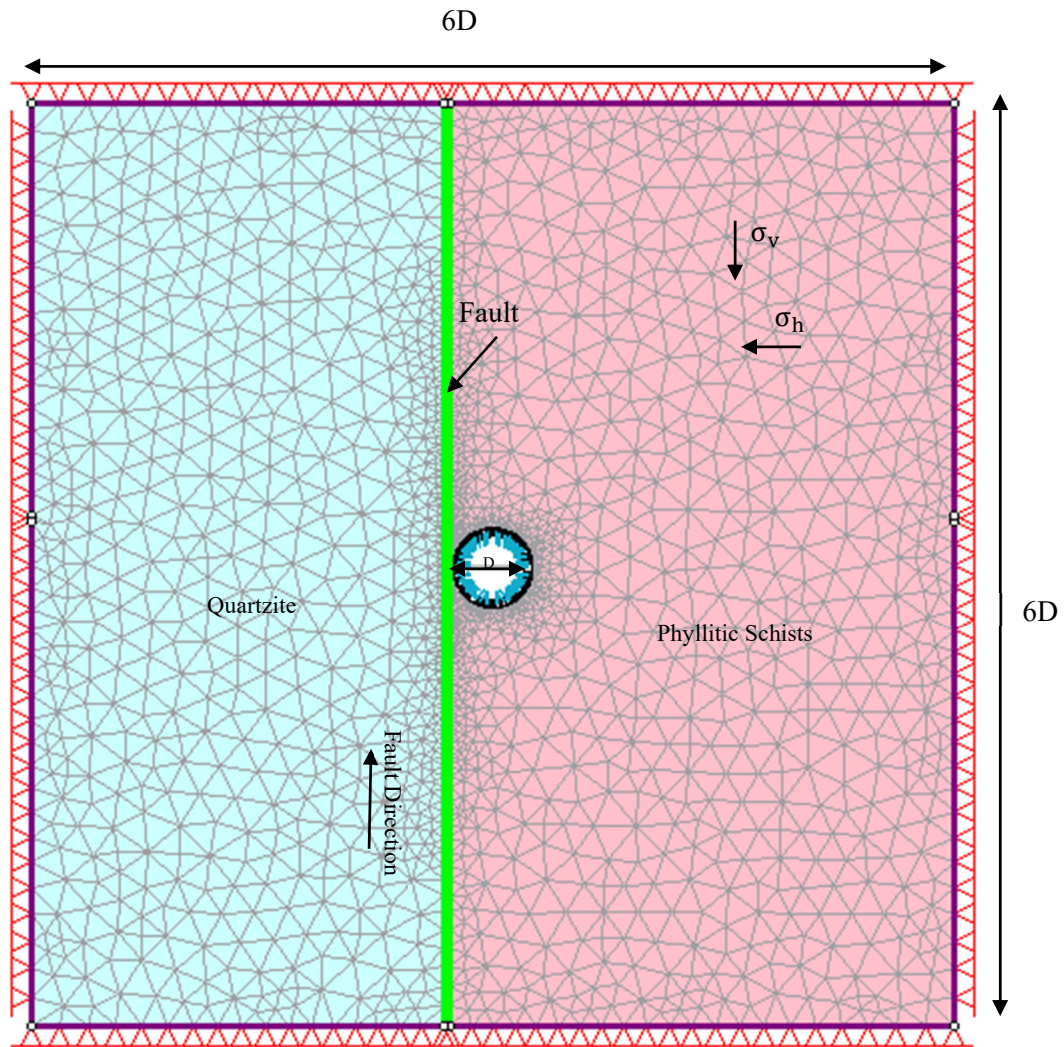


Figure 4-16 Circular Tunnel with Left Side Wall Fault in RS2

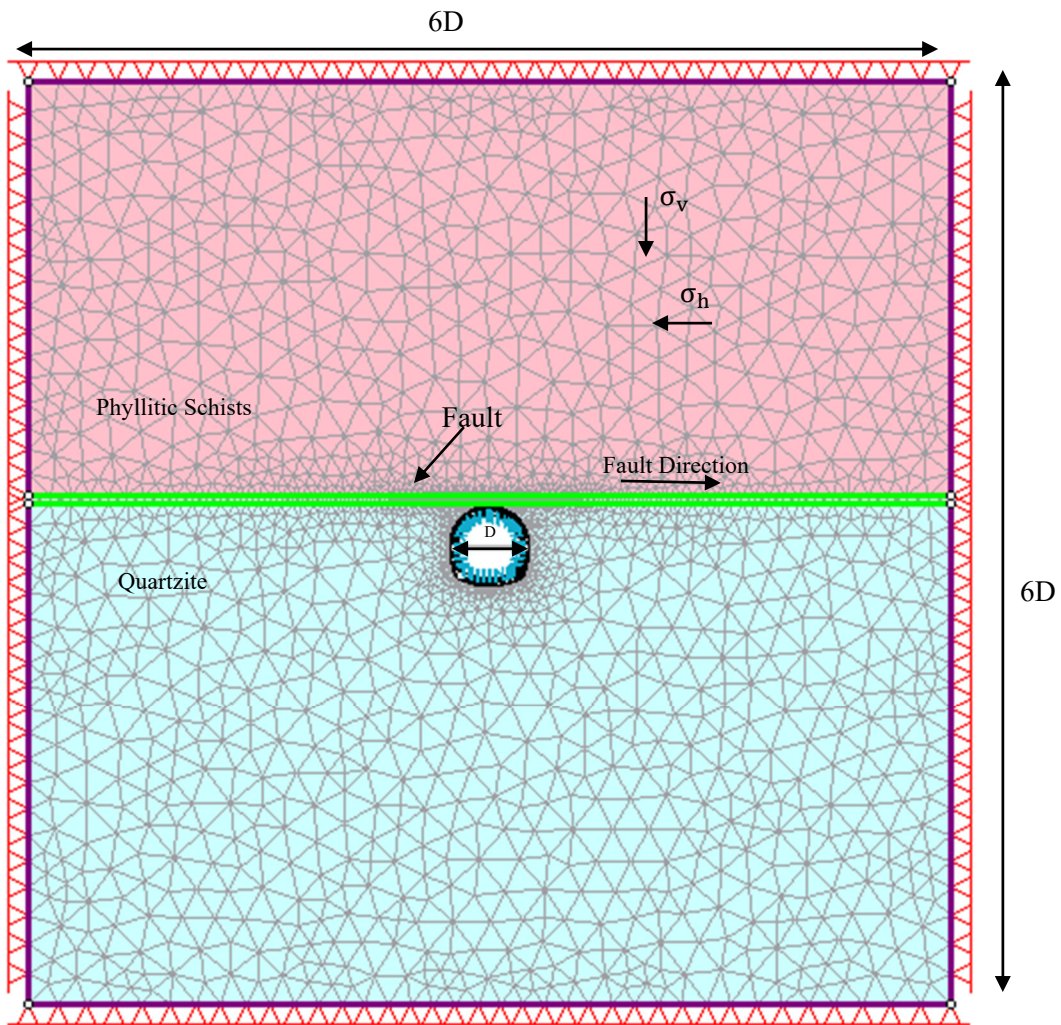


Figure 4-17 Horse Shoe Tunnel with Crown Fault in RS2

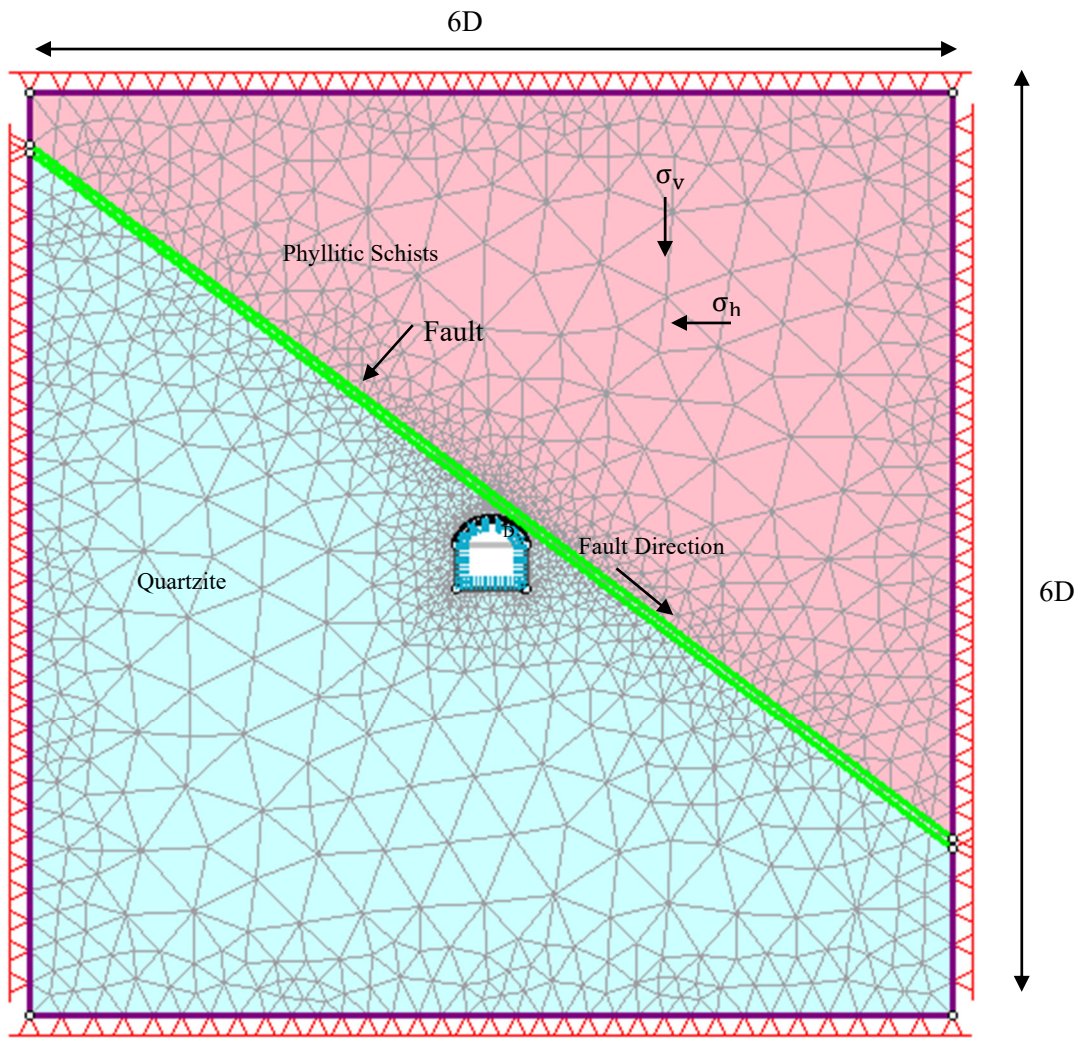


Figure 4-18 Inverted D Tunnel with Right Shoulder Fault in RS2

4.3 Effects of fault in different shape of tunnel

Deformation or displacement of the surrounding rock mass, shear force, bending moment and axial force in tunnel lining is a direct index of the stability of the surrounding rock mass for tunneling and underground excavations. Hence, in this section displacement and the vector field of the displacement of the surrounding rock mass are analyzed for different cases. When a fault is near a tunnel the surrounding rock mass of the tunnel is divided into two sections by the fault. One section contains the tunnel while another does not contain fault (Figure 4-16, Figure 4-17, Figure 4-18). The fault can change the continuous displacement field of the non-faulted surrounding rock mass to a discontinuous displacement field. The analysis in three different sections of Inverted D, horseshoe and circular section are as follows:

a) Inverted D Tunnel

In inverted D tunnel, the displacement of 8.5 mm is maximum at left shoulder at point 'J' due to crown fault. Figure 4-19 show displacement at the tunnel lining at different fault locations. On the basis of the location following results have been obtained. Point 'C' i.e., common point invert and has maximum displacement of 6 mm due to invert fault. Point 'F' of the right shoulder has maximum displacement of 4.8 mm due to right side wall fault. Point 'H' of crown has maximum displacement of 5.8 mm due to right side wall fault. Point 'J' of left shoulder has maximum displacement due to crown fault. Point 'K' of left side wall has maximum displacement of 8 mm due to crown fault.

For invert and right, side wall invert fault is critical. Similarly, Right side wall fault is critical for right shoulder and crown. Crown fault is critical for left side shoulder and left side wall.

The displacement is comparatively maximum at the crown and invert section. The crown fault, left shoulder fault, right side wall fault and right bottom fault are critical faults for the deformation in crown section of tunnel, left shoulder and right shoulder. Similarly, right side wall also has higher deformation due to invert fault. The deformation is maximum in the left side wall due to crown fault. Similarly, deformation in invert is more due to the invert fault. Hence for displacement in inverted D tunnel crown and invert fault are more critical faults.

Table 4-1 shows ratio of increase in displacements in tunnel lining positions due to different fault locations. In comparison without fault, RLS_d is maximum at Points 'A' and 'B' with values of 27.6 and 20.6 respectively. Similarly, RI_d is maximum at points 'c' and 'D' with values of 100.5 and 66.9 respectively. RRB_d is maximum at points D with value of 42.7. $RRSW_d$ is maximum at points E, F, G with values of 45.5, 42.9, and 63.8 respectively. RC_d is maximum at I, J, L with values of 73.8, 227.2 and 193.9 respectively. RLS_d is maximum at point L with the value of 89.8.

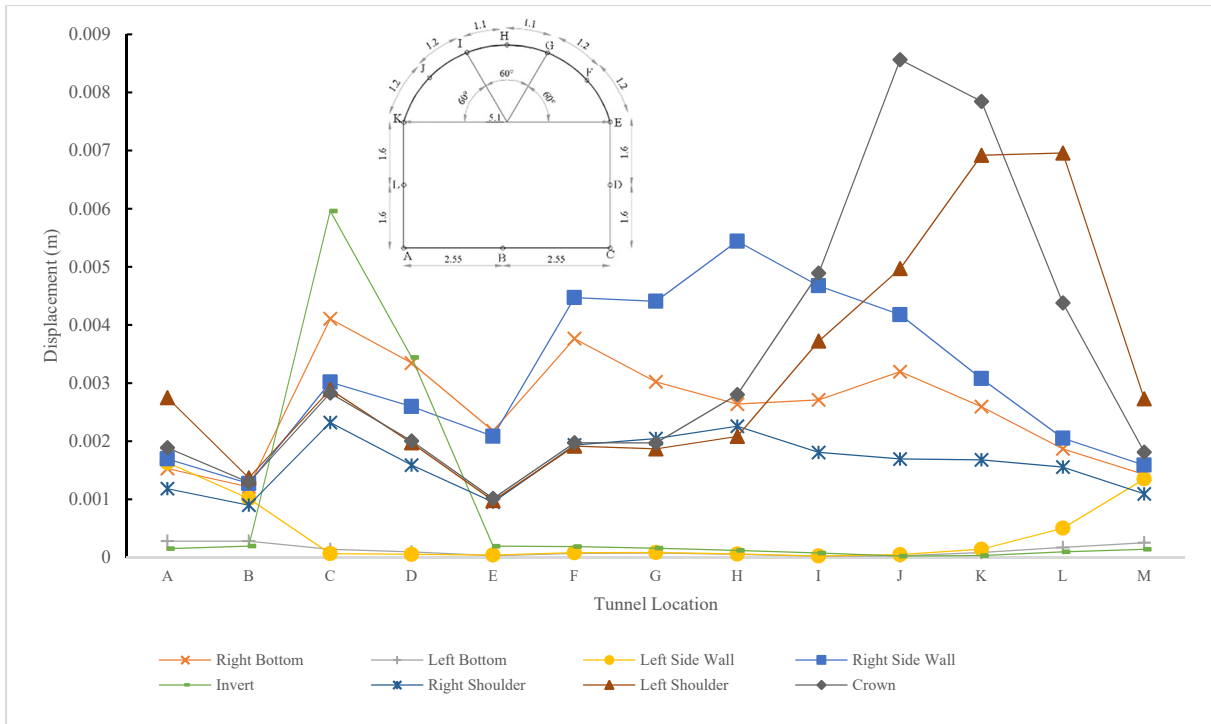


Figure 4-19 Displacement at tunnel locations at different Fault locations inverted D tunnel.

Table 4-1 Ratio of increase in displacements in tunnel lining positions due to different fault locations inverted D tunnel.

Locations	RC _d	RLS _d	RRS _d	RI _d	RRSW _d	RLSW _d	RLB _d	RRB _d	Maximum ratio
A	19.0	27.6	11.9	1.5	17.0	16.4	2.8	15.4	27.6
B	19.5	20.6	13.6	3.0	19.2	15.3	4.2	18.3	20.6
C	47.7	48.7	39.2	100.5	50.9	1.1	2.4	69.3	100.5
D	39.0	38.3	30.9	66.9	50.4	1.1	1.9	65.0	66.9
E	19.9	19.2	18.7	3.8	40.9	0.8	0.6	42.7	42.7
F	20.1	19.5	19.7	1.9	45.5	0.8	0.7	38.3	45.5
G	19.2	18.2	19.9	1.6	42.9	0.8	0.8	29.4	42.9
H	32.9	24.4	26.5	1.4	63.8	0.7	0.7	31.0	63.8
I	73.8	56.1	27.3	1.1	70.5	0.4	0.4	40.9	73.8
J	227.2	131.8	45.0	0.6	110.8	1.3	0.7	84.8	227.2
K	193.9	171.0	41.5	0.8	76.1	3.5	2.1	64.2	193.9
L	56.5	89.8	20.1	1.2	26.5	6.5	2.2	24.1	89.8

Left shoulder fault is critical for point A and B. Invert fault is critical for points C and D. Right side wall fault is critical for F, G and H. Right bottom fault is critical for point E. Crown fault is critical for points I, J, and K. Left shoulder fault is critical for point L.

Similarly, in inverted D tunnel, the axial force of 2.25 MN is maximum at point 'G' due to right shoulder fault. Figure 4-19 Displacement at tunnel locations at different Fault locations On the basis of the location following results have been obtained. Point 'C' i.e common point invert and has maximum axial force of 1.25 MN due to right shoulder fault. Point 'F' of the right shoulder has maximum axial force of 2.25 MN due to right shoulder fault. Point 'H' of crown has maximum axial force of 2 MN due to right right shoulder fault. Point 'J' of left shoulder has maximum axial force 1.75 MN due to right shoulder fault. Point 'K' of left side wall has maximum axial force of 0.75 MN due to right shoulder.

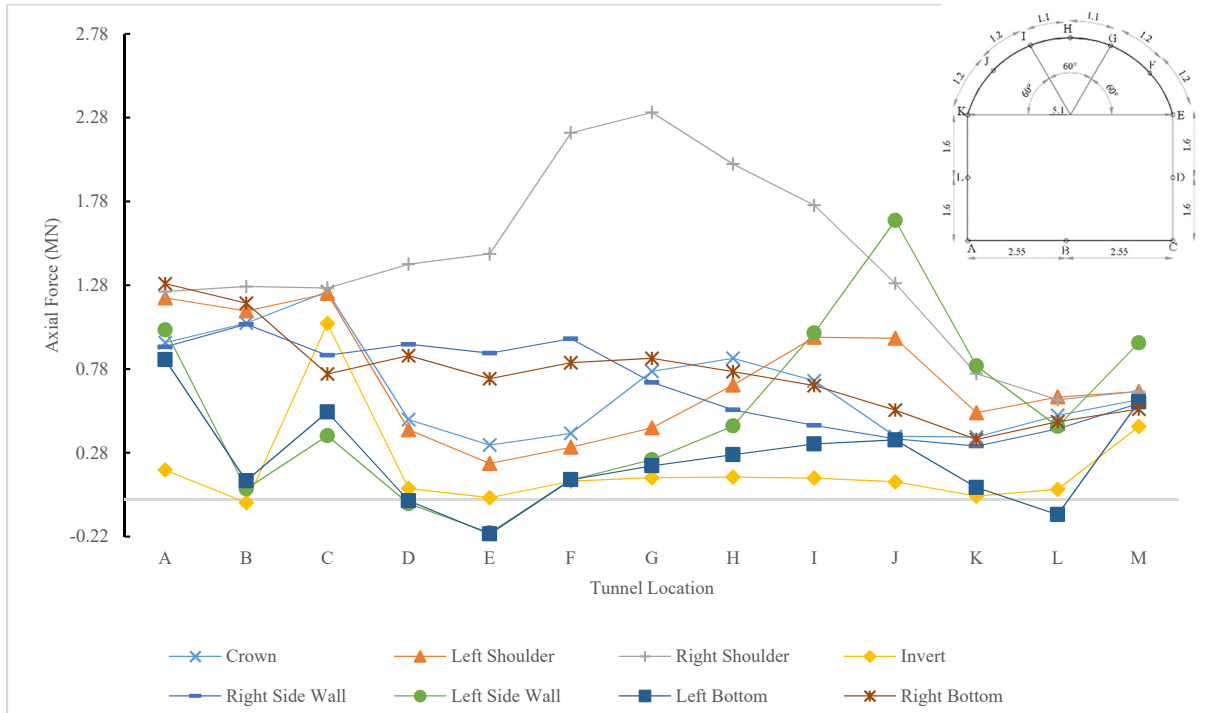


Figure 4-20 Axial force at tunnel locations at different Fault locations inverted D tunnel.

Table 4-2 Ratio of increase in axial force in tunnel lining positions due to different fault location inverted D tunnel

Location	RC _a	RLS _a	RRS _a	RI _a	RRSW _a	RLSW _a	RLB _a	RRB _a	Maximum ratio
A	1.8	2.3	2.4	0.3	1.7	1.9	1.6	2.4	2.4
B	16.2	17.3	19.5	-0.3	16.1	1.0	1.7	18.0	19.5
C	2.3	2.3	2.3	1.9	1.6	0.7	1.0	1.4	2.3
D	23.6	20.6	69.4	3.3	45.8	-1.1	-0.3	42.5	69.4
E	-1.5	-1.0	-6.7	-0.1	-4.0	0.9	0.9	-3.3	0.9
F	2.4	1.9	13.2	0.7	5.8	0.7	0.7	4.9	13.2
G	3.4	1.9	10.1	0.6	3.1	1.0	0.9	3.7	10.1
H	3.6	2.9	8.6	0.6	2.3	1.9	1.2	3.3	8.6
I	3.1	4.3	7.8	0.6	2.0	4.4	1.5	3.0	7.8
J	2.6	6.6	8.8	0.7	2.5	11.4	2.4	3.7	11.4

K	-4.9	-6.8	-9.9	-0.3	-4.2	-10.5	-1.0	-4.7	-0.3
L	11.5	14.0	13.6	1.4	9.7	10.0	-2.0	10.6	14.0

Table 4-2 shows ratio of increase in axial force in tunnel lining due to different fault location in inverted D tunnel. In comparison without fault, RRS_a is maximum at Points A, B, C, D, E, F, G, H, and I with values of 2.4, 19.5, 2.3, 69.4, -6.7, 13.2, 10.1, 8.6, and 7.8 respectively. Similarly, $RLSW_a$ is maximum at points J and K with values of 11.4 and -10.5 respectively. RLS_a is maximum at points L with with value of 14.0.

Similarly, in inverted D tunnel, the bending moment of 0.11 MNm is maximum at point 'D' due to right shoulder fault. Figure 4-19 shows displacement at tunnel locations due to different fault locations in inverted D tunnel. On the basis of the location following results have been obtained. Point 'C' i.e., common point invert and has maximum the bending moment of -0.14 MNm due to right shoulder fault. Point 'F' of the right shoulder has maximum the bending moment of 0.13 MNm due to right shoulder fault. Point 'H' of crown has maximum the bending moment of -0.02 MNm due to right shoulder fault. Point 'J' of left shoulder has maximum the bending moment -0.03 MNm due to right shoulder fault. Point 'L' of left side wall has maximum the bending moment of 0.06 MNm due to right shoulder.

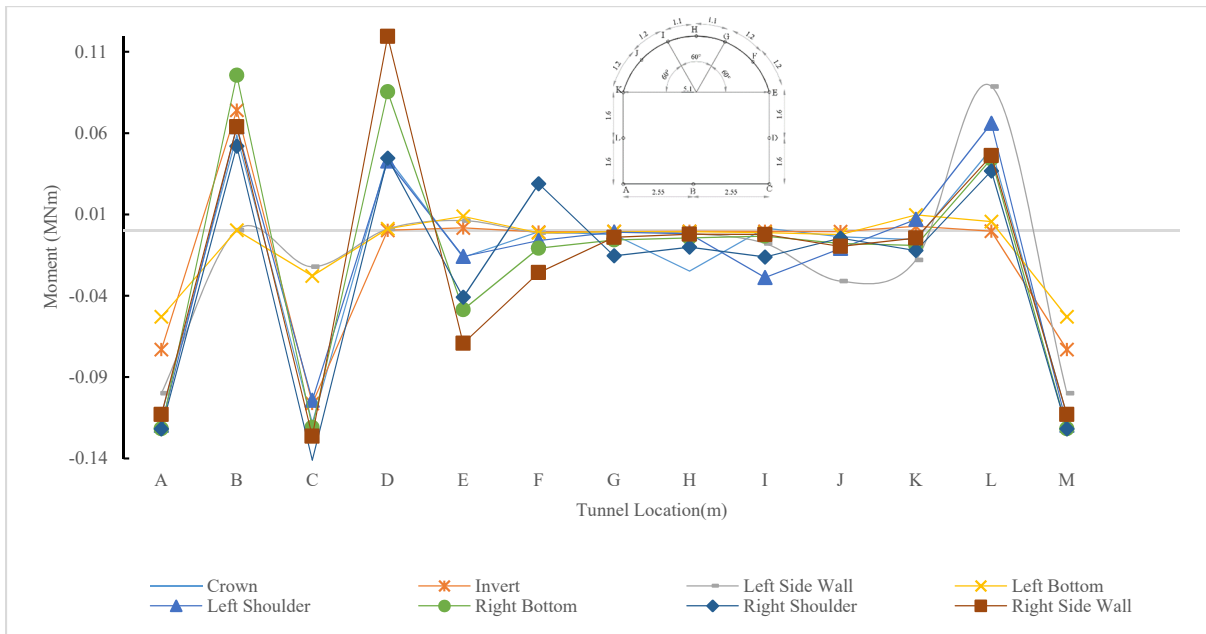


Figure 4-21 Moment at tunnel locations at different Fault locations inverted D tunnel.

Table 4-3 Ratio of increase in moment in tunnel lining positions due to different fault locations inverted D tunnel.

Locations	RC _m	RLS _m	RRS _m	RI _m	RRSW _m	RLSW _m	RLB _m	RRB _m	Maximum ratio
A	1.6	1.6	1.7	1.0	1.5	1.4	0.7	1.7	1.7
B	35.5	38.8	31.5	45.0	38.8	0.2	0.2	58.0	58.0
C	1.5	1.3	1.8	1.3	1.6	0.3	0.4	1.5	1.8
D	7.4	7.1	7.4	0.0	19.8	0.2	0.2	14.2	19.8
E	-0.7	-0.7	-1.7	0.1	-2.9	0.3	0.4	-2.0	-1.7
F	0.1	0.8	-3.9	0.1	3.5	0.2	0.2	1.4	-3.9
G	0.8	0.3	5.1	0.2	1.3	0.2	0.2	1.9	5.1
H	9.3	0.7	3.8	0.1	0.8	0.6	0.2	1.6	9.3
I	-0.5	9.2	5.2	0.1	0.7	2.5	0.4	1.1	9.2
J	0.5	1.4	0.6	0.1	1.2	3.8	0.3	1.0	3.8
K	-0.2	0.2	-0.3	0.1	-0.1	-0.5	0.3	-0.3	-0.5
L	6.2	8.1	4.5	0.0	5.7	10.9	0.7	5.4	10.9

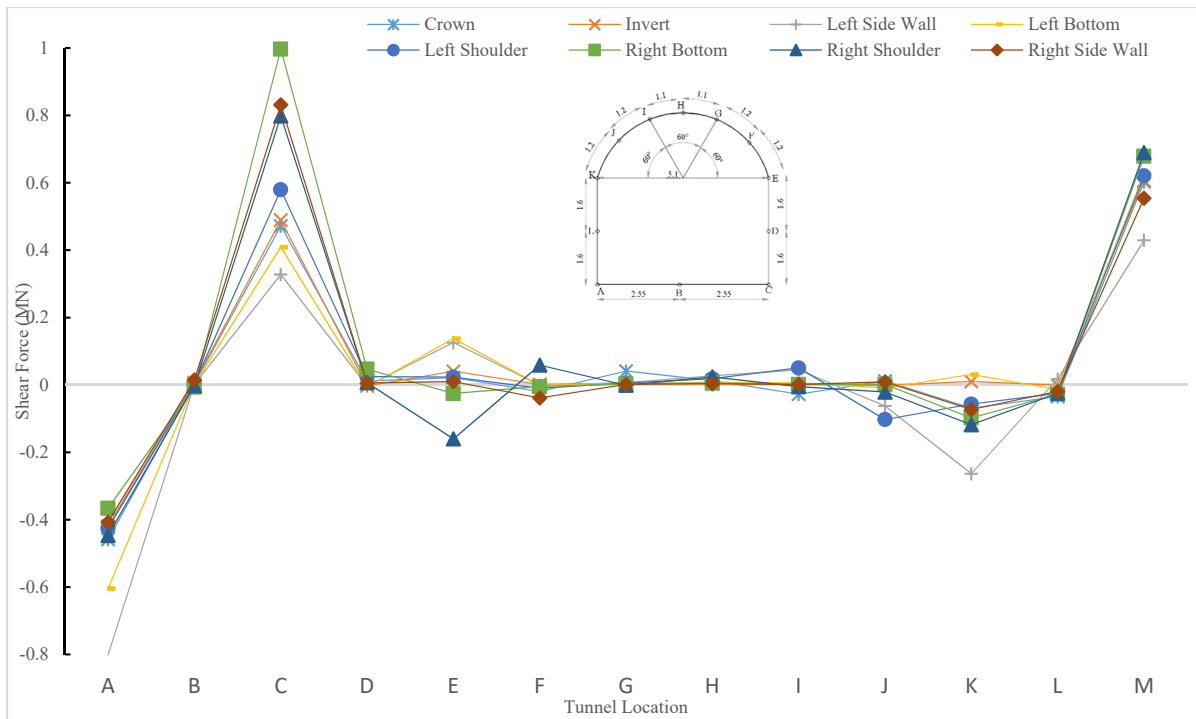


Figure 4-22 Shear Force at tunnel locations at different Fault locations inverted D tunnel.

Table 4-4 Ratio of increase in shear force in tunnel lining positions due to different fault locations inverted D tunnel.

Locations	RC _s	RLS _s	RRS _s	RI _s	RRSW _s	RLSW _s	RLB _s	RRB _s	Maximum ratio
A	0.8	0.8	0.8	0.8	0.7	1.4	1.1	0.7	1.4
B	0.9	1.0	-0.4	1.6	3.3	0.4	0.5	-1.4	3.3
C	0.7	0.8	1.2	0.7	1.2	0.5	0.6	1.5	1.5

D	6.9	14.7	4.0	-1.6	3.4	-1.6	-3.8	28.0	28.0
E	0.1	0.1	-0.7	0.2	0.0	0.5	0.6	-0.1	0.6
F	1.6	0.8	-4.9	-0.1	3.2	0.0	0.1	0.4	3.2
G	14.3	2.1	-0.3	1.2	0.6	2.4	1.3	1.0	14.3
H	1.5	2.2	2.8	0.4	0.5	3.2	1.0	0.7	3.2
I	-8.6	16.2	-1.6	0.7	0.5	14.3	1.9	0.5	16.2
J	1.1	-9.3	-1.9	-0.1	0.8	-5.6	-0.8	0.2	-9.3
K	-0.9	-0.7	-1.5	0.1	-0.9	-3.4	0.4	-1.2	-3.4
L	1.7	1.3	1.2	0.0	1.0	-0.9	0.7	1.4	1.7

Similarly, in inverted D tunnel, shear force of 1 MN is maximum at point 'C' due to right bottom fault. Figure 4-19 shows the displacement at tunnel locations at different fault locations. On the basis of the location following results have been obtained. Point 'C' i.e. common point invert and has maximum the shear force of -0.1 MN due to right bottom fault. Point 'F' of the right shoulder has maximum the shear force of 0.13 MN due to right shoulder fault. Point 'H' of crown has maximum the shear force of -0.1 MN due to right right shoulder fault. Point 'J' of left shoulder has maximum the shear force -0.1 MN due to crown fault. Point K of left side wall has maximum the shear force of 0.3 MN due to left side wall fault.

b) Horseshoe Tunnel

In horseshoe tunnel, the displacement of 11 mm is maximum at crown at point 'H' due to crown fault. Figure 4-23 shows displacement at different tunnel locations due to different fault in horseshoe tunnel. On the basis of the location following results have been obtained. Point 'C' i.e., common point invert and has maximum displacement of 4 mm due to invert fault. Point 'F' of the right shoulder has maximum displacement of 8 mm due to right shoulder fault. Point 'H' of crown has maximum displacement of 11 mm due to right side wall fault. Point 'J' of left shoulder has maximum displacement of 9 mm due to left shoulder fault. Point 'K' of left side wall has maximum displacement of 4 mm due to left shoulder fault.

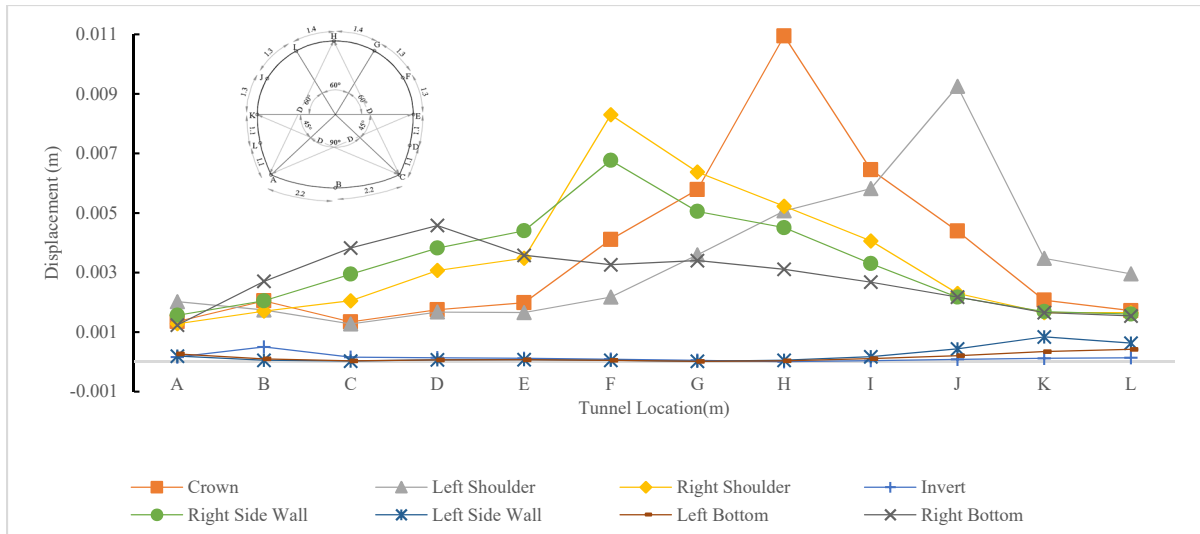


Figure 4-23 Displacement at tunnel locations at different Fault locations Horseshoe Tunnel

Table 4-5 Ratio of increase in displacements in tunnel lining positions due to different Fault locations Horseshoe Tunnel

Locations	RC _d	RLS _d	RRS _d	RI _d	RRSW _d	RLSW _d	RLB _d	RRB _d	Maximum ratio
A	72.3	107.9	68.5	8.7	83.7	10.5	14.4	66.0	107.9
B	47.9	40.7	39.9	11.7	48.0	1.3	2.4	63.3	63.3
C	25.0	23.7	38.1	3.0	54.7	0.6	0.7	71.0	71.0
D	20.1	19.3	35.3	1.6	43.9	0.8	0.8	52.6	52.6
E	20.4	17.0	35.8	1.2	45.3	0.8	0.8	36.8	45.3
F	49.4	26.2	99.6	1.1	81.3	0.7	0.7	39.2	99.6
G	100.3	62.4	110.6	0.9	87.7	0.4	0.3	59.0	110.6
H	323.3	149.9	154.5	0.2	133.3	1.7	1.1	91.9	323.3
I	133.1	120.0	83.8	0.9	68.1	3.6	2.3	55.3	133.1
J	56.2	118.4	29.4	1.1	27.8	5.6	2.7	27.9	118.4
K	20.4	34.2	16.3	1.2	16.6	8.3	3.4	16.3	34.2
L	20.1	34.5	19.3	1.7	18.8	7.4	4.9	18.0	34.5

Table 4-5 shows ratio of increase in displacements in tunnel lining positions due to different fault locations in Horseshoe Tunnel. In comparison without fault, RLS_d is maximum at Points ‘A’ with value of 107.9. RRB_d is maximum at points B, C, and D with value of 63.3, 71.0 and 52.6 respectively. RRSW_d is maximum at point E with values of 45.3. RRS_d is maximum at F, G with values of 99.6 and 110.6 respectively. RC_d is maximum at points H and I with the value of 323.3 and 133.1 respectively. RLS_d is maximum at points J, K and L with the values of 118.4, 34.2 and 34.5 respectively. Left shoulder fault is critical for point A. Right bottom fault is critical for points B, C and D respectively. Right side wall fault is

critical for E. Right shoulder fault is critical for point F and G. Crown fault is critical for points H and I. left shoulder fault is critical for point J, K and L.

Similarly, in horseshoe tunnel, the axial force of 1.25 MN is maximum at point ‘B’ due to left side wall fault. Figure 4-24 shows the axial force at tunnel locations due to different fault locations in horseshoe tunnel. Figure 4-19 shows displacement at tunnel locations due to different fault locations. On the basis of the analysis on the basis of tunnel location following results have been obtained. Point ‘C’ i.e., common point invert and has maximum axial force of 1.25 MN due to right shoulder fault. Point ‘F’ of the right shoulder has maximum axial force of 0.7 MN due to left shoulder fault. Point ‘H’ of crown has maximum axial force of 0.5 MN due to right bottom fault. Point ‘J’ of left shoulder has maximum axial force 0.5 MN due to left side wall fault. Point ‘K’ of left side wall has maximum axial force of 0.9 MN due to left side wall. Similarly, Figure 4-25 shows the moment distribution at tunnel locations due to different fault locations in horseshoe tunnel. Figure 4-25 shows moment distribution at different tunnel locations due to different fault locations. Figure 4-26 shows the shear force distribution at tunnel locations at different fault locations.

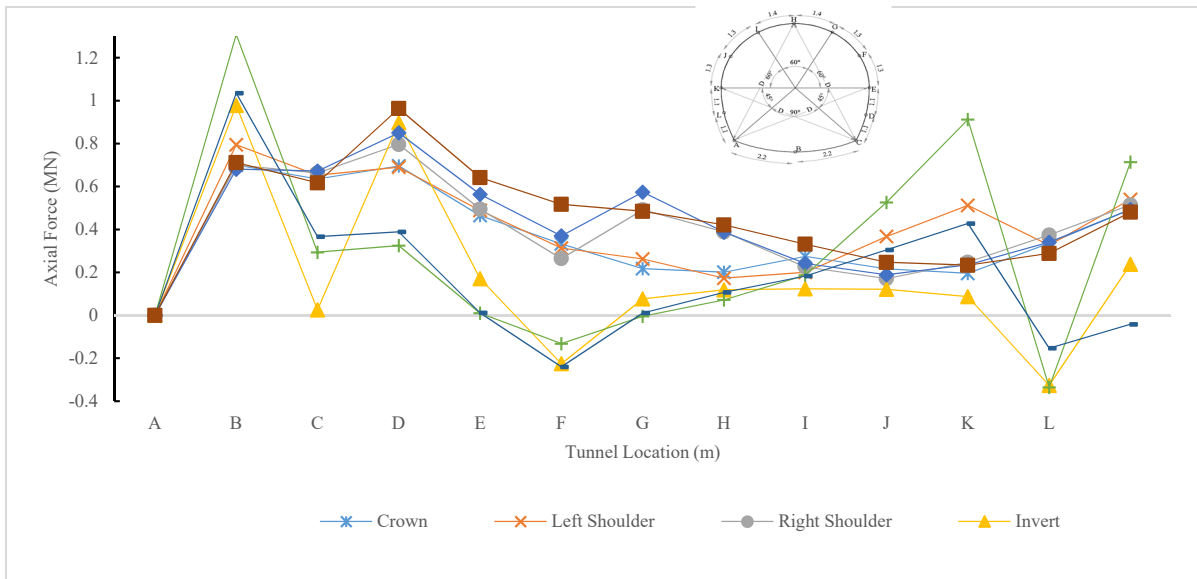


Figure 4-24 Axial force at tunnel locations at different Fault locations horseshoe tunnel

Table 4-6 Ratio of increase in axial force in tunnel lining positions due to different fault locations horseshoe tunnel

Locations	RC _a	RLS _a	RRS _a	RI _a	RRSW _a	RLSW _a	RLB _a	RRB _a	Maximum ratio
A	2.3	2.6	2.3	3.1	2.2	4.2	3.3	2.3	4.2
B	4.5	4.6	4.7	0.2	4.7	2.1	2.6	4.4	4.7
C	2.2	2.1	2.5	2.8	2.6	1.0	1.2	3.0	3.0

D	18.9	19.9	20.2	7.0	23.0	0.4	0.5	26.2	26.2
E	-3.4	-3.2	-2.7	2.3	-3.8	1.4	2.5	-5.3	-3.4
F	7.6	9.2	17.1	2.7	20.0	-0.1	0.4	16.9	20.0
G	2.7	2.3	5.1	1.6	5.1	1.0	1.4	5.6	5.6
H	3.3	2.4	2.7	1.5	2.9	2.2	2.2	3.9	3.9
I	2.8	4.7	2.2	1.5	2.4	6.7	3.9	3.1	6.7
J	5.6	14.6	7.1	2.5	6.7	26.1	12.2	6.7	26.1
K	-2.0	-2.0	-2.3	2.0	-2.1	2.0	0.9	-1.8	-2.3
L	10.1	11.1	10.6	4.9	10.1	14.7	-0.9	9.9	14.7

Table 4-6 show increase in axial force in tunnel lining due to different fault location in horseshoe tunnel. In comparison without fault, $RLSW_a$ is maximum at Points A with values of 4.2. Similarly, $RLSW_a$ is maximum at points B with values of 4.7. RRB_a is maximum at points C and D with value of 3.0 and 26.2. RC_a is maximum at points E with value of -3.4, $RRSWA_a$ is maximum at points F with value of 20, RRB_a at points G with the value of 5.6. Similarly, Table 4-7 show ratio of increase in moment in tunnel lining positions due to different fault locations horseshoe tunnel. Table 4-8 show ratio of increase in shear force in tunnel lining positions due to different fault location horseshoe tunnel.

Similarly, in horseshoe tunnel, the bending moment of 0.11 MNm is maximum at point 'E' due to right bottom fault. Figure 4-19 Displacement at tunnel locations at different Fault locations On the basis of the location following results have been obtained. Point 'C' i.e common point invert and has maximum the bending moment of 0.02 MNm due to invert fault. Point 'F' of the right shoulder has maximum the bending moment of -0.04 MNm due to right side wall fault. Point 'H' of crown has maximum the bending moment of 0.05 MNm due to right shoulder fault. Point 'J' of left shoulder has maximum the bending moment - 0.02 MNm due to right bottom fault. Point 'L' of left side wall has maximum the bending moment of - 0.02 MNm due to left shoulder.

Similarly, horse shoe tunnel, the shear force of -0.6 MN is maximum at point 'A' due to left side wall fault. Figure 4-19 shows Displacement at tunnel locations at different Fault locations. On the basis of the location following results have been obtained. Point 'C' i.e., common point invert and has maximum the shear force of -0.4 MN due to invert fault. Point 'F' of the right shoulder has maximum the shear force of 0.01 MN due to right bottom fault. Point 'H' of crown has maximum the shear force of -0.01 MN due to right bottom fault. Point 'J' of left shoulder has maximum the shear force -0.05 MN due to right shoulder fault. Point K of left side wall has maximum the shear force of 0.2 MN due to right side wall fault.

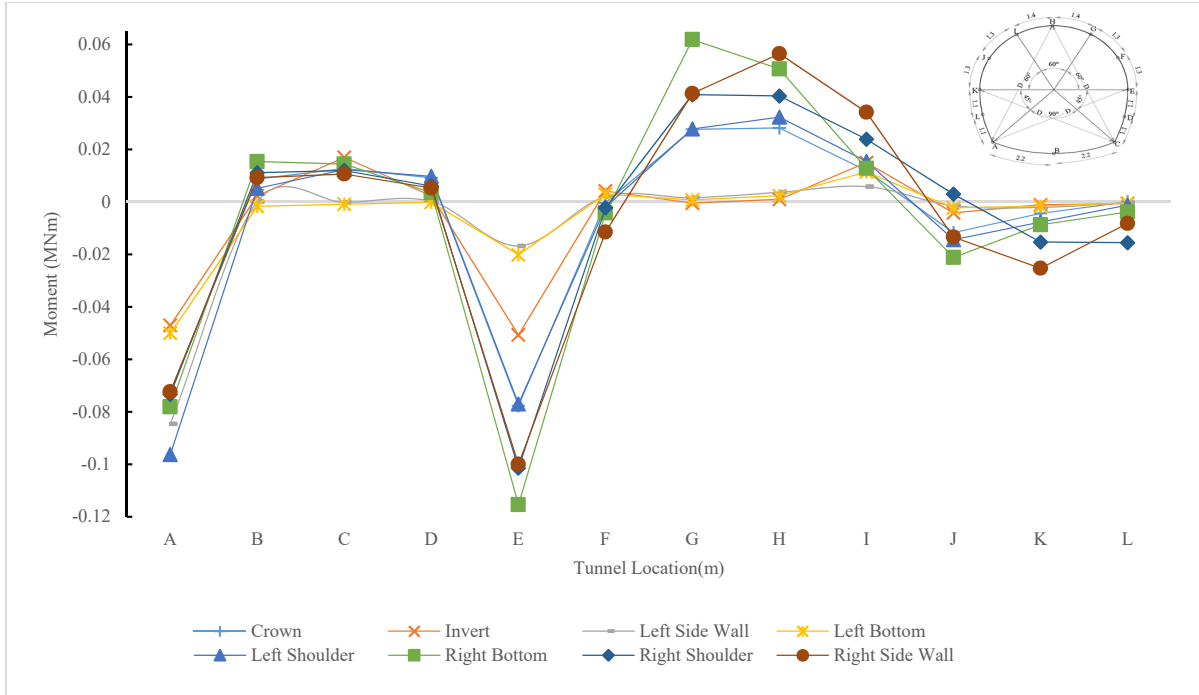


Figure 4-25 Moment at tunnel locations at different Fault locations horseshoe tunnel

Table 4-7 Ratio of increase in moment in tunnel lining positions due to different fault locations horseshoe tunnel

Locations	RC _m	RLS _m	RRS _m	RI _m	RRSW _m	RLSW _m	RLB _m	RRB _m	Maximum ratio
A	4.5	2.9	5.3	3.1	6.0	4.9	4.6	4.5	6.0
B	41.9	11.4	0.6	-8.0	25.0	73.8	53.3	44.4	73.8
C	-91.9	-120.8	11.4	64.5	-81.2	-104.9	-88.8	-70.9	64.5
D	53.8	13.5	1.0	-1.0	57.2	20.8	35.7	31.3	57.2
E	4.6	3.0	1.0	1.2	4.5	6.8	6.0	5.9	6.8
F	-0.1	1.7	0.8	1.2	-0.8	-1.7	-0.9	-4.7	-4.7
G	39.1	-0.7	2.3	1.0	39.3	87.5	57.7	58.5	87.5
H	10.9	0.4	1.4	0.9	12.6	19.7	15.7	22.0	22.0
I	1.6	2.0	0.8	1.5	2.0	1.7	3.1	4.5	4.5
J	4.7	1.7	0.6	0.9	5.8	8.5	-1.2	5.4	8.5
K	2.5	0.6	1.2	0.9	4.3	4.9	8.6	14.2	14.2
L	-0.2	1.2	0.5	0.8	2.3	7.3	29.7	15.6	29.7

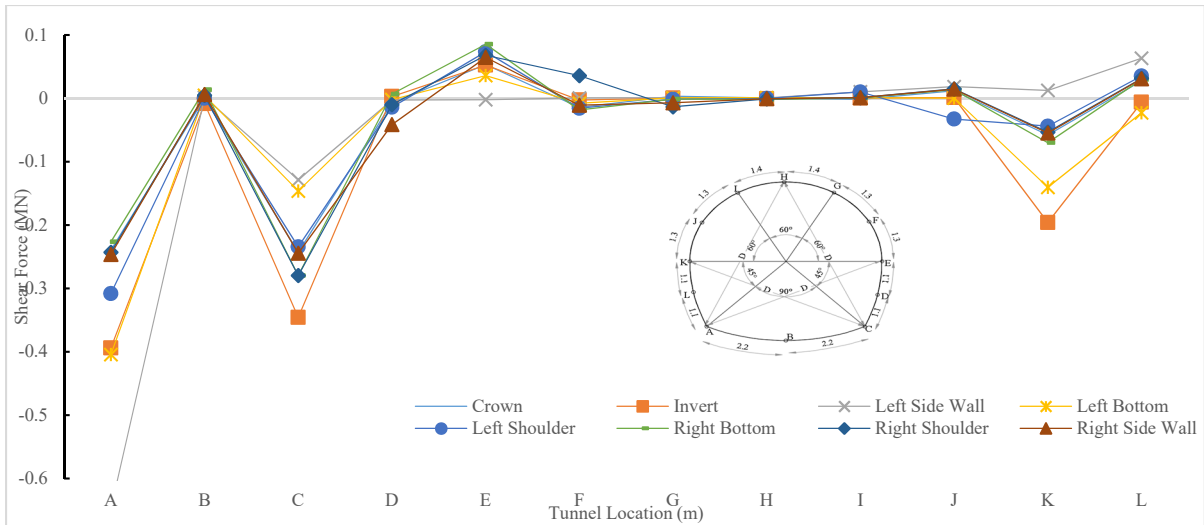


Figure 4-26 Shear force at tunnel locations at different fault locations horseshoe tunnel

Table 4-8 Ratio of increase in shear force in tunnel lining positions due to different fault location horseshoe tunnel

Locations	RC _s	RLS _s	RRS _s	RI _s	RRSW _s	RLSW _s	RLB _s	RRB _s	Maximum ratio
A	1.8	2.9	4.8	3.0	2.3	1.7	1.8	1.8	4.8
B	0.3	-5.2	0.9	2.9	0.1	8.5	2.9	3.7	8.5
C	1.9	2.7	1.0	1.2	1.8	2.2	2.2	1.9	2.7
D	5.8	-2.4	2.3	1.6	11.8	-5.7	8.3	35.1	35.1
E	9.6	9.4	-0.4	6.5	13.2	15.4	12.2	11.6	15.4
F	2.7	0.5	-0.1	1.5	2.9	3.4	-6.7	2.0	3.4
G	23.0	3.4	6.6	5.2	-10.4	-8.0	-92.1	-48.9	23.0
H	-2.0	3.1	-2.0	-4.2	0.7	7.8	3.8	3.0	7.8
I	-2.6	0.6	14.3	1.1	14.2	0.6	1.4	1.4	14.3
J	1.9	0.2	3.0	0.1	-5.2	2.2	2.4	2.3	3.0
K	4.4	14.9	-1.0	10.7	3.3	5.3	4.1	4.2	14.9
L	-27.8	6.2	-63.7	22.9	-35.5	-30.0	-31.6	-31.0	-31.6

c) Circular Tunnel

In circular tunnel, the displacement of 11 mm is maximum at crown at point 'H' due to crown fault. Figure 4-27 shows displacement at different tunnel locations due to different fault in circular tunnel. On the basis of the location following results have been obtained. Point 'C' i.e common point invert and has maximum displacement of 3.8 mm due to invert fault. Point 'F' of the right shoulder has maximum displacement of 8 mm due to right shoulder fault. Point 'H' of crown has maximum displacement of 11

mm due to right side wall fault. Point ‘J’ of left shoulder has maximum displacement of 9 mm due to left shoulder fault. Point ‘K’ of left side wall has maximum displacement of 4 mm due to left shoulder fault.

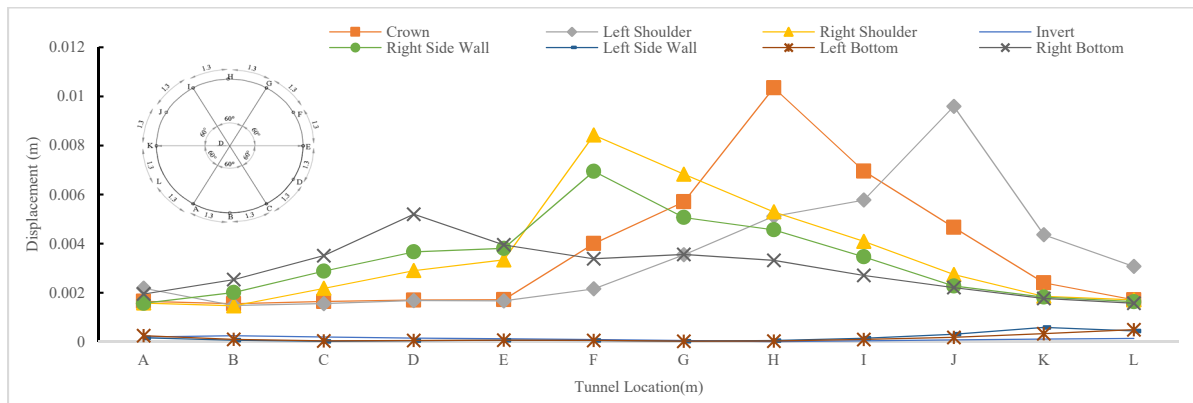


Figure 4-27 Displacement at tunnel locations at different Fault locations circular tunnel

Table 4-9 Ratio of increase in displacement in tunnel lining positions due to different fault locations

Locations	RC _d	RLS _d	RRS _d	RI _d	RRSW _d	RLSW _d	RLB _d	RRB _d	Maximum ratio
A	32.5	43.1	31.2	3.8	30.9	3.2	4.9	38.5	43.1
B	49.2	47.0	46.4	7.8	63.7	2.1	3.1	80.4	80.4
C	33.2	31.4	44.1	4.0	58.2	0.4	0.8	71.0	71.0
D	22.8	22.5	38.9	2.0	49.2	0.6	0.7	69.7	69.7
E	19.7	19.1	38.3	1.4	43.7	0.7	0.8	45.4	45.4
F	50.2	27.0	105.5	1.1	87.0	0.7	0.7	42.4	105.5
G	101.6	63.1	121.5	1.0	90.2	0.4	0.4	63.3	121.5
H	308.1	152.3	157.6	0.3	135.9	1.5	0.9	98.8	308.1
I	150.6	125.0	88.6	0.8	75.0	3.1	2.1	58.6	150.6
J	64.9	133.6	38.2	1.1	31.6	4.3	2.5	30.8	133.6
K	25.4	46.1	19.6	1.2	19.2	6.2	3.5	18.7	46.1
L	21.1	37.7	21.0	1.7	20.1	5.4	6.1	19.3	37.7

Table 4-9 shows ratio of increase in displacement in tunnel lining positions due to different fault locations in circular Tunnel. In comparison without fault, RLS_d is maximum at Points ‘A’ with value of 43.1. RRB_d is maximum at points B, C, D and E with value of 80.4, 71.0, 69.7 and 45.4 respectively. RRS_d is maximum at point F and G with values of 105.5 and 121.5. RC_d is maximum at points H and I with the value of 308.1 and 150.6 respectively. RLS_d is maximum at points J, K and L with the values of 133.6, 46.1 and 37.7 respectively. Left shoulder fault is critical for point A. Right bottom fault is critical for points B, C D and E respectively. Right shoulder fault is critical for point F and G. Crown fault is critical for points H and I. Left shoulder fault is critical for point J, K and L.

Similarly, in circular tunnel, the axial force of 1.25 MN is maximum at point ‘A’ due to right side wall fault. Figure 4-28 shows axial force at tunnel locations due to different fault locations in circular tunnel. Figure 4-19 shows displacement at tunnel locations due to different Fault locations in circular tunnel. On the basis of the location following results have been obtained. Point ‘C’ i.e common point invert and has maximum axial force of 0.72 MN due to right shoulder fault. Point ‘F’ of the right shoulder has maximum axial force of 0.47 MN due to right side wall fault. Point ‘H’ of crown has maximum axial force of 0.27 MN due to right bottom fault. Point ‘J’ of left shoulder has maximum axial force of 0.27 MN due to right bottom fault. Point ‘J’ of left shoulder has maximum axial force 0.57 MN due to left side wall fault. Point ‘K’ of left side wall has maximum axial force of 0.9 MN due to left side wall fault. Similarly, Figure 4-29 shows moment distribution at tunnel locations due to different fault locations in circular tunnel. Figure 4-30 shows shear force at tunnel locations due to different fault locations in circular tunnel.

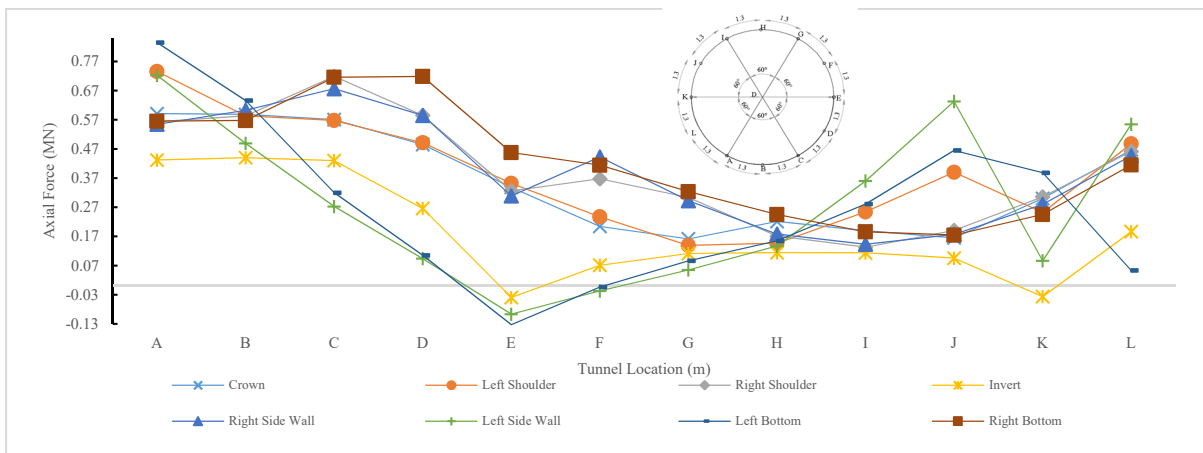


Figure 4-28 Axial Force at tunnel locations at different Fault locations in circular tunnel

Table 4-10 Ratio of increase in axial force in tunnel lining positions due to different fault locations in circular tunnel

Locations	RC _a	RLS _a	RRS _a	RI _a	RRSW _a	RLSW _a	RLB _a	RRB _a	Maximum ratio
A	3.4	4.3	3.3	2.5	3.2	4.2	4.9	3.3	4.9
B	2.8	2.7	2.7	2.1	2.8	2.3	3.0	2.7	3.0
C	3.3	3.3	4.2	2.5	3.9	1.6	1.9	4.2	4.2
D	5.8	5.8	6.9	3.2	6.9	1.1	1.3	8.5	8.5
E	-5.2	-5.4	-5.0	0.6	-4.8	1.5	2.0	-7.0	-5.4
F	8.9	10.4	16.0	3.1	19.3	-0.7	-0.1	18.1	19.3
G	2.5	2.2	4.8	1.8	4.6	0.9	1.4	5.1	5.1
H	3.1	2.1	2.4	1.6	2.5	2.0	2.2	3.5	3.5
I	2.8	3.8	2.0	1.7	2.1	5.4	4.2	2.8	5.4
J	3.6	8.5	4.1	2.1	3.8	13.7	10.1	3.8	13.7

K	-12.5	-10.5	-12.7	1.5	-11.7	-3.6	-16.2	-10.2	-16.2
L	10.0	10.4	9.8	4.0	9.5	11.8	1.1	8.9	11.8

Table 4-10 shows ratio of increase in axial force in tunnel lining positions due to different fault locations circular tunnel. In comparison without fault, RRS_a is maximum at Points C with values of 4.2. Similarly, RLB_a is maximum at points A and B with values of 4.9 and 3.0. RRB_a is maximum at points D with with value of 8.5. RLS_a is maximum at points E with value of -5.4, $RRSWA_a$ is maximum at points F with value of 19.3, RRB_a at points G and H with the value of 5.1 and 3.5. $RLSW_a$ at points I and J with the value of 5.4 and 13.7. RLB_a at points K with the value of -16.2. $RLSW_a$ at points L with the value 11.8. Similarly, Table 4-11 shows ratio of increase in moment in tunnel lining positions due to different fault locations circular tunnel. Table 4-12 shows ratio of increase in shear force in tunnel lining positions due to different fault locations circular tunnel.

Similarly, in circular, the bending moment of -0.10 MNm is maximum at point 'E' due to right bottom fault. Figure 4-19 shows displacement at tunnel locations due to different fault locations in circular tunnel. On the basis of the location following results have been obtained. Point 'C' i.e., common point invert and has maximum the bending moment of 0.02 MNm due to left bottom. Point 'F' of the right shoulder has maximum the bending moment of -0.02 MNm due to right side wall fault. Point 'H' of crown has maximum the bending moment of 0.01 MNm due to right shoulder fault. Point 'J' of left shoulder has maximum the bending moment -0.02 MNm due to right bottom fault. Point 'L' of left side wall has maximum the bending moment of -0.02 MNm due to left shoulder.

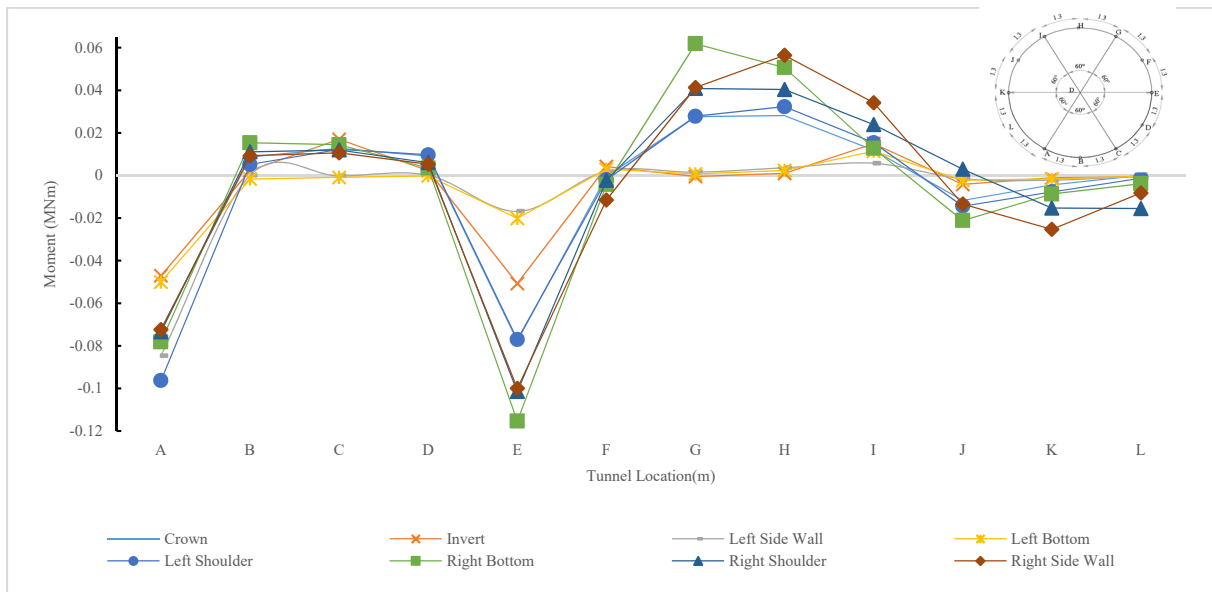


Figure 4-29 Moment at tunnel locations at different Fault locations in circular tunnel

Table 4-11 Ratio of increase in moment in tunnel lining positions due to different fault locations in circular tunnel

Locations	RC _m	RLS _m	RRS _m	RI _m	RRSW _m	RLSW _m	RLB _m	RRB _m	Maximum ratio
A	10.5	5.2	13.2	24.0	25.8	11.4	10.8	14.1	25.8
B	6.6	-1.3	4.3	11.6	12.5	4.8	5.0	4.9	12.5
C	9.4	-9.2	2.7	7.0	8.7	4.4	7.5	7.2	9.4
D	7.5	-3.1	1.7	3.0	5.7	7.8	11.3	7.1	11.3
E	9.0	4.8	0.9	1.8	10.0	31.4	26.6	18.3	31.4
F	24.5	16.0	-0.6	-0.1	13.9	126.9	53.0	90.6	126.9
G	22.3	-5.1	2.5	2.3	14.1	48.9	40.5	0.4	48.9
H	-43.7	4.7	0.3	0.3	-45.0	-120.4	-58.2	-82.7	-120.4
I	2.0	1.8	1.2	1.3	2.6	2.7	3.5	4.0	4.0
J	6.8	4.6	0.5	1.8	7.5	16.4	0.5	1.3	16.4
K	2.8	0.7	1.3	1.2	4.4	5.5	4.2	9.4	9.4
L	0.9	1.5	0.7	1.0	3.9	8.2	27.6	19.8	27.6

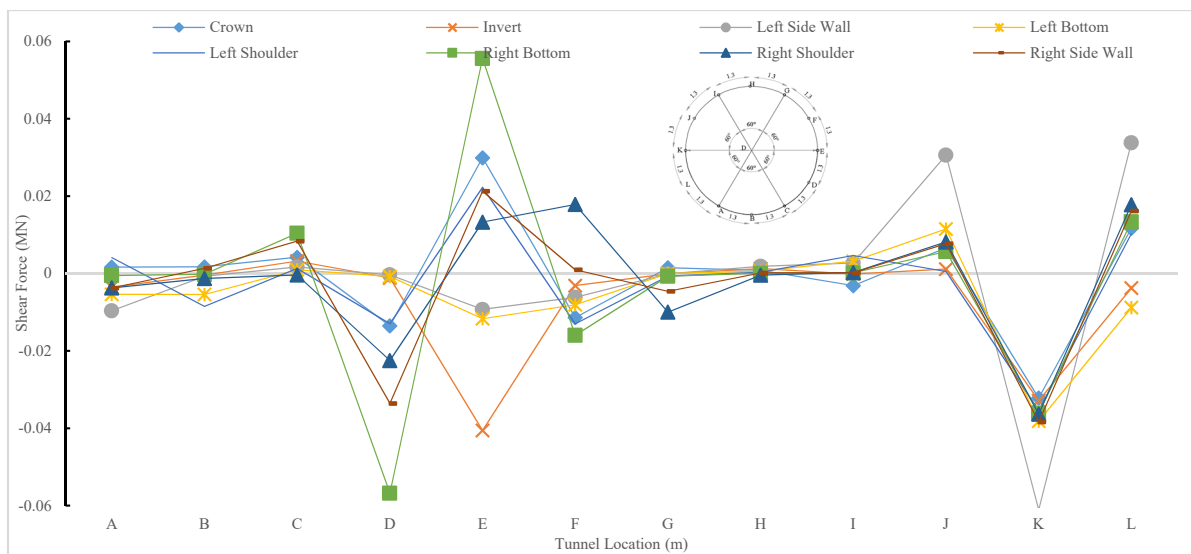


Figure 4-30 Shear Force at tunnel locations at different Fault locations circular tunnel

Similarly, circular tunnel, the shear force of -0.06 MN is maximum at point ‘K’ due to left side wall fault. Figure 4-19 shows displacement at tunnel locations due to different fault locations. On the basis of the location following results have been obtained. Point ‘C’ i.e., common point invert and has maximum the shear force of -0.01 MN due to right shoulder fault. Point ‘F’ of the right shoulder has maximum the shear force of -0.01 MN due to right bottom fault. Point ‘H’ of crown has maximum the shear force of -0.01 MN due to right shoulder fault. Point ‘J’ of left shoulder has maximum the shear force 0 MN. Point K of left side wall has maximum the shear force of -0.06 MN due to left shoulder fault.

Table 4-12 Ratio of increase in shear force in tunnel lining positions due to different fault locations in circular tunnel

Locations	RC _s	RLS _s	RRS _s	RI _s	RRSW _s	RLSW _s	RLB _s	RRB _s	Maximum ratio
A	-1.4	3.0	8.2	4.6	-3.5	0.4	3.2	3.2	8.2
B	-5.3	1.3	2.2	16.9	26.4	0.6	3.9	-4.3	26.4
C	3.3	2.5	1.3	0.7	1.0	8.1	-0.3	6.5	8.1
D	33.5	2.8	0.8	1.9	32.1	140.8	55.7	83.2	140.8
E	-1.9	2.5	0.6	0.7	-1.4	-3.5	-0.8	-1.3	-3.5
F	1.6	0.4	0.9	1.1	1.8	2.2	-2.5	-0.1	-2.5
G	6.2	-0.4	-0.4	0.0	-2.7	-2.9	-41.0	-18.8	-41.0
H	0.9	1.3	2.0	0.6	0.3	0.1	-0.4	0.2	2.0
I	-70.3	-2.6	61.6	71.6	105.4	4.5	6.1	4.5	105.4
J	8.7	1.5	39.8	15.0	0.7	7.4	10.6	10.1	39.8
K	1.7	1.7	3.2	2.0	1.9	1.9	1.9	2.0	3.2
L	-5.1	1.6	-14.6	3.8	-4.5	-5.8	-7.7	-7.0	-14.6

4.4 Analysis of structurally controlled instabilities

The analysis for structurally formed wedges in headrace tunnel of Modi Khola Hydroelectric Project due to discontinuities have been done as explained in section 4.2 (b). The data of the structural discontinuity such as bedding plane and joint plane has been listed in Table 3-2 . The analysis has been done to three sections of the headrace tunnel. They are i) 90 m to 400 m ii) 400 to 500 and iii) 500 to 700 m. The field stress has been taken as the principal stress in faulted geometry as $\sigma_1 = 2.08$ MPa, $\sigma_3 = 1.33$ MPa, $\sigma_2 = 1.33$ MPa (Chhushyabaga et. al., 2020). The analysis results of three section have been shown as follows. Figure 4-31 show Normal stress distribution in perimeter wedge at chainage of 99 to 400 m of Headrace tunnel of Modi Khola Hydropower Project. Figure 4-32 show Normal stress distribution in perimeter wedge at chainage of 400 to 500 m of Headrace tunnel of Modi Khola Hydropower Project. Figure 4-33 Normal stress distribution in perimeter wedge at chainage of 500 m to 700 m of Headrace tunnel of Modi Khola Hydropower Project.

The distribution of the normal stress show that the wedges formed in all the section are structurally stable against the sliding failure. The wedges formed cannot slide inside the tunnel as the factor of safety of all the wedges are well above 2.5 limit. Analysis of structurally controlled instabilities for three section of the headrace tunnel i) 90 m to 400 m ii) 400 to 500 and iii) 500 to 700 m show wedges are formed around the tunnel due to the intersection of the joint planes. They are safe against the sliding failure inside the tunnel with factor of safety greater than 2.5. Hence, there is no any requirement of support in the tunnel for structurally controlled failures. The support system is to be provided for the stress induced failure which has been done by modelling of fault and tunnel in 4.2 (b). Figure 4 -31 shows normal stress distribution in

perimeter wedge at chainage of 99 to 400 m of Headrace tunnel of Modi Khola Hydropower Project. Figure 4-32 shows normal stress distribution in perimeter wedge at chainage of 400 to 500 m of headrace tunnel of Modi Khola Hydropower Project. Figure 4-33 shows normal stress distribution in perimeter wedge at chainage of 500 m to 700 m of headrace tunnel of Modi Khola Hydropower Project. It is found out that the factor of the safety of the wedges formed at the crown and invert wedges are greater in comparison to that of the wedges formed at the side walls.

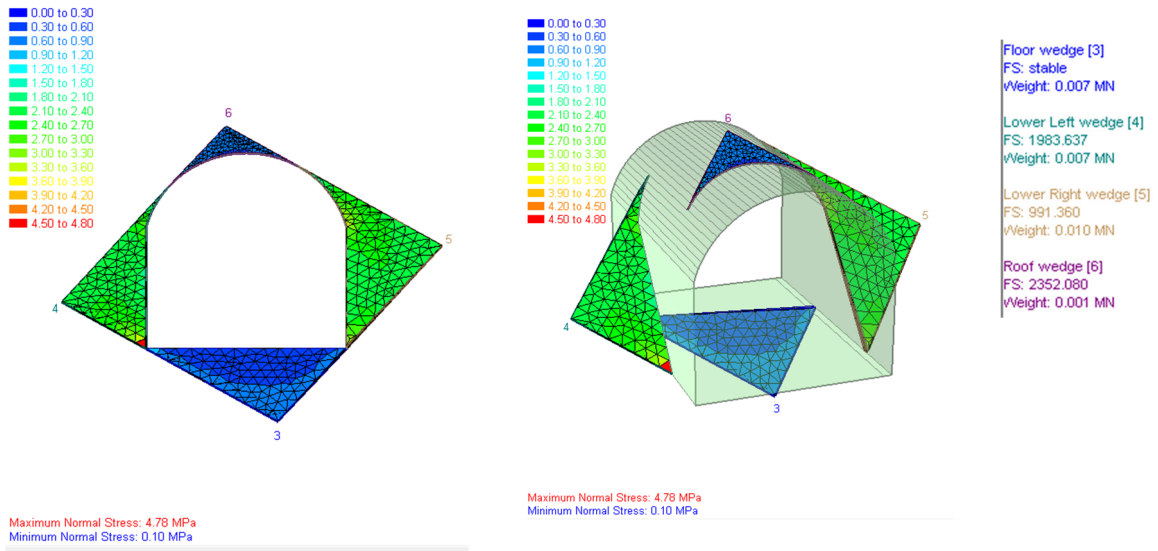


Figure 4-31 Normal stress distribution in perimeter wedge at chainage of 99 to 400 m of Headrace tunnel of Modi Khola Hydropower Project

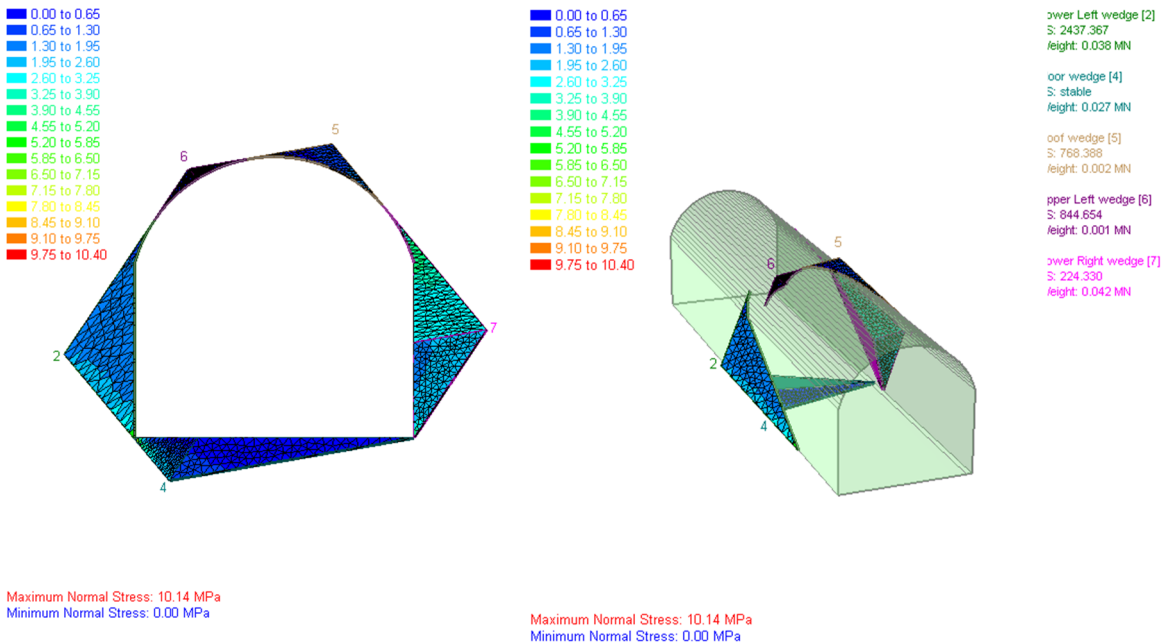


Figure 4-32 Normal stress distribution in perimeter wedge at chainage of 400 to 500 m of Headrace tunnel of Modi Khola Hydropower Project.

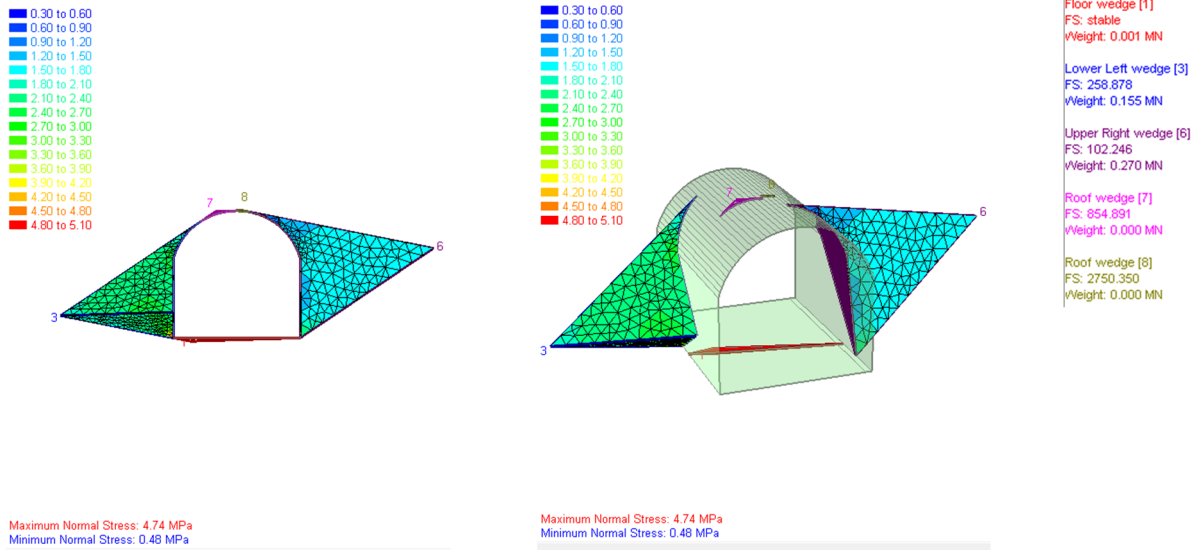


Figure 4-33 Normal stress distribution in perimeter wedge at chainage of 500 m to 700 m of Headrace tunnel of Modi Khola Hydropower Project

4.5 Conclusion

With the analysis of structurally controlled instabilities, it can be concluded that the wedges formed in the crown and invert have greater factor of safety in comparison to that of the wedges formed at the side walls. The stress distribution in the wedge show that wedges formed at the crown and invert are at low stress in comparison to that of the wedges formed at the side walls.

- In the absence of fault, the displacement of the surrounding rock mass reduces gradually from the tunnel limit to the boundary of the outer surrounding rock mass and becomes zero on the boundary.
- With presence of a fault, the displacements of the surrounding rock mass have discontinuous nature.
- The displacement is concentrated more to the tunnel and fault boundary.
- The displacement of tunnel and rock mass surrounding tunnel are more directed towards the movement of the fault.
- From the results obtained from the displacement, crown fault is more critical.
- In inverted D tunnel, when the fault is located in crown of the tunnel the displacement is maximum in the crown of the tunnel.

Table 4-13 Ratio of increase in displacement, axial force, bending moment and shear force

	Inverted D Tunnel		Horseshoe Tunnel		Circular Tunnel	
	Tunnel Section Location /(Ratio)	Fault	Tunnel Section Location /(Ratio)	Fault	Tunnel Section Location /(Ratio)	Fault
Displacement	Left Shoulder (227.2)	Crown	Crown (323.3)	Crown	Crown (308.1)	Crown
Axial Force	Right Side Wall (69.4)	Right Shoulder	Right Side Wall (26.2)	Right Bottom	Right Shoulder (19.3)	Right Side Wall
Bending Moment	Invert (58.0)	Right Bottom	Right Bottom (104.0)	Left Side Wall	Right Shoulder (126.9)	Right Side Wall
Shear Force	Right Side Wall (28.0)	Right Bottom	Right Side Wall (35.1)	Right Bottom	Right Side Wall (140.8)	Left Side Wall

The nature or the path followed by the of the internal forces in the tunnel lining is similar in nature but the magnitude increased in the location respective to the fault. The presence of the fault has increased the internal forces such as axial force, bending moment and shear force in the corresponding position of the fault. It has been illustrated in Table 4-13.

The distribution of the displacements, shear force, bending moment and axial force is uniform and smooth in circular tunnel. It is due to the uniform circular cross section. But in case of the horseshoe and inverted D tunnels the distribution of the displacements, shear force, axial force and bending moment are not uniform. It is due to non-uniform cross-sectional shapes. There is sharp change in cross sectional shape. The results can be concluded in Table 4-14 Critical faults at critical points of tunnel lining in terms of shear force, bending moment, axial force and displacements. It shows which fault is critical in different position of tunnel in terms of shear force, bending moment, axial force and displacement. For example, Right bottom and Right-side wall of circular tunnel are critical in shear force due to right bottom fault.

Table 4-14 Critical faults at critical points of tunnel lining in terms of shear force, bending moment, axial force and displacements

Parameter	Circular Tunnel		Horseshoe Tunnel		Inverted D Tunnel	
	Positions of tunnel lining	Critical Fault	Positions of tunnel lining	Critical Fault	Positions of tunnel lining	Critical Fault
Shear Force	Right bottom and Right Side Wall	Right Bottom Fault	Left Bottom-	Left Side Wall Fault	Left Bottom	Left Side Wall Fault
	Left shoulder and Left Side Wall	Left Side Wall Fault	Right Bottom	Invert Fault	Right Bottom	Right Bottom Fault
	-	-	Left Side Wall	Right Side Wall Fault	Right Side Wall	Right Shoulder Fault
	-	-	-	-	Left Side Wall	Left Side Wall Fault
Bending Moment	Left Bottom	Left Shoulder Fault	Left Bottom	Left Side Fault	Right Bottom	Right Bottom Fault
	Right Side Wall	Right Bottom Fault	Right Bottom	Right Side Fault	Invert	Right Bottom Fault
	Right Shoulder	Right Bottom Fault	Right Shoulder	Right Bottom Fault	Right Bottom	Left Shoulder Fault
	Crown	Right Side Wall Fault	Crown	Right Side Wall Fault	Right Side Wall	Right Side Wall Fault
	-	-	Left Side Wall	Right Side Wall Fault	Left Side Wall	Left Side Wall Fault
Axial Force	Left shoulder	Crown Fault	Invert-	Left Side Wall Fault	Left Bottom	Right Bottom Fault
	Right Bottom	Right Bottom Fault	Right Shoulder	Right Bottom Fault	Right Bottom	Right Shoulder Fault
	Right Side Wall	Right Bottom	Right Shoulder	Right Bottom	Right Side Wall	Right Shoulder Fault
	Right Shoulder	Right Side Wall Fault	Left Side Wall	Left Side Wall Fault	Crown	Right Shoulder Fault
	Left Shoulder	Left Side Wall Fault	Left Bottom	Left Side Wall Fault	Left Shoulder	Left Side Wall Fault
	Left Side Wall	Left Bottom Fault	-	-	-	-
Displacement	Left Bottom	Left Shoulder Fault	Crown	Crown Fault	Crown	Crown Fault
	Right Bottom	Invert Fault,	Right shulder	Right Shoulder Fault	Right shoulder	Right Shoulder Fault
	Left Side Wall	Right Bottom Fault	Left shoulder	Left Shoulder Fault	Left shoulder	Left Shoulder Fault

Hence, we can conclude that tunnel lining becomes critical in terms of displacement, shear force, axial force and bending moment when there is presence of fault. However, it is not proportional for all the sections i.e a fault that is located in specific place does not increase the parameter of stress or displacement in same place. It may or may not increase the parameter of stress or displacement. For example, the displacement has increased in circular and horse shoe tunnel in crown, right shoulder and left shoulder

when the fault is located crown, right shoulder and left shoulder respectively. However, it is not in the case of inverted D tunnel.

Similarly, the shear force, bending moment and axial force in the tunnel lining don't increase in the place where the the fault is located. For example, in case inverted D tunnel, there is maximum shear force at right bottom and right-side wall due to right bottom fault. Similarly, in case of horseshoe tunnel, shear force in left bottom is maximum due to left side wall fault and in case of circular tunnel left bottom has maximum shear force due to left side wall fault. It is similar with the case of bending moment, displacement and axial force in all three-cross section of tunnel.

However, from Table 4-14 we can see that the circular tunnel show more uniformity in the effect in tunnel lining due to the fault position than inverted D and horseshoe tunnel. i.e., the fault and its effect in tunnel lining location are proportional in the same side where as Inverted D show least uniformity i.e., the fault and its effect in the tunnel lining is random.

5 Tunnel design system in Fault

Articulated design suggested by Russo et. al, 2002 has been used for the design of the tunnel support using 2D Numerical Modelling in RS2. This strategy of the design consists in reducing the lining segments and leaving independent sections over a certain across the fault. When there is fault rupture, it helps to concentrate the movement at the joints linking the segments, and to limit the movement of the ground on a certain distance. This concentrates potential damages in the tunnel support at some elements only, without propagation of the damage to other elements. The maximum length of any single element depends on width of the cross section, expected movement of the fault, compressibility of the surrounding soil, element kinematics (Russo et. al, 2002).

Tunnel acts longitudinally as an embedded beam whose extremities are displaced by the lateral offset or displacement of the fault. Some assumption made are made i.e., the fault ruptures with higher probability by a uniformly distribution of displacement or offset across the fault boundaries, displacement which is expected is mainly in x-y plane. Therefore, the shear strain (γ) in the fault rock or soil can be reasonably assumed according to the movement of fault with geological records.

The implementation of the design procedure has been done as follows:

- Inverted-D have been used.
- Eight locations of fault have been done as fault definition and location done in section 4.2.2.
- The maximum acceptable shear resistance of the joint has been defined on an equivalent elastic model.
- In modelling in RS2, strain at Locking has been implemented for the analysis of the articulated design.
- The length of the sliding gap is specified in terms of an equivalent or circumferential strain in the liner.
- The strain is averaged over the entire length of liner being considered. The sliding gap does not have a physical location on the RS2 model, the effect of the gap is averaged over the entire liner.
- The value of Strain at Locking depends on the length of liner you are considering. Example: for a fully lined, circular tunnel of 6 meter diameter, and a total Sliding Gap = 1 meter, the Strain at Locking = $100/(\pi \times 6) \% = 5.3 \%$.
- If more than one sliding gap exists, then add up the total gap length, and divide by the total liner length, to determine the Strain at Locking.

At the installation stage of a sliding gap liner, the axial stiffness and axial force in the liner is always zero regardless of the liner strain (i.e. the gap is never closed at the installation stage). After each stage of

modelling, RS2 checks the liner axial strain. If the strain in the liner is less than the Strain at Locking, then the liner has zero axial stiffness in the next stage. If the axial strain in the liner is greater than or equal to the Strain at Locking, then the gap closes at the next stage, and the axial stiffness will be set to that defined which is equivalent to (EA/L) . The liner then have have axial forces in it after the nextstage. Up to rupture of the joints (weak sections) the tunnel will be sheared and bent by surrounding rock and soil as an embedded beam. Once the joints shear resistance attained, each segment will be free to move independently according to external loads. So, for the sliding gap liner to work correctly, modelling have been multiple stages (15 stages) with the liner installed and in general relax the boundary stresses over a number of stages. Figure 5-1 show tunnel support details.

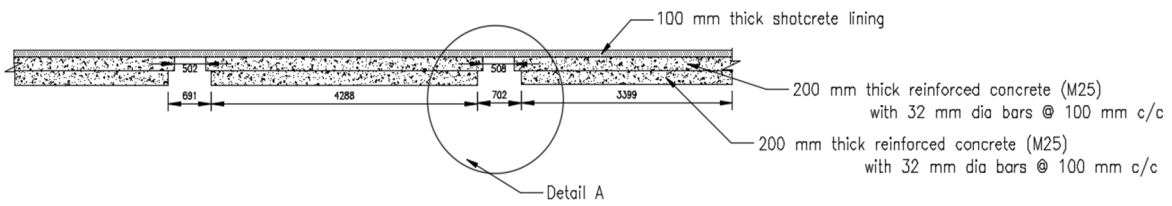
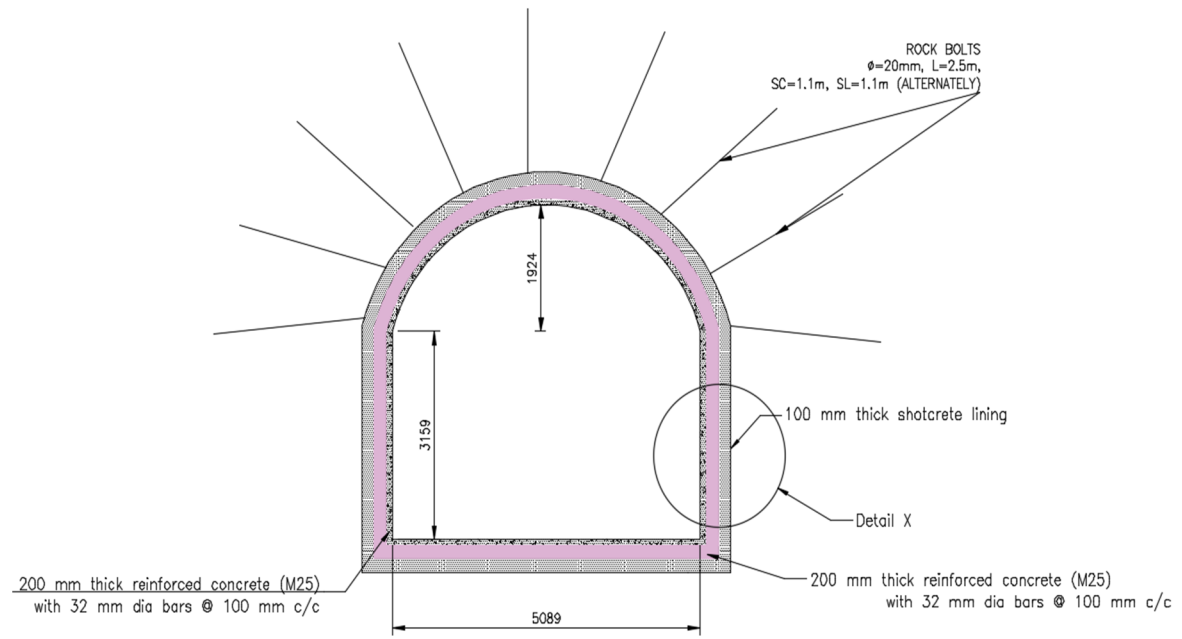
Design of Tunnel Support for Crown Fault

The support consists of 100 mm shotcrete (25 MPa), 20 mm dia anchored rock bolts @ 1 m c/c and 400 mm reinforced concrete (25 MPa). The tunnel support details are shown in Figure 5-1. This support has been designed for all the fault cases defined in the section 4.2.2. The support capacity curve showed that it failed due to moment when the articulated design was not used (Figure 5-9). With the application of articulated design of 15 percent strain locking, the support capacity curve showed that it was safe for axial, shear and bending moment (Figure 5-8).

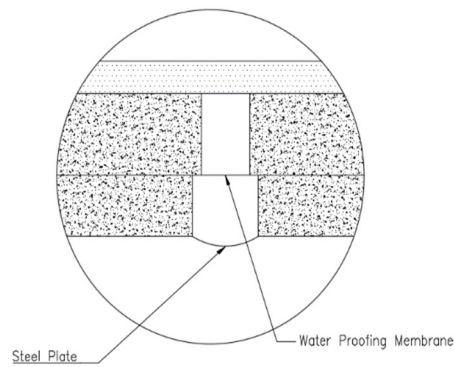
The maximum shear force 1.246 MN, -1.114 MN were obtained when the fault was located above the crown of the tunnel (Figure 5-3). The support consists of 100 mm shotcrete (25 MPa), 20 mm dia anchored rock bolts @ 1 m c/c and 400 mm reinforced concrete (25 MPa). The support capacity curve showed that it failed due to moment. With the application of articulated design of 15 percent strain locking, the maximum shear force was reduced to 0.535 MN, -0.526 MN (Figure 5-2).

Similarly, the maximum Moment of 0.195 MNm, -0.468 MNm were obtained when the fault was located above the crown of the tunnel (Figure 5-5). The support consists of 100 mm shotcrete (25 MPa), 20 mm dia anchored rock bolts @ 1 m c/c and 400 mm reinforced concrete (25 MPa). With the application of articulated design of 15 percent strain locking, the maximum moment was reduced to 0.157 MNm, -0.283 MNm (Figure 5-4).

Also, The Axial force of 1.421 MN, -0.436 MN were obtained when the fault was located above the crown of the tunnel (Figure 5-7). The support consists of 100 mm shotcrete (25 MPa), 20 mm diameter anchored rock bolts @ 1 m c/c and 400 mm reinforced concrete (25 MPa). With the application of articulated design of 15 percent strain locking, the maximum axial force was reduced to 0 MN (Figure 5-6).



Detail X



Detail A

Figure 5-1 Tunnel Support Details

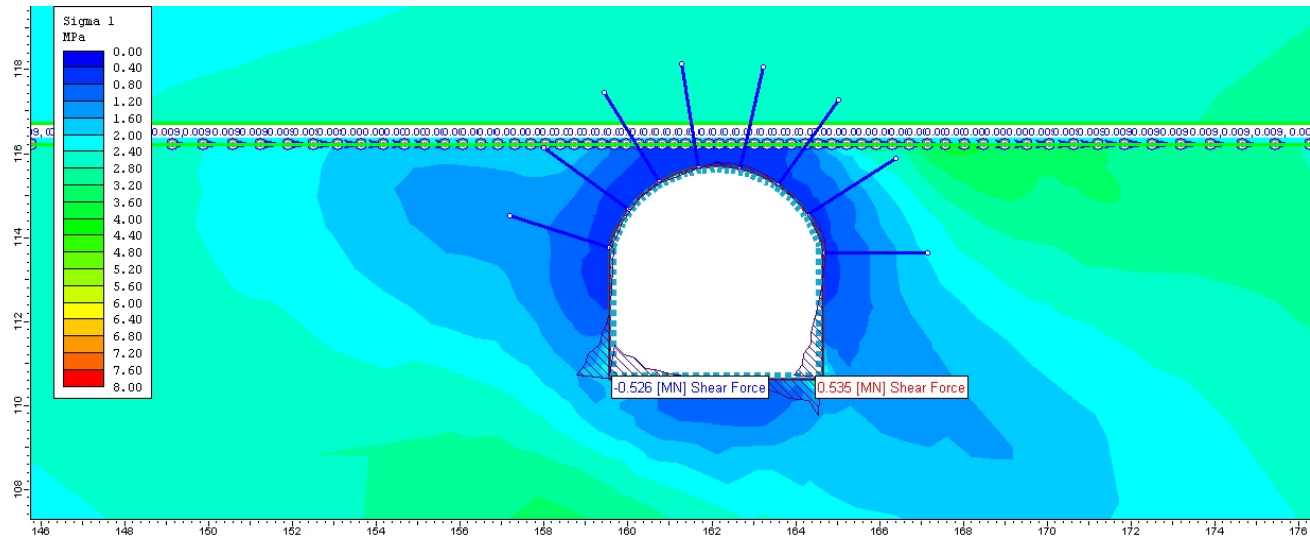


Figure 5-2 Shear force distribution with articulated design Crown Fault

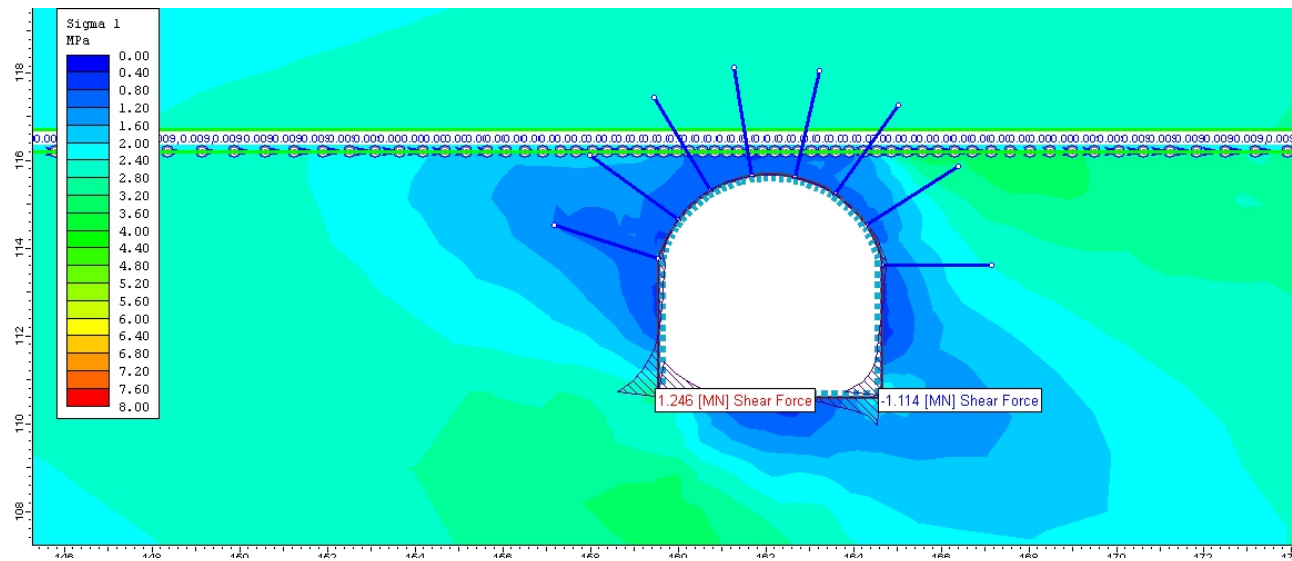


Figure 5-3 Shear force distribution without articulated design Crown Fault

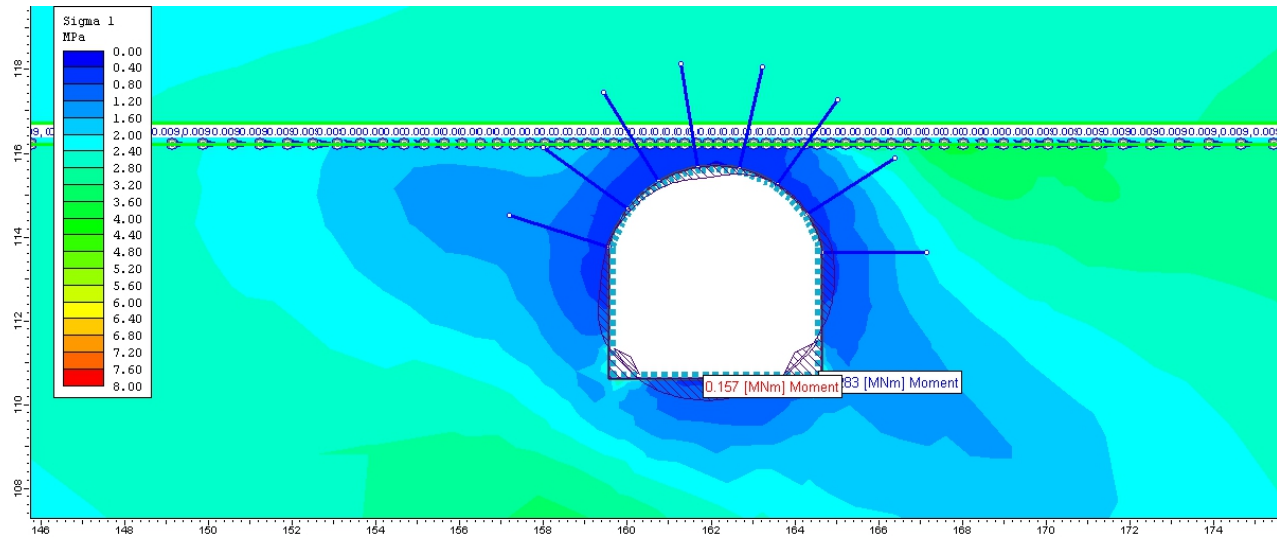


Figure 5-4 Moment distribution with articulated design Crown Fault

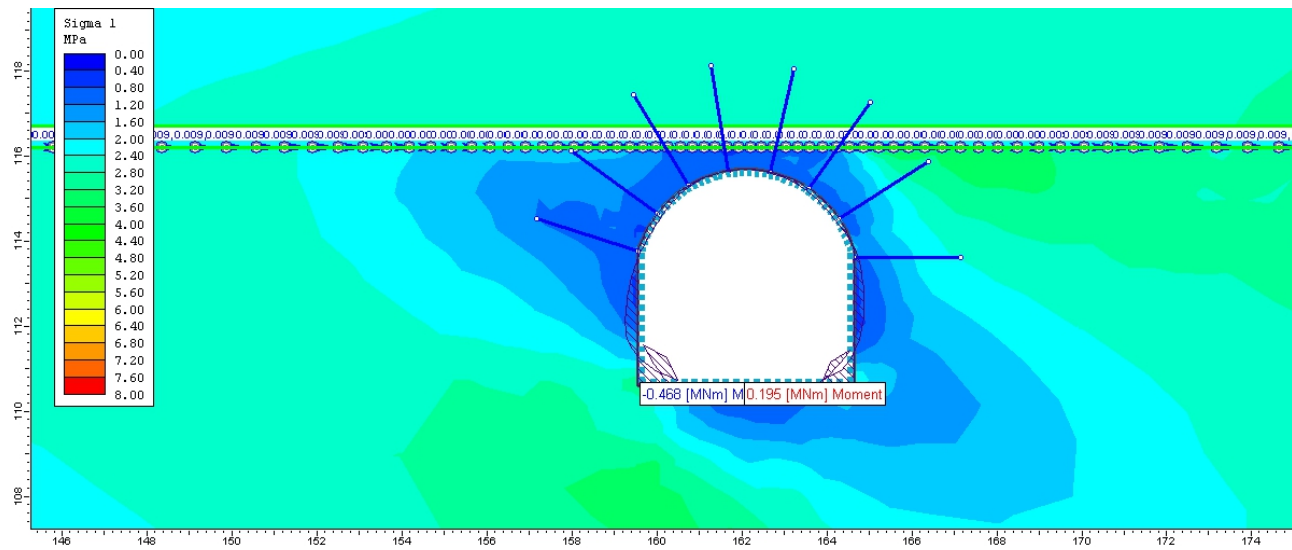


Figure 5-5 Moment distribution without articulated design Crown Fault

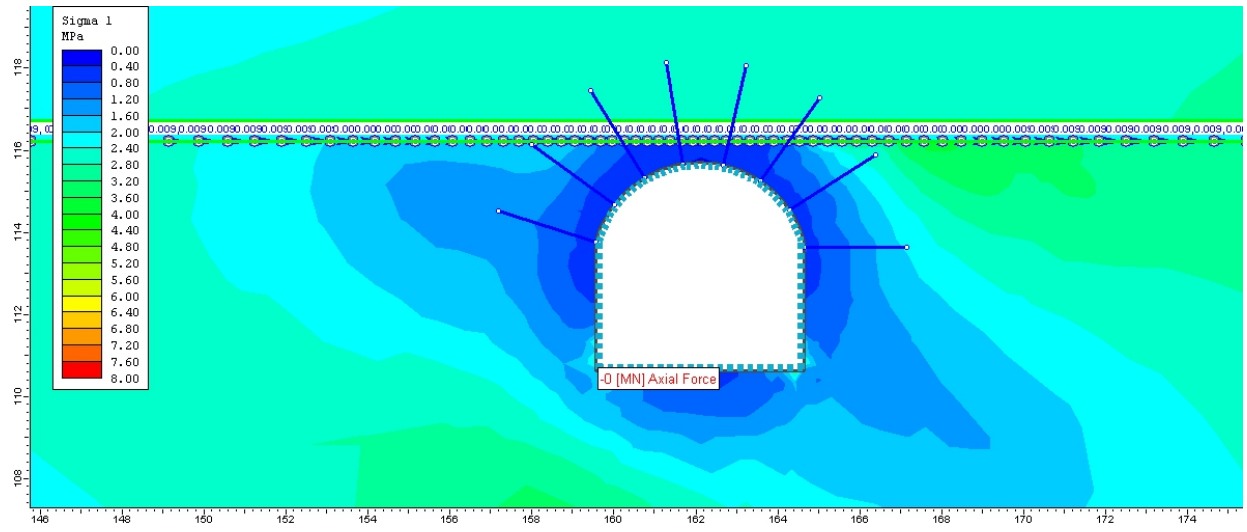


Figure 5-6 Axial Force distribution with articulated design Crown Fault

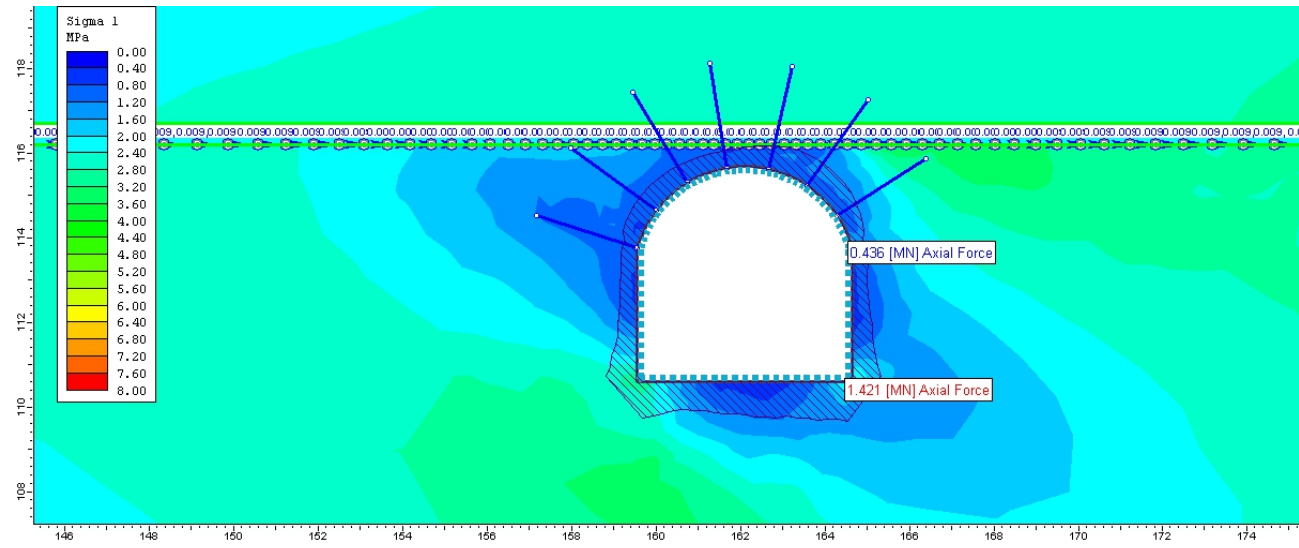


Figure 5-7 Axial Force distribution without articulated design Crown Fault

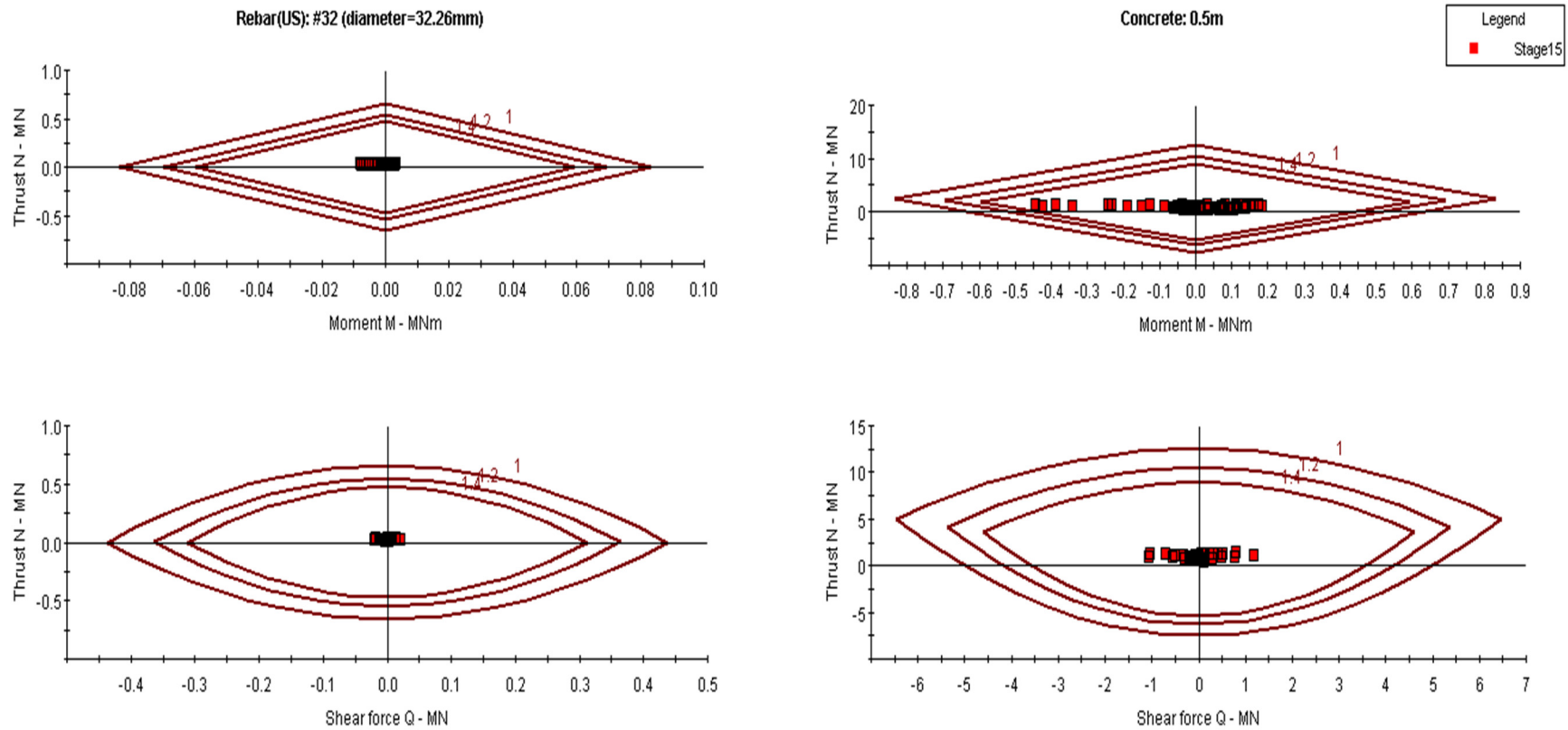


Figure 5-8 Support capacity plot with articulated design

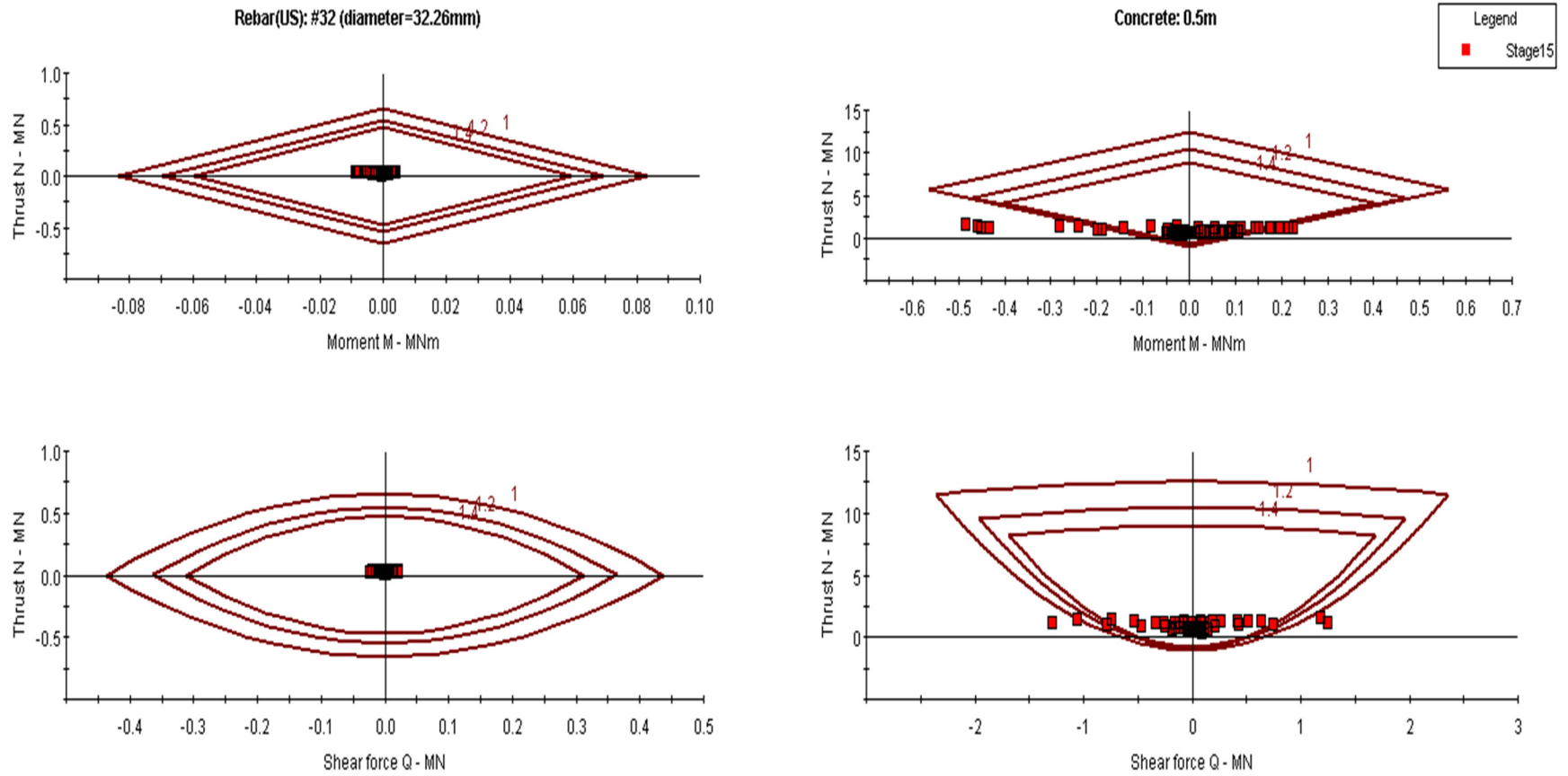


Figure 5-9 Support capacity plot without articulated design

Similarly, the stress distribution, with and without the articulated design for the different fault locations defined in 4.2.2 are as follows.

Design of Tunnel Support for Invert Fault

The maximum shear force 5.283 MN was obtained when the fault was located above the crown of the tunnel (Figure 5-15). The support consists of 100 mm shotcrete (25 MPa), 20 mm diameter anchored rock bolts @ 1 m c/c and 400 mm reinforced concrete (25 MPa). With the application of articulated design of 15 percent strain locking, the maximum shear force was reduced to 4.909 MN (Figure 5-12).

Similarly, the maximum Moment of 0.218 MNm, -0.742 MNm were obtained when the fault was located above the crown of the tunnel (Figure 5-14). The support consists of 100 mm shotcrete (25 MPa), 20 mm diameter anchored rock bolts @ 1 m c/c and 400 mm reinforced concrete (25 MPa). With the application of articulated design of 15 percent strain locking, the maximum moment was reduced to 0.19 MNm, -0.67 MNm (Figure 5-11).

Also, The Axial force of 4.487 MN, -1.166 MN were obtained when the fault was located above the crown of the tunnel (Figure 5-13). The support consists of 100 mm shotcrete (25 MPa), 20 mm diameter anchored rock bolts @ 1 m c/c and 400 mm reinforced concrete (25 MPa). With the application of articulated design of 15 percent strain locking, the maximum axial force was reduced to 0 MN (Figure 5-10).

Design of Tunnel Support for Left Bottom Fault

The maximum shear force 2.97 MN were obtained when the fault was located above the crown of the tunnel (Figure 5-21). The support consists of 100 mm shotcrete (25 MPa), 20 mm diameter anchored rock bolts @ 1 m c/c and 400 mm reinforced concrete (25 MPa). The support capacity curve showed that it failed due to moment. With the application of articulated design of 15 percent strain locking, the maximum shear force was reduced to 2.743 MN (Figure 5-18).

Similarly, maximum Moment of 0.152 MNm, -0.465 MNm were obtained when the fault was located above the crown of the tunnel (Figure 5-20). The support consists of 100 mm shotcrete (25 MPa), 20 mm diameter anchored rock bolts @ 1 m c/c and 400 mm reinforced concrete (25 MPa). With the application of articulated design of 15 percent strain locking, the maximum moment was reduced to 0.108 MNm, -0.433 MNm (Figure 5-17).

Also, The Axial force of 2.93 MN, -0.287 MN were obtained when the fault was located above the crown of the tunnel (Figure 5-19). The support consists of 100 mm shotcrete (25 MPa), 20 mm diameter anchored rock bolts @ 1 m c/c and 400 mm reinforced concrete (25 MPa). With the application of articulated design of 15 percent strain locking, the maximum axial force was reduced to 0 MN (Figure 5-16).

Design of Tunnel Support for Left Shoulder Fault

The maximum shear force 1.328 MN, -1.359 MN were obtained when the fault was located above the crown of the tunnel (Figure 5-27). The support consists of 100 mm shotcrete (25 MPa), 20 mm diameter anchored rock bolts @ 1 m c/c and 400 mm reinforced concrete (25 MPa). The support capacity curve showed that it failed due to moment. With the application of articulated design of 15 percent strain locking, the maximum shear force was reduced to 0.728 MN, -0.64 MN (Figure 5-24).

Similarly, the maximum moment of 0.239 MNm were obtained when the fault was located above the crown of the tunnel (Figure 5-26). The support consists of 100 mm shotcrete (25 MPa), 20 mm diameter anchored rock bolts @ 1 m c/c and 400 mm reinforced concrete (25 MPa). With the application of articulated design of 15 percent strain locking, the maximum moment was reduced to 0.193 MNm (Figure 5-23).

Also, the axial force of 1.623 MN, -0.375 MN were obtained when the fault was located above the crown of the tunnel (Figure 5-25). The support consists of 100 mm shotcrete (25 MPa), 20 mm diameter anchored rock bolts @ 1 m c/c and 400 mm reinforced concrete (25 MPa). With the application of articulated design of 15 percent strain locking, the maximum axial force was reduced to 0 MN (Figure 5-22).

Design of Tunnel Support for Left Side Wall Fault

The maximum shear force 3.352 MN were obtained when the fault was located above the crown of the tunnel (Figure 5-33). The support consists of 100 mm shotcrete (25 MPa), 20 mm diameter anchored rock bolts @ 1 m c/c and 400 mm reinforced concrete (25 MPa). The support capacity curve showed that it failed due to moment. With the application of articulated design of 15 percent strain locking, the maximum shear force was reduced to 3.811 MN (Figure 5-30).

Similarly, the maximum moment of 0.155 MNm, -0.572 MNm were obtained when the fault was located above the crown of the tunnel (Figure 5-32). The support consists of 100 mm shotcrete (25 MPa), 20 mm diameter anchored rock bolts @ 1 m c/c and 400 mm reinforced concrete (25 MPa). With the

application of articulated design of 15 percent strain locking, the maximum moment was reduced to 0.144 MNm, -0.542 MNm (Figure 5-29).

Also, The Axial force of 3.039 MN, -2.417 MN were obtained when the fault was located above the crown of the tunnel (Figure 5-31). The support consists of 100 mm shotcrete (25 MPa), 20 mm diameter anchored rock bolts @ 1 m c/c and 400 mm reinforced concrete (25 MPa). With the application of articulated design of 15 percent strain locking, the maximum axial force was reduced to 0 MN (Figure 5-28).

Design of Tunnel Support for Right Bottom Fault

The maximum shear force 0.64 MN, -0.572 MN were obtained when the fault was located above the crown of the tunnel (Figure 5-37). The support consists of 100 mm shotcrete (25 MPa), 20 mm diameter anchored rock bolts @ 1 m c/c and 400 mm reinforced concrete (25 MPa). The support capacity curve showed that it failed due to moment. With the application of articulated design of 15 percent strain locking, the maximum shear force was reduced to 0.314 MN, -0.267 MN (Figure 5-36).

Similarly, The maximum Moment of 0.109 MNm, -0.24 MNm were obtained when the fault was located above the crown of the tunnel (Figure 5-39). The support consists of 100 mm shotcrete (25 MPa), 20 mm diameter anchored rock bolts @ 1 m c/c and 400 mm reinforced concrete (25 MPa). With the application of articulated design of 15 percent strain locking, the maximum moment was reduced to 0.083 MNm, -0.146 MNm (Figure 5-35).

Also, axial force of 0.75 MN, -0.193 MN were obtained when the fault was located above the crown of the tunnel (Figure 5-38). The support consists of 100 mm shotcrete (25 MPa), 20 mm diameter anchored rock bolts @ 1 m c/c and 400 mm reinforced concrete (25 MPa). With the application of articulated design of 15 percent strain locking, the maximum axial force was reduced to 0 MN (Figure 5-34).

Design of Tunnel Support for Right Shoulder Fault

The maximum shear force 0.837 MN were obtained when the fault was located above the crown of the tunnel (Figure 5-45). The support consists of 100 mm shotcrete (25 MPa), 20 mm diameter anchored rock bolts @ 1 m c/c and 400 mm reinforced concrete (25 MPa). The support capacity curve showed that it failed due to moment. With the application of articulated design of 15 percent strain locking, the maximum shear force was reduced to 0.395 MN (Figure 5-42).

Similarly, the maximum moment of 0.145 MNm, -0.336 MNm were obtained when the fault was located above the crown of the tunnel (Figure 5-44). The support consists of 100 mm shotcrete (25 MPa), 20 mm diameter anchored rock bolts @ 1 m c/c and 400 mm reinforced concrete (25 MPa). With the application of articulated design of 15 percent strain locking, the maximum moment was reduced to 0.103 MNm, -0.185 MNm (Figure 5-41).

Also, The Axial force of 0.896 MN, -0.34 MN were obtained when the fault was located above the crown of the tunnel (Figure 5-43). The support consists of 100 mm shotcrete (25 MPa), 20 mm diameter anchored rock bolts @ 1 m c/c and 400 mm reinforced concrete (25 MPa). With the application of articulated design of 15 percent strain locking, the maximum axial force was reduced to 0 MN (Figure 5-40).

Design of Tunnel Support for Right Side Wall

The maximum shear force 1.168 MN were obtained when the fault was located above the crown of the tunnel (Figure 5-51). The support consists of 100 mm shotcrete (25 MPa), 20 mm diameter anchored rock bolts @ 1 m c/c and 400 mm reinforced concrete (25 MPa). The support capacity curve showed that it failed due to moment. With the application of articulated design of 15 percent strain locking, the maximum shear force was reduced to 0.458 MN (Figure 5-48).

Similarly, the maximum moment of 0.187 MNm, -0.462 MNm were obtained when the fault was located above the crown of the tunnel (Figure 5-50). The support consists of 100 mm shotcrete (25 MPa), 20 mm diameter anchored rock bolts @ 1 m c/c and 400 mm reinforced concrete (25 MPa). With the application of articulated design of 15 percent strain locking, the maximum moment was reduced to 0.12 MNm, -0.2 MNm (Figure 5-47).

Also, the axial force of 1.296 MN, -0.223 MN were obtained when the fault was located above the crown of the tunnel (Figure 5-49). The support consists of 100 mm shotcrete (25 MPa), 20 mm diameter anchored rock bolts @ 1 m c/c and 400 mm reinforced concrete (25 MPa). With the application of articulated design of 15 percent strain locking, the maximum axial force was reduced to 0 MN (Figure 5-46).

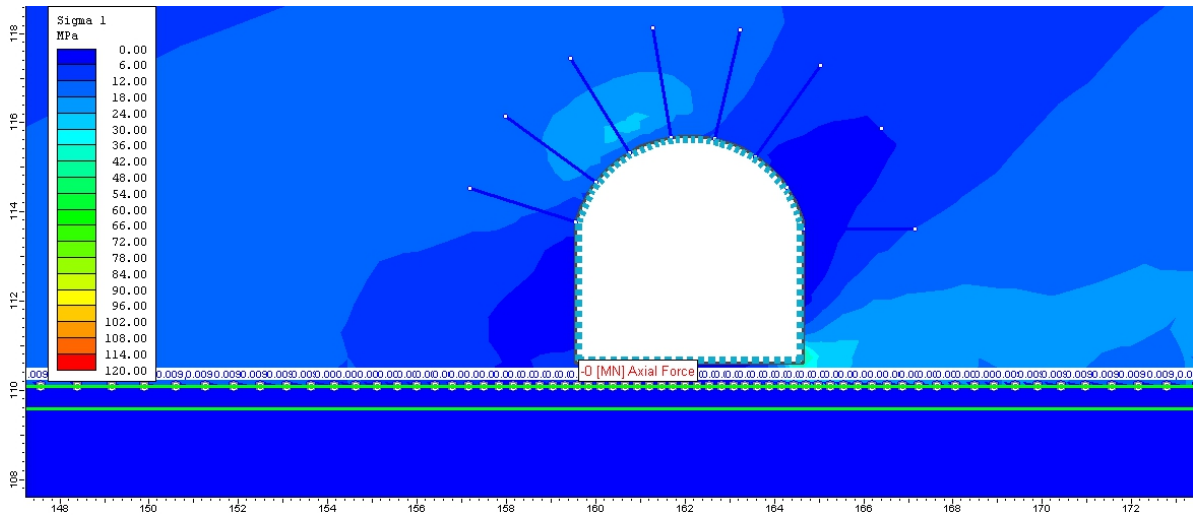


Figure 5-10 Axial Force Distribution with articulated design Invert Fault

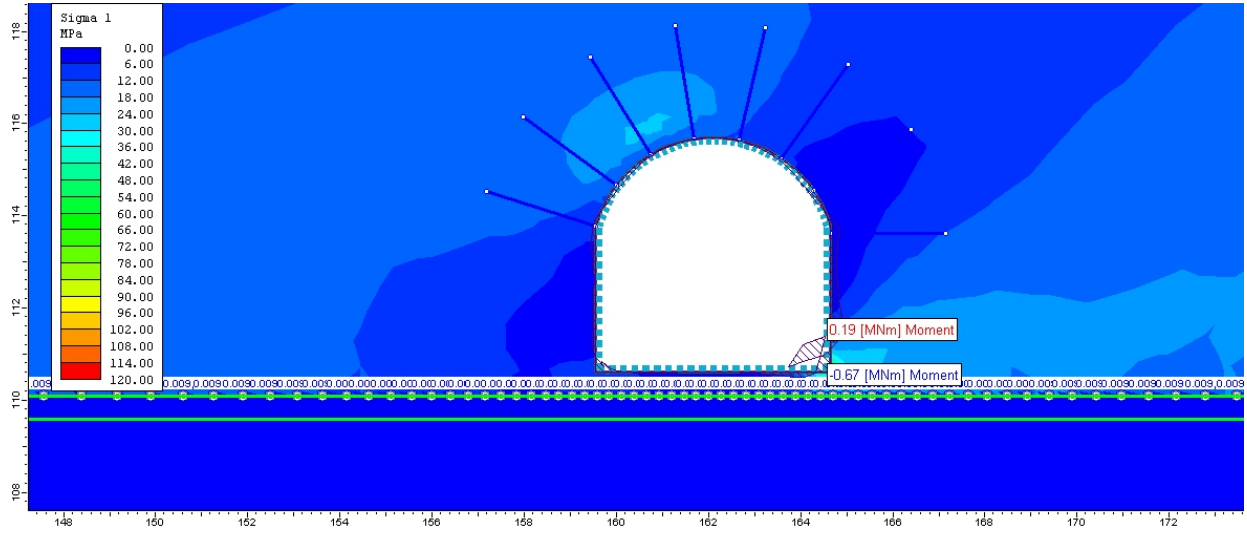


Figure 5-11 Moment Distribution with articulated design Invert Fault

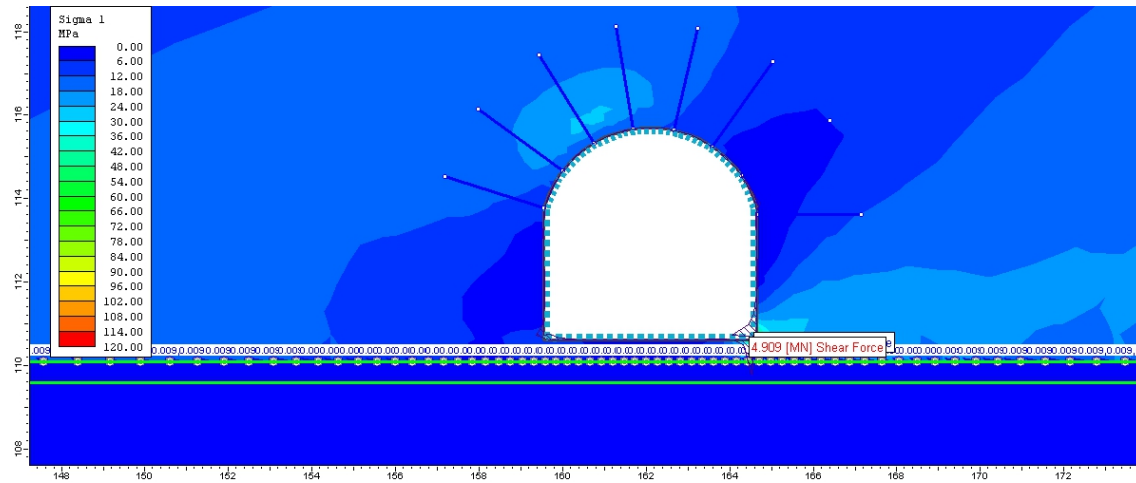


Figure 5-12 Shear Force Distribution with articulated design Invert Fault

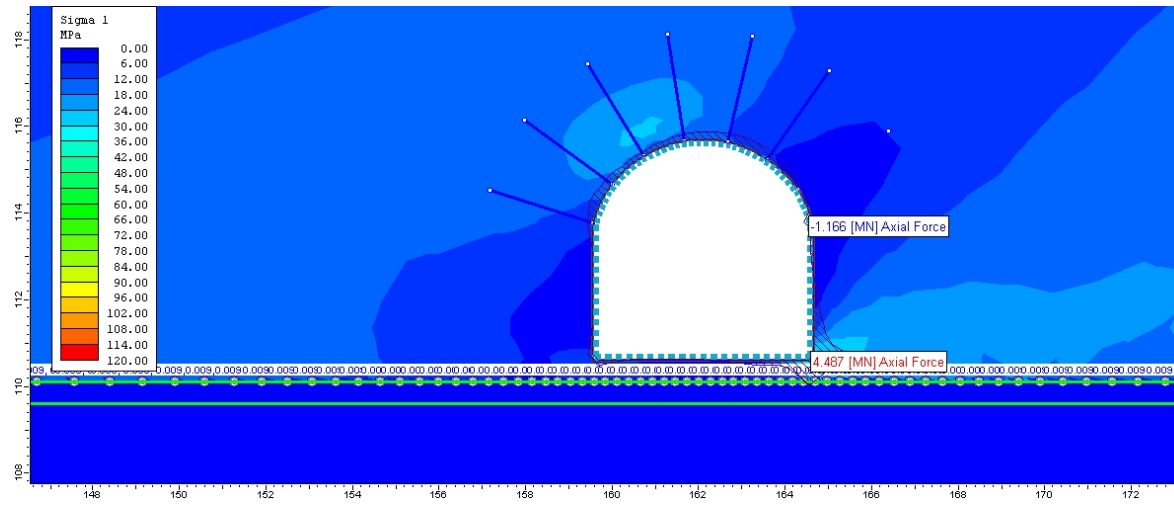


Figure 5-13 Axial Force distribution without articulated design for Invert Fault

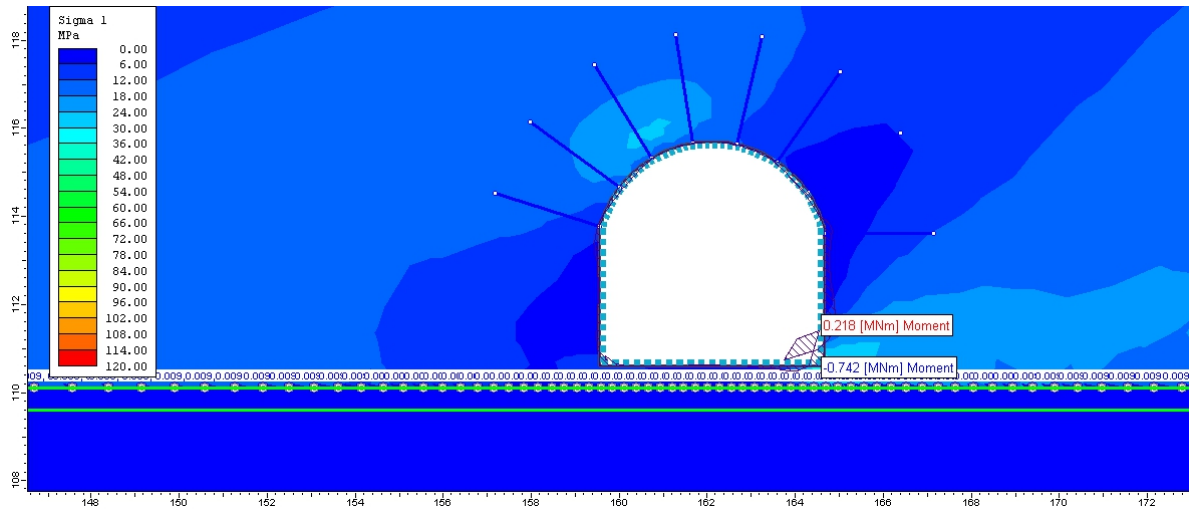


Figure 5-14 Moment distribution without articulated design for Invert Fault

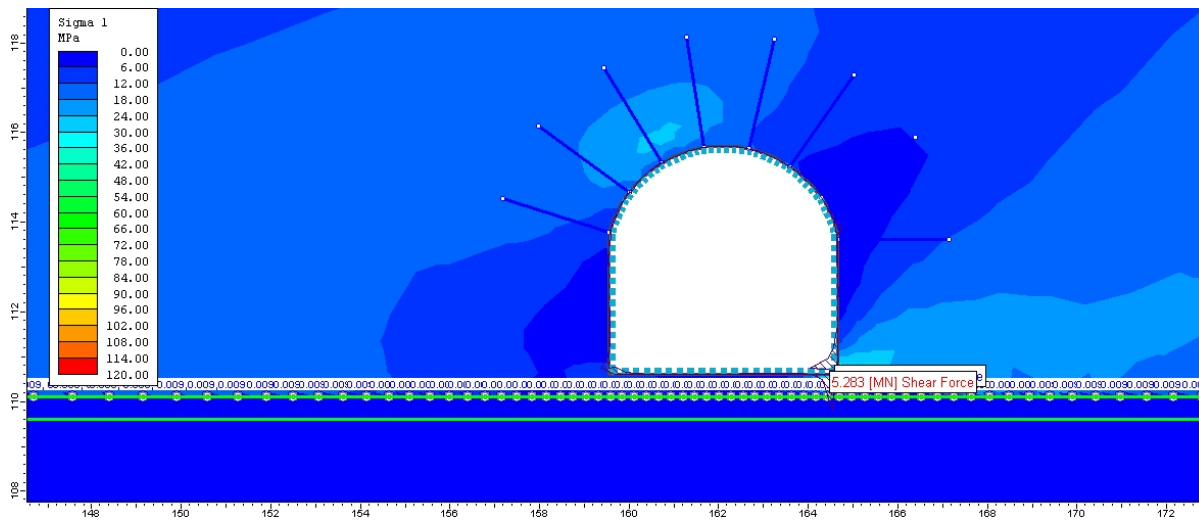


Figure 5-15 Shear Force distribution without articulated design for Invert Fault

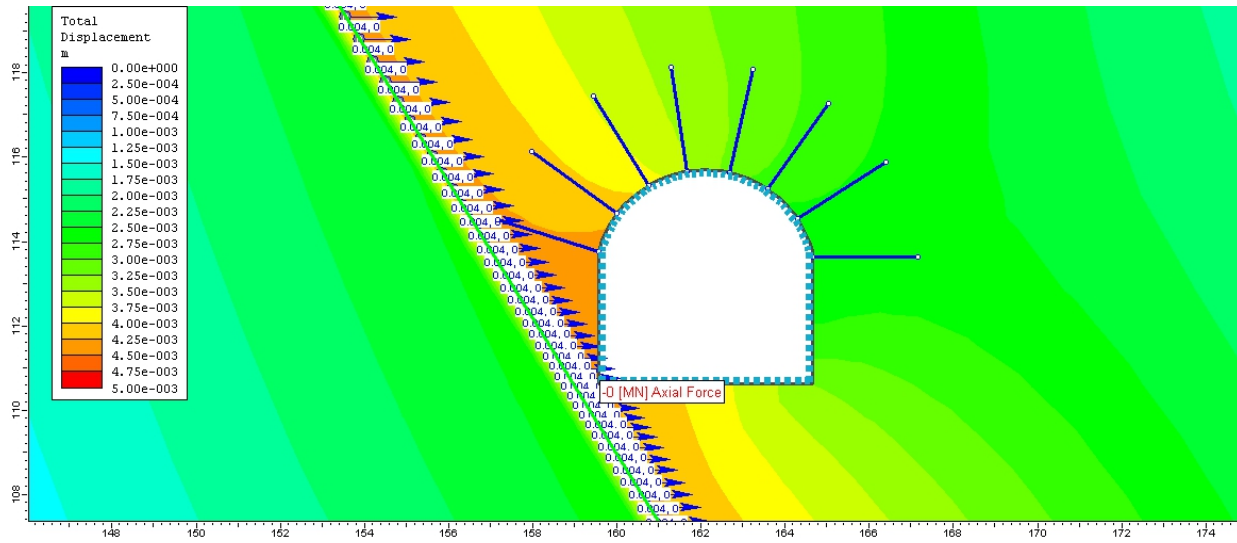


Figure 5-16 Axial Force Distribution with articulated design for Left Bottom Fault

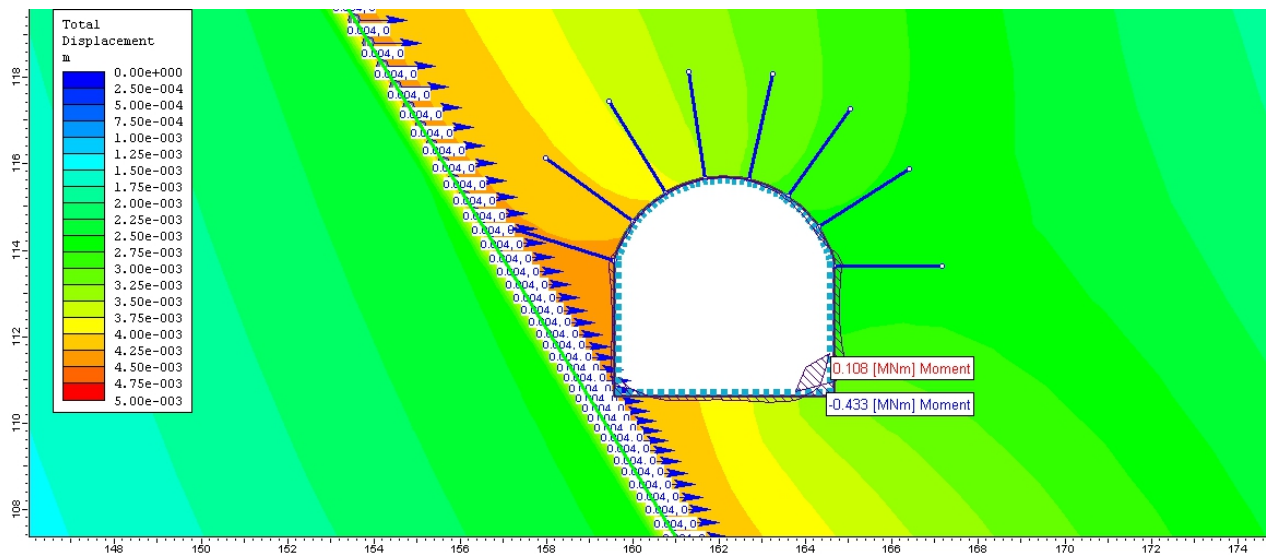


Figure 5-17 Moment Distribution with articulated design for Left Bottom Fault

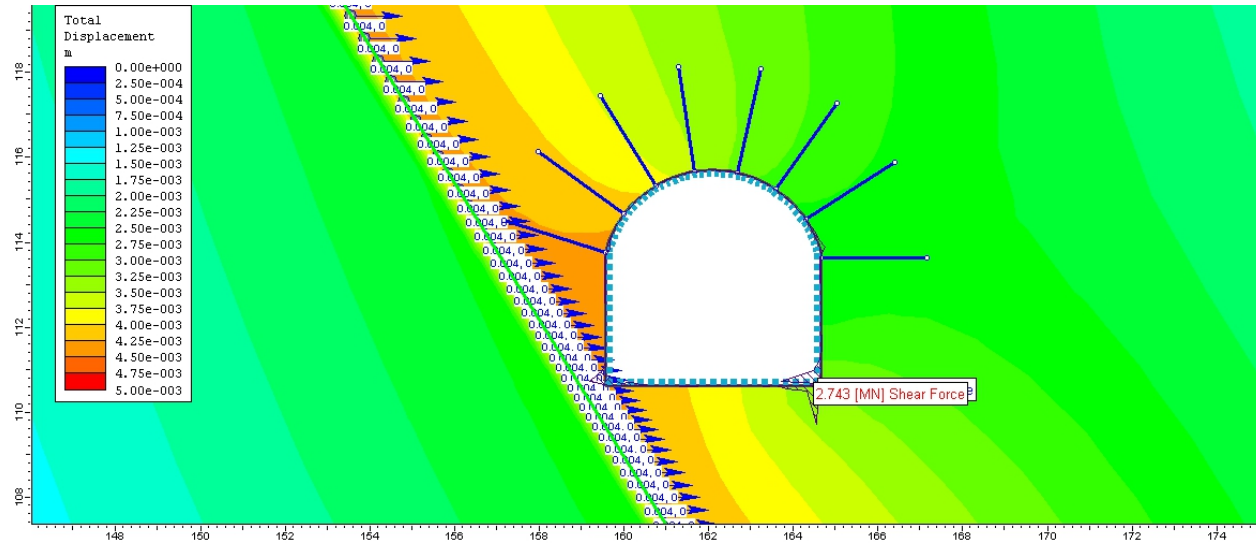


Figure 5-18 Shear Force Distribution with articulated design for Left Bottom Fault

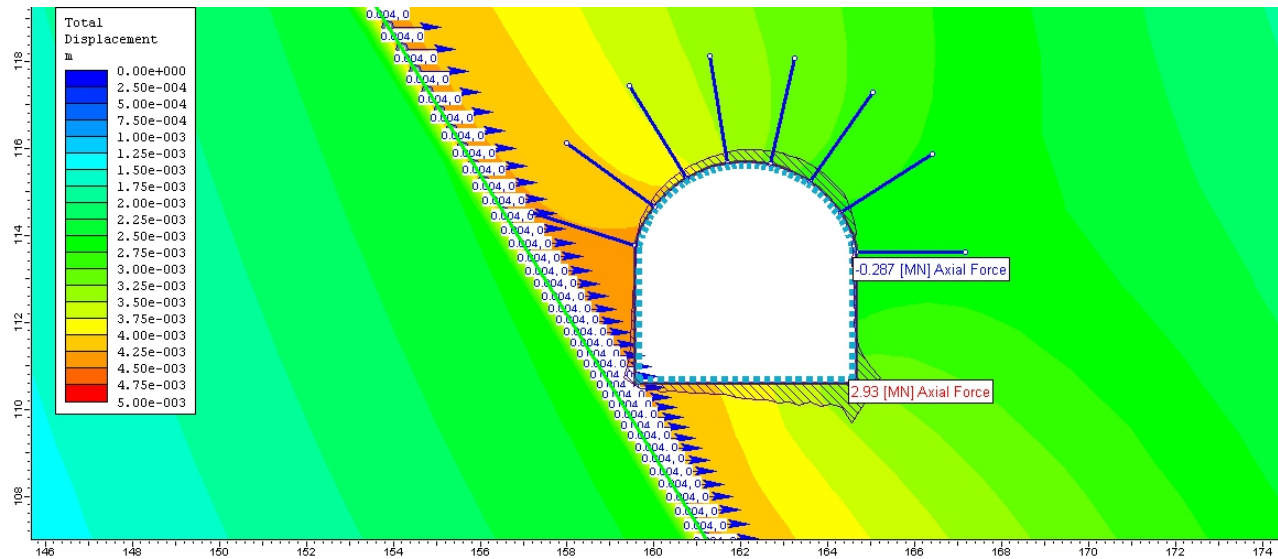


Figure 5-19 Axial Force Distribution without articulated design for Left Bottom Fault

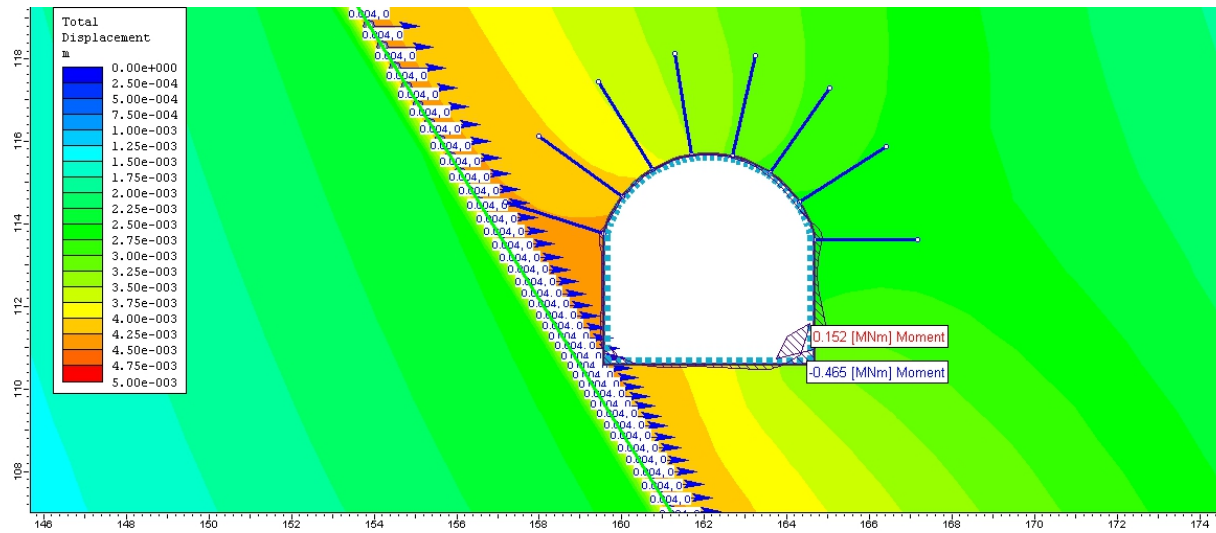


Figure 5-20 Moment Distribution without articulated design for Left Bottom Fault

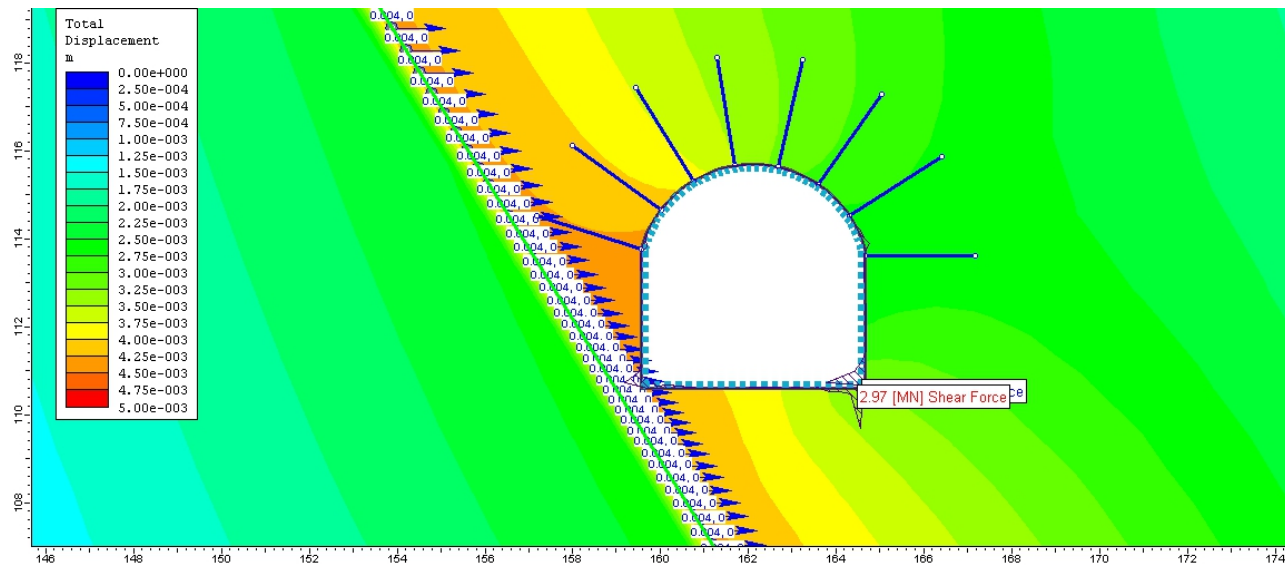


Figure 5-21 Shear Distribution without articulated design for Left Bottom Fault

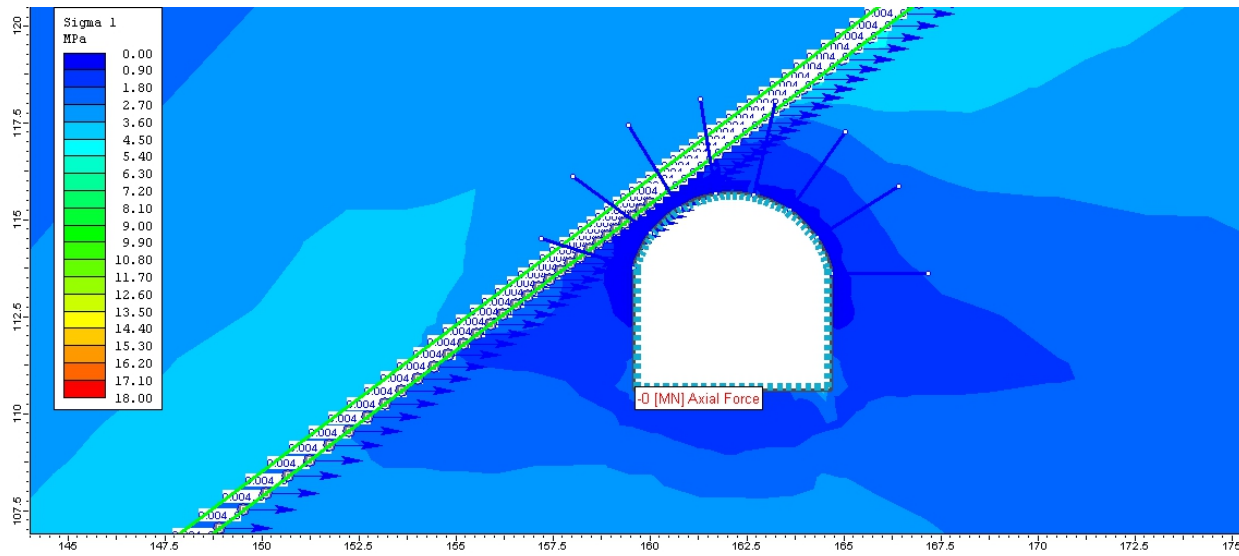


Figure 5-22 Axial Distribution with articulated design for Left Shoulder Fault

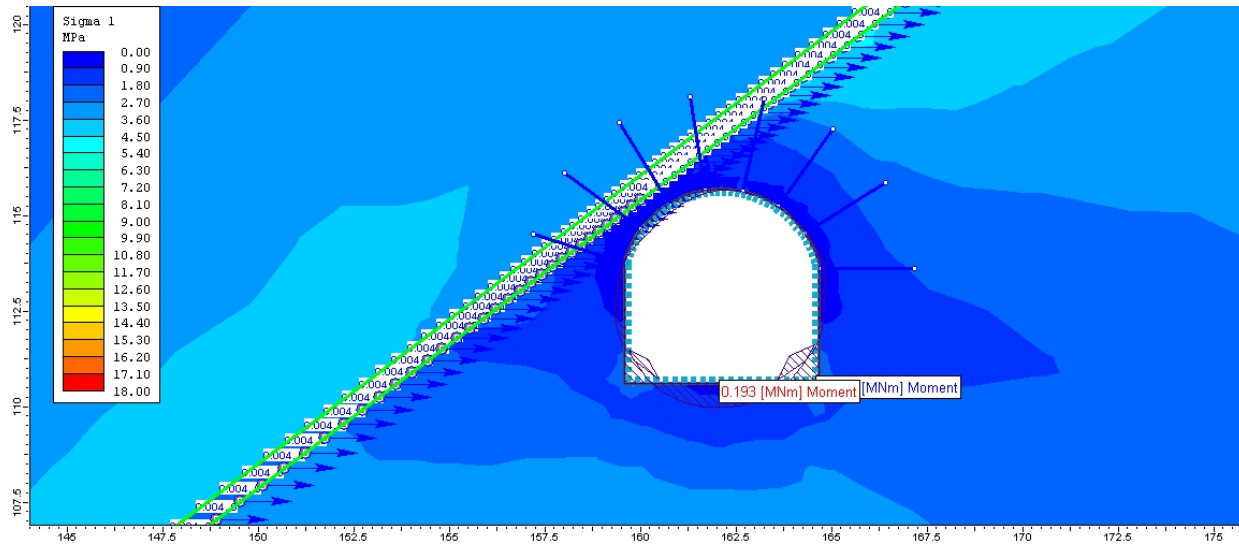


Figure 5-23 Moment Distribution with articulated design for Left Shoulder Fault

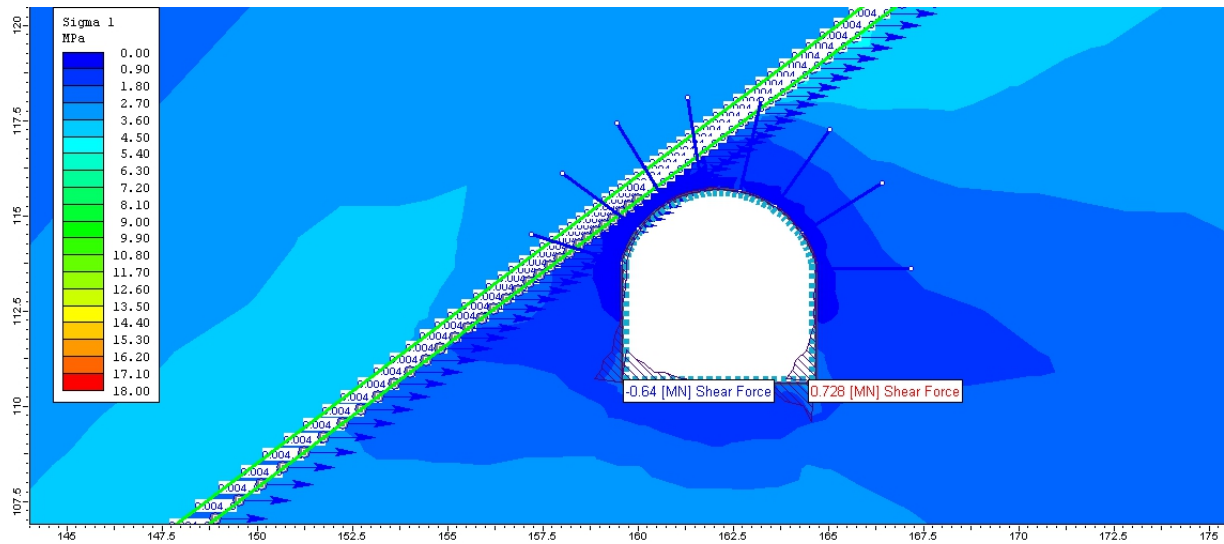


Figure 5-24 Shear Distribution with articulated design for Left Shoulder Fault

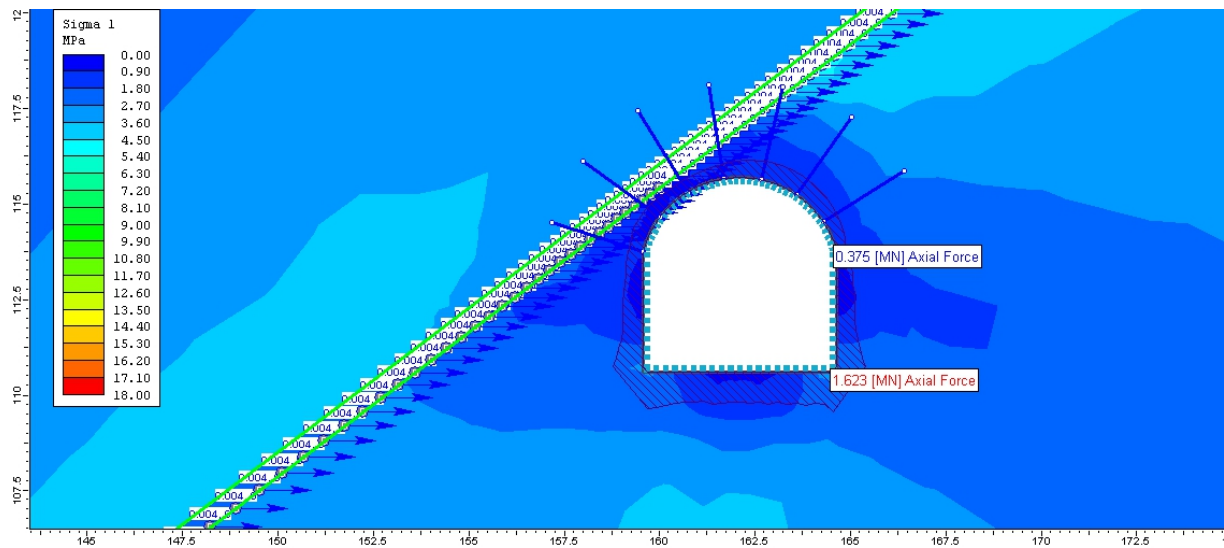


Figure 5-25 Axial Distribution without articulated design for Left Shoulder Fault

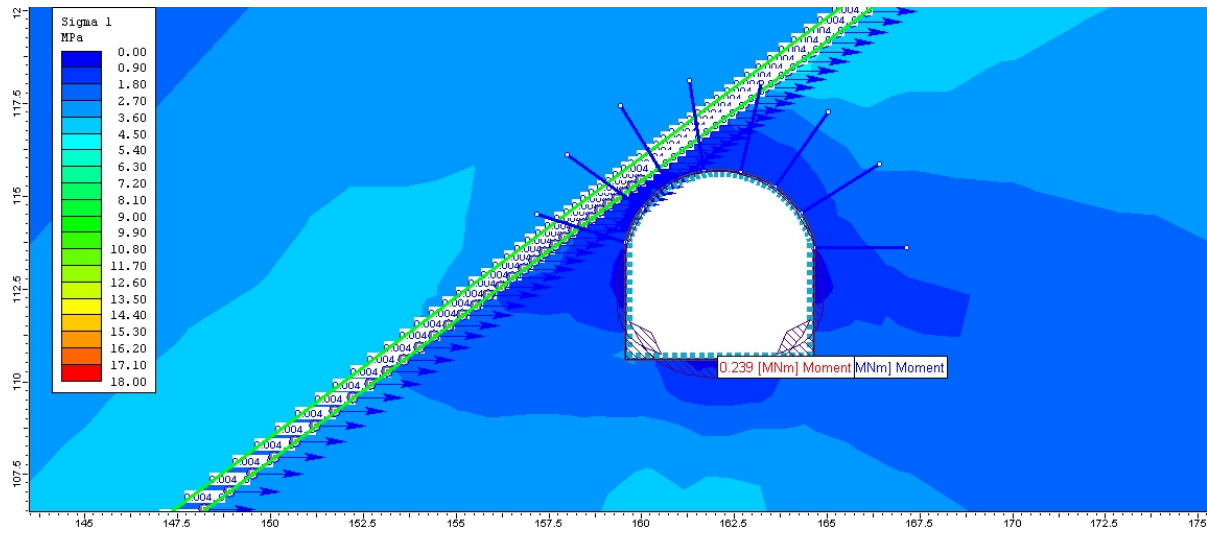


Figure 5-26 Moment Distribution without articulated design for Left Shoulder Fault

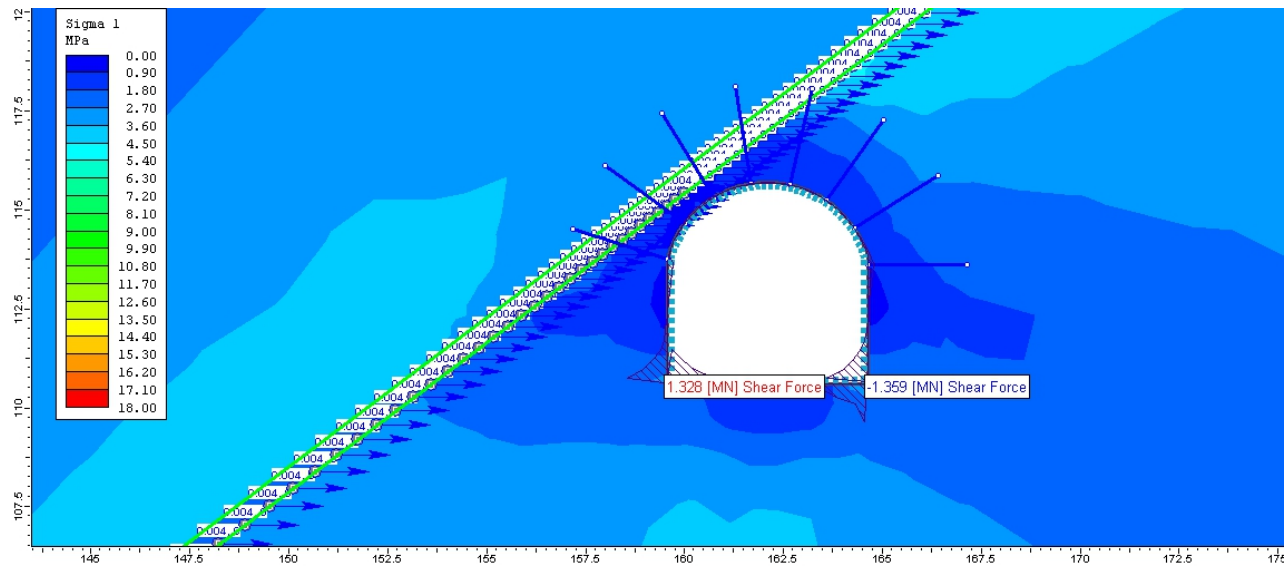


Figure 5-27 Shear Distribution without articulated design for Left Shoulder Fault

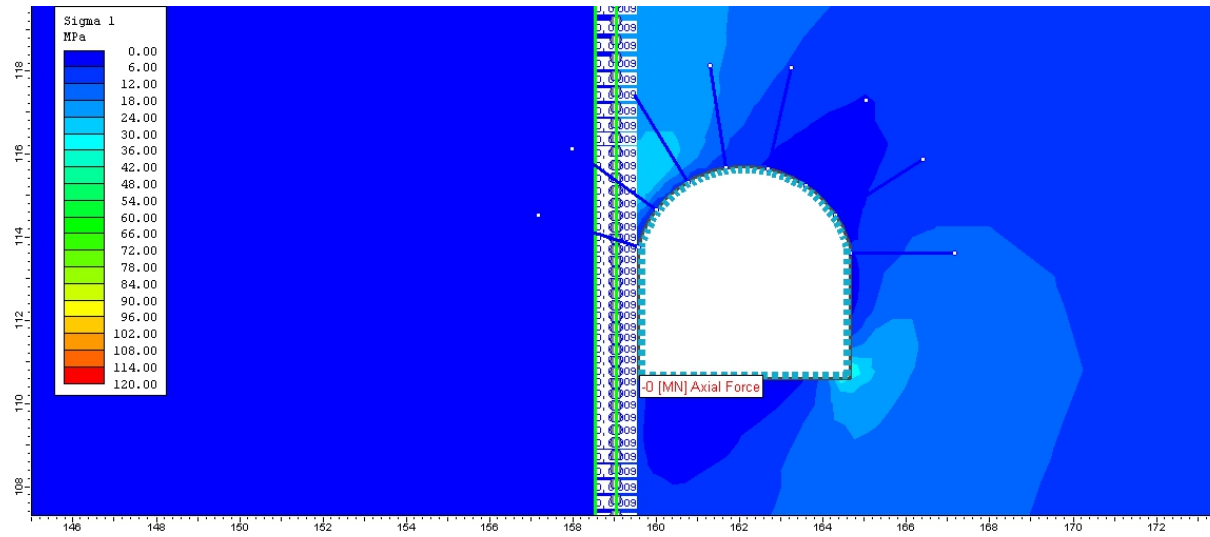


Figure 5-28 Axial Distribution with articulated design for Left Side Wall Fault

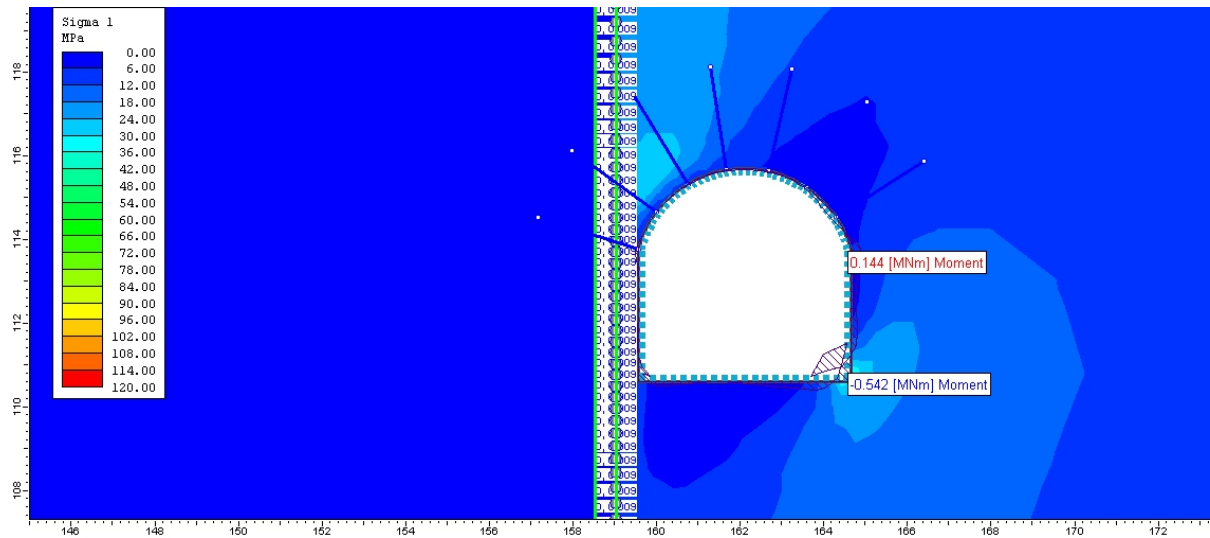


Figure 5-29 Moment Distribution with articulated design for Left Side Wall Fault

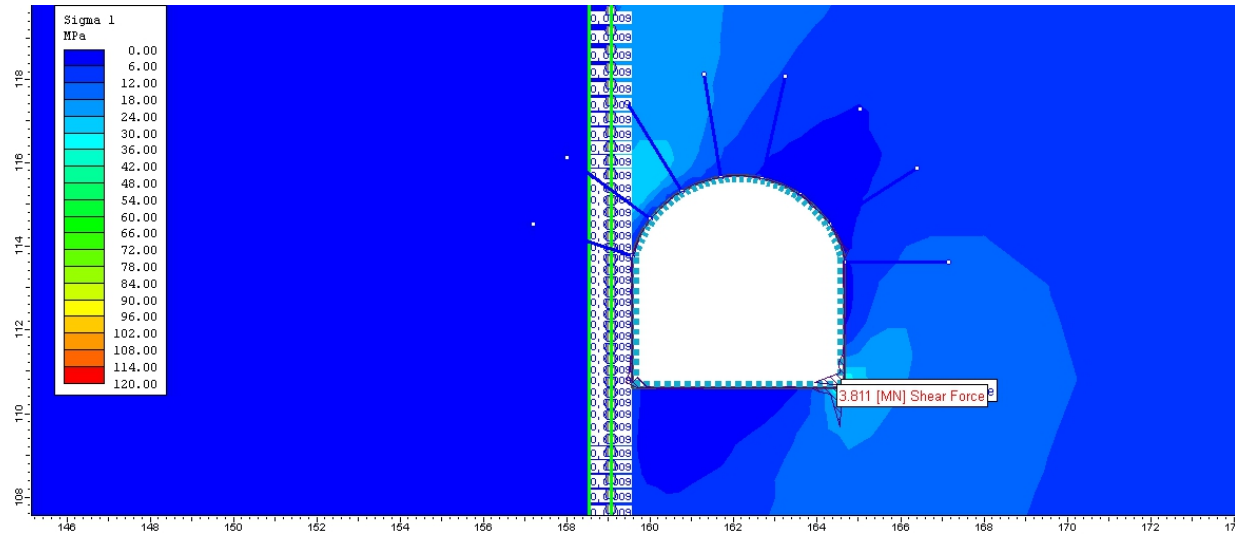


Figure 5-30 Shear Distribution with articulated design for Left Side Wall Fault

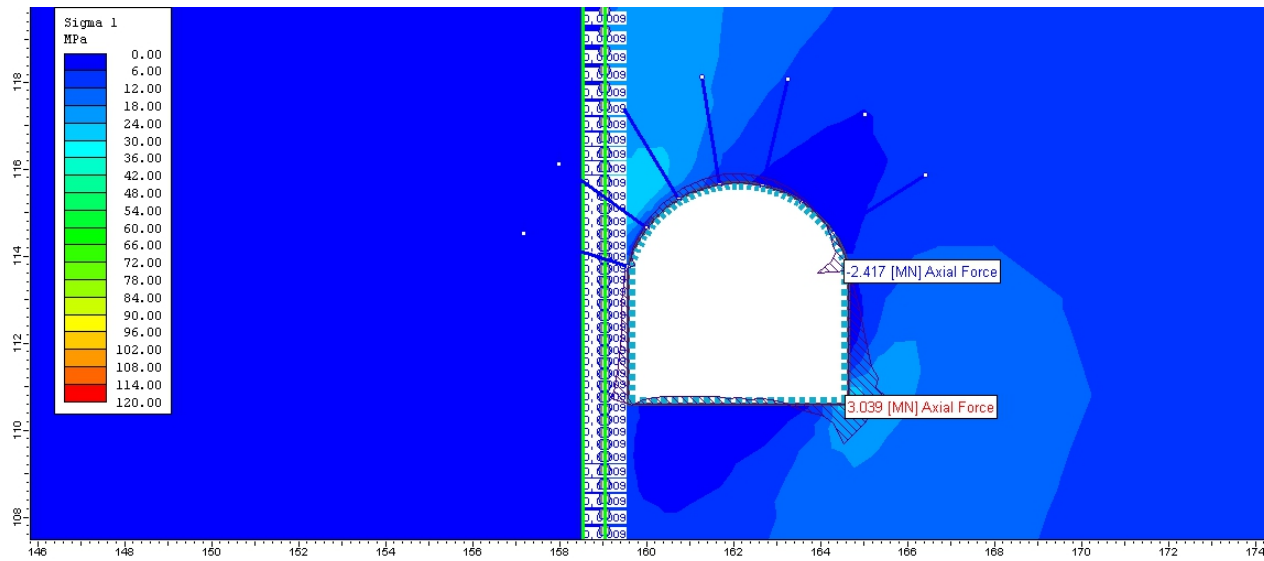


Figure 5-31 Axial Distribution without articulated design for Left Side Wall Fault

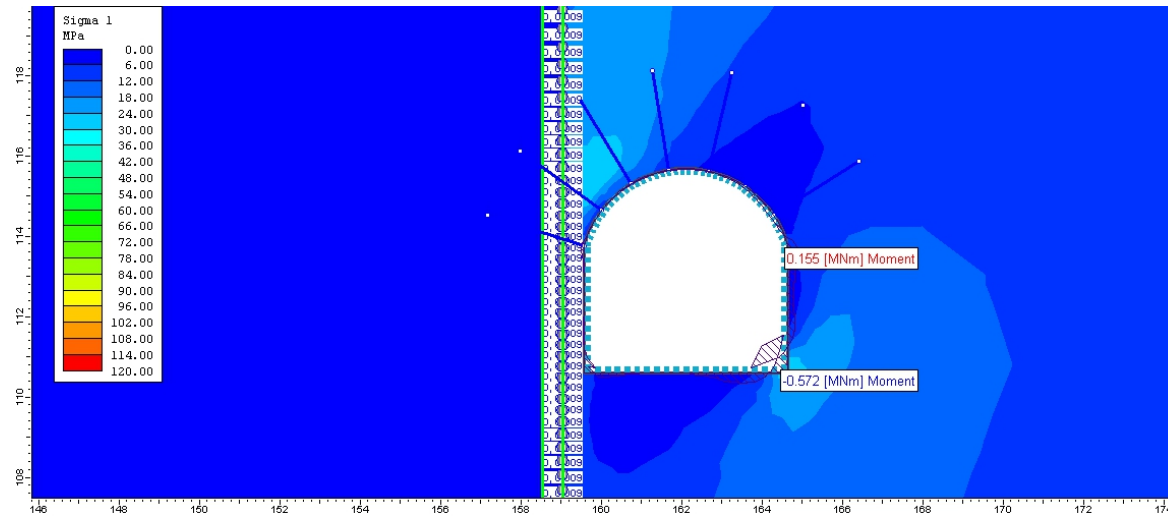


Figure 5-32 Moment Distribution without articulated design for Left Side Wall Fault

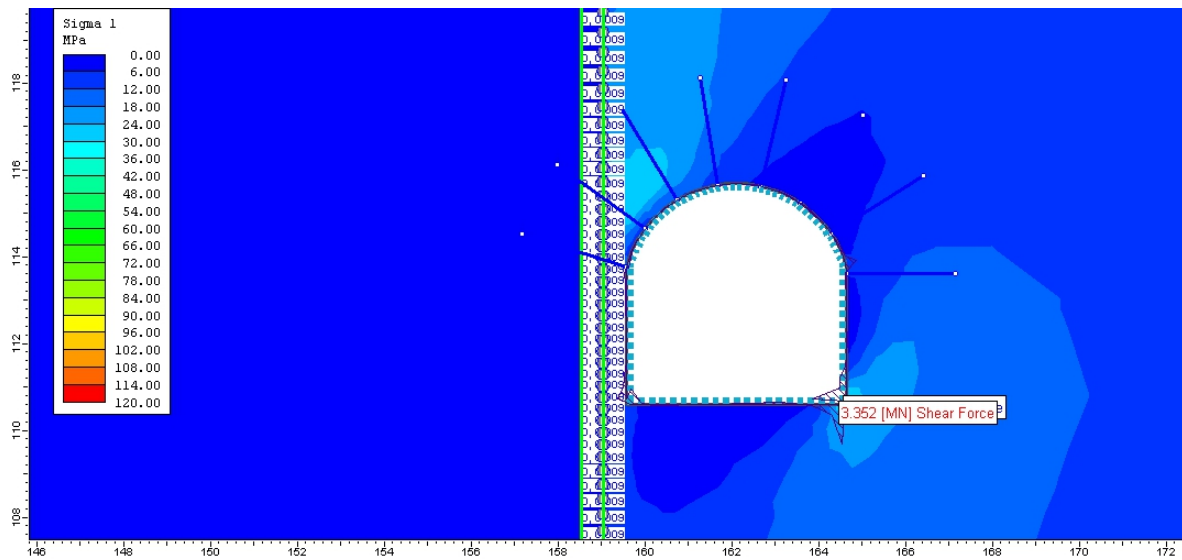


Figure 5-33 Shear Distribution without articulated design for Left Side Wall Fault

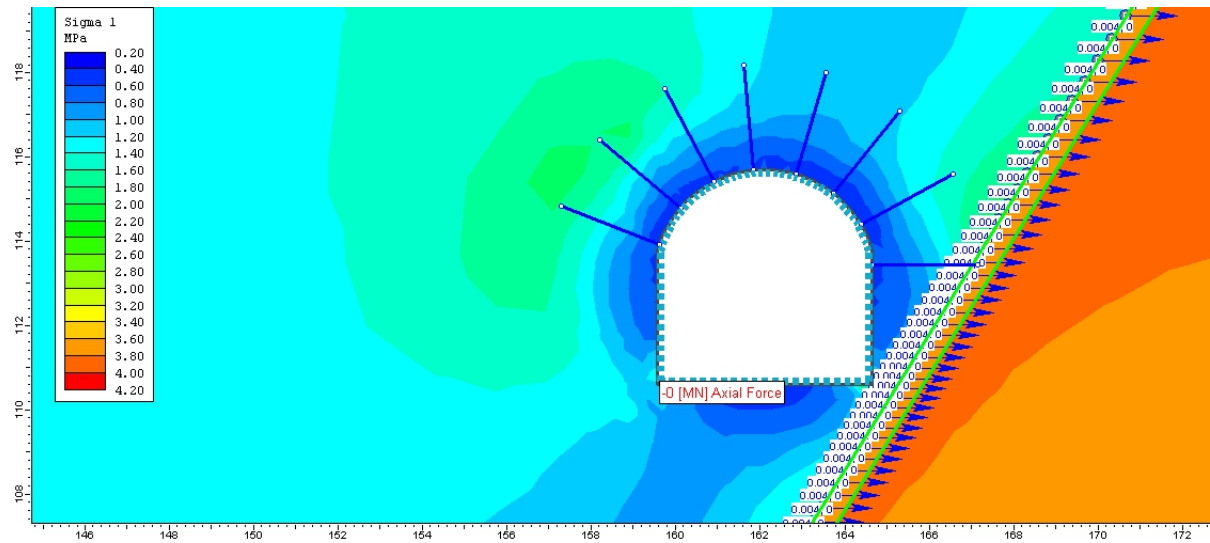


Figure 5-34 Axial Distribution with articulated design for Right Bottom Fault

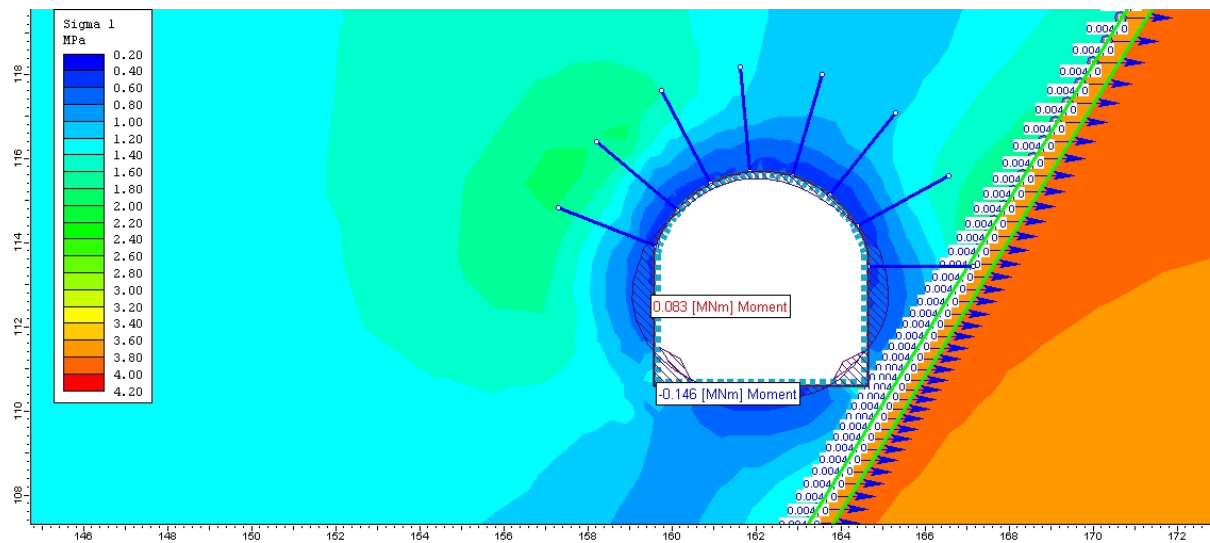


Figure 5-35 Moment Distribution with articulated design for Right Bottom Fault

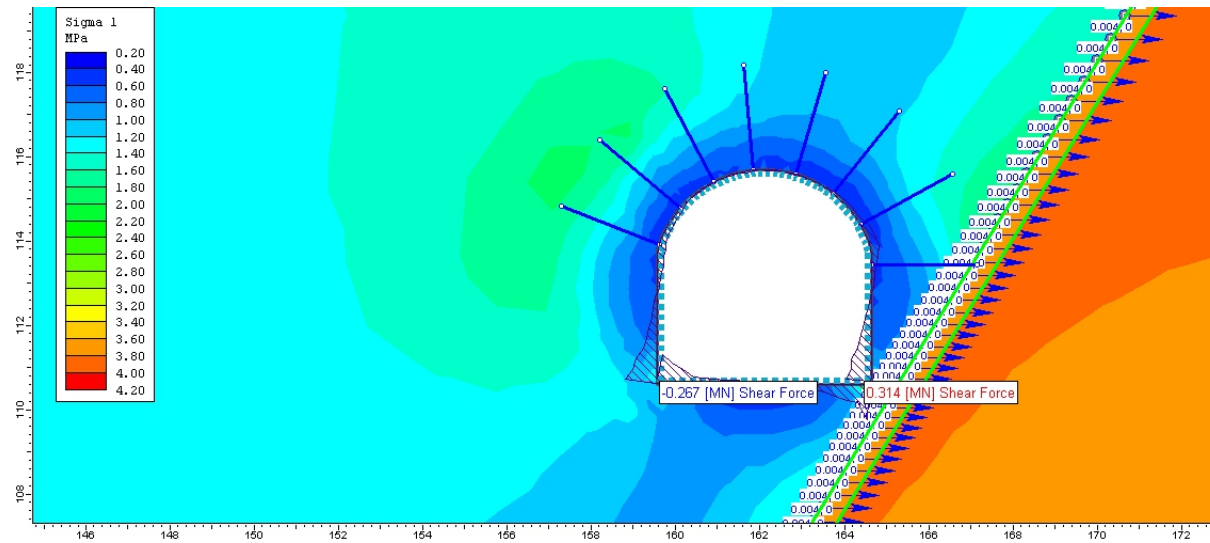


Figure 5-36 Shear Distribution with articulated design for Right Bottom Fault

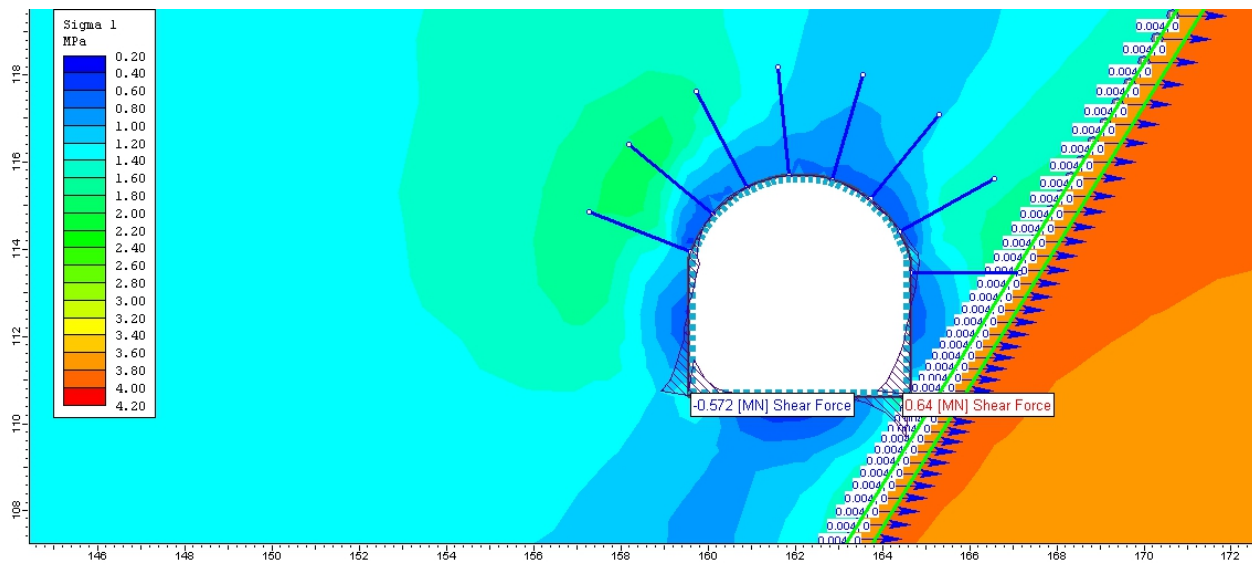


Figure 5-37 Shear Distribution without articulated design for Right Bottom Fault

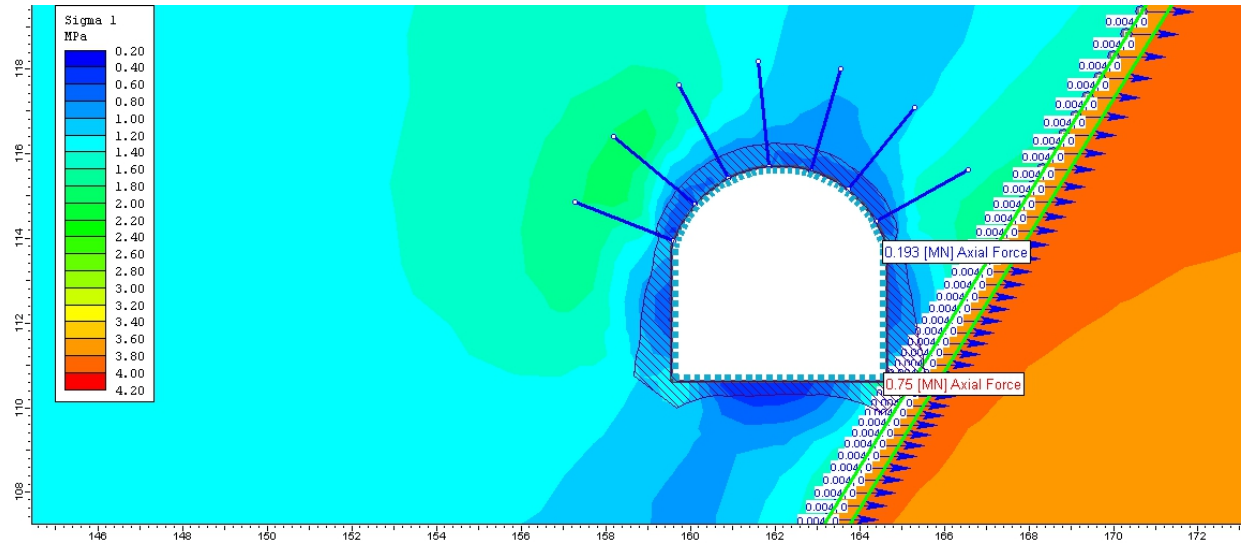


Figure 5-38 Axial Distribution without articulated design for Right Bottom Fault

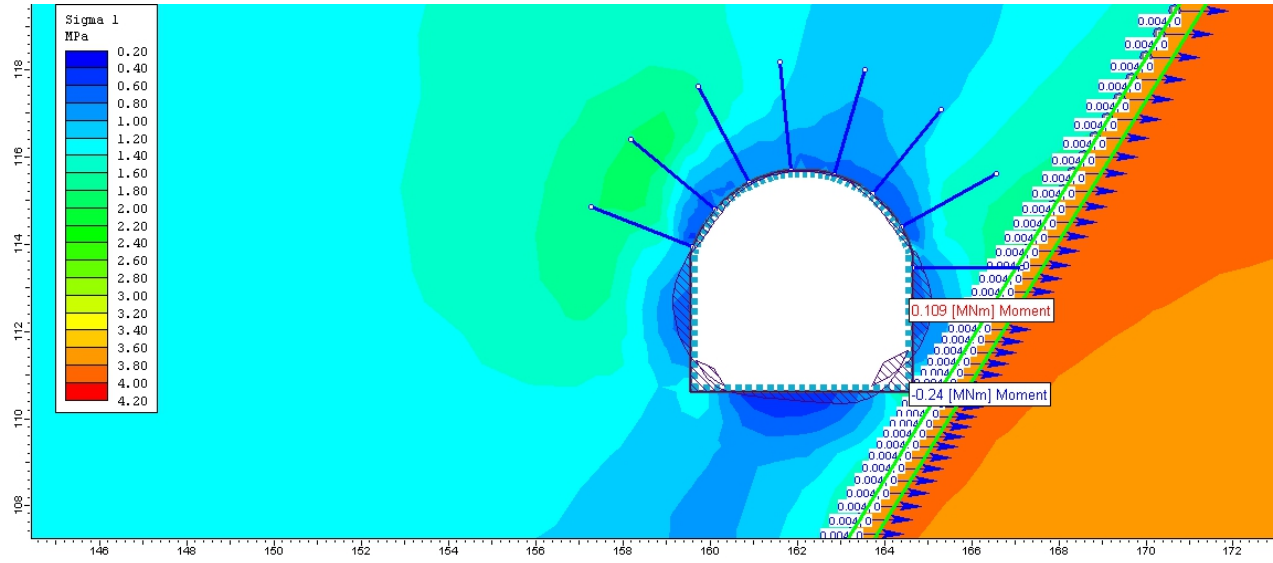


Figure 5-39 Moment Distribution without articulated design for Right Bottom Fault

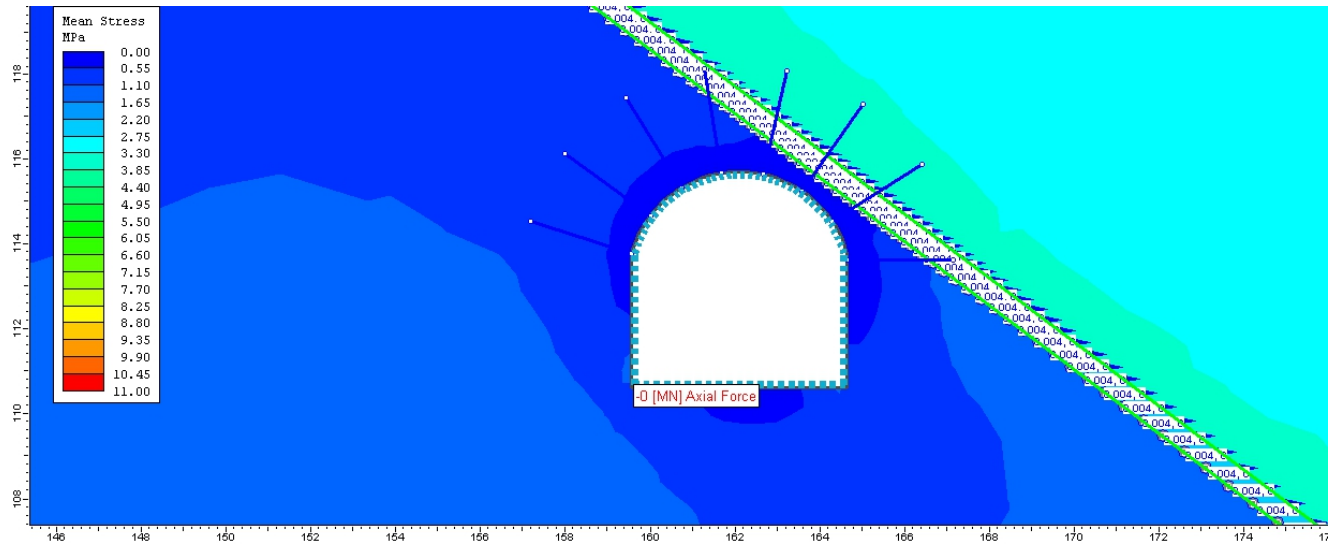


Figure 5-40 Axial Distribution with articulated design for Right Shoulder Fault

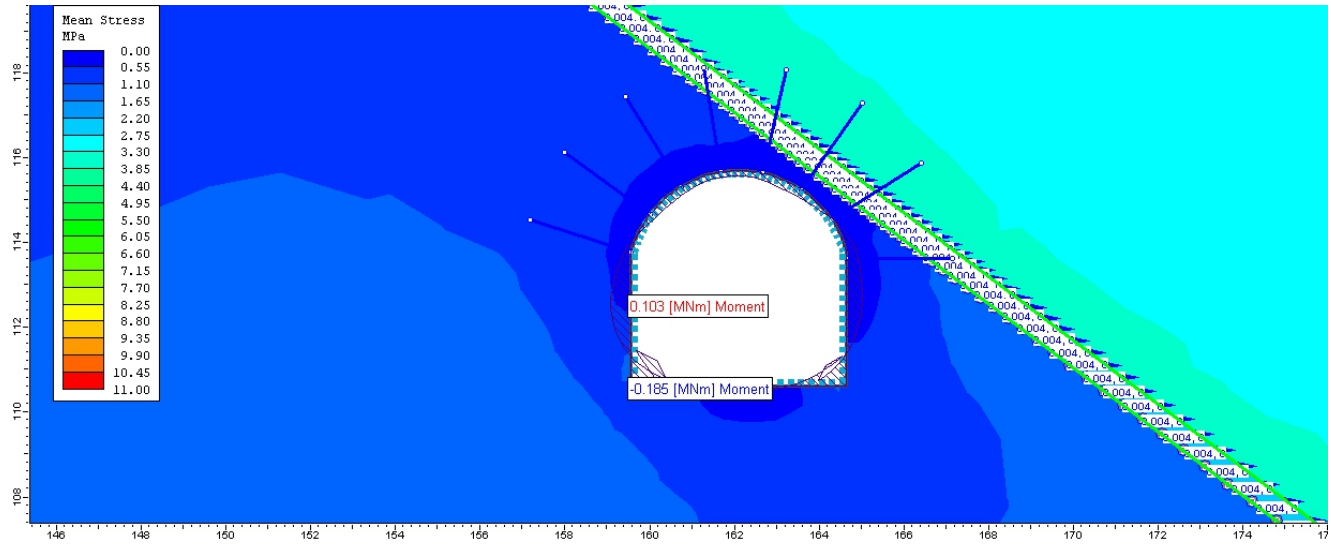


Figure 5-41 Moment Distribution with articulated design for Right Shoulder Fault

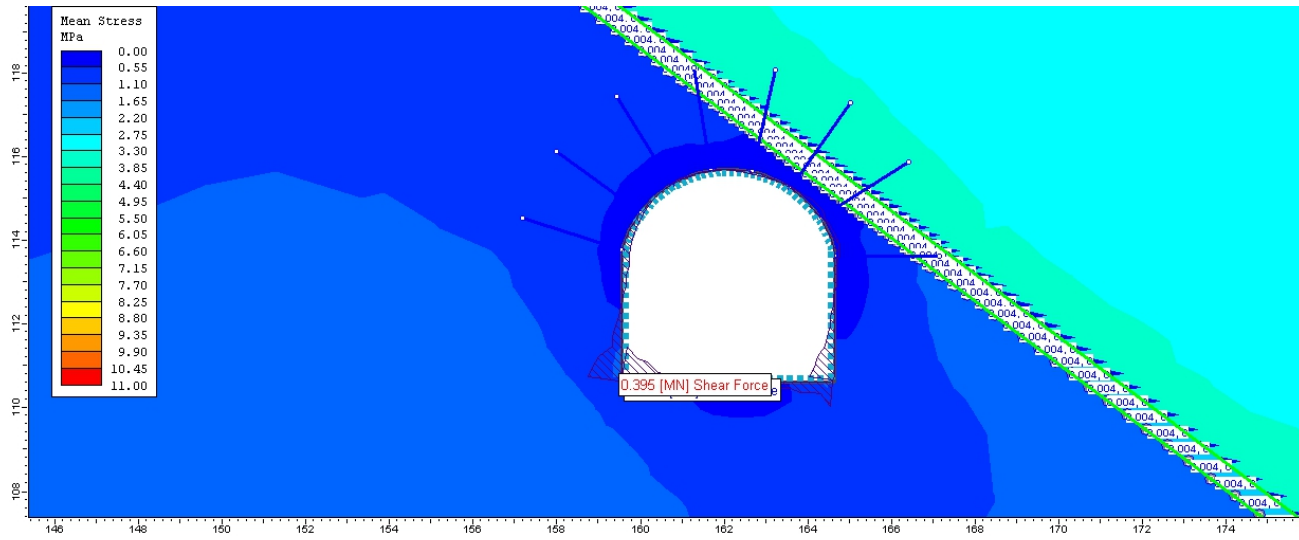


Figure 5-42 Shear Distribution with articulated design for Right Shoulder Fault

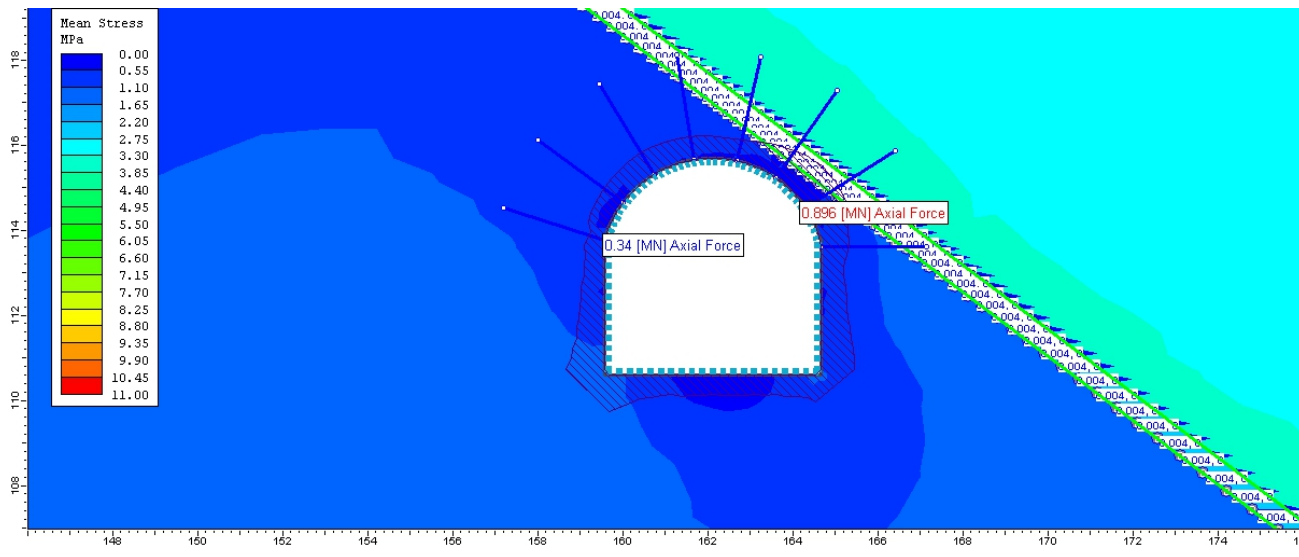


Figure 5-43 Axial Distribution without articulated design for Right Shoulder Fault

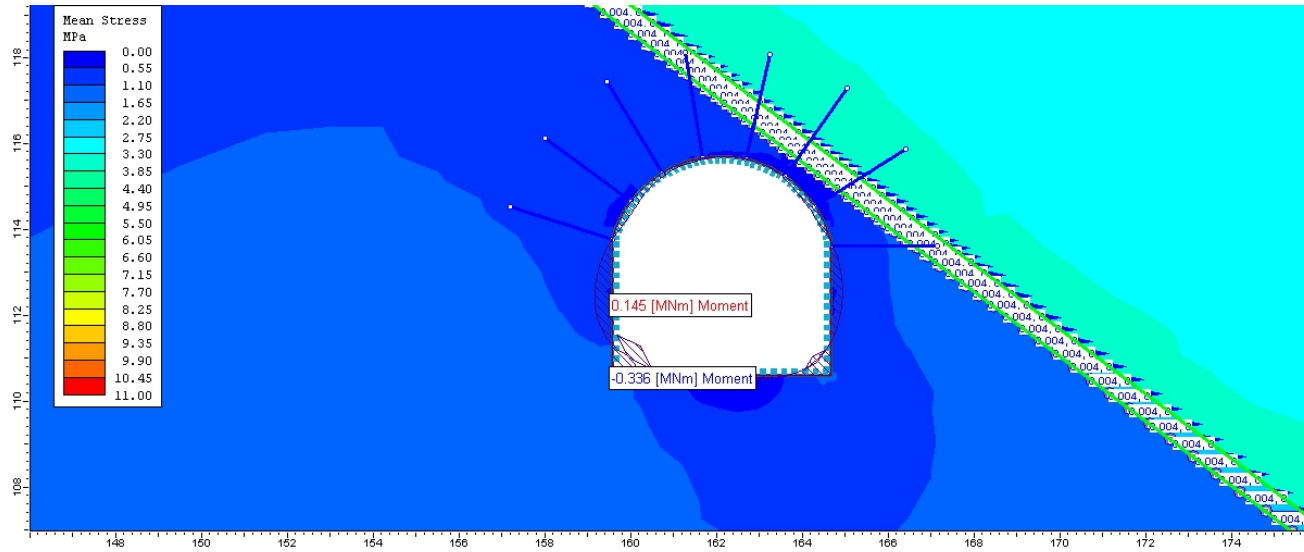


Figure 5-44 Moment Distribution without articulated design for Right Shoulder Fault

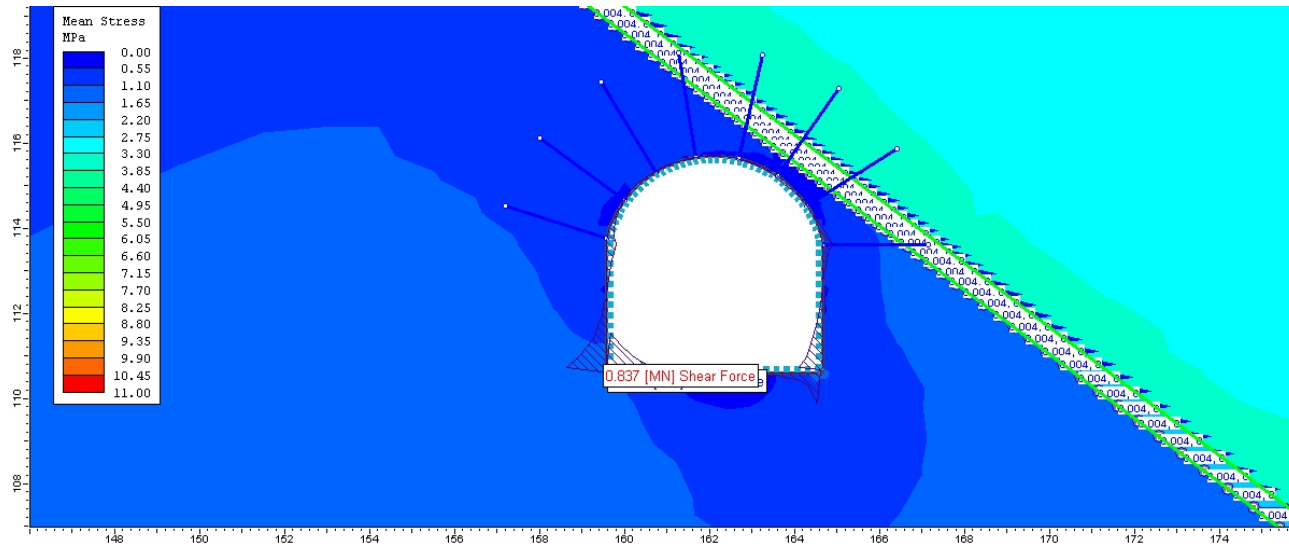


Figure 5-45 Shear Distribution without articulated design for Right Shoulder Fault

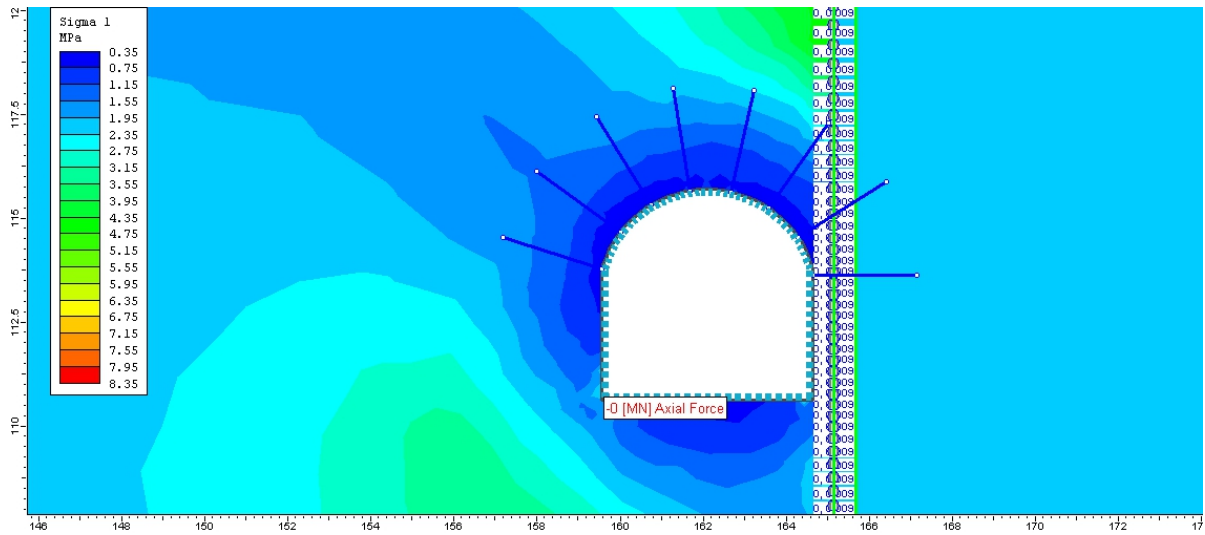


Figure 5-46 Axial Distribution with articulated design for Right Side Wall

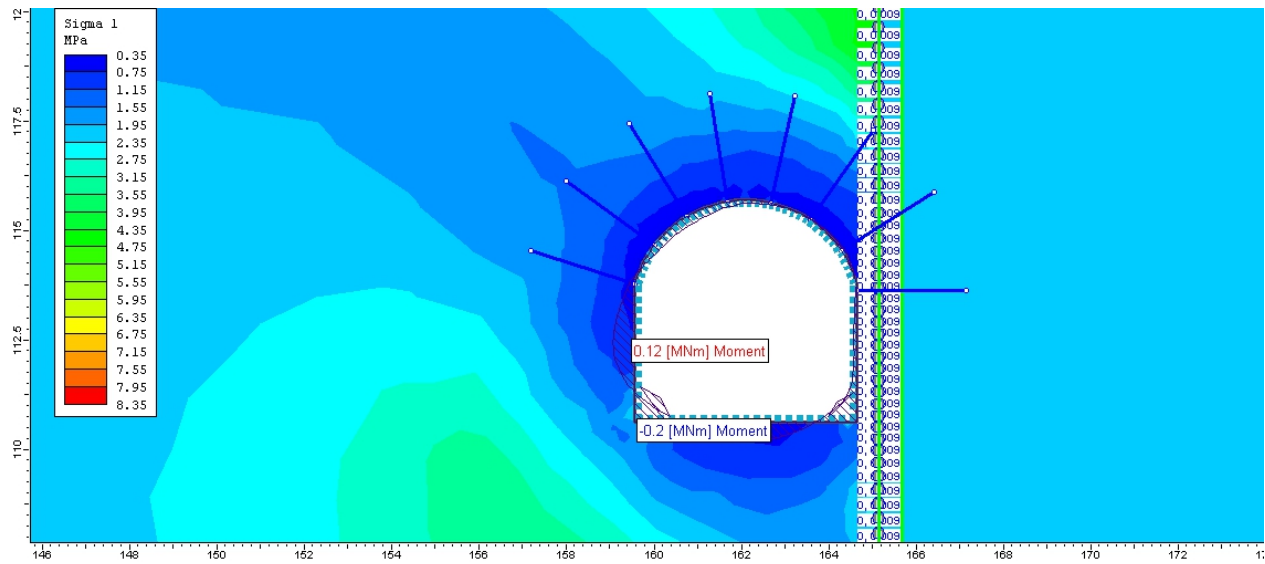


Figure 5-47 Moment Distribution with articulated design for Right Side Wall

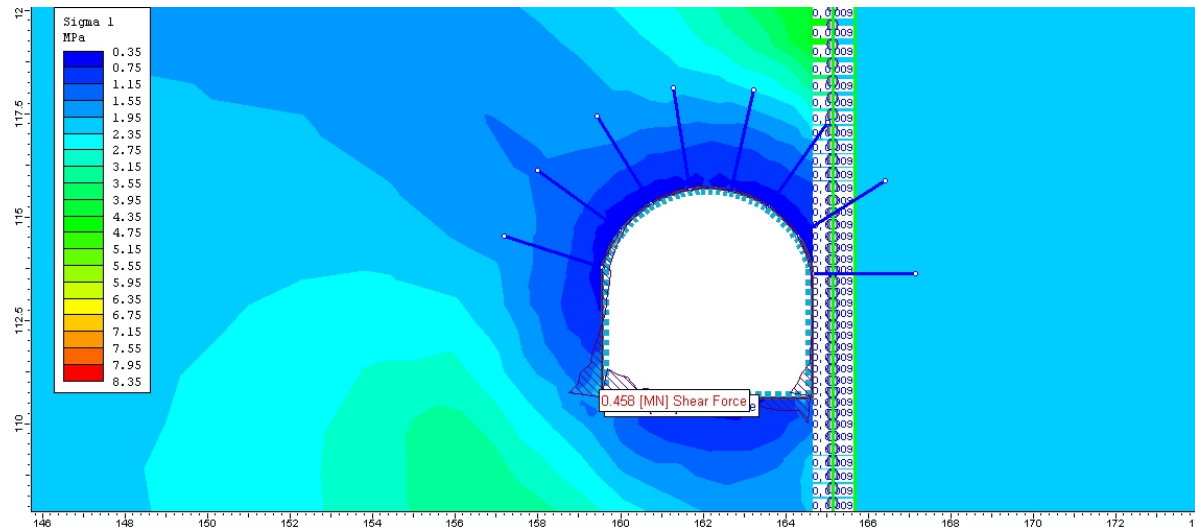


Figure 5-48 Shear Distribution with articulated design for Right Side Wall

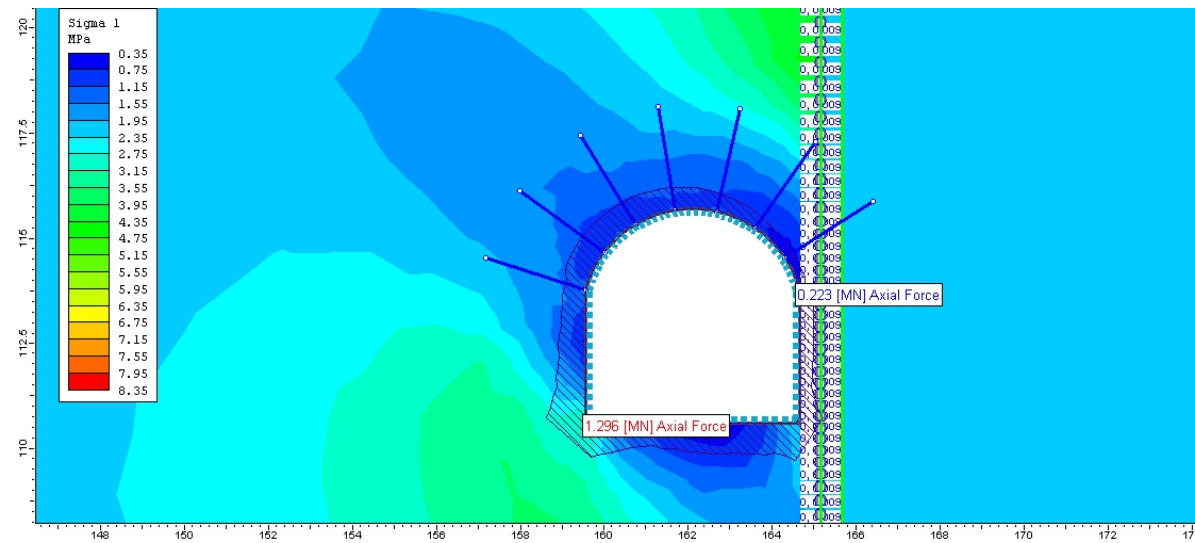


Figure 5-49 Axial Distribution without articulated design for Right Side Wall

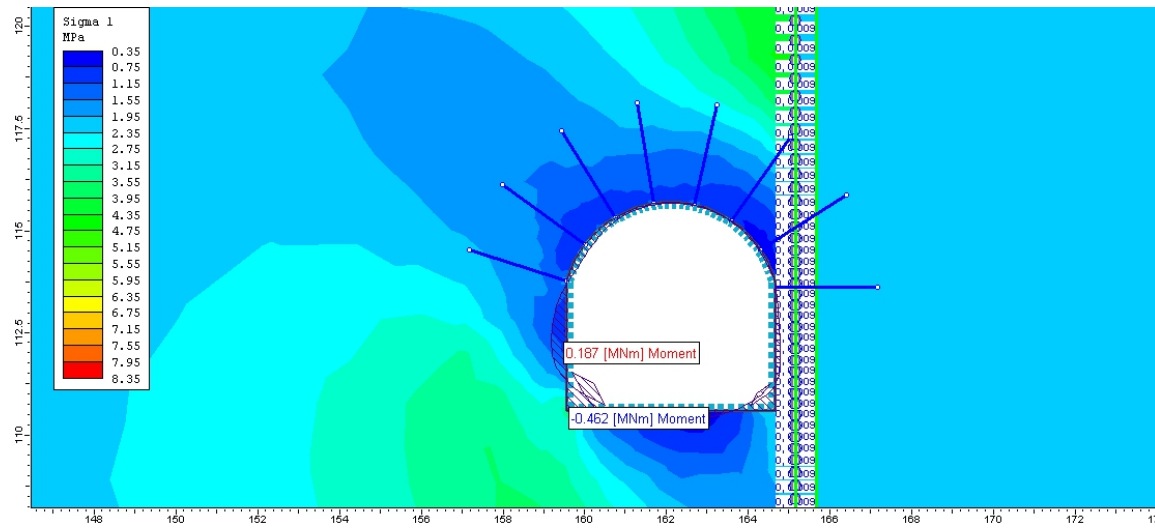


Figure 5-50 Moment Distribution without articulated design for Right Side Wall

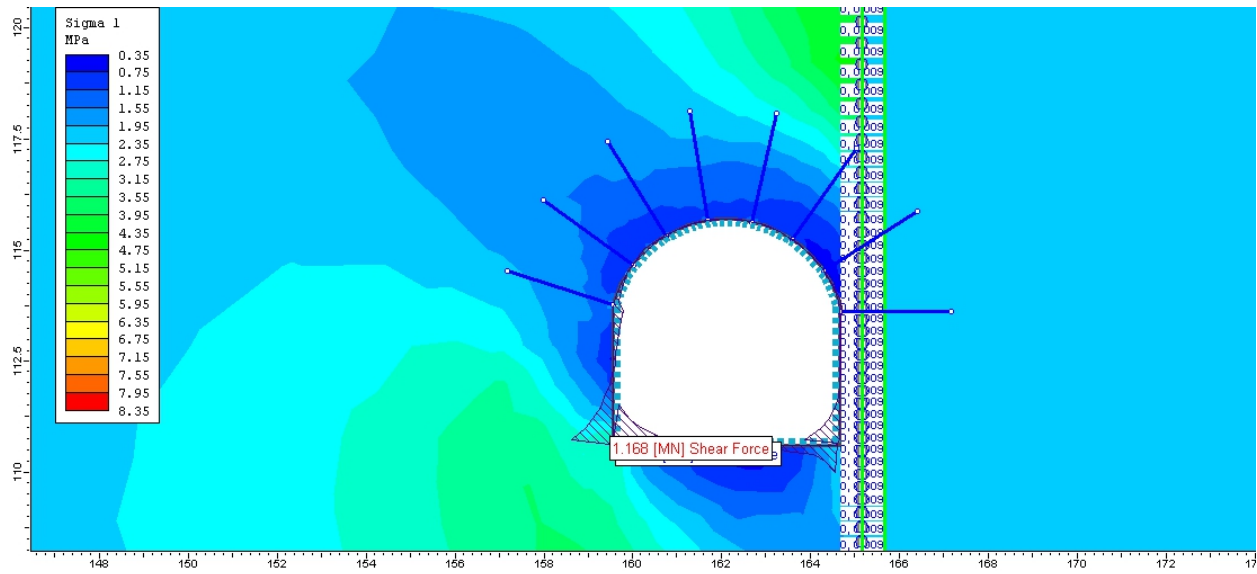


Figure 5-51 Shear force distribution without articulated design for Right Side Wall

Discussion

The results obtained from the design of tunnel support using articulated support using eight cases of fault location at different tunnel location such as crown, invert, left shoulder, right shoulder, right side wall, left side wall, left side bottom, right side bottom has shown the location of fault has significant effect on the tunnel in stability. The shear force, moment, axial force is dependent on the fault location. It has been found out that there is maximum moment of 0.24 MNm when the fault is located at the left shoulder of the tunnel. Similarly, the minimum moment of 0.11 MNm has been obtained when the fault is located at right bottom of the tunnel. Figure 5-52 shows the comparison of maximum moment with and without articulated design for different fault location. The stress condition, tunnel geometry, strength properties of rock mass, failure criterion of the rock mass, modelling criterion is same for all the modelling.

The reason for the different in the magnitude of the moment is the combine mechanism of gravitational stress and direction of the fault displacement. In the case of the fault located at the left shoulder of the tunnel, the gravitational rock mass above the tunnel and fault displacement is moving in the direction inward of the tunnel (Figure 5-26) where as in the case of the fault located in the right bottom of the shoulder the fault displacement is in the direction outward of the tunnel opening (Figure 5-39). Using articulated method of design with 15 percent sliding gap in the tunnel support, the moment has reduced significantly. It has been found out that there has been reduction of 19.5 %, 12.8 %, 28.9 %, 19.2 %, 7.1 %, 23.9 %, 29.0 %, 35.8 % of moment in tunnel support for Crown fault, Invert fault, Left Bottom fault, Left Shoulder fault, Left Side Wall fault, Right Bottom fault, Right Shoulder fault, Right Side Wall fault respectively (Figure 5-52). Similarly, it has also been found out that there has been reduction of 57.1 %, 7.1 %, 7.6 %, 45.2 %, -13.7 %, 50.9 %, 52.8 %, 60.8 % of shear force in tunnel support for Crown fault, Invert fault, Left Bottom fault, Left Shoulder fault, Left Side Wall fault, Right Bottom fault, Right Shoulder fault, Right Side Wall fault respectively (Figure 5-53). Hence articulated design of tunnel support has proved to be effective in reducing the effect in shear force and bending moment acting in the tunnel support due to fault rupture.

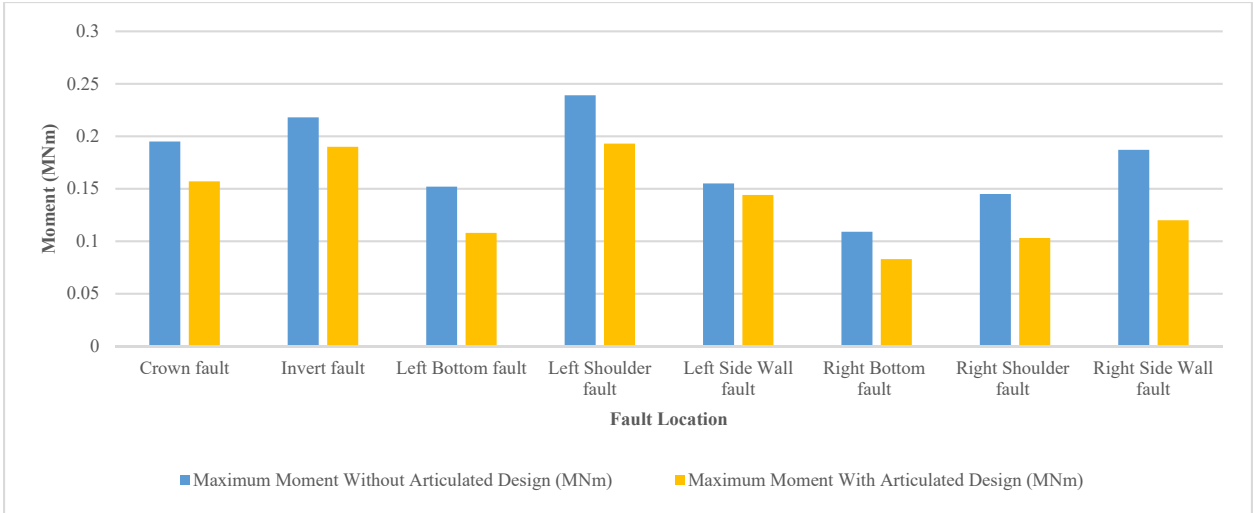


Figure 5-52 Comparison of Maximum Moment with and without Articulated Design for Different fault location

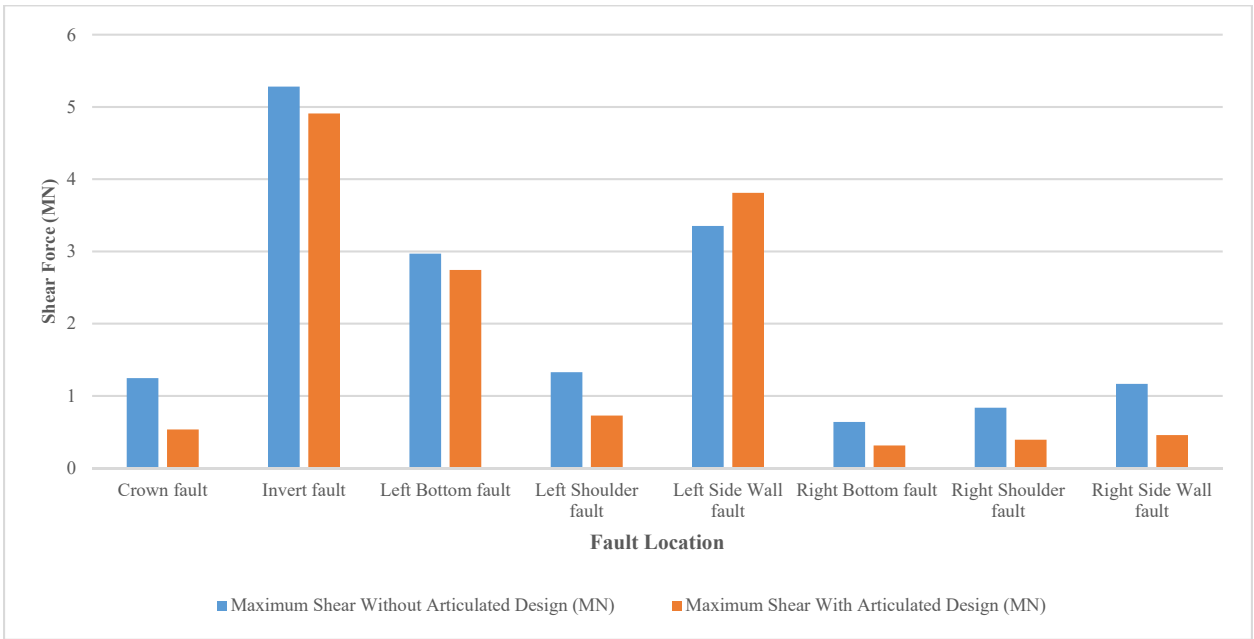


Figure 5-53 Comparison of Maximum Shear force with and without articulated Design for different fault location

6 Conclusion and Recommendation

Tunnelling in the lesser Himalaya is very challenging and difficult due to presence of fault and thrust zones. Quartzite, Gneisses, Phyllite, Slate, limestone, Metabasic, Chlorite schist, sand stones are the common types of the rock mass found in the fault and thrust zone in this zone. These rock masses are unstable when tunnel and underground structures are excavated. They encounter problems such as squeezing, high pressure and deformation, flowing ground condition, water in rush, cavity formation and high pressure leading to support failure of the tunnel. This requires a design of the tunnel support with consideration of the weak rock mass of the fault and thrust zone. Most of the hydropower projects in located in fault and thrust zone in lesser Himalaya have encountered and solves those problems mentioned above with measures of the support based on the site conditions. It includes stabilization of the fractured rock mass with drainage of ground water and use of final support for the movement of ground due to fault. Some of conclusions which can be drawn from this study are as follows:

- Elastic plastic model of rock mass is suitable for the modelling of tunnel in faulted rock mass. The validation of numerical model of Modi Khola Hydropower Project showed that there is variation of 1.71 % and 5.2 % of modelled deformation with field measured deformations at hill side spring line and hill side bottom respectively
- Articulated design approach (Russo et. al, 2002), Analytical Method using CCM approach (Carranza-Torres and Fairhurst, 2000), and Empirical method (Marinos et. al. 2007;, Marinos et al., 2011; Marinos, 2014;, Marinos, 2019) are three methods which can be used in design of tunnel in faulted rock mass.
- Tunnel lining becomes critical in terms of displacement, shear force, axial force and bending moment when there is presence of fault. However, it is not proportional for all three tunnel sections i.e., a fault that is located in specific place does not increase the parameter of stress or displacement in same place. It may or may not increase the parameter of stress or displacement. For example, the displacement has increased in circular and horse shoe tunnel in crown, right shoulder and left shoulder when the fault is located crown, right shoulder and left shoulder respectively. However, it is not in the case of inverted D tunnel.
- The shear force, bending moment and axial force in the tunnel lining do not increase in the place where the fault is located. For example: in case inverted D tunnel, there is maximum shear force at right bottom and right side wall due to right bottom fault. Similarly, in case of horseshoe tunnel, shear force in left bottom is maximum due to left side wall fault and in case of circular tunnel left bottom has maximum shear force due to left side wall fault. It is similar with the case of bending moment, displacement and axial force in all three-cross section of tunnel.

- Circular tunnel show more uniformity in the effect in tunnel lining due to the fault position than inverted D and horseshoe tunnel. i.e., the fault and its effect in tunnel lining location are proportional in the same side where as Inverted D show least uniformity i.e., the fault and its effect in the tunnel lining is random.
- Wedges formed are safe for sliding with (FOS > 2.5) based on the stability analysis of wedge formed around the tunnel
- Articulated design performs well in reduction of shear force and bending moment significantly in the presence of fault. The results obtained show that the tunnel support using articulated system have served well to reduce the bending moment and shear force in tunnel lining of Reinforced Cement Concrete 36 % and 61 % respectively.

Hence, is recommended that Stability analysis of wedge, and Articulated design methodology should be used to design the tunnel support in faulted rock mass in case of Nepal Himalaya.

7 References

- Ader, T., Avouac, J. P., Liu-Zeng, J., Lyon-Caen, H., Bollinger, L., Galetzka, J., ... & Flouzat, M. (2012). Convergence rate across the Nepal Himalaya and interseismic coupling on the Main Himalayan Thrust: Implications for seismic hazard. *Journal of Geo..*
- Anderson, E. M. (1951). *The dynamics of faulting and dyke formation with applications to Britain*. Oliver and Boyd.
- Barton, N. R. (1988). Barton, 1988. Rock mass classification and tunnel reinforcement using the Q-system. ASTM, STP 984. *ASTM STP 984*.
- Barton, N. R., & Bandis, S. C. (2017). Characterization and modeling of the shear strength, stiffness and hydraulic behavior of rock joints for engineering purposes. *Rock Mechanics and Engineering*, 1, 1-40.
- Barton, N., & Bandis, S. (1982, January). Effects of block size on the shear behavior of jointed rock. In *The 23rd US symposium on rock mechanics (USRMS)*. American Rock Mechanics Association.
- Barton, N., Lien, R., & Lunde, J. (1974). Engineering classification of rock masses for the design of tunnel support. *Rock mechanics*, 6(4), 189-236.
- Basnet, C. B., Shrestha, P. K., & Panthi, K. K. (2013). Analysis of Squeezing Phenomenon in the Headrace Tunnel of Chameliya Project, Nepal.
- Bhasin, R., Singh, R. B., Dhawan, A. K., and Sharma, V. M. (1995). Geotechnical evaluation and a review of remedial measures in limiting deformations in distressed zones in a powerhouse cavern, *Conf. on Design and Construction of Underground Structures, New Delhi, India*, pp. 145–152.
- Bieniawski, Z. (1974). *Geomechanics classification of rock masses and its application in tunneling*.
- Bieniawski, Z. T. (1989). *Engineering rock mass classifications: a complete manual for engineers and geologists in mining, civil, and petroleum engineering*. John Wiley & Sons.
- BTS/ICE (2004). *Tunnel Lining Design Guide*, Thomas Telford, London.
- Byrne, G., Everett, J. P., & Schwartz, K. (1995). *A guide to practical geotechnical engineering in southern Africa*. Franki.

- Cai, M., Kaiser, P. K., Tasaka, Y., And Minami M.,2007, Determination of residual strength parameters of jointed rock masses using the GSI system. *International Journal of Rock Mechanics and Mining Sciences*, Volume 44, Issue 2, 247-265.
- Carranza-Torres, C., & Fairhurst, C. (2000). Application of the convergence-confinement method of tunnel design to rock masses that satisfy the Hoek-Brown failure criterion. *Tunnelling and underground space technology*, 15(2), 187-213.
- Caulfield, R., Kieffer, D. S., Tsztoo, D. F., & Cain, B. (2005, June). Seismic design measures for the retrofit of the claremont tunnel. In *Jacobs Associates, Rapid Excavation and Tunneling Conference (RETC) Proceedings*; Jacobs Associates: San Francisco.
- Chamlagain, D., & Niroula, G. P. (2020). Contribution of Fault Geometry on Probabilistic Seismic Hazard Assessment in Intermontane Basin: An example from Kathmandu Valley. *Journal of Nepal Geological Society*, 60, 21-36.
- Chapman, D., Metje, N., & Stärk, A. (2017). *Introduction to tunnel construction*. Crc Press.
- Chen, W. P., & Molnar, P. (1977). Seismic moments of major earthquakes and the average rate of slip in central Asia. *Journal of Geophysical Research*, 82(20), 2945-2969.
- Chhushyabaga, B., Karki, S., & Khadka, S. S. (2020). Fault induced problems in hydropower tunnels in Nepal: A case study. *Lowland Technology International*, 21(4, March), 255-267.
- Chhushyabaga, B., Karki, S., & Khadka, S. S. (2020, August). Tunnel support design in fault zone in hydropower project in the Nepal Himalaya: a case study. In *Journal of Physics: Conference Series* (Vol. 1608, No. 1, p. 012009). IOP Publishing.
- Childs, C., Manzocchi, T., Walsh, J. J., Bonson, C. G., Nicol, A., & Schöpfer, M. P. (2009). A geometric model of fault zone and fault rock thickness variations. *Journal of Structural Geology*, 31(2), 117-127.
- Dahal, R. K. (2006). *Geology for Technical Students: A Text Book for Bachelor Level Students: Environmental Science, Civil Engineering, Forestry and Earth Hazard*. Bhrikuti Academic Publications.
- Dalgıç, S. (2002). Tunneling in squeezing rock, the Bolu tunnel, Anatolian Motorway, Turkey. *Engineering Geology*, 67(1-2), 73-96.

- Desai, D. B., Merritt, J. L., & Chang, B. (1991, November). 'Shake and slip to survive'-tunnel design: Proc 1989 Rapid Excavation and Tunnelling Conference, Los Angeles, 11–14 June 1989 P13–30. Publ Littleton: SME, 1989. In International Journal of Rock M.
- Di Giacomo, D., Storchak, D.A., Safronova, N., Ozgo, P., Harris, J., Verney, R. and Bondár, I., 2014. A New ISC Service: The Bibliography of Seismic Events, *Seismol. Res. Lett.*, 85, 2, 354-360, doi: 10.1785/0220130143.
- Dinis, J. C. C. (2009). Assessment of rock mass parameters based on the monitoring data from the Koralm Investigation Tunnels.
- Dwivedi, R. D., Singh, M., Viladkar, M. N., & Goel, R. K. (2014). Estimation of support pressure during tunnelling through squeezing grounds. *Engineering geology*, 168, 9-22..
- Eberhardt, E. (2012). The hoek–brown failure criterion. *Rock mechanics and rock engineering*, 45(6), 981-988.
- Feng, X. T. (Ed.). (2017). *Rock Mechanics and Engineering Volume 5: Surface and Underground Projects*. CRC Press.
- Gautam, D. (2017). Mapping surface motion parameters and liquefaction susceptibility in Tribhuvan International Airport, Nepal. *Geomatics, Natural Hazards and Risk*, 8(2), 1173-1184.
- Gautam, D. (2017). Unearthed lessons of 25 April 2015 Gorkha earthquake (MW 7.8): geotechnical earthquake engineering perspectives. *Geomatics, Natural Hazards and Risk*, 8(2), 1358-1382.
- Goel, R. K., Jethwa, J. L., & Paithankar, A. G. (1995a). Tunnelling in the Himalayas: problems and solutions. In *International Journal of Rock Mechanics and Mining Sciences and Geomechanics Abstracts* (Vol. 8, No. 32, pp. 415A-416A).
- Goel, R. K., Jethwa, J. L., & Paithankar, A. G. (1995b). Tunnelling through the young Himalayas—a case history of the Maneri-Uttarkashi power tunnel. *Engineering Geology*, 39(1-2), 31-44.
- Goel, R.K.,Jethwa,J.L.andPaithankar,A.G.(1995b).Tunnellingthroughtheyoung.
- Goodman, R. E., & Shi, G. H. (1985). Block theory and its application to rock engineering.
- Gregor, T., Garrod, B., & Young, D. (2007, May). Analyses of underground structures crossing an active fault in Coronado, California. In *Proceedings of the World Tunnel Congress 2007 and the 33rd ITA/AITES Annual General Assembly: Underground space-the 4t*.

- Grimstad, E., & Barton, N. (1993). Updating of the Q-system for NMT. Int. In Symposium on Sprayed Concrete-Modern use of wet mix sprayed concrete for underground support, Fagernes (Editors Kompen, Opshall and Berg, Norwegian Concrete Association, Oslo).
- Guevara Briceño, R. 2004. Túnel Yacambú-Quibor, Experiencia de Construcción - Reparación Tramo entre las Progresivas 12+800 a 12+950. In Sociedad Venezolana de Geotecnia (Ed.), Actas del XVII Seminario Venezolano de Geotecnia. Geoinfraestructura: la Geote.
- Hack, H. R. G. K. (2006). Discontinuous rock mechanics: lecture note: also as e-book.
- Himal Hydro and General Construction Ltd (2001) Construction report. Modi Khola Hydroelectric Project, Nepal.
- Hochella, M. F., Eggleston, C. M., Elings, V. B., Parks, G. A., Brown, G. E., Wu, C. M., & Kjoller, K. (1989). Mineralogy in two dimensions: Scanning tunneling microscopy of semiconducting minerals with implications for geochemical reactivity. American Mi.
- Hoek, E. (2002). A brief history of the development of the Hoek-Brown failure criterion.
- Hoek, E. (2018). Support for very weak rock associated with faults and shear zones. In Rock support and reinforcement practice in mining (pp. 19-32). Routledge.
- Hoek, E. (November 20-22, 1998). Tunnel support in weak rock. Taipei, Taiwan: Keynote address, Symposium of Sedimentary Rock Engineering.
- Hoek, E. and Diederichs, M.S., 2006, Empirical estimation of rock mass modulus, International Journal of Rock Mechanics & Mining Sciences 43, 203-215.
- Hoek, E., & Brown, E. T. (1997). Practical estimates of rock mass strength. International journal of rock mechanics, mining sciences, 34, 1165-1186.
- Hoek, E., & Brown, E. T. (2019). The Hoek–Brown failure criterion and GSI–2018 edition. Journal of Rock Mechanics and Geotechnical Engineering, 11(3), 445-463.
- Hoek, E., & Marinos, P. (2000). Predicting tunnel squeezing problems in weak heterogeneous rock masses. Tunnels and tunnelling international, 32(11), 45-51.
- Hoek, E., Carranza-Torres, C., Diederichs, M., & Corkum, B. (2008, February). Integration of geotechnical and structural design in tunnelling—2008 Kersten Lecture. In Proceedings University of Minnesota 56th Annual Geotechnical Engineering Conference, Min.

- Hoek, E., Carranza-Torres, C., Diederichs, M., & Corkum, B. (2008, February). The 2008 Kersten Lecture Integration of geotechnical and structural design in tunneling. In 56th annual geotechnical engineering conference (pp. 1-53).
- Jethwa, J. L., Singh, B., Singh, Bhawani and Mithal, R. S. (1980). Influence of geology on tunnelling conditions and deformational behavior of supports in faulted zones – A case history of Chhibro-Khodri tunnel in India, *Engineering Geology*, Vol. 16, No. 3.
- Karki, S., Chhushyabaga, B., & Khadka, S. S. (2020, August). An Overview of Design and Construction practices of Himalayan Hydropower tunnels. In *Journal of Physics: Conference Series* (Vol. 1608, No. 1, p. 012008). IOP Publishing.
- Khadka, S. S. (2019). Tunnel Closure Analysis of Hydropower Tunnels in Lesser Himalayan Region of Nepal through Case Studies. Retrieved from Rock Mechanics and Underground Structure Lab: http://rmlab.ku.edu.np/wpcontent/uploads/2019/09/PhD-Thesis__Full.
- Kim, K., & Yoo, C. H. (2002). Design loading for deeply buried box culverts. Highway Research Center. Report No. IR-02-03. Auburn University, Alabama, p 215.
- Kontogianni, V. A., & Stiros, S. C. (2003). Earthquakes and seismic faulting: effects on tunnels. *Turkish Journal of Earth Sciences*, 12(1), 153-156.
- Kun, M., & Onargan, T. (2013). Influence of the fault zone in shallow tunneling: A case study of Izmir Metro Tunnel. *Tunnelling and Underground Space Technology*, 33, 34-45.
- Labuz, J. F., & Zang, A. (2012). Mohr–Coulomb Failure Criterion. *Rock Mech Rock Eng*, 45 , pp.975-979.
- Lang, T. A. (1961). Theory and practice of rock bolting. *Transactions of the American Institute of Mining, Metallurgical and Petroleum Engineers*, 220, 333-348.
- Lanzano, G., Bilotta, E., & Russo, G. (2008). Tunnels under seismic loading: a review of damage case histories and protection methods. *Strategies for reduction of the seismic risk*, Publisher StreGa, 65-75.
- Lorig, L. J., & Varona, P. (2013). Guidelines for numerical modelling of rock support for mines. Australian Centre for Geomechanics, Perth: ISBN 978-0-9806154-7-0.
- Maidl, B., Schmid, L., Ritz, W., & Herrenknecht, M. (2008). *Hardrock tunnel boring machines*. John Wiley & Sons.

- Mandal, P. (2018). Evidence of a Large Triggered Event in the Nepal Himalaya Following the Gorkha Earthquake: Implications Toward Enhanced Seismic Hazard. *Pure and Applied Geophysics*, 175(8), 2807-2819.
- Marinos V, Fortsakis P, Prountzopoulos G. Estimation of geotechnical properties and classification of geotechnical behaviour in tunnelling for flysch rock masses. In: Anagnostopoulos A, Pachakis M, Tsatsanifos C editors. *Proceedings of the 15th European C*.
- Marinos, P., Marinos, V., & Hoek, E. (2007, May). Geological Strength Index (GSI). A characterization tool for assessing engineering properties for rock masses. In *Proceedings International Workshop on Rock Mass Classification for Underground Mining*, Mark.
- Marinos, V. (2014). Tunnel behaviour and support associated with the weak rock masses of flysch. *Journal of Rock Mechanics and Geotechnical Engineering*, 6(3), 227-239.
- Marinos, V. (2019). A revised, geotechnical classification GSI system for tectonically disturbed heterogeneous rock masses, such as flysch. *Bulletin of Engineering Geology and the Environment*, 78(2), 899-912.
- Marinos, V. I. I. I., Marinos, P., & Hoek, E. (2005). The geological strength index: applications and limitations. *Bulletin of Engineering Geology and the Environment*, 64(1), 55-65.
- Marinos, V. P. (2012). Assessing rock mass behaviour for tunnelling. *Environmental & Engineering Geoscience*, 18(4), 327-341.
- Moffat, R., Sotomayor, J., & Beltrán, J. F. (2015). Estimating tunnel wall displacements using a simple sensor based on a Brillouin optical time domain reflectometer apparatus. *International Journal of Rock Mechanics and Mining Sciences*, 75, 233-243.
- Nepal Electricity Authority (1997). *Detailed Design Report of Kulekhani III Hydroelectric Project*. Kathmandu, Nepal.: Nepal Electricity Authority.
- Nilsen, B. (2000). *New trends in rock slope stability analyses*.
- Palmstrom, A. (1995). *RMi-a rock mass characterization system for rock engineering purposes*.
- Panthi K K and Shrestha P K 2018 *Estimating Tunnel Strain in the Weak and Schistose Rock Mass*.
- Panthi, K. K. (2006). *Analysis of engineering geological uncertainties related to tunnelling in Himalayan rock mass conditions*.

- Panthi, K. K. (2012). Probabilistic Approach for Assessing Rock Mass Quality in the Tunnel. *Hydro Nepal: Journal of Water, Energy and Environment*, 11, 6-11.
- Panthi, K. K., & Nilsen, B. (2007). Uncertainty analysis of tunnel squeezing for two tunnel cases from Nepal Himalaya. *International Journal of Rock Mechanics and Mining Sciences*, 44(1), 67-76.
- Paudel, T. R., Dangol, V., & Sharma, R. H. (1998). Construction phase engineering geological study in Modi Khola hydroelectric project, Parbat district, western Nepal. *Journal of Nepal Geological Society*, 18, 343-355.
- Perri, G. (2007, July). Behavior category and design loads for conventionally excavated tunnels. In 11th ISRM congress. OnePetro.
- Priest, S. D. (2005). Determination of Shear Strength and Three-dimensional Yield Strength for the Hoek-Brown Criterion. *Rock Mech. Rock Engng.*, 38(4), 229-327.
- RocLab, User's Guide, 2002 Rocscience Inc.
- Rocscience, Inc. (2005). RocSupport – Rock support interaction and deformation analysis for tunnels.
- Russo, M., Germani, G., & Amberg, W. (2002, October). Design and construction of large tunnel through active faults: a recent application. In *Proceedings of the International Conference of Tunneling and Underground Space Use* (pp. 16-18).
- Shahidi, A. R., & Vafaeian, M. (2005). Analysis of longitudinal profile of the tunnels in the active faulted zone and designing the flexible lining (for Koohrang-III tunnel). *Tunnelling and underground space technology*, 20(3), 213-221.
- Shrestha, P. K., & Panthi, K. K. (2014). Groundwater effect on faulted rock mass: an evaluation of Modi Khola pressure tunnel in the Nepal Himalaya. *Rock mechanics and rock engineering*, 47(3), 1021-1035.
- Unlu, T., Gercek, H. (2003). Effect of Poisson's ratio on the normalized radial displacements.
- Zhang, L. F., Li, R. H., Liu, H., Fang, Z. B., Wang, H. B., Yuan, Y., & Yu, H. T. (2020, October). A Review on Seismic Response and Aseismic Measures of Fault-crossing Tunnels. In *IOP Conference Series: Earth and Environmental Science* (Vol. 570, No. 5, p.
- Zhang, X., Jiang, Y., & Maegawa, K. (2020). Mountain tunnel under earthquake force: A review of possible causes of damages and restoration methods. *Journal of Rock Mechanics and Geotechnical Engineering*, 12(2), 414-426.

- Zhang, Z., Chen, F., Li, N., Swoboda, G., & Liu, N. (2017). Influence of fault on the surrounding rock stability of a tunnel: Location and thickness. *Tunnelling and Underground Space Technology*, 61, 1-11.
- Zhao, J. (2000). Applicability of Mohr-Coulomb and Hoek-Brown strength criteria to the dynamic strength of brittle rock. *International Journal of Rock Mechanics & Mining Sciences*, 37 , pp. 1115-1121.
- Zoback, M. L. (1992). First-and second-order patterns of stress in the lithosphere: The World Stress Map Project. *Journal of Geophysical Research: Solid Earth*, 97(B8), 11703-11728.

Annex

A. Convergence Confinement Method

Convergence Confinement Method is tunnel design approach which is basically a two-dimensional plane strain model of a hole in an infinite pre-stressed slab. The effect of the third dimension i.e., distance to tunnel face is introduced by successive release of an internal pressure, which corresponds to the primary stress at the starting point. Convergence confinement method can be applied to study tunnel behavior along the different stages of excavation. The study of tunnel behavior allows the definition of different solutions to the support and excavation types needed to a safe tunnelling construction.

There are closed mathematical solutions for elastic and elasto-plastic material and isotropic stress conditions. The displacement response of the tunnel perimeter versus the internal stress is called Ground Reaction Curve (GRC). In the case of a supported tunnel the load release on the rock mass is partially absorbed by yielding of the rock and partially transferred to the support. The load transfer from the rock mass into the support is represented by the Support Characteristic Curve (SCC). The tunnel deformation behavior ahead and behind of the face is represented by the longitudinal displacement profile (LDP).

Ground Reaction Curve (GRC)

Carranza-Torres and Fairhurst in 2000 describe, GRC as the relationship between the decreasing internal pressure p_i and the increasing radial displacement of the wall u_r and plastic zone surrounding the tunnel. The internal pressure is the idealized way of modelling the support and the relief due to the tunnel advance. It is defined as the pressure acting around the perimeter of the tunnel in a certain cross section. shows the decrease of the p_i value for an unsupported tunnel.

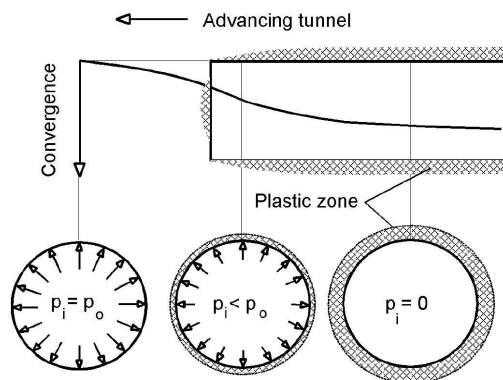


Figure 7-1 Assumed support pressure p_i at different positions (Hoek, 1998)

The critical internal pressure p_i^{cr} is the value at which plastic deformation begins to develop. This means that if the internal pressure falls below this value, a failed area surrounding the tunnel develops. The critical internal pressure is given by

$$p_i^{cr} = \frac{2p_0 + \sigma_{cm}}{1 + k} \quad \text{Eq.(a)}$$

If the internal support pressure is greater than the critical value, the behavior of the rock mass will be elastic; meaning that no failure occurs. In this condition the elastic displacement of the tunnel wall u_{ie} is given by

$$u_{ie} = \frac{r_0(1+U)}{E}(p_0 - p_i) \quad \text{Eq.(b)}$$

Where U is the Poisson's ratio, E is the deformation modulus and r_0 is the initial tunnel radius. When the internal pressure p_i is less than the critical internal pressure p_i^{cr} , failure occurs and a region of extension r_p develops around the tunnel. In this condition the plastic radius zone r_p is given by

$$r_p = r_0 \left[\frac{2(p_0(k-1) + \sigma_{cm})}{(k+1)((k-1)p_i + \sigma_{cm})} \right]^{\frac{1}{k-1}} \quad \text{Eq.(c)}$$

It is therefore possible to predict the ground reaction either under elastic or plastic conditions using the above formula.

Longitudinal Deformation Profile (LDP)

In a tunnel the LDP is defined as the deformation of the tunnel wall along the longitudinal axis, ahead of and behind the face. Deformation starts about two to four tunnel diameters in front of the face, i.e. into the rock mass. However, this value differs from author to author depending also on the rock mass behavior. Therefore, care must be taken when performing calculations. The total closure at the face u_0 under elastic conditions is about one-third of the maximum short term radial displacement u_{max} for an unsupported tunnel calculated from plain strain analysis.

The radial displacement ends about two to four tunnel diameters behind the face for linear elastic rock, but it can reach several tunnel diameters if elasto-plastic behavior is observed. The estimation of the normalized LDP, as explained by Unlu and Gercek (2003), was developed by several researchers who defined equations for the elastic behavior of the tunnel. This best fit curve is used to calculate the tunnel face displacement and is given by .

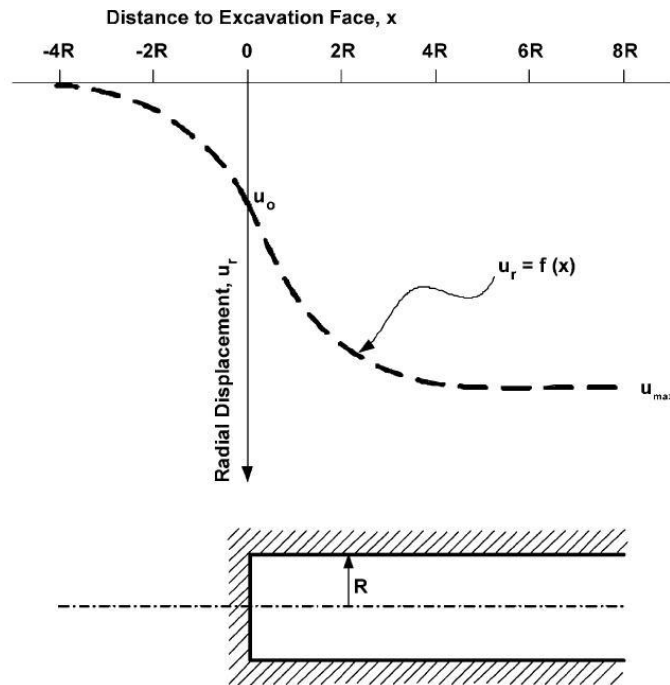


Figure 7-2 Longitudinal displacement profile (Unlu and Gercek,2003).

$$\frac{u_r}{u_{max}} = 1 + e^{\frac{d_t}{1.10} - 1.7} \quad \text{Eq.(d)}$$

Where $d_t = x/r_0$, u_r is the average radial displacement at a specified longitudinal position x , and r_0 is the tunnel radius. x is the distance measured from the tunnel face, being positive towards the excavated zone ($x > 0$) and negative into the unexcavated rock ($x < 0$).

A large bullet shaped plastic yielding zone develops in three dimensions on the advancing front (Hoek et. al., 2008). To take into account the influence of this large plastic zone a normalized plastic zone radius r_p/r_0 must be considered and a new equation is therefore defined by .

$$\frac{u_0}{u_{max}} = \frac{1}{3} e^{-0.15p_r} \quad \text{Eq.(e)}$$

Support Characteristic Curve (SCC)

The SCC is the relation between the increasing pressure on the support, p_s , with increasing radial displacement. When support is installed the initial support pressure is considered to be zero, becoming greater with the increasing load induced by convergence. The pressure carried by the support depends on the stiffness, the distance from the face when it was installed and the maximum loading bearing capacity

p_s^{\max} of the support chosen. The support reacts like a system formed by springs, meaning that induced loads from the rock mass are gradually transferred until equilibrium or the p_s^{\max} is reached.

Equations are published for the calculation of the stiffness and capacity of different support systems; however, they often refer to an ideal state given by homogeneous conditions around a perfectly circular tunnel. Therefore, equations must not be used to define precise support characteristics but to have a general idea how the different support types will work.

B. Rock Mass Classification

Knowledge, understanding of geological material and its implication in design, advances in site investigation methods has led to development of geotechnical classification systems and quantification of rock masses. The most common empirical methods for tunneling are Rock Mass Rating (RMR) (Bieniawski, 1989). Rock Mass Quality (Q system) (Barton et al 1974) and Geological Strength Index (GSI) (Marinos et. Al.,2005; Hoek and Brown,2019) in the Himalayan region of Nepal. These three empirical methods incorporate geological geotechnical parameters to obtain a quantitative value of their rock mass quality

Rock Mass Rating (RMR, Bieniawski (1989))

Bieniawski (1989) published the details of a rock mass classification called the Geomechanics Classification or the Rock Mass Rating (RMR) system to classify the rock mass give a rating number (RMR) and provide the support on the basis of RMR value.

A given site is divided into several geological structural units in such a way that each type of rock mass is represented by a separate geological unit. The following six parameters are used to classify a rock mass using the RMR system: i) uniaxial compressive strength of rock material, ii) Rock Quality Designation (RQD), iii) joint or discontinuity spacing, iv) joint conditions, v) groundwater conditions, and vi) joint orientation. The rating from each six parameters is used for evaluating the RMR of rock mass.

Table 7-1 Guidelines for excavation and support of rock tunnels based on the RMR system (Bieniawski, 1989)

Rock mass class	Excavation	Supports		
		Rock bolts (20 mm dia. Fully grouted)	Conventional shotcrete	Steel sets
Very good rock RMR =81-100	Full face 3 m advance	Generally, no support required except for occasional spot bolting		
Good Rock RMR= 61-80	Full face 1.0-1.5 m advance. Complete support 20 m from face	Locally, bolts in crown 3 m long, spaced 2.5 m, with occasional mesh	50 mm in crown where required	None

Fair rock RMR= 41-60	Heading and bench. 1.5 -3 m advance in heading. Commence support after each blast. Complete support 10 m from face.	Systematic bolts 4 m long, spaced 1.5-2 m in crown and walls with wire mesh in crown	50-100 mm in crown and 30 mm in sides	None
Poor rock RMR= 21-40	Top heading and bench. 1.0 - 1.5 m advance in top heading. Install support concurrently with excavation 10 m from face.	Systematic bolts 4-5 m long, spaced 1-1.5 m in crown and wall with wire mesh.	100-150 mm in crown and 10 mm in sides	Light to medium ribs spaced 1.5 m where required.
Very poor rock RMR<20	Multiple drift 0.5-1.5 m advance in top heading. Install support concurrently with excavation. Shotcrete as soon as possible after blasting	Systematic bolts 5-6 m long, spaced 1-1.5 m in crown and walls with wire mesh. Bolt invert	150-200 mm in crown 150 mm in sides and 50 mm on face	Medium to heavy ribs spaced 0.75 m with steel lagging and forepoling if required. Close invert

Guidelines for selection of tunnel support is presented in , based on the RMR values, which is applicable to tunnels excavated with conventional drilling and blasting method. These guidelines depend upon the factors like depth below surface (to take care of overburden pressure or in situ stress), tunnel size and shape and method of excavation.

Rock Mass Quality (Q- system, Barton et al. (1974))

Barton et al. (1974) proposed the Rock Mass Quality (Q) System of rock mass classification with a numerical value i.e., Q value and tunnel support on the basis of Q value. The Q-System is based on a numerical assessment of the rock mass quality using six different parameters given Eq.(f)

$$Q = \frac{RQD}{J_n} \cdot \frac{J_r}{J_a} \cdot \frac{J_w}{SRF} \quad \text{Eq.(f)}$$

where, RQD is the Rock Quality Designation, J_n is the joint set number, J_r , is the joint roughness number, J_a , is the joint alteration number, J_w , is the joint water reduction factor and SRF is the stress reduction factor

The three quotients in the Q system can be explained as follows: the quotient RQD/J_n is a crude measure of the block or particle size, the second quotient J_r/J_a represents the roughness and frictional characteristics of the wall or filling materials, and the third quotient J_w/SRF consists of two parameters. While J_w can be directly related to water pressure values across the joint, while SRF bears more complicated relationship

with a number of factors such as 1) loosening load in the case of an excavation through shear zones and clay bearing rock, 2) rock stress in competent rock, and 3) squeezing loads in plastic incompetent rock.

For various rock conditions, the rating (numerical values) to these six parameters are assigned. The details of rating can be found in Barton et al, 1974. The goal of Q-system is preliminary empirical design of support system for tunnels and caverns (). The ratings of these parameters obtained for a given rock mass is substituted in 17. to get rock mass quality Q. In addition to the Q- value two other factors are decisive for the support design in underground openings. These factors are the safety requirements and the dimension, i.e., the span or height of the underground opening. Generally, there will be an increasing need for support with increasing span and increasing wall height. Safety requirements will depend on the purpose of the excavation.

One of the benefits of the RMR system is that it is relatively easy to use. The result produced by the RMR classification, however, is rather conservative. This can lead to an overestimation of the support measures (Maidl et al. 2008). As the RMR system and the Q-method are empirical methods they have their own deficiencies. As there are some reasonably consistent relationships between these systems, it is advantageous to apply both systems to the field data as a mutual check. There is an empirical relationship between the RMR and the Q-value as shown in Eq.(g) (Barton 2002).

$$\text{RMR} \sim 15 \log Q + 50 \quad \text{Eq.(g)}$$

For most tunnels for civil engineering projects, the ground can be considered as a continuum and tunnels are designed on this basis, i.e. the movement of the ground towards the excavation will load the lining. Rock mass classification systems such as RMR and Q-method are best used where the ground strength adequately exceeds the ground stresses and a support system, which increases the strength and stiffness of the discontinuities is appropriate. Where the ground requires a continuous structural lining for support, such is the case for weaker rocks, continuum analysis methods are more appropriate (BTS/ICE 2004). Palmström and Broch (2006) investigated Q-method and showed that Q-method is most applicable within outside this area () with supplementary calculations and methods of evaluation are recommended. For poorer quality ground outside the area as shown in , support criteria are very sensitive to small changes in the rating values.

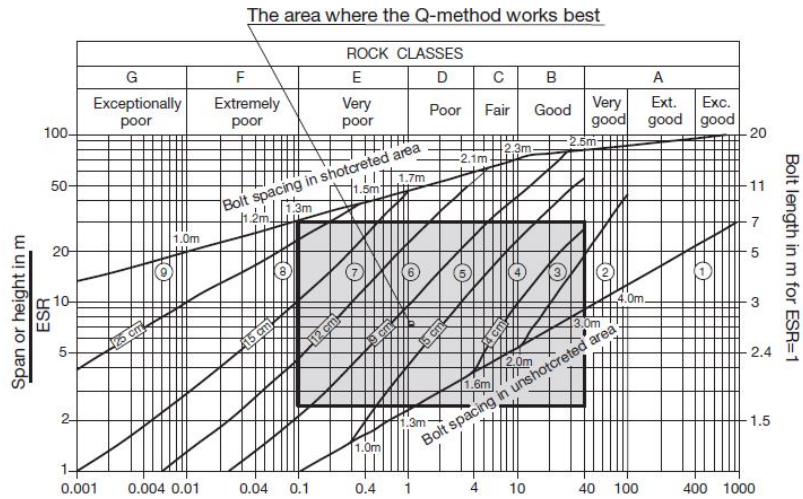
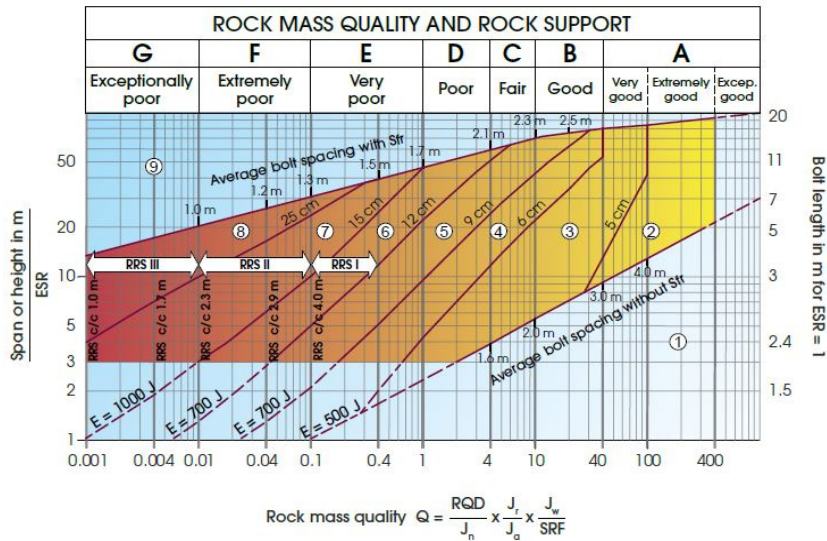


Figure 7-3 Analysis chart by Palmström and Broch (2006)



Support categories

- ① Unsupported or spot bolting
- ② Spot bolting, **SB**
- ③ Systematic bolting, fibre reinforced sprayed concrete, 5-6 cm, **B+Sfr**
- ④ Fibre reinforced sprayed concrete and bolting, 6-9 cm, **Sfr (E500)-B**
- ⑤ Fibre reinforced sprayed concrete and bolting, 9-12 cm, **Sfr (E700)-B**
- ⑥ Fibre reinforced sprayed concrete and bolting, 12-15 cm + reinforced ribs of sprayed concrete and bolting, **Sfr (E700)+RRS I +B**
- ⑦ Fibre reinforced sprayed concrete >15 cm + reinforced ribs of sprayed concrete and bolting, **Sfr (E1000)+RRS II +B**
- ⑧ Cast concrete lining, **CCA** or **Sfr (E1000)+RRS III +B**
- ⑨ Special evaluation

Bolts spacing is mainly based on $\phi 20$ mm
 E = Energy absorption in fibre reinforced sprayed concrete
 ESR = Excavation Support Ratio
 Areas with dashed lines have no empirical data

RRS - spacing related to Q-value

- I** S130/6 $\phi 16 - \phi 20$ (span 10m)
D40/6+2 $\phi 16-20$ (span 20m)
- II** S135/6 $\phi 16-20$ (span 5m)
D45/6+2 $\phi 16-20$ (span 10m)
D55/6+4 $\phi 20$ (span 20m)
- III** D40/6+4 $\phi 16-20$ (span 5 m)
D55/6+4 $\phi 20$ (span 10 m)
Special evaluation (span 20 m)

S130/6 = Single layer of 6 rebars, 30 cm thickness of sprayed concrete
 D = Double layer of rebars
 $\phi 16$ = Rebar diameter is 16 mm
 c/c = RSS spacing, centre - centre

Figure 7-4 Support recommendations based on Q values Barton et al. (1974)

Geological Strength Index (GSI)

The geological strength index (GSI) is a system of rock-mass characterization, proposed by Hoek (1995), for reliable input data, related to rock-mass properties required as inputs into numerical analysis or closed form solutions for designing tunnels, slopes or foundations in rocks. The geological character of rock material with the visual assessment of the mass is used as a direct input to the selection of parameters relevant for the prediction of rock-mass strength and deformability. This approach enables a rock mass to be considered as a mechanical continuum without losing the influence geology has on its mechanical properties. It also provides a field method for characterizing difficult-to-describe rock masses. presents the general chart for GSI to estimate the rock mass parameters for poor and weak rock mass.

GEOLOGICAL STRENGTH INDEX		SURFACE CONDITIONS				
<p>From the description of structure and surface conditions of the rock mass, pick an appropriate box in this chart. Estimate the average value of the Geological Strength Index (GSI) from the contours. Do not attempt to be too precise. Quoting a range of GSI from 36 to 42 is more realistic than stating that GSI = 38. It is also important to recognize that the Hoek-Brown criterion should only be applied to rock masses where the size of the individual blocks or pieces is small compared with the size of the excavation under consideration. When individual block sizes are more than approximately one quarter of the excavation dimension, failure will generally be structurally controlled and the Hoek-Brown criterion should not be used.</p>		<p>VERY GOOD Very rough, fresh unweathered surfaces</p>	<p>GOOD Rough, slightly weathered, iron stained surfaces</p>	<p>FAIR Smooth, moderately weathered and altered surfaces</p>	<p>POOR Slit-sided, highly weathered surfaces with compactings or fillings of angular fragments</p>	<p>VERY POOR Slit-sided, highly weathered surfaces with soft clay coatings or fillings</p>
STRUCTURE		DECREASING SURFACE QUALITY →				
 <p>INTACT OR MASSIVE – intact rock specimens or massive in situ rock with very few widely spaced discontinuities</p>		90	80	N/A	N/A	N/A
 <p>BLOCKY - very well interlocked undisturbed rock mass consisting of cubical blocks formed by three orthogonal discontinuity sets</p>			70			
 <p>VERY BLOCKY - interlocked, partially disturbed rock mass with multifaceted angular blocks formed by four or more discontinuity sets</p>			60	50		
 <p>BLOCKY/DISTURBED - folded and/or faulted with angular blocks formed by many intersecting discontinuity sets</p>				40	30	
 <p>DISINTEGRATED - poorly interlocked, heavily broken rock mass with a mixture of angular and rounded rock pieces</p>					20	
 <p>FOLIATED/LAMINATED – Folded and tectonically sheared foliated rocks. Schistosity prevails over any other discontinuity set, resulting in complete lack of blockiness</p>		N/A	N/A			10
						5

Figure 7-5 General chart for GSI (Marinos et al., 2005)

C. Published Papers

1. **B Chhushyabaga**, S Karki, SS Khadka, " Tunnel support design in fault zone in hydropower project in the Nepal Himalaya: a case study ", Journal of Physics: Conference Series 1608 (1), 012009
2. **B Chhushyabaga**, S Karki, SS Khadka, "Fault induced problems in hydropower tunnels in Nepal: A case study" March 2020, Lowland Technology International 21,255-267.
3. **B Chhushyabaga**, S Karki, SS Khadka, "Stability Analysis of Jointed Rock mass for the Underground Structures in the Himalaya", December 2019, Nepal Tunnelling Conference 2019, "Knowledge Sharing on Tunnel Design and Construction" Kathmandu, Nepal
4. S Karki, **B Chhushyabaga**, SS Khadka, " An Overview of Design and Construction practices of Himalayan Hydropower tunnels" Journal of Physics: Conference Series 1608 (1), 012008
5. S Karki, B Karki, **B Chhushyabaga**, SS Khadka, "Design and Analysis of Squeezing Ground Hydropower Tunnel in the Himalaya through a Case Study", March 2020, Lowland Technology International 21, 268-278.
6. S Khadka., S Karki., **B Chhushyabaga**, R K Maskey, "Assessment and Numerical Analysis of Hydropower Tunnel in Lesser Himalayan Region of Nepal- A Case Study." June 2019, Journal of Physics Conference Series 1266:012015 DOI: 10.1088/1742-6596/1266/1/012015 Conference: Journal of Physics: Conference Series Volume: Volume 1266